THE SIMULTANEOUS INVESTIGATION OF THE ISOBARIC INTEGRAL HEAT OF VAPORIZATION AND VAPOR-LIQUID EQUILIBRIA DATA OF METHANE-ETHYLENE MIXTURES AT HIGH PRESSURES

By

PHILIP COCHRAN TULLY

Bachelor of Science
Iowa State University
Ames, Iowa
1947

Master of Science
University of Pittsburgh
1955

Submitted to the Faculty of the Graduate School of
the Oklahoma State University
in partial fulfillment of the requirements
for the degree of
DOCTOR OF PHILOSOPHY
August, 1965

THE SIMULTANEOUS INVESTIGATION OF THE ISOBARIC INTEGRAL HEAT OF VAPORIZATION AND VAPOR-LIQUID EQUILIBRIA DATA OF METHANE-ETHYLENE MIXTURES AT HIGH PRESSURES

Thesis Approved:

Wayne C. Edmister
Thesis Adviser

Kenneth J. Bell

J. A. Weibelt

John B. West

J. H. Boggs
Dean of the Graduate School

PREFACE

The isobaric integral heats of vaporization of three methane-ethylene mixtures were measured at 20 and 40 atmospheres in a calorimeter especially designed for this purpose. These data were obtained to provide information about the non-ideal behavior of hydrocarbon mixtures. They are compared to values calculated by three different methods to illustrate the application of these data to a theoretical problem involving non-ideal behavior. Thermodynamic consistency tests are made on the enthalpy data using vapor-liquid equilibria data obtained simultaneously.

The advice and guidance given by the members of the author's Doctoral Committee, Professors K. J. Bell, W. C. Edmister, J. B. West, and J. A. Wiebelt, are appreciated. The author is particularly grateful to his major adviser, Professor W. C. Edmister, for the great amount of time he has given to this dissertation.

The author thanks the National Science Foundation for the research assistantship during the 1961-63 school years and the Ford Foundation for financial assistance. Appreciation is extended to Phillips Petroleum Co., Hoskins Manufacturing Co., F. W. Glitch and Sons, the Research Apparatus Development Laboratory personnel, and Mr. Eugene McCroskey for their contributions which aided in the construction and operation of the calorimeter.

TABLE OF CONTENTS

LIST OF TABLES

LIST OF FIGURES

LIST OF PLATES

CHAPTER I

INTRODUCTION

The purpose of this research was to obtain experimental heat of vaporization data for an investigation of the non-ideal behavior of hydrocarbon mixtures. This necessitated the development of a new experimental capability with certain features.

The first feature required was a high pressure rating because hydrocarbon mixtures are generally more non-ideal at elevated pressures. The cricondenbar for most of these two phase systems is about 2500 psia. A 2000 psi limit was selected to permit the investigation of many mixtures without making the design requirements excessive.

The second feature selected was a low-temperature capability. The temperature of gas-liquid hydrocarbon mixtures ranges upward from 112° K (-258° F), the normal boiling point of methane. The apparatus was specifically designed for the lower end of the range, 110° to 285° K (-262° to +54° F), because of the current interest in cryogenic processes such as the production of liquid oxygen, nitrogen, hydrogen, and helium. The temperature range could be extended to 500° K (440° F) to include more mixtures by changing the heat transfer media.

In this high pressure and low temperature range, there are two hydrocarbon mixtures of interest whose systems lie entirely within the range: methane-ethylene and methane-ethane. Methane-ethylene was selected because it should be more non-ideal than the methane-ethane.

In addition, this mixture is of greater industrial importance because more than a billion pounds of ethylene are purified annually by the removal of small quantities of methane.

The third design feature of the apparatus was a capability for sampling the co-existing phases. These composition data, together with the heats of vaporization, would make the isobaric thermodynamic consistency tests possible.

There are many facets to a theoretical study of the non-ideal behavior of hydrocarbon mixtures. Some of these are solution theory; prediction of critical properties, compressibility factors, and equilibrium distribution ratios (K-values); development and evaluation of methods for calculating heats of mixing, heats of vaporization, and heats of condensation, etc. Most of these are beyond the scope of this research. To illustrate the use of the experimental data, an evaluation is made of three methods for calculating the isobaric integral heat of vaporization.

The data are also used in performing three different isobaric thermodynamic consistency tests in differential and integral form. All three tests used have been developed recently. They are the Thompson-Edmister (45) test, the Edmister (10) test, and a modified Thompson-Edmister test, heretofore unpublished.

CHAPTER II

THEORY

The theoretical aspects of this investigation are discussed in this chapter in three sections; heats of vaporization of binary mixtures, calculation methods, and consistency tests.

Heats of Vaporization of Binary Mixtures

For a binary mixture with two coexisting phases, the Phase Rule allows two degrees of freedom. These two degrees of freedom can be selected as follows: pressure-temperature, pressure-composition, and temperature-composition. Each constraint requires a different type of vaporization, as discussed below.

Differential Heat of Vaporization and Condensation

The differential heat of vaporization is measured at constant temperature and pressure. It is the amount of heat required to produce one mole of equilibrium vapor from a quantity of liquid so large that its composition does not change during the process. The following analysis is from Schroeder and Edmister (36). By heat balance

$$(\Delta H_v)_{P,T} = \underline{H}^V - \underline{H}^L - (y-x)\left(\frac{\partial \underline{H}^L}{\partial x}\right)_{P,T} \qquad (1)$$

where $(\Delta H_v)_{P,T}$ = molal differential heat of vaporization

$\underline{H}^V$ = molal enthalpy of equilibrium vapor y

$\underline{H}^L$ = molal enthalpy of equilibrium liquid x

$\left(\frac{\partial \underline{H}^L}{\partial x}\right)_{P,T}$ = slope of line BPDH.

A list of symbols is appended at the end of this dissertation.

The enthalpy-concentration diagram of one mole of a binary solution at constant pressure is shown in Figure 1 (36). The heats of vaporization of pure components 1 and 2 are represented by lines AB and CD, respectively. CA is the saturated liquid line; DB is the saturated vapor line. A typical isotherm is represented by line EBPVG. Comparing Equation 1 with Figure 1, it can be seen that

$\underline{H}^V$ = Enthalpy at point V

$\underline{H}^L$ = Enthalpy at point BP

$\left(\frac{\partial \underline{H}^L}{\partial x}\right)_{P,T}$ = Slope of line BPDH

$(\Delta H_v)_{P,T}$ = V - DH

The differential heat of condensation is not equal and opposite to the differential heat of vaporization. By heat balance (36),

$$(\Delta H_c)_{P,T} = \underline{H}^L - \underline{H}^V - (x-y)\left(\frac{\partial \underline{H}^V}{\partial y}\right)_{P,T} \qquad (2)$$

where $(\Delta H_c)_{P,T}$ = differential heat of condensation

= BP - CP

$\left(\frac{\partial \underline{H}^V}{\partial y}\right)_{P,T}$ = slope of line CPV

Isobaric Integral Heat of Vaporization

The isobaric integral heat of vaporization $(\Delta H_v)_{P,x}$ is measured at constant pressure and composition. It is the amount of heat required to vaporize completely one mole of liquid mixture. During the vaporization process the temperature rises from the bubble point of the binary to its dew point. In Figure 1, this isobaric path is

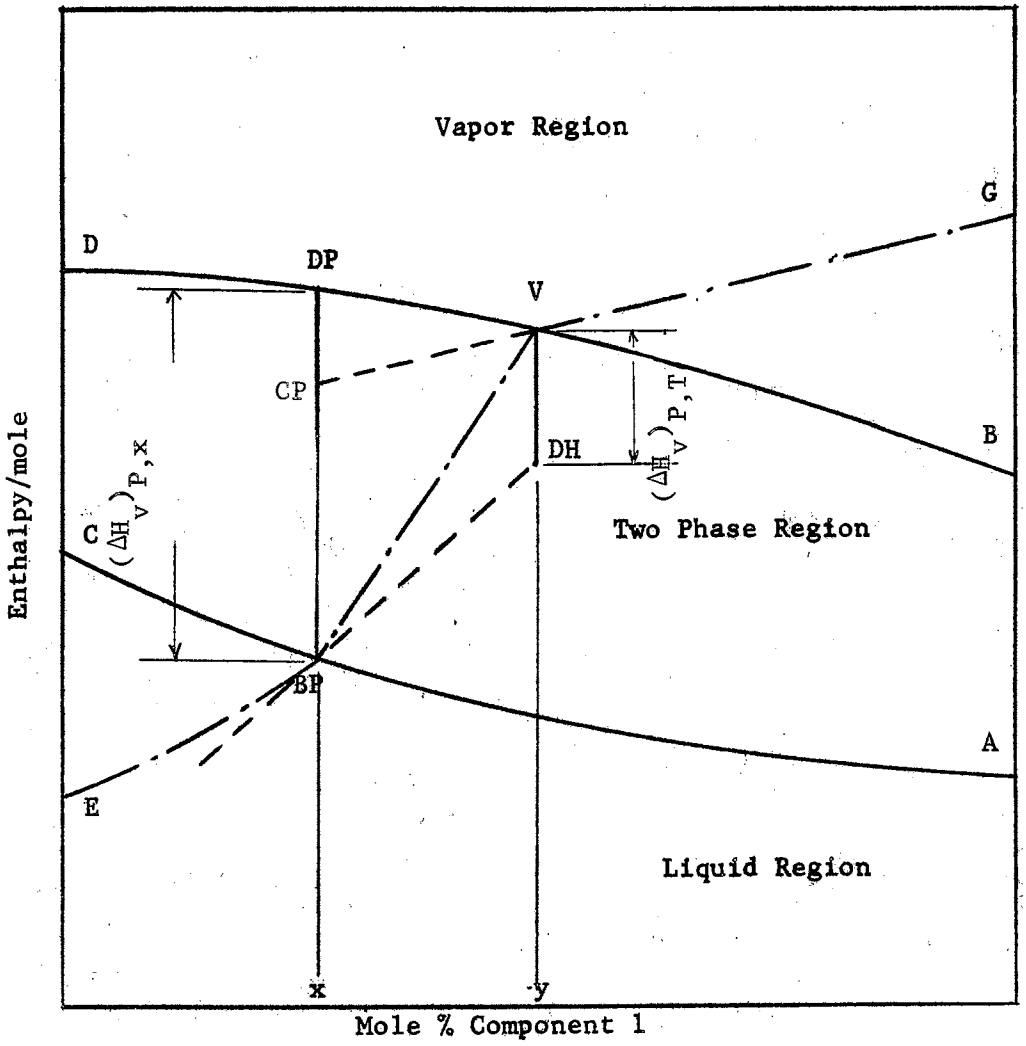

Figure 1

Enthalpy-Concentration Diagram
for a Binary Solution at Constant Pressure

Source: Schroeder-Edmister (36)

represented by the line BPDP, which is equal to BPCP plus CPDP. Since

$$BPCP = -(\Delta H_c)_{P,T} = CP - BP$$

and

$$CPDP = (C_P^V)_{y^\#}(T_{DP}-T_{BP}) = DP - CP$$

$$(\Delta H_v)_{P,x} = -(\Delta H_c)_{P,T} + (C_P^V)_{y^\#}(T_{DP}-T_{BP}) = DP - BP \qquad (3)$$

where

$(C_P^V)_{y^\#}$ = heat capacity of constant composition vapor, $y^\#$

T_{DP} = dew point temperature of constant composition vapor $y^\# = x$

T_{BP} = bubble point temperature of same constant composition liquid x

Isothermal Integral Heat of Vaporization

The isothermal integral heat of vaporization $(\Delta H_v)_{T,x}$ is determined at constant temperature and composition. It is the amount of heat required to vaporize completely one mole of liquid mixture at constant temperature, accomplished by decreasing the pressure. Since the isobaric integral heat of vaporization could be replaced by a combination of isothermal integral vaporization, heating the vapor produced to the dew point temperature and compressing it to the original pressure

$$(\Delta H_v)_{P,x} = (\Delta H_v)_{T,x} + (C_P^V)_{y^\#}(T_{DP}-T_{BP}) + \Delta H_{com} \qquad (4)$$

where ΔH_{com} = enthalpy change on compressing the vapor from the isothermal dew point pressure to the original bubble point pressure. Combining Equations 3 and 4 and solving for $(\Delta H_v)_{T,x}$

$$(\Delta H_v)_{T,x} = -\left[(\Delta H_c)_{P,T} + \Delta H_{com}\right] \qquad (5)$$

This variable pressure path cannot be shown on the isobaric curves of Figure 1.

Other Diagrams

The temperature-composition diagram for a binary solution at constant pressure is shown in Figure 2. The paths of the differential heat of vaporization BPV and the isobaric integral heat of vaporization BPDP are shown.

The enthalpy-temperature diagram for a binary solution at constant composition is shown in Figure 3 (9.). The isobar P through the two-phase region is drawn as a straight line for simplicity; it is not intended to imply that the isobaric integral heat of vaporization proceeds along this path. The linear isobar P in the subcooled liquid and superheated vapor regions implies that the heat capacities are independent of temperature. Figure 3 is ideally suited for portraying the isothermal integral heat of vaporization BPV.

Calculation Methods

Methods have been developed for calculating the different heats of vaporization from other types of data which are more generally available, such as pressure-volume-temperature (PVT) data, vapor-liquid equilibria (VLE) data, pure component properties, equations of state, generalized enthalpy correlations, etc. Several of these methods are presented here.

Differential Heat of Vaporization and Condensation

Sage and Lacey (32) derived an expression for $(\Delta H_v)_{P,T}$ using the basic relationships

$$\bar{H}_i - H_i^\circ = -RT^2 \left(\frac{\partial \ln \bar{f}_i}{\partial T}\right)_{P,N_i} \qquad (6)$$

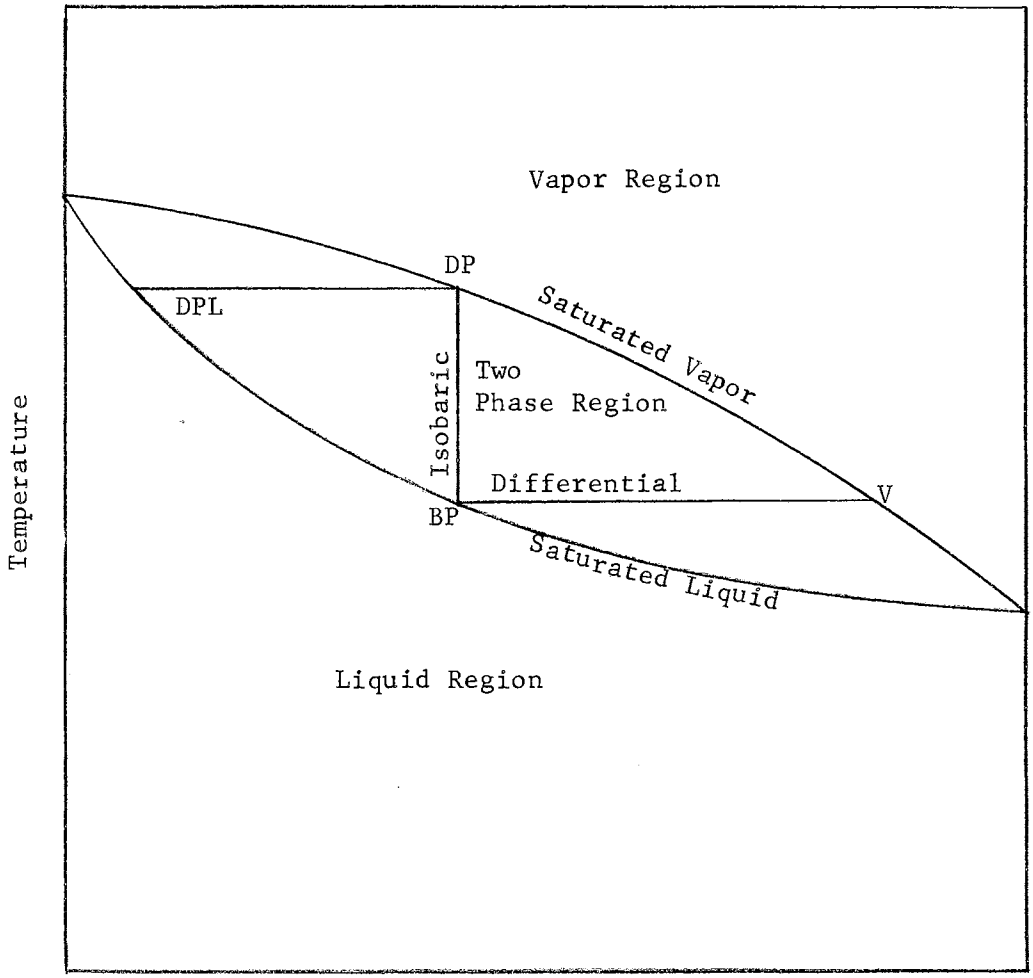

Figure 2

Temperature-Composition Diagram
for a Binary Solution at Constant Pressure

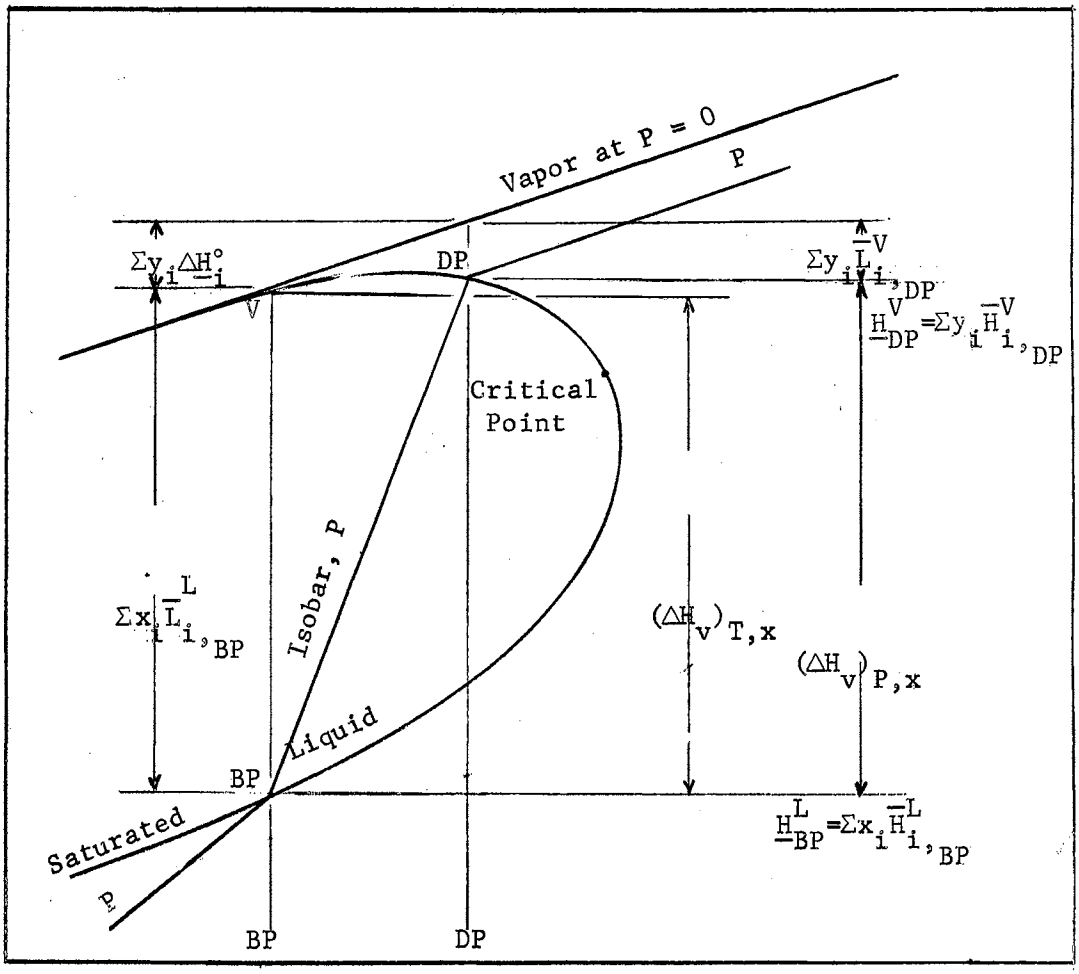

Figure 3

Enthalpy-Temperature Diagram for a
Binary Solution at Constant Composition

Source: Edmister (9)

$$\bar{V}_i^L = RT\left(\frac{\partial \ln \bar{f}_i^L}{\partial P}\right)_{T,x_i} \tag{7}$$

$$\left(\frac{\partial \ln \bar{f}_i^L}{\partial T}\right)_{x_i} = \left(\frac{\partial \ln \bar{f}_i^V}{\partial T}\right)_{x_i} \tag{8}$$

and the definition of $(\Delta H_v)_{P,T}$

$$(\Delta H_v)_{P,T} = \left[y_1 \Delta\bar{V}_1 + (1-y_1)\,\Delta\bar{V}_2\right] T\left(\frac{dP}{dT}\right)_x$$

to give

$$\bar{H}_i^V - \bar{H}_i^L = (\Delta\bar{H}_{v_i})_{P,T} = T\left(\bar{V}_i^V - \bar{V}_i^L\right)\left(\frac{\partial P}{\partial T}\right)_{x_i} + RT^2\left(\frac{\partial \ln \bar{f}_i^V}{\partial y_i}\right)_{P,T}\left(\frac{\partial y_i}{\partial T}\right)_{x_i} \tag{9}$$

where $\left(\frac{\partial P}{\partial T}\right)_{x_i}$ = the slope of the vapor pressure curve for constant liquid composition.

Equation 9 requires knowledge of the PVT and VLE data and saturated liquid and vapor partial volumes of the system under consideration, which limits its utility.

Differential Heat of Condensation

Sage and Lacey (32) continued their derivation to develop a similar equation for the differential heat of condensation, using the definition

$$-(\Delta H_c)_{P,T} = \left[x_1 \Delta\bar{V}_1 + (1-x_1)\,\Delta\bar{V}_2\right] T\left(\frac{dP}{dT}\right)_y$$

to give

$$\bar{H}_i^L - \bar{H}_i^V = (\Delta\bar{H}_c)_{P,T} = T\left(\bar{V}_i^V - \bar{V}_i^L\right)\left(\frac{\partial P}{\partial T}\right)_{y_i} - RT^2\left(\frac{\partial \ln \bar{f}_i^L}{\partial x_i}\right)_{P,T}\left(\frac{\partial x_i}{\partial T}\right)_{y_i} \tag{10}$$

which requires the same knowledge as before, and has the same utility.

Stiehl, Hobson, and Weber (36) also developed a method for calculating the differential heat of condensation. Their method requires less data than that of Sage and Lacey, but depends much more on the equation of state. Since the condensation is isothermal, isobaric, and the vapor phase has constant composition, they applied the Clapeyron equation

$$\left(\frac{\partial P}{\partial T}\right)_y = \frac{\Delta S}{\Delta V} = \frac{(\Delta H_c)_{P,T}}{T(\Delta V_c)_{P,T}} \tag{11}$$

to mixtures and an equation given by Dodge (8)

$$\Delta V = V_x^L - V_y^V + (y-x)\left(\frac{\partial V^V}{\partial y}\right)_{P,T} \tag{12}$$

in their development. In Equation 11 $(\partial P/\partial T)_y$ is the slope of the dew point pressure-temperature curve of the mixture. In Equation 12, $(\partial V^V/\partial y)_{P,T}$ is the slope of the $(V^V$ vs. $y)_{P,T}$ curve at its intersection with the saturated vapor curve. It is plotted from the superheated vapor region to the saturated vapor line. Although $(\partial V^V/\partial y)_{P,T} = \overline{V}_1^V - \overline{V}_2^V$, the graphical technique does not require the partial volumes per se. The authors used precise dew point PVT data and the Benedict-Webb-Rubin (4) equation of state to calculate the slope and volume terms.

Application of this method is therefore limited to the availability of PVT and VLE data and an equation of state which adequately describes the vapor behavior of the system in question.

Knowledge of the saturated liquid and vapor partial volumes is not required, which makes the Stiehl, et al., method more convenient. The authors also point out that Equation 11 is very sensitive to values of $(\partial P/\partial T)_y$, which must be determined with the highest possible degree of accuracy. It is also sensitive to $(\partial V^V/\partial y)_{P,T}$, which is found from an equation of state (BWR).

Isobaric Integral Heat of Vaporization

In Chapter VI, the experimental enthalpy data obtained in this investigation are compared with values calculated by the three methods presented below.

Edmister K-Value Approximation Method

Edmister (9) developed a method for calculating the isobaric integral heat of vaporization of multicomponent hydrocarbon mixtures from K-values and bubble and dew point temperatures. The complete derivation is given in Appendix I. The first simplifying approximation was

$$\left(\frac{\bar{f}^L_{i_{T_{DP}}}}{\bar{f}^L_{i_{T_{BP}}}}\right)_{x_{BP}} \approx \left(\frac{\bar{f}^L_{i_{T_{DP}x_{DP}}}}{\bar{f}^L_{i_{T_{BP}x_{BP}}}}\right) \tag{13a}$$

and

$$\left(\frac{\bar{f}^V_{i_{T_{DP}}}}{\bar{f}^V_{i_{T_{BP}}}}\right)_{y^{\#}_{DP}} \approx \left(\frac{\bar{f}^V_{i_{T_{DP}y_{DP}}}}{\bar{f}^V_{i_{T_{BP}y_{BP}}}}\right) \tag{13b}$$

The second approximation was

$$T^2_{BP} \approx T_{BP}T_{DP} \approx T^2_{DP} \tag{14}$$

These approximations resulted in

$$(\Delta H_v)_{P,x} = \frac{RT_{BP}T_{DP}}{(T_{DP}-T_{BP})} \sum z_i \ln \frac{K_{i_{DP}}}{K_{i_{BP}}} + \sum z_i \Delta H^\circ_i \tag{15}$$

This equation was programmed on the IBM 1620 computer to carry out the calculations given in Chapter VI.

Edmister-Persyn-Erbar Method

Edmister, Persyn and Erbar (11, 12) have developed a computer

program for calculating consistent K-values, saturated liquid and vapor enthalpies, and partial enthalpies of multicomponent hydrocarbon mixtures. They combined the works of Redlich and Kwong (30), API Research Project 44 (2), Chao and Seader (6), Grayson and Streed (13), and Pitzer, et al. (23), with their own correction factors to produce the final program. The pertinent details of the method are presented in Appendix I. The calculations in Chapter VI were carried out on an IBM 1401 computer using a program supplied by the authors (12).

Yen-Alexander Method

Yen and Alexander (49) have developed mathematical expressions for the generalized enthalpy correction charts of Lydersen, Greenkorn and Hougen (24). The equations are primarily for computer application. Those equations which were programmed for the IBM 1620 computer to calculate the isobaric integral heats of vaporization of methane-ethylene mixtures are given in Appendix I.

Isothermal Integral Heat of Vaporization

The isothermal integral heat of vaporization can be calculated by the method of Bahlke and Kay (3). Their derivation was essentially as follows:

The combined form of the First and Second Laws of Thermodynamics

$$dH = TdS + VdP \tag{16}$$

is differentiated with respect to V at constant T to give

$$\left(\frac{dH}{dV}\right)_{T,x} = T\left(\frac{dS}{dV}\right)_{T,x} + V\left(\frac{dP}{dV}\right)_{T,x}$$

$$= T\left(\frac{dP}{dT}\right)_{V,x} + V\left(\frac{dP}{dV}\right)_{T,x} \tag{17}$$

Integrating

$$(\Delta H_v)_{T,x} = T \int_{V^L}^{V^V} \left(\frac{dP}{dT}\right)_V dV + \int_{P_{BP}}^{P_{DP}} VdP \qquad (18)$$

The values of the integrals are determined graphically from PVT data on the system in question. Here again, this limits the utility of their method, although it is thermodynamically rigorous.

Consistency Tests

Thermodynamic consistency tests are derived from basic equations to compare two types of experimental data. Isobaric consistency tests usually compare enthalpy data with fugacities and/or vapor-liquid equilibria (VLE) data. The experimental apparatus used in this investigation was designed to collect enthalpy and VLE data simultaneously for use in isobaric consistency tests.

Until recently, the consistency equations of Adler, et al. (1), provided the best approach to experimental thermodynamic consistency tests because they used observables rather than derived or calculated quantities. Their derivation assumed that the vapor obeyed the Lewis and Randall rule (22). Since deviations from this rule are more significant at high pressures, the results of applying their equations to the high pressure data of this work would be questionable.

Thompson and Edmister (45) made a rigorous derivation of similar equations which do not assume that the Lewis and Randall rule applies. Their derivation is given in Appendix J. Their test was carried out on these data. Results are discussed in Chapter VI.

Recently, Edmister (10) developed a new consistency test as derived

below.

Isobaric Case

From Dodge (8)

$$d \ln f = \frac{\bar{H}^\circ - \bar{H}}{RT^2} dT \tag{19}$$

Writing Equation 19 for each component in the liquid and vapor phases

$$x_1 \, d \ln \bar{f}_1^L + x_2 \, d \ln \bar{f}_2^L = \frac{\bar{H}^\circ - \bar{H}^L}{RT^2} dT \tag{20a}$$

and

$$y_1 \, d \ln \bar{f}_1^V + y_2 \, d \ln \bar{f}_2^V = \frac{\bar{H}^\circ - \bar{H}^V}{RT^2} dT \tag{20b}$$

Replacing x_2 by $1-x_1$, y_2 by $1-y_1$, and since at equilibrium

$$d \ln \bar{f}_i^V = d \ln \bar{f}_i^L \tag{21}$$

$$(y_1 - x_1)(d \ln \bar{f}_1^V - d \ln \bar{f}_2^V) = \frac{\bar{H}^L - \bar{H}^V}{RT^2} dT \tag{22}$$

or

$$(y_1 - x_1)\left(\frac{d \ln \frac{\bar{f}_1^V}{\bar{f}_2^V}}{dT}\right) = \frac{\bar{H}^L - \bar{H}^V}{RT^2} \tag{23}$$

From the definition of fugacity coefficient

$$\phi_i = \frac{\bar{f}_i^V}{Py_i} \tag{24}$$

$$\ln \bar{f}_i^V = \ln \phi_i + \ln P + \ln y_i \tag{25}$$

and

$$\ln \frac{\bar{f}_1^V}{\bar{f}_2^V} = \ln \frac{\phi_1}{\phi_2} + \ln \frac{y_1}{y_2} \tag{26}$$

Substituting Equation 26 into Equation 23

$$(y_1-x_1)\left(\frac{d \ln \frac{\phi_1}{\phi_2}}{dT} + \frac{d \ln \frac{y_1}{y_2}}{dT}\right) = \frac{\underline{H}^L-\underline{H}^V}{RT^2} \tag{27}$$

which is the isobaric consistency test in differential form. In integral form

$$\int_{T_1}^{T_2} (y_1-x_1)\, d \ln \frac{\phi_1}{\phi_2} + \int_{T_1}^{T_2} (y_1-x_1)\, d \ln \frac{y_1}{y_2} = \int_{T_1}^{T_2} \frac{\underline{H}^L-\underline{H}^V}{RT^2}\, dT \tag{28}$$

By using integration by parts, the same analytical functions required for Equation 27 can be used in Equation 28.

Isothermal Case

For constant temperature conditions

$$d \ln f = \frac{\underline{V}}{RT}\, dP \tag{29}$$

Following the same scheme used in the isobaric case

$$(y_1-x_1)(d \ln \bar{f}_1^V - d \ln \bar{f}_2^V) = \frac{\underline{V}^V-\underline{V}^L}{RT}\, dP \tag{30}$$

which is analogous to Equation 22. The resulting isothermal test in differential form is

$$(y_1-x_1)\left(\frac{d \ln \frac{\phi_1}{\phi_2}}{dP} + \frac{d \ln \frac{y_1}{y_2}}{dP}\right) = \frac{\underline{V}^V-\underline{V}^L}{RT} \tag{31}$$

In integral form

$$\int_{P_1}^{P_2} (y_1-x_1)\, d \ln \frac{\phi_1}{\phi_2} + \int_{P_1}^{P_2} (y_1-x_1)\, d \ln \frac{y_1}{y_2} = \int_{P_1}^{P_2} \frac{V^V - V^L}{RT}\, dP \qquad (32)$$

The differential form of the consistency test (Equations 27 and 31) is evaluated point by point. As such it is much more sensitive than the integral test, which averages the experimental results over the range under investigation.

The logarithm of the fugacity coefficient ratio is easily determined from the Redlich-Kwong (30) equation of state by

$$\ln \frac{\phi_1}{\phi_2} = (Z-1) \frac{B_1-B_2}{B} - \frac{A^2}{B}\left(2 \frac{A_1-A_2}{A} - \frac{B_1-B_2}{B}\right) \ln\left(1 + \frac{BP}{Z}\right) \qquad (33)$$

(The value of Z must be determined by successive approximations of the original R-K (30) equation in Z form.) These ratios are tabulated in Table F-I. From this table it is obvious that the calculated value of $\ln \phi_1/\phi_2$ is of secondary importance compared to the observed value of $\ln y_1/y_2$.

The isobaric thermodynamic consistency tests were carried out in differential and integral form as given by Equations 27 and 28. Values of each term are tabulated in Appendix F. Results are discussed in Chapter VI.

The Thompson-Edmister (45) test was modified to put it in a form which could be integrated by parts. These modifications are presented in Appendix J. Results of the test are presented and discussed in Chapter VI.

CHAPTER III

PRIOR INVESTIGATIONS

The first experimental determination of the isobaric integral heat of vaporization was made by Dana (7) in 1925. Subsequent experiments, all since early 1950, have utilized the principal feature of the Dana calorimeter. In his own words, "The principal feature of the calorimeter consists of the thermal isolation of a small volume of the liquid by means of a glass bulb, surrounded by a vacuum jacket, communicating with a large volume of the liquid through a capillary tube." In addition to this feature, other investigators have incorporated their own modifications for their particular experiments. The calorimeter used in this investigation, discussed in Chapter IV, is the first to be adapted for high pressure experiments. Some of the important features and modifications of previous investigators will be discussed here.

Dana (7) investigated the oxygen-nitrogen system at atmospheric pressure ($\approx$ -310° F). A schematic diagram of his calorimeter is shown in Figure 4. The liquid in the bulb was vaporized by the immersion heater. Steady state operation of the calorimeter required the same amount of material to leave the system, through the outlet at the top, that entered it, via the capillary at the bottom of the bulb if there were no losses or accumulation. Thus, the composition of the exit

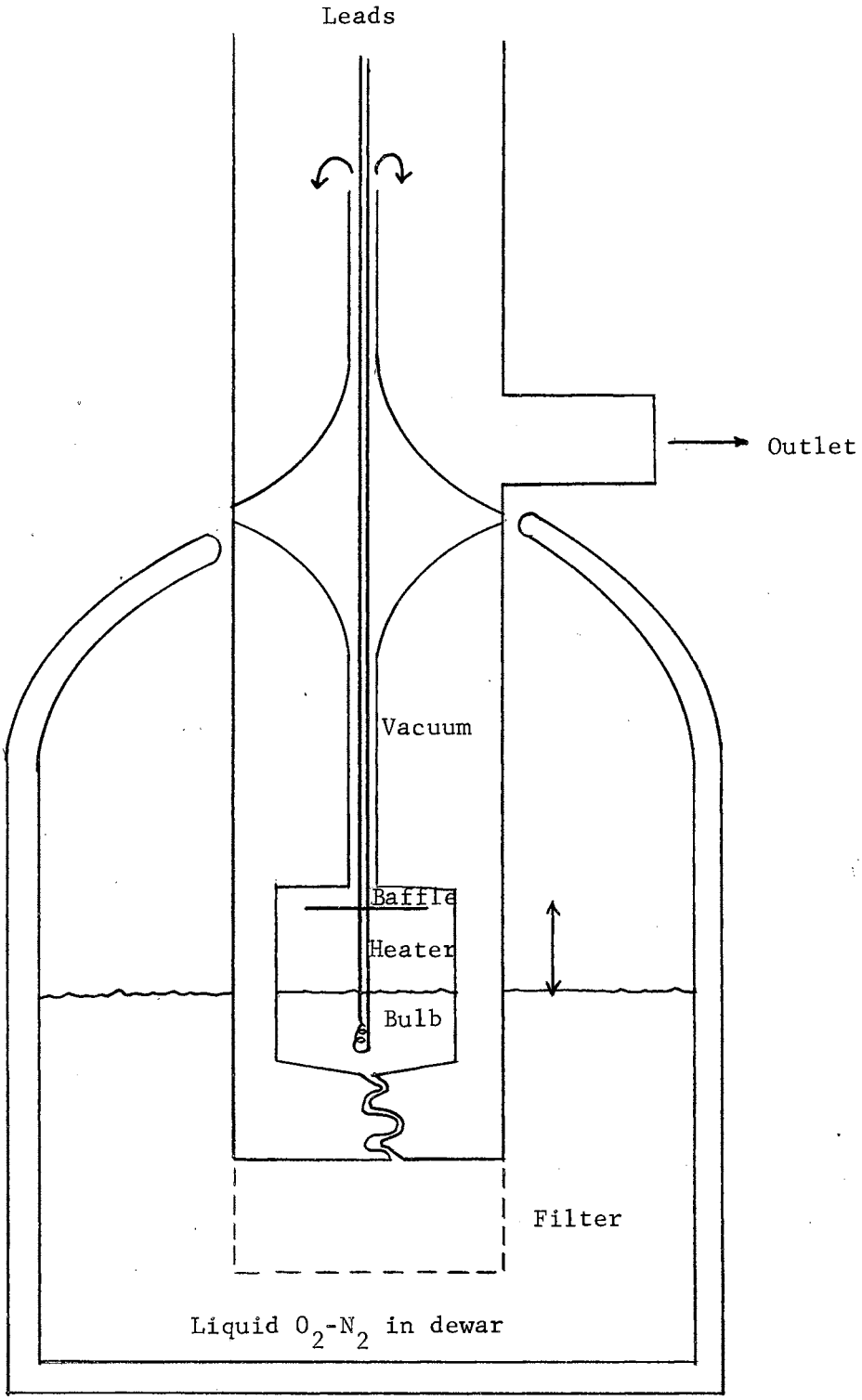

Figure 4

Original Dana Calorimeter

Source: Dana (7)

stream was the same as that of the mixture in the flask. This required the bulb composition to be that of a liquid in equilibrium with a vapor whose composition was that of the condensate or flask liquid.

The heat of vaporization was determined from the electrical energy supplied to the heater. As vaporization proceeded, the bulb was lowered slowly into the large volume of liquid to maintain a constant liquid level in the bulb. Dana stated his precision as 0.2 per cent.

Schroeder (35, 42) modified the Dana calorimeter to operate above room temperature. He substituted an ordinary flask for the dewar used by Dana, and placed it in an electric heating mantle. The methanol-benzene mixtures flowed from the flask through a small capillary tube to a vacuum jacketed, silvered glass bulb where they were vaporized by an immersion heater. The vapors rose through a glass column to a condenser; the condensate was collected in a receiver. Schroeder assumed that heat was lost from the bulb to the flask by conduction and convection. He calculated the heat transfer coefficient across the bulb and calibrated the apparatus for the radiation and convection losses. A sensible heat correction was made for the difference between the flask temperature and the mixture bubble point temperature. He estimated his precision at 1 per cent and calculated his average deviation to be 1.2 per cent.

Tallmadge (40, 41, 42) modified Schroeder's apparatus by replacing the electric mantle with an oil bath. A non-silvered, vacuum-jacketed bulb was used. A resistance heater was placed around the top of the glass column just below the rubber stopper which sealed it. This

heater prevented reflux in the column and was calibrated to eliminate the heat loss up the column. Experiments conducted on pure components indicated that the uncorrected latent heat of vaporization minus the sensible heat correction was a linear function of the temperature difference between the bulb and the flask. The uncorrected latent heat was measured at two values of bulb-flask ΔT, while holding immersion and top heater input constant. The sensible heat correction was applied and the results plotted against ΔT. A straight line was extrapolated from the two points to zero ΔT. The measurements were repeated using a different immersion heater input, corrections applied, and results plotted again. If the zero intercept was the same for both lines, it was assumed that the top heater wattage was correct. If they were not the same, the top heater wattage was changed and the calibration repeated.

The calibration procedure was repeated for each pure component, each of which had a different bubble point. The correct top heater wattage was plotted against the temperature difference between the bubble point and room temperature. This curve was linear and was used to determine the correct top heater wattage for any bubble point in the calibrated range.

Tallmadge then calculated a heat transfer coefficient for the bulb, from which he made another correction to the observed latent heat of pures and mixtures minus the sensible heat correction. The average deviation of pure acetone, benzene, methanol, and chloroform latent heats was 0.09 per cent. The average deviation of the isobaric integral heats of vaporization of acetone-chloroform, acetone-benzene, and benzene-methanol mixtures was 0.07 per cent.

Tallmadge sampled the bulb mixture at the end of each run by removing the bulb from the flask and draining it into a receiver. The composition was determined by refractive index.

Schnelle (33, 34) made extensive revisions to the Tallmadge apparatus. All rubber stoppers were replaced by ground-glass joints. A hypodermic needle sampling tube was inserted through the top of the glass column into the bulb so that mixtures could be sampled without removing the bulb from the flask. A thermocouple well was also added in the top of the column, and the immersion heater leads were sealed into the top. Pressure taps were added to the flask and condenser to elevate the pressure to 760 mm Hg, which was controlled by a Cartesian manostat. The laboratory was air conditioned to minimize daily fluctuations. He calibrated the calorimeter and applied corrections in the same manner as Tallmadge. His cumulative error on the acetone-chloroform system was calculated to be 0.1 per cent.

During the initial phases of this high pressure investigation, some work was carried out at atmospheric pressure on an improved version of Schnelle's apparatus. New features added to the glass calorimeter included a bubble cap above the heater bulb for improved vapor-liquid contact, a stirrer in the main flask, additional hypodermic sampling probes, and more thermocouple wells for obtaining a temperature profile across the entire calorimeter. Kumar (21) used this apparatus.

Concurrent with the work of Schroeder and Tallmadge, Plewes, et al. (26, 27, 28) were working on their own version of the Dana calorimeter for conducting experiments at 300 and 760 mm Hg. Vapor-liquid equilibria data were not obtained simultaneously in the calorimeter but taken from the literature. The immersion heater was encap-

sulated for studying corrosive mixtures. Data were obtained on water binaries on methanol, ethanol, n-propanol, acetone, and formic acid.

Plewes and co-workers did not discuss the heat leak problem, although their apparatus contained heat leaks similar to those of Tallmadge. The magnitude of the radiation heat loss from the bulb was reduced by silvering. In the initial experiments (26), the power input was measured with only moderate precision, which probably masked the heat loss effects caused by a 15° ΔT. The precision of power input measurement was increased in the later experiments (27, 28), but the systems studied produced only a 3° ΔT, for which heat loss corrections were neglected.

Stein and Martin (37) made a glass, adiabatic flow Dana calorimeter which had a unique modification to eliminate heat leak. Instead of immersing the vacuum-jacketed bulb in the bubble point mixture, they placed it in a large volume of the dew point mixture, which underwent vaporization simultaneously with the liquid in the bulb. With the liquids inside and outside the bulb at the dew point temperature, there was no temperature difference across the vacuum-jacketed bulb, and consequently no heat leak. The bubble point liquid was in a thermostatically controlled vessel adjacent to the calorimeter. They collected data on the water binaries of i-propanol and acetone. They calculated their combined enthalpy error to be $\pm$ 0.3 per cent and their composition error to be $\pm$ 0.1 mole per cent.

In summary, all of the previous investigators have used glass Dana calorimeters at atmospheric pressure or below. All studies except that by Dana were above ambient temperature. The present investigation

was made in a stainless steel calorimeter at 20 and 40 atmospheres absolute and low temperatures (166° K or -161° F).

CHAPTER IV

EXPERIMENTAL APPARATUS

The design requirements of a calorimeter-equilibrium cell for the simultaneous determination of the isobaric integral heat of vaporization and vapor-liquid equilibria data will be considered first, followed by a detailed description of each component of the calorimeter, overall schematic flow diagram, and electrical circuitry.

Design Requirements

General Considerations

Inasmuch as the temperatures and pressures encountered in two-phase equilibrium hydrocarbon mixtures cover a wide range, it was decided to design and construct a calorimeter specifically for handling the lighter systems, such as the methane binaries of ethane and ethylene. This required a low-temperature capability of about 150° K (-190° F) and a pressure capability well in excess of 1000 psi. A level of 2000 psi was arbitrarily selected, which would cover most possibilities. A safety factor of 4 was used on all high pressure designs.

The general configuration required was that of a distillation set-up, i.e., charge reservoir and reboiler, vapor-liquid contactor and condenser.

It was also required that the design be such that the calorimeter could be disassembled to make revisions or locate leaks.

Specific Requirements

Three different constant-temperature zones were required for steady-state operation of the isobaric integral heat of vaporization calorimeter: one for the reservoir containing the charge at the bubble point, one for the equilibrium still at the dew point, and one for the condenser at a temperature sufficiently below the bubble point to condense completely the dew point vapor, which should have the same composition as the original bubble point liquid. Each zone was complete with stirrer, heater, heat sink, vacuum jacket, temperature indicator and sensor, and controller.

A vaporizing bulb was necessary to isolate the mixture to be vaporized (dew point liquid) from the bulk of the charge (bubble point liquid) in the reservoir. This zone contained the heater and was connected to the reservoir in such a way that bubble point liquid was free to flow into the zone to replenish vaporized mixture. This bulb will be called the "reboiler tube."

Because the reservoir was maintained at the bubble point temperature, there was a strong tendency for vapors to be produced and accumulate in the reservoir. This accumulation would expel a like volume of liquid into the reboiler tube and condenser. Therefore, a refluxing arrangement was provided to condense any vapors that might form.

The vapor-liquid contactor provided an arrangement for thorough contacting of vapor and liquid. A bubble cap was selected for this purpose. Inasmuch as any inventory change on the tray would affect the

results, a liquid level sensor was provided. This part of the calorimeter will be called the "equilibrium cell."

Sampling lines were provided for withdrawing samples of the bubble point vapor in the reservoir, the dew point liquid in the reboiler and on the tray, and the dew point vapor between the reboiler and tray. The bubble point liquid was sampled when the reservoir vapor sample line was flooded, and the dew point vapor was sampled from the external condenser sample bomb.

The external condenser was provided as a means of collecting a sample during a timed run. It consisted of a sample bomb connected in parallel with the calorimeter condenser.

Various experimental quantities had to be measured, including the pressure in the calorimeter, the energy dissipated in the heater, the vacuum in the jackets and transfer lines, and the thermocouple emf's.

Construction Details

The details of construction of each component of the calorimeter are shown in Figures 5 through 11. Actual photographs appear in Plates I through VII. Details are discussed below.

Reservoir Constant-Temperature Zone

The reservoir constant-temperature zone, shown in Figure 5 and Plate I was made by nesting two Type 302, deep-drawn, stainless steel beakers, and silver soldering the outer lip of the smaller, 6-1/4 in. I.D., beaker to the inner edge of the larger, 7-1/4 in. I.D., beaker. Three 1/4 in. NPT and four 1/8 in. NPT stainless steel collars were silver soldered between the inner and outer walls to accept Conax pack-

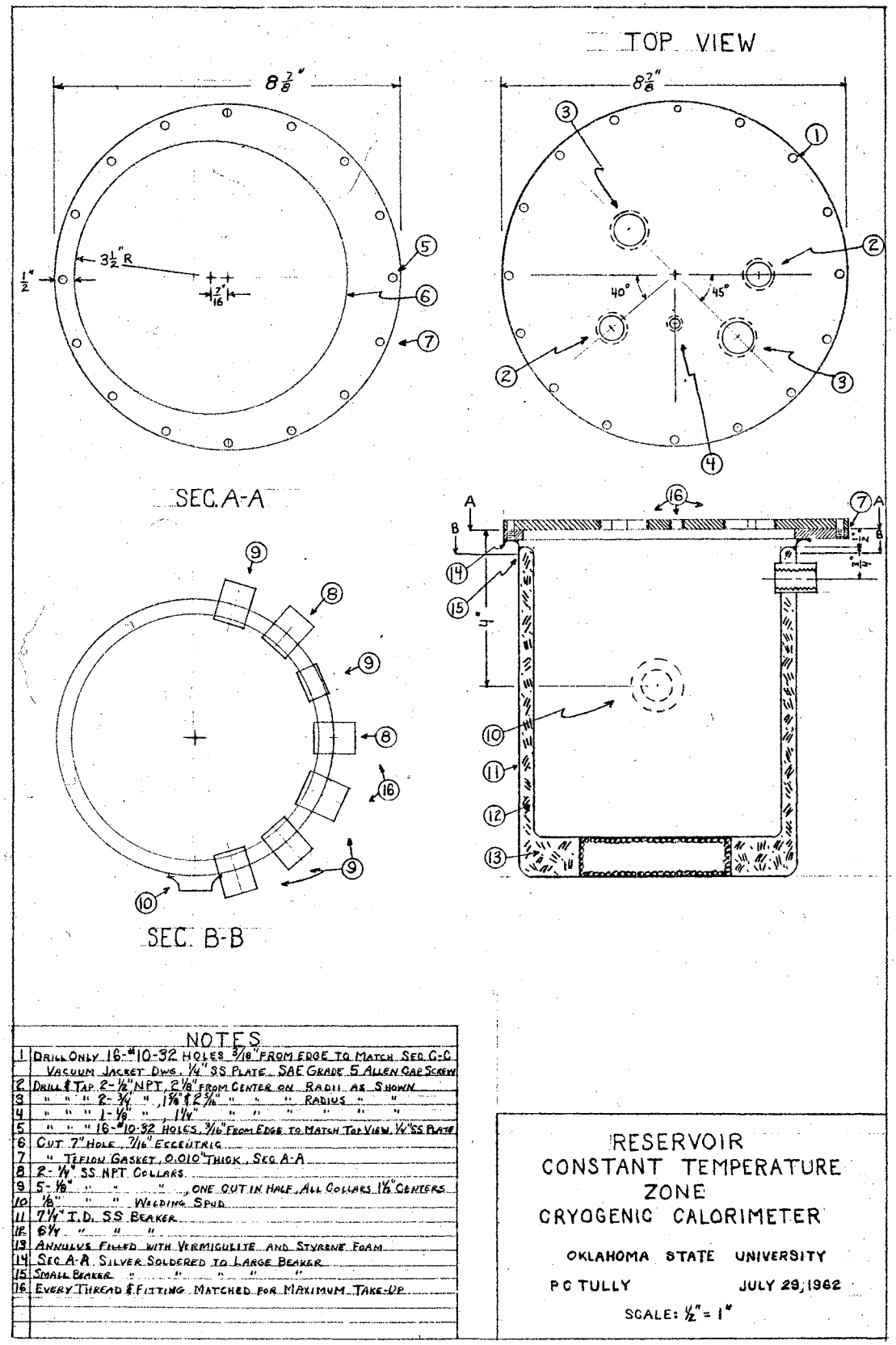

Figure 5

Reservoir Constant Temperature Zone

Plate I.

Reservoir Constant Temperature Zone

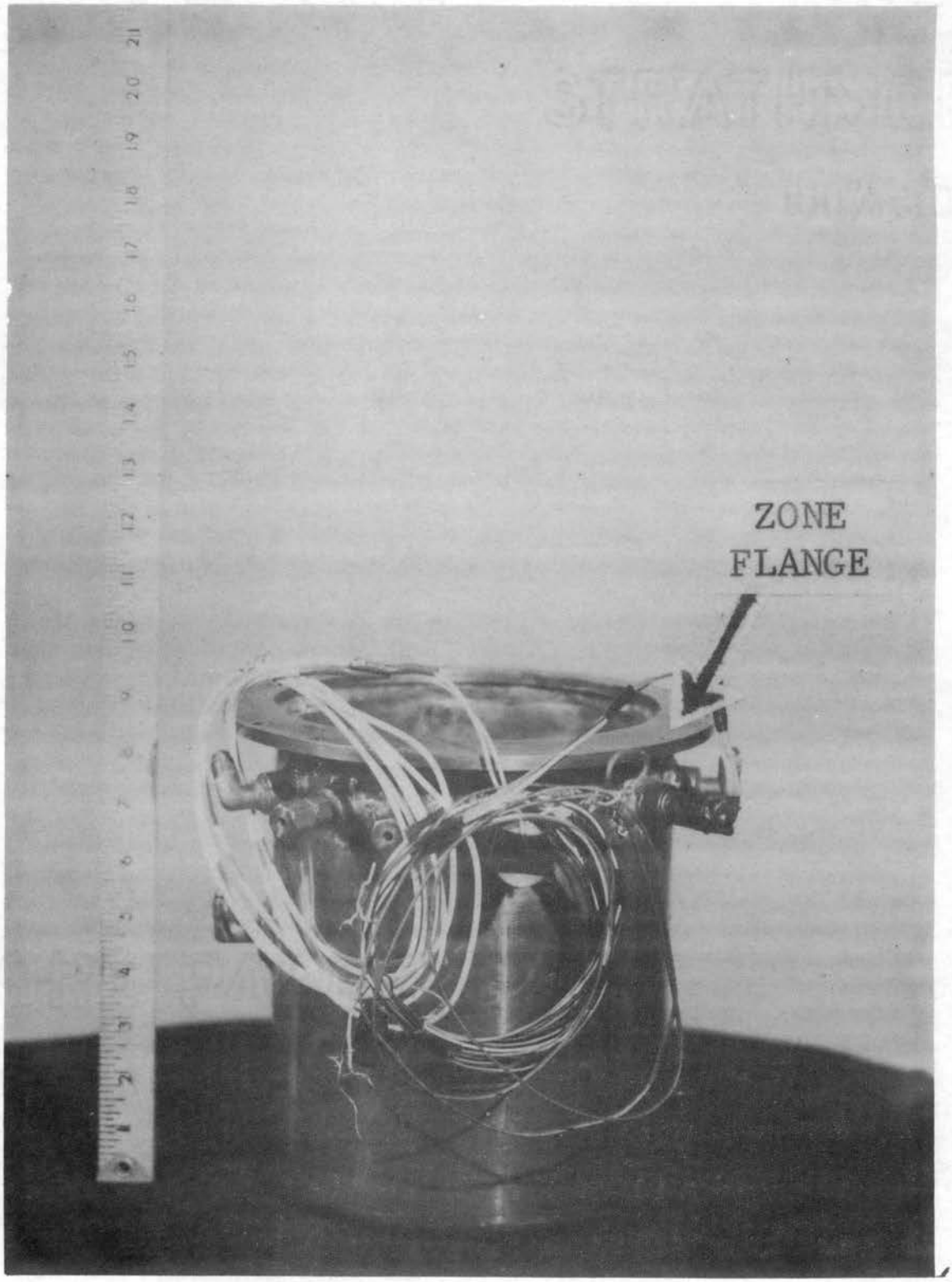

ing glands and flared copper tubing fittings for connecting thermocouples, heater leads, a thermostatic fluid transfer line, and a nitrogen blow-down and vent line. A 1/8 in. stainless steel welding spud was silver soldered in the outer beaker to attach the vacuum line. The annular space was filled with expanded mica to reduce radiation heat transfer. The zone flange, shown in Plate I, was silver soldered to the lip of the outer beaker for joining the two major portions of the calorimeter.

Three midget thermocouple glands, Conax MTG-20-A2, were used to bring three copper-constantan pairs through the zone walls for the reservoir, zone, and condensate thermocouples. These thermocouples were well tempered by making two circlesaround the inside of the zone before the bi-metallic junction was made. One MTG-20-A4 was used to bring the four leads to the Rosemount Engineering Model 104 platinum resistance sensor mounted inside the zone. These leads were also well tempered.

Two immersion heaters were installed inside the zone to provide the necessary heat source for temperature control. One 300-watt heater was connected in series with a variable 12-ohm ballast resistor to the Hallikainen Thermotrol unit for that zone. The external ballast resistor permitted adjustment of the controller heat input to suit operating conditions without disassembling the calorimeter. One 275-watt booster heater was connected directly to the 110-volt AC supply via a single pole-single throw (SPST) switch to raise the zone temperature rapidly. The four heater leads were brought through the zone walls by a Conax TG-14-A4 packing gland. Virtually all of the Conax glands were equipped

with natural magnesium silicate, or "lava," sealants to withstand cryogenic temperatures.

Reservoir

The reservoir, shown in Figure 6 and Plates II and III, was made from a 4-5/8 in. piece of IPS Schedule 80, Type 304, stainless steel pipe. The bottom closure was a 1 inch thick disc of Type 304 stainless steel, threaded and back-welded in place. The top closure was made by a 7/8 in. x 5-1/2 in. O.D. blind flange, using an O-ring and groove for sealing. The O-ring was a Teflon coated, stainless steel tube, Advanced Products #4000-3-3-TCV. Three holes were drilled and tapped in the blind flange for the reboiler and stirrer Conax glands, and the reflux street ell. The bolting ring was threaded to the body of the reservoir and back welded at the proper index. Eight 5/16 in. Allen cap screws were used to tighten the blind flange. The three connections in the blind flange and the condenser-return street ell in the reservoir body were back-soldered inside and outside to reduce the possibility of leakage. A 1/4 in. NPT stainless steel union with a 0.002-inch copper gasket inserted in the seat was used to connect the condenser return to the street ell.

One Conax MTG-20-A2 copper-constantan thermocouple gland was inserted through the wall of the reservoir to measure the bubble-point liquid temperature. This thermocouple was tempered by passing one coil around the inside of the reservoir. Another MTG-20-A2 was inserted in a tee in the condenser return line to measure the temperature of the condensate.

The reservoir stirring shaft was fabricated from 5/16 in. centerless ground, Type 303, stainless steel shafting. The impeller was made

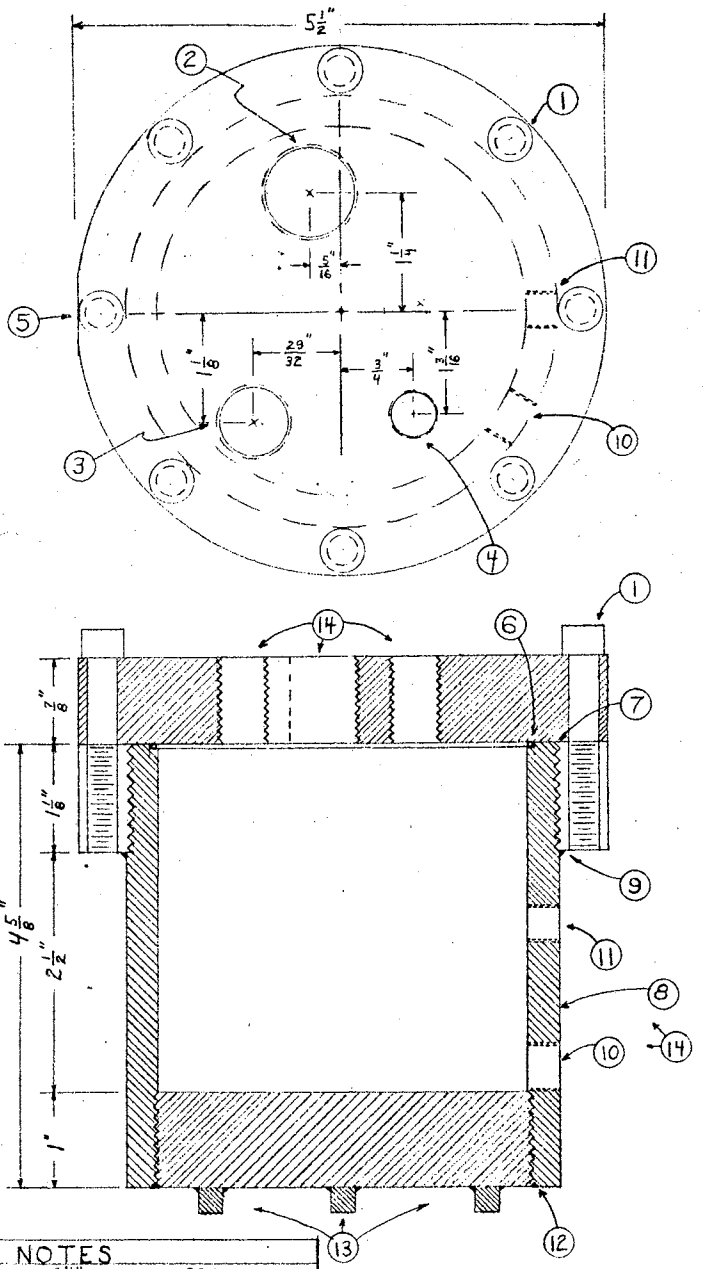

NOTES

1	8-5/16 Allen Cap Screws on 2½" Radius, Type 304 Stainless
2	Drill & Tap ¾" NPT as Shown
3	" " ½" " " "
4	" " ¼" " " "
5	Flat to Bolt Head
6	4000-3-3-TQV Advanced Products Stainless Teflon Coated "O" Ring in Groove .042"-.047" Deep, 3.850" Max. I.D. by 4.007"-4.012" O.D., Finest Emery Surface on Three Sides
7	4½" x 16 Thread
8	4" IPS Sch. 80 Type 304 S.S. Pipe
9	Silver Solder After Trial Assembly in C.T. Zone
10	Drill & Tap ¼" NPT 1¼" Up from Bottom
11	" " ⅛" " 2¾" " " " 30° from ⑩
12	3.9" x 16 Thread, Back Soldered
13	4-¼" Cubes on 1½" Radius, Silver Soldered to Plug
14	Every Thread & Fitting Matched for Maximum Take-Up

RESERVOIR
CRYOGENIC CALORIMETER

OKLAHOMA STATE UNIVERSITY

PC TULLY AUG 15, 1962

FULL SCALE

Figure 6

Reservoir

Plate II.

Reservoir, Reboiler Tube, and Condenser

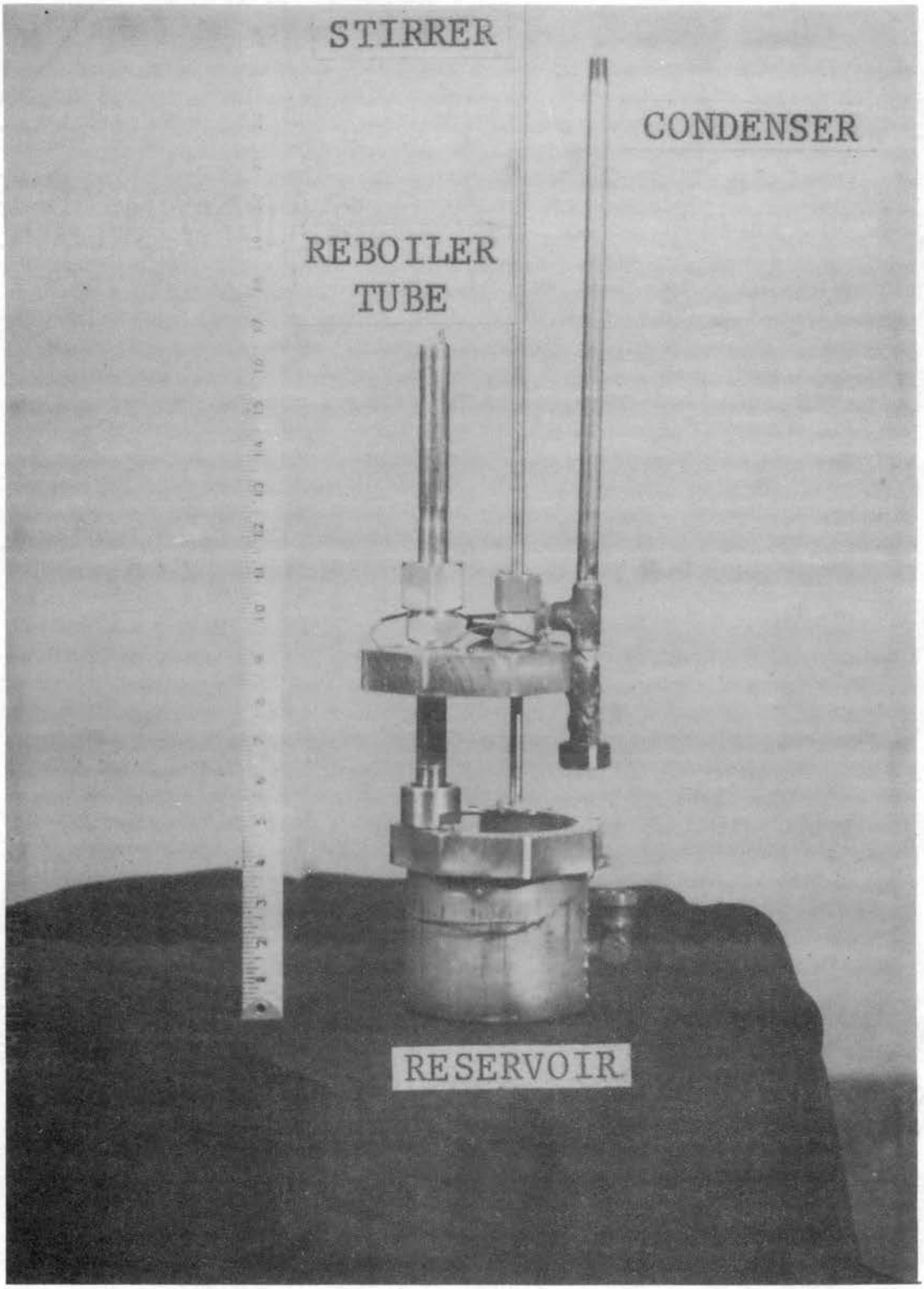

Plate III.

High Pressure Components, Exposed View

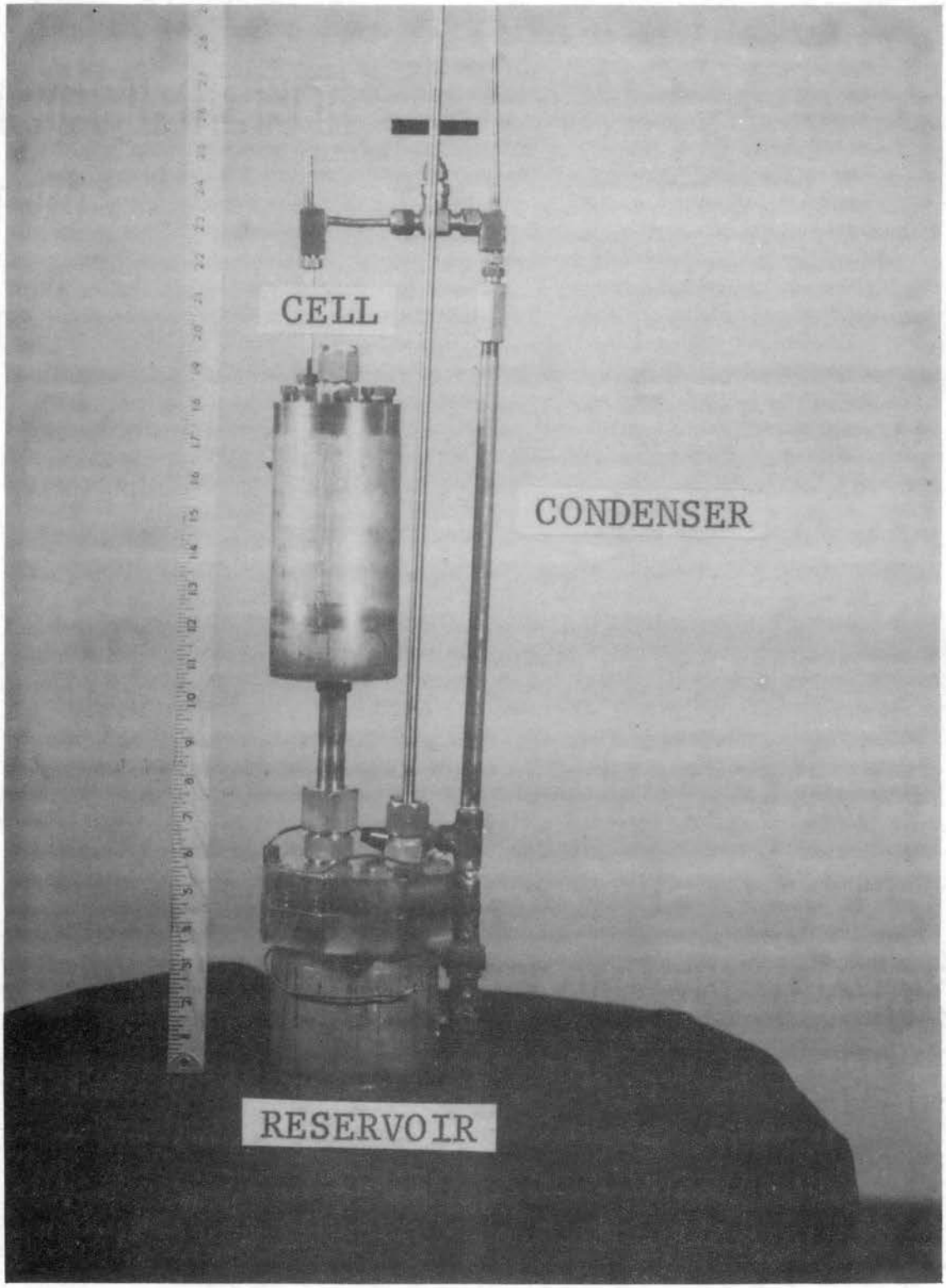

from a 1 inch disc of 22-gauge stainless steel sheeting, and had four vanes.

The reflux street ell was drilled and tapped for a 1/8 in. NPT Conax packing gland, MPG-2, 1/16 in. bore. This was for the reservoir vapor sample line, 1/16 in. O.D. by 0.020 in. I.D.

Reboiler Tube

The reboiler tube, shown in Figure 11 and Plate II, was made from a 12 in. piece of heavy-wall steel aircraft tubing, 1/2 in. I.D. by 3/4 in. O.D. The top end was drilled and tapped 3/8 in. NPT for a plug to be used for reservoir pressure testing. The bottom end was equipped with a threaded collar and retaining nut to permit insertion of different sizes of stainless steel orifice plates for controlling flow of liquid into the reboiler.

The heater in the reboiler tube was an encapsulated type made from a piece of 1/4 in. copper tubing, which was turned down in a lathe to about 0.220 in. O.D. and drilled out to about 0.200 in. I.D. to reduce the wall thickness and resistance to heat transfer.

The bottom was closed by rolling the thin copper wall to the center and putting a dot of silver solder over the minute hole. Two small legs were attached to the bottom to prevent the capsule from seating itself against the reboiler orifice plate, which would stop the flow of liquid into the reboiler.

About 17 in. of 30-gauge Chromel A heating wire, donated by Hoskins Mfg. Co., was wound on a ceramic support and coated with Sauereisen cement. When the heating element was thoroughly dried, it was inserted into the copper capsule, which had been filled with fresh Sauereisen.

The leads were soldered to 18-gauge, silver-plated, Teflon-coated copper wire, and placed in ceramic to prevent flexural fatigue.

Condenser

The condenser, also shown in Figure 11 and Plates II and III, was made very simply from a short piece of 1/4 in., Schedule 40, Type 304 stainless steel pipe.

Plate III is a photograph showing an exposed view of the reservoir, reboiler tube, stirrer, and condenser.

Equilibrium Cell

The main body of the cell, detailed in Figure 7 and shown in Plate III, was constructed from a 7-1/2 in. piece of 3 in. IPS Schedule 80, Type 304 stainless steel pipe. The bottom closure was formed from a disc of Type 304 stainless steel, 7/8 in. thick, and was drilled and tapped 3/4 in. NPT for the PG-5, 3/4 in. bore, Conax packing gland that sealed the top of the reboiler tube to the equilibrium cell.

The bubble-cap tray, shown in the exploded view of cell, Plate IV, was located about midway in the cell to minimize entrainment from the reboiler and the bubble cap. The bubble cap itself was a standard 2 in., soft steel model donated by F. W. Glitch and Sons. A Delta-Sonics point liquid level sensor was mounted on the bubble cap to detect any decrease in tray liquid inventory during a run.

The top closure, also shown in Plate IV, was made by a 1/2 in. thick lens ring, Type 303 stainless steel, and was drilled and tapped for five Conax packing glands, which permitted insertion of three sample lines, four mineral-insulated, copper-constantan Conax thermocouples 1/16 in. O.D., and two heater leads, plus the 1/4 in. by 1/8 in.

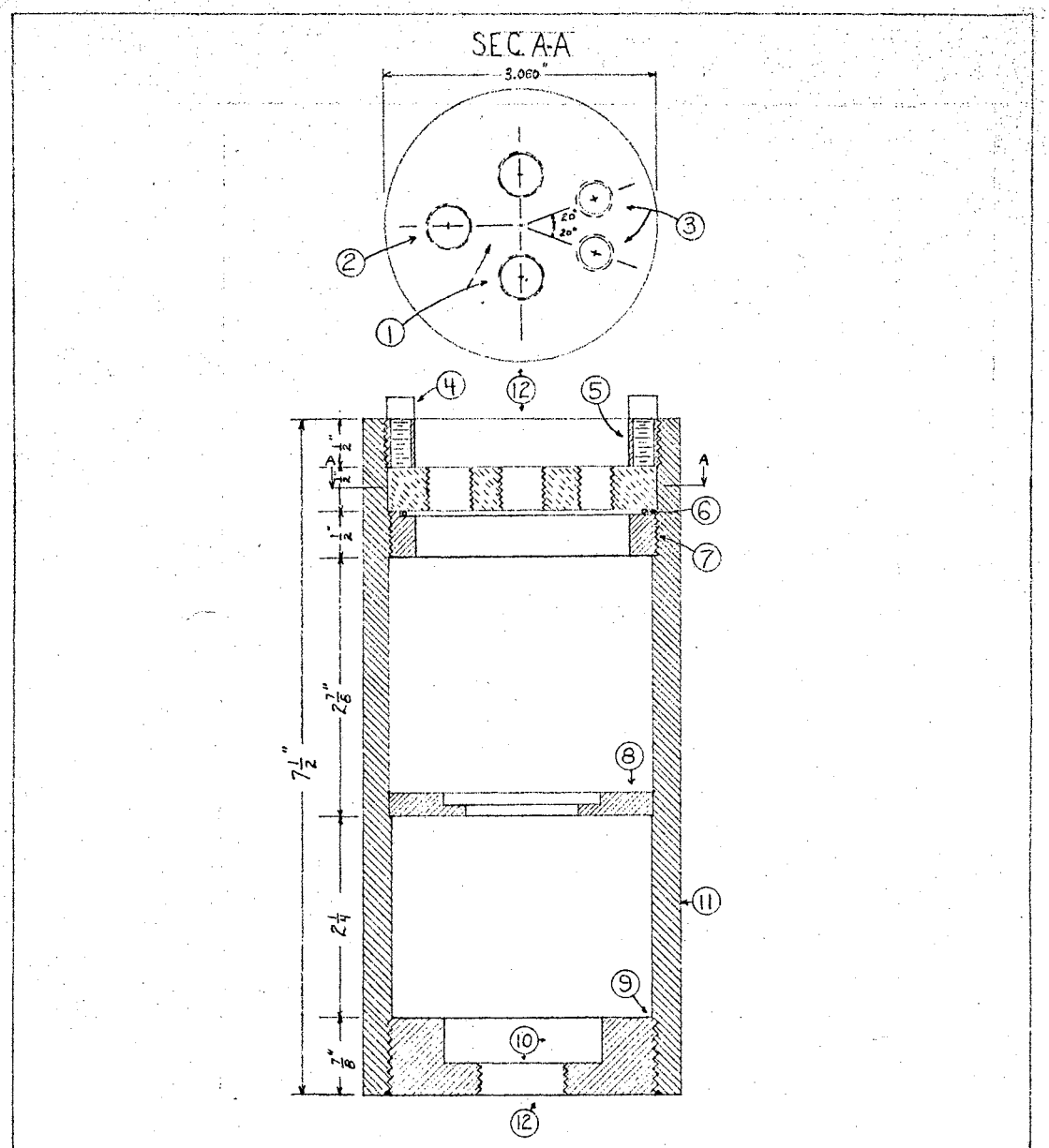

NOTES

1	Drill & Tap 2-1/4 NPT 9/16" From Center on Radius as Shown. Type 303 SS
2	" " 1-1/4" " 13/16" " " " " " "
3	" " 2-1/8" " 7/8" " " " Radii " "
4	" " 8-1/4" Allen Cap Screws. SAE Grade 5 on 1.4" Radius
5	Bolt Ring 2.375" I.D. by 3.2" x 16 Thread O.D. Type 303 Stainless
6	Teflon Coated SS "O" Ring Advanced Products #2750-3-3-TGV in Groove 0.042"-0.047" Deep by 2.757"-2.762" O.D. Finest Finish
7	Gasket Ring 2.375" I.D. by 3.06 x 16 Thread O.D. Type 303 SS
8	Tray 2.930" O.D. With 1/8" Hole. Countersink 1/8" Deep by 1 3/4" O.D. Spring Retainer. Liquid Tight Fit. 1/4" SS Plate. Type 304
9	3.030" x 16 Thread. Back Soldered. Type 303 Stainless Steel
10	Drill & Tap 3/4" NPT. Countersink 1/2" Deep by 1 3/4" O.D. Thread Matched With Bottom of Equilibrium Constant Temperature Zone
11	3" IPS Sch. 80 Pipe Type 304 Stainless
12	Every Thread & Fitting Matched for Maximum Take-Up

EQUILIBRIUM STILL
CRYOGENIC CALORIMETER

OKLAHOMA STATE UNIVERSITY

P C TULLY AUG 17, 1962

FULL SCALE

Figure 7

Equilibrium Still

Plate IV.

Equilibrium Cell, Exploded View

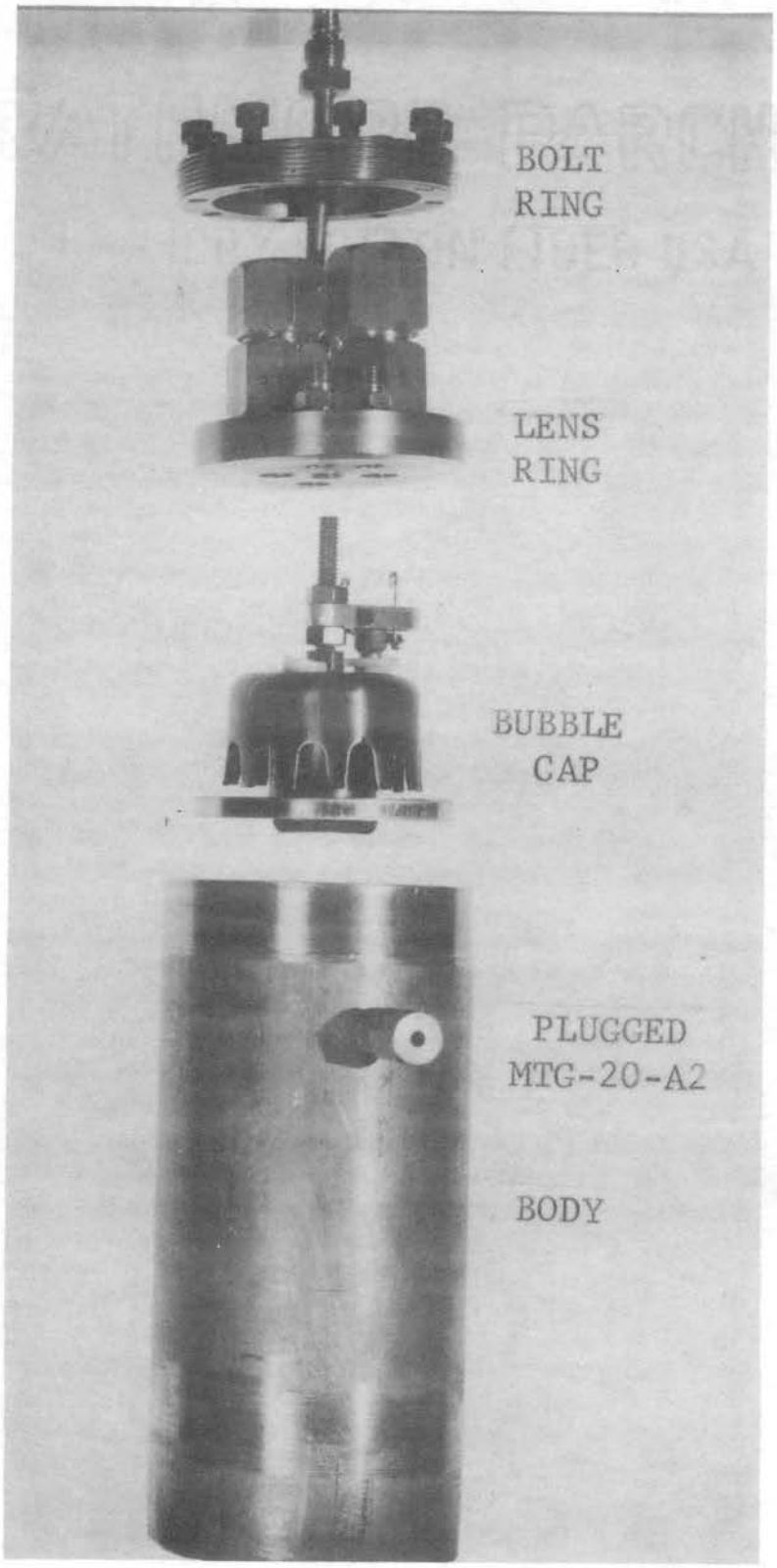

stainless steel tubing which formed the cell overhead line to the condenser. All Conax fittings were back-soldered with soft solder. The lens ring seat was recessed from the inner wall of the cell so that the permanent distortion caused by sealing would not interfere with the removal of the bubble-cap tray. The lens ring was held in place by a threaded stainless steel bolt ring, shown in Plate IV, containing eight 1/4 in. Allen cap screws.

The side wall of the cell was drilled and tapped 1/8 in. NPT to accept a plugged Conax MTG-20-A2 packing gland, also shown in Plate IV, which prevented rotation of the cell body during assembly.

Plate III shows the three high-pressure components (reservoir, cell, and condenser) as they would appear assembled inside their respective constant-temperature zones. This exposed configuration is pictured to illustrate the recycling path of material flow. It is not intended as a guide to assembly of the calorimeter.

Equilibrium Cell Constant-Temperature Zone

The equilibrium cell constant-temperature zone is detailed in Figure 8. The inner wall of this zone was made from 22-gauge Type 302 stainless steel with a crimped and silver-soldered side seam. The irregular cross-sectional shape, shown in Plate VI, was necessary to accommodate two different constant-temperature zones inside one common circular vacuum jacket, shown in Figure 10 and Plates V and VI. The bottom, 1/4 in. stainless steel plate of the constant-temperature zone was silver-soldered in place, while the cover was bolted to the zone with #5-40 Allen cap screws. A 0.010-in. Teflon gasket sealed the cover to the zone, and a copper gasket was used to seal the cap screws

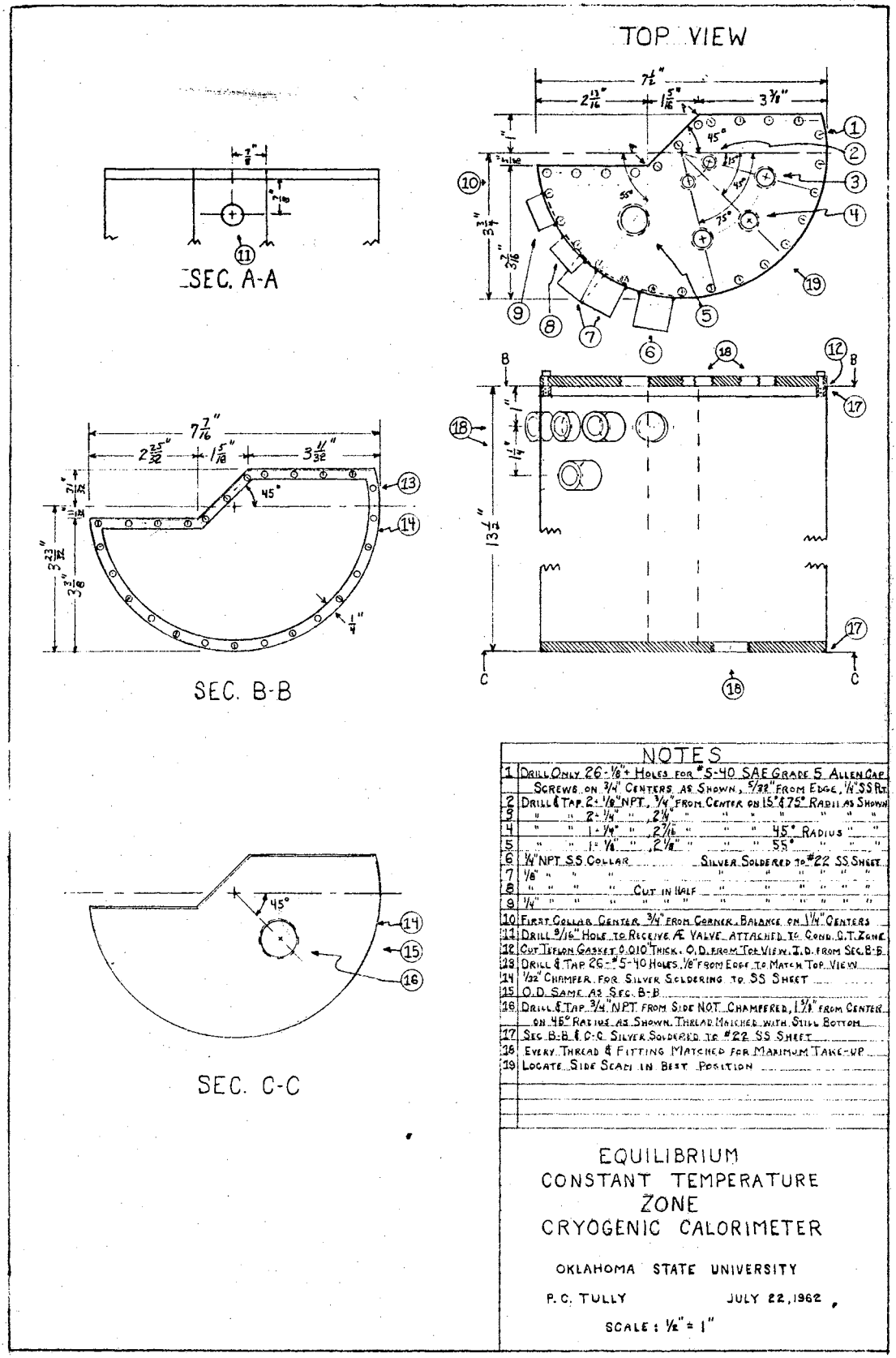

Figure 8

Equilibrium Constant Temperature Zone

Plate V.

Vacuum Jacket

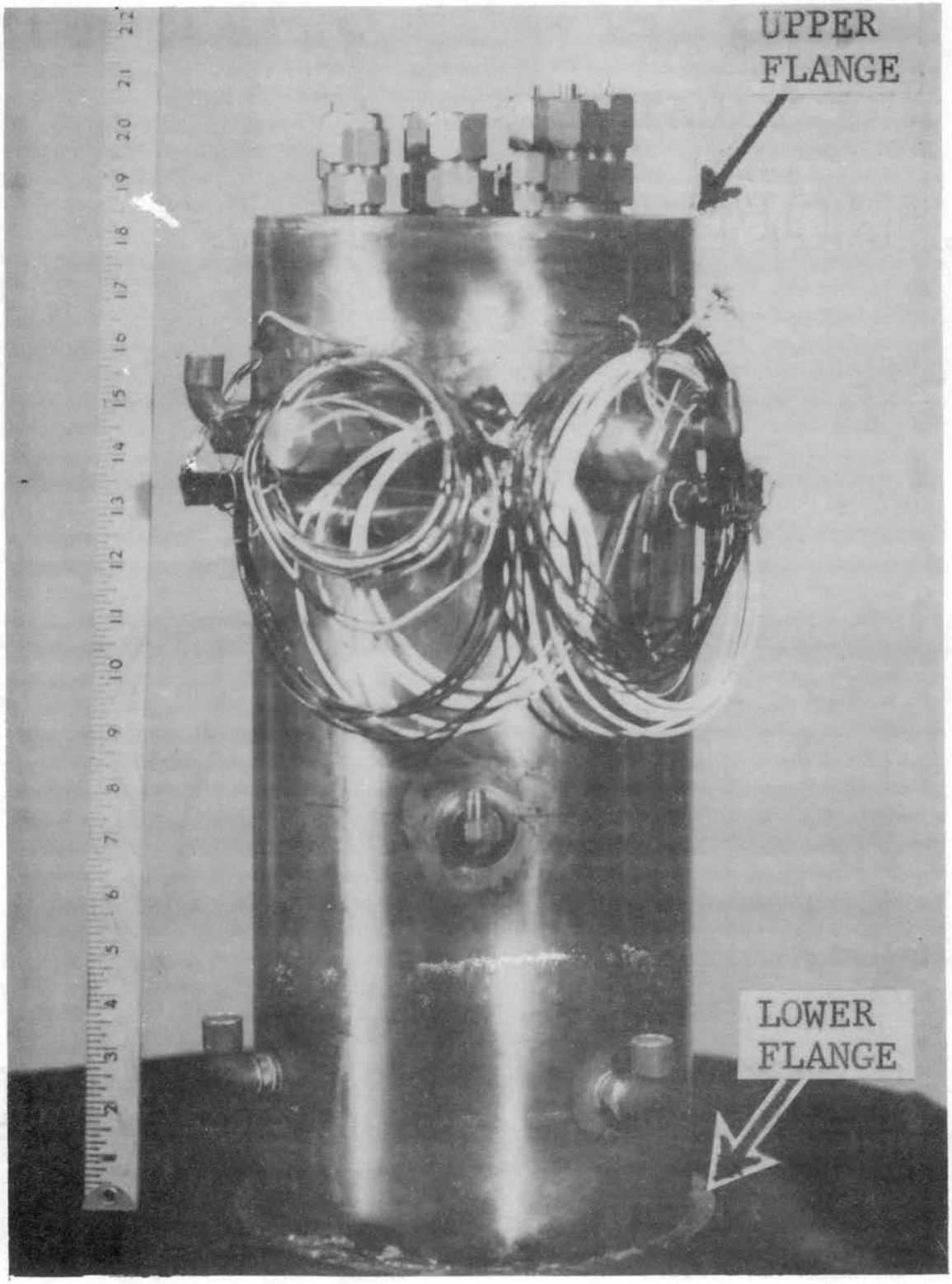

Plate VI.

Top View of Isobaric Heat of Vaporization Calorimeter

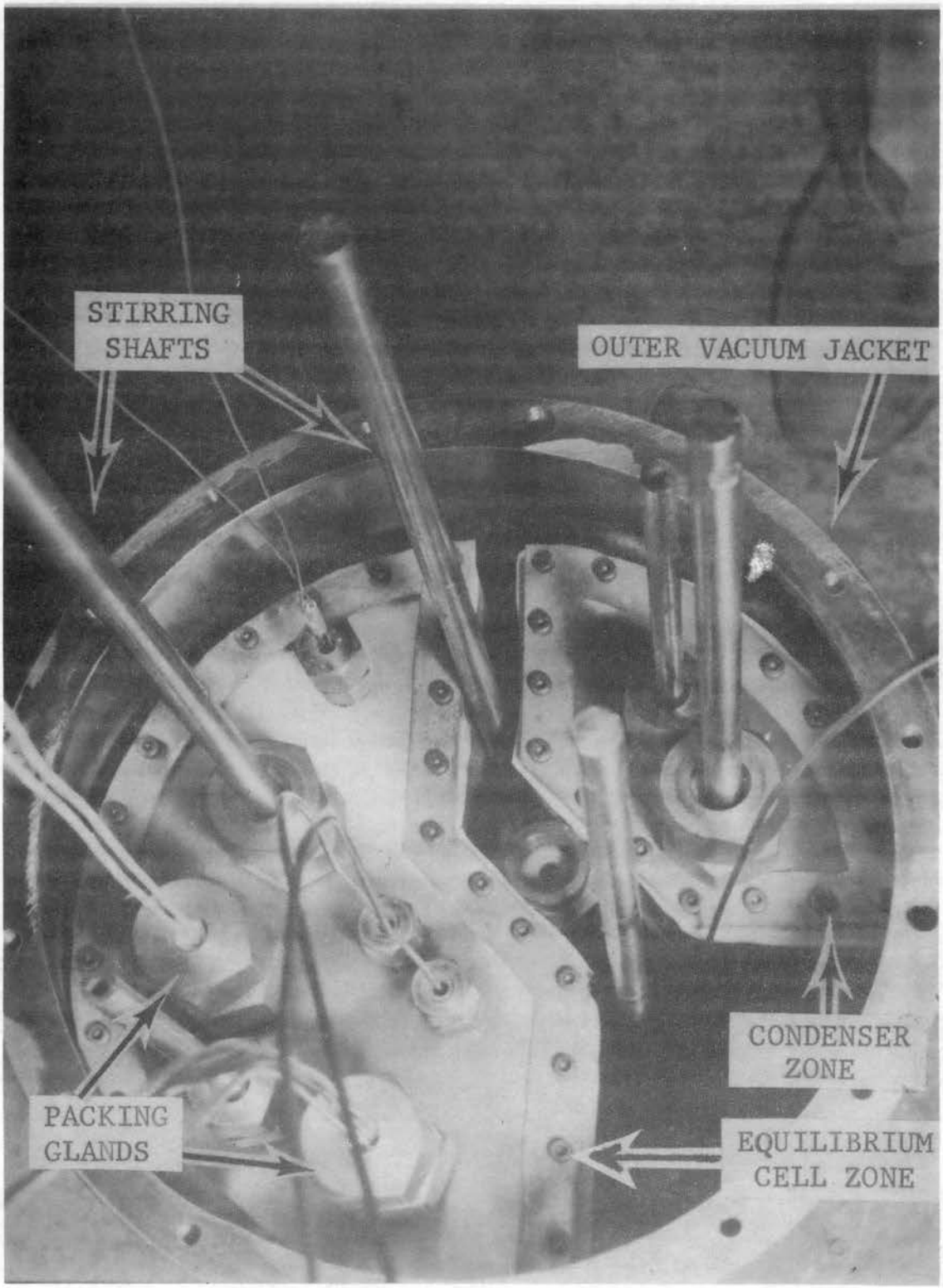

to the cover. Seven different holes were drilled and tapped in the cover for various Conax packing glands which brought out all of the equilibrium cell wire, thermocouples, etc., plus one for the stirring shaft, which was similar to the reservoir stirrer.

Seven different 1/4 in. and 1/8 in. NPT pipe collars were silver-soldered to the wall of this zone to accept the Conax fittings and other piping connections that were essential for zone operation. The thermostatic fluid was brought in as close to the bottom as possible, with a vent connection near the top. The zone thermocouple, sensor, and heater leads were well tempered inside the zone.

A 300-watt immersion heater was connected in series with an external, variable 100-ohm ballast resistor to the temperature controller. A 475-watt booster heater was provided in this zone for increasing set-point temperature rapidly.

Condenser Constant-Temperature Zone

This zone, detailed in Figure 9 and pictured in Plate VI, is quite similar to the equilibrium cell constant-temperature zone; only the major differences will be mentioned.

The cross-section was designed to utilize as much of the remaining interior as was necessary. This zone was not equipped with a booster heater like the other two zones, but only one oversized heater, about 800 watts, made of about 50 feet of high-temperature, asbestos-insulated, chromel thermocouple wire. However, the ballast resistor technique was utilized here as in the other zones. Inasmuch as the condenser duty was estimated to be quite high in this zone, a refrigerant coil of 1/4 in. copper tubing was provided for using liquid nitrogen or other suitable coolants. The equilibrium cell zone was joined to the condenser

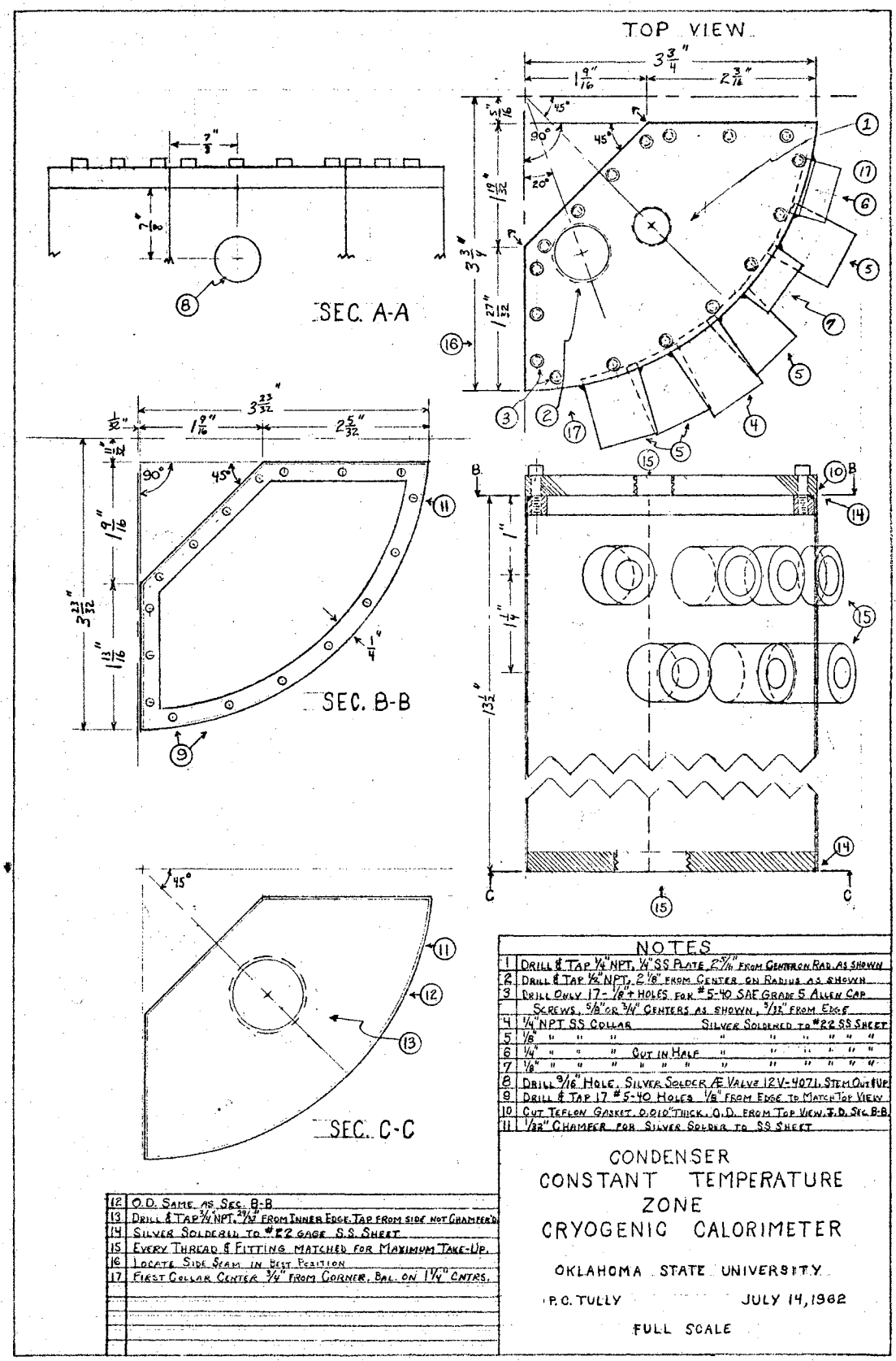

Figure 9

Condenser Constant Temperature Zone

zone by a high-pressure needle valve, shown in Figure 11 and Plate VI, which was used for switching flow from the internal condenser to the external condenser.

Vacuum Jacket

The equilibrium cell and condenser constant-temperature zones were surrounded by a common circular vacuum jacket, shown in Figure 10 and Plates V and VI, and rolled out of #22-gauge Type 302 stainless steel sheeting, through which all of the connections of the two inner zones were silver-soldered. The bottom of the zone was left open, and was fitted with a lower flange for 16 #10-32 Allen cap screws, which bolted the vacuum jacket to the reservoir constant-temperature zone cover. The top cover was sealed to the upper flange with Teflon and copper gaskets like the two inner zones, and was drilled and tapped for the numerous Conax packing glands required for stirrers, sample lines, thermocouples and lead wires. In addition to the 12 #10-32 cap screws which secured the top cover, provision was made for attaching four 1/4 in. all-threads, by which the entire calorimeter was suspended from a phenolic-impregnated plate. The vacuum connection was made via a 1/8 in. stainless steel welding spud which was silver-soldered in the wall of the jacket. Figure 11 is a cross-sectional view of the assembled calorimeter, a photograph of which appears in Plate VII.

Stirrer Drive and Suspension

The phenolic plate mentioned above was inserted in the suspension to block the direct flow of heat from the stirrer drive plate to the calorimeter. This plate was hung from a 1/4 in. aluminum plate by four 1/4 in. all-threads, each of which was inserted in a spacer tube.

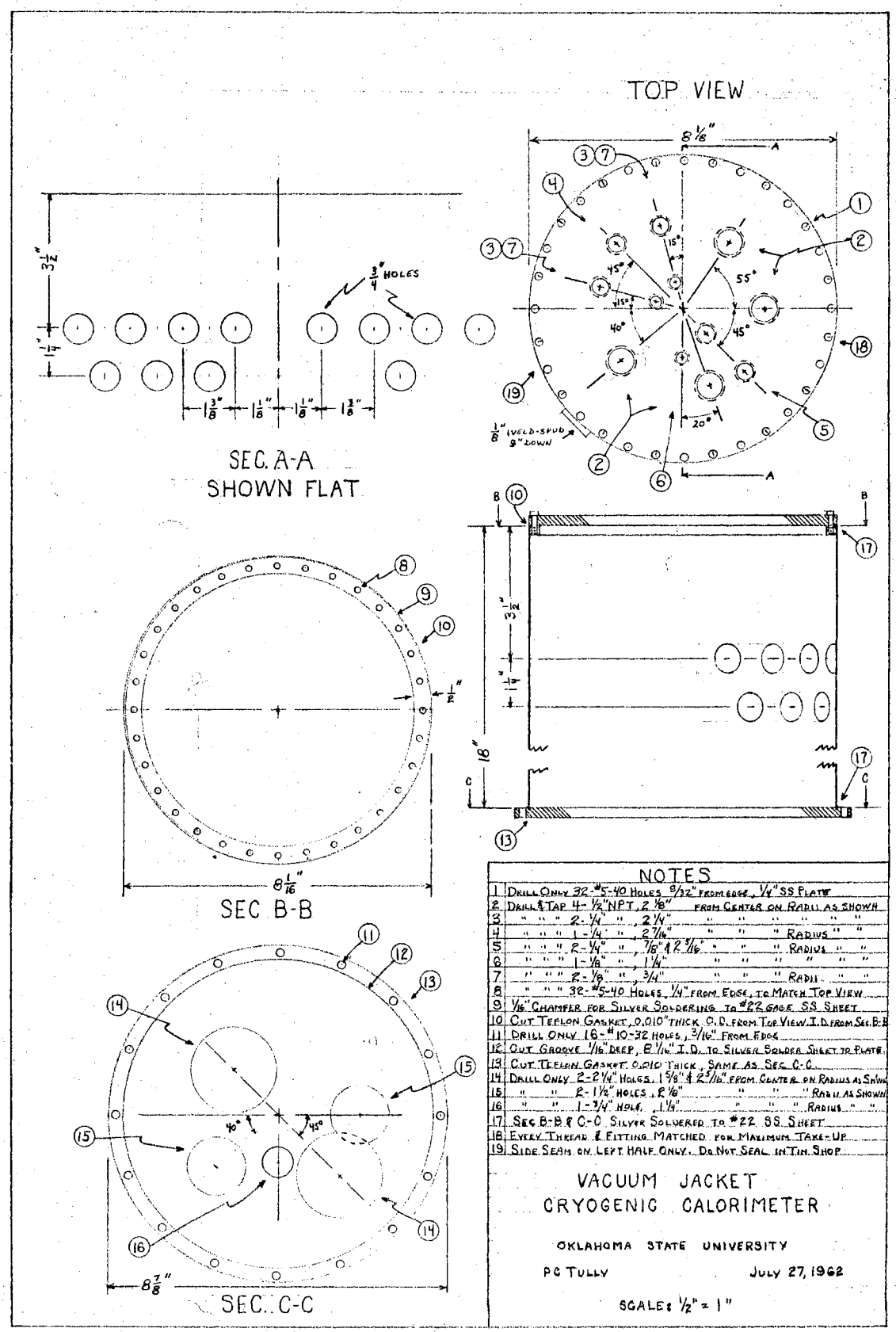

Figure 10

Vacuum Jacket

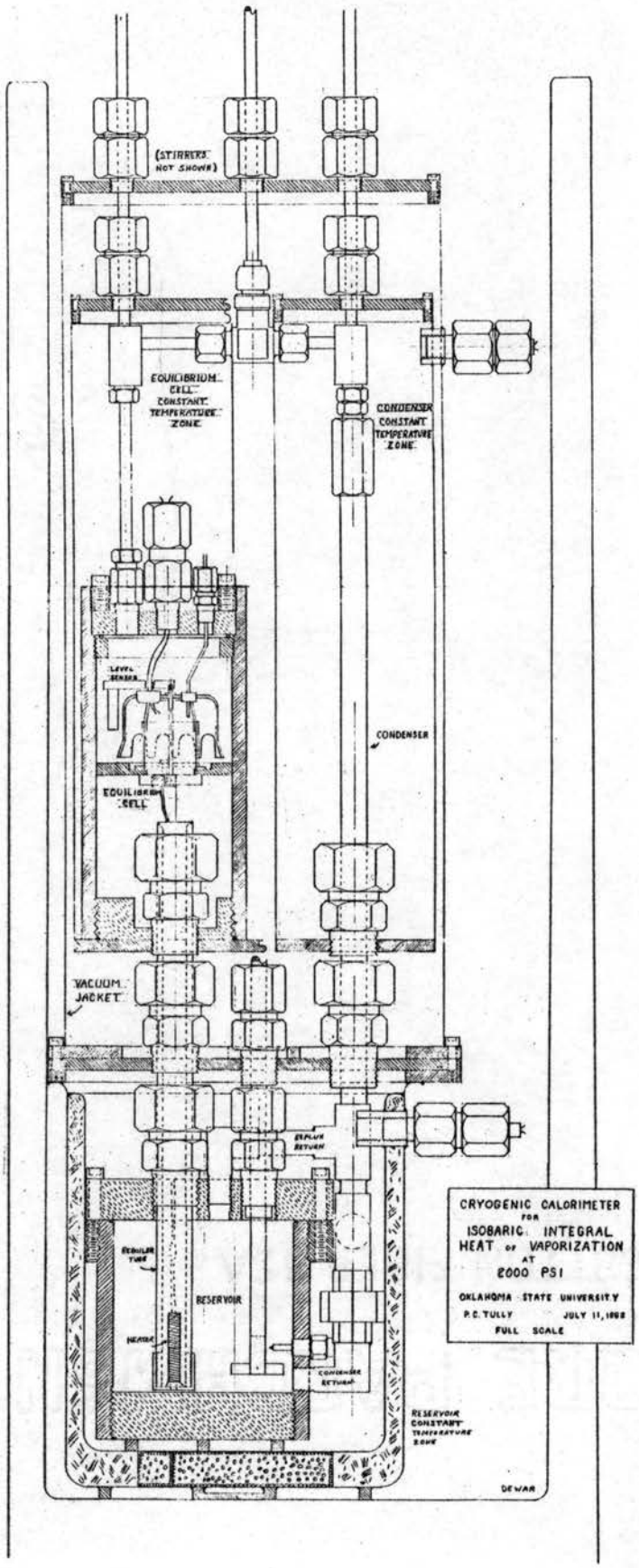

Figure 11

Calorimeter

Plate VII.

Assembled Calorimeter

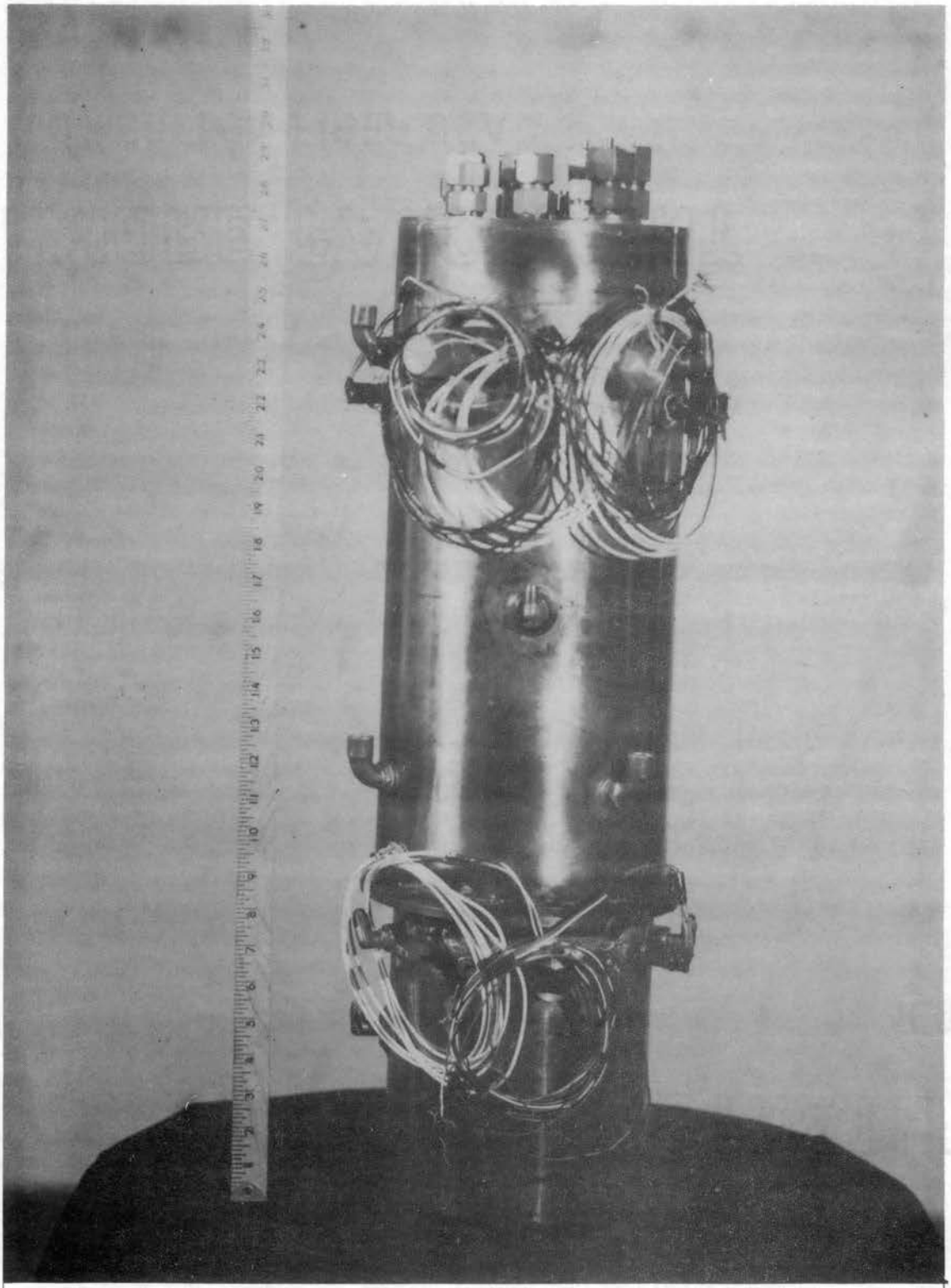

In the 1/4 in. aluminum plate were mounted four floating bearings for the four stirrer shafts. The drive gears were connected to each shaft and were driven by a small bull gear. The bull gear was powered by a 1/2 hp Boston Gear Co. 10-to-1 gearhead motor, which resulted in a shaft speed of about 225 rpm. The motor and gear plate were mounted on two cross members of double slotted angle, which were supported at their extremities by a seven foot tower made of heavy duty, punched angle iron. Vibrations were dampened by using mounting blocks of expanded polystyrene foam.

Flow Diagram

The schematic flow diagram of the apparatus for determination of the isobaric integral heat of vaporization is shown in Figure 12. (The sample lines for vapor-liquid equilibria data have been omitted for simplicity.) All high pressure piping consisted of 1/4 in. O.D. x 1/8 in. I.D. Type 316 stainless steel tubing using high pressure Ermeto elbows, tees, crosses, etc. Hydromatics Flo-bal valves with either Teflon or nylon seats and seals were used to direct the flow. Generally, vacuum piping was made of 5/8 in. O.D. x 1/2 in. I.D. hard-drawn copper tubing using soft-soldered (sweated) fittings. Vacuum valves were 1/2 in. brass Jamesbury HV and Hydromatics Flo-bal's. Thermostatic fluid transfer lines were usually 5/8 in. O.D. hard-drawn copper tubing also, insulated with 4 inches of polystyrene foam. Ohio Brass Co. 3/8 in. brass globe valves or 1/4 in. and 3/8 in. brass Hoke valves were used.

Briefly, the sequence of operations went as follows (a more detailed description will be given in Chapter V):

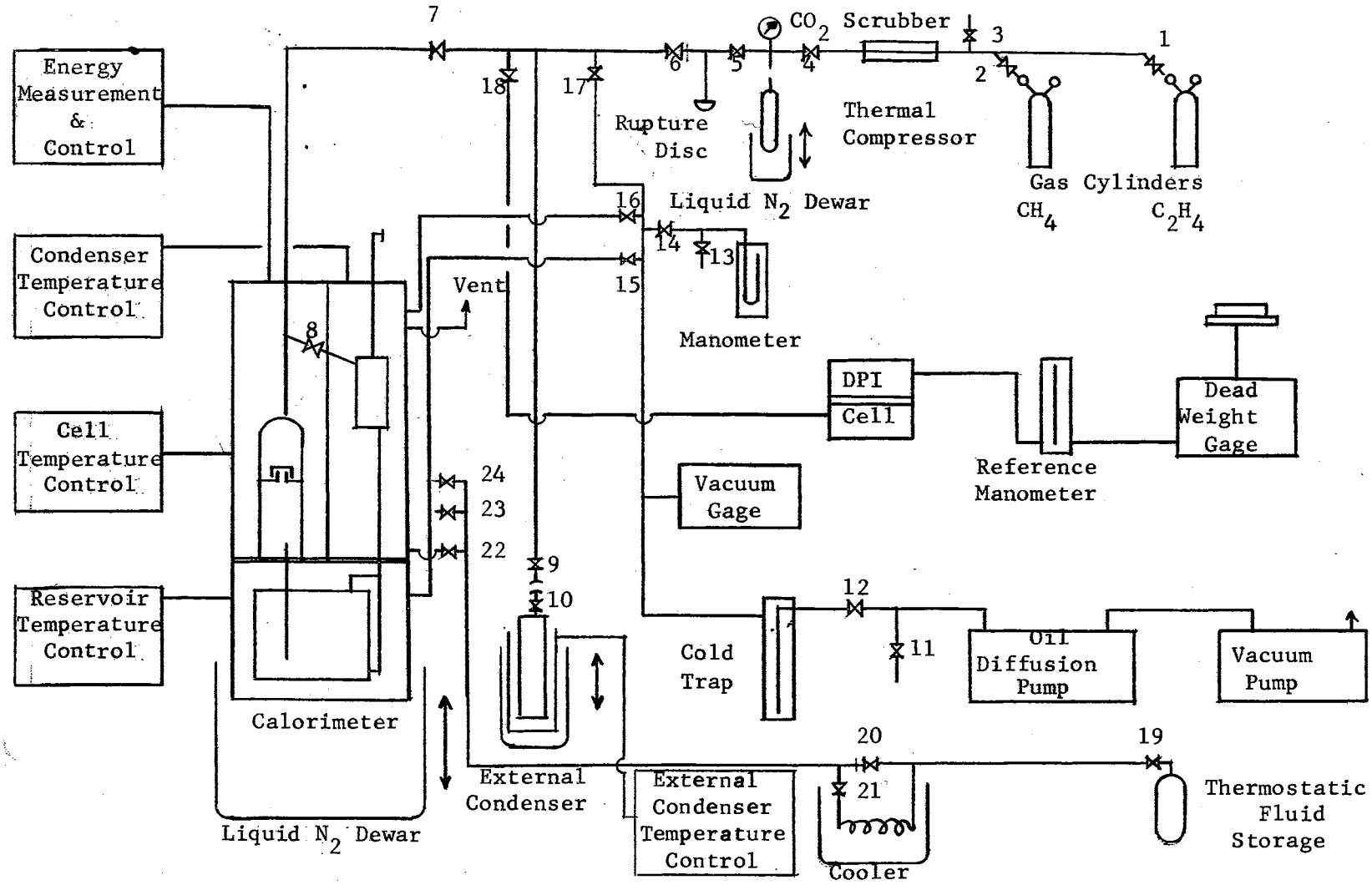

Figure 12

Schematic Flow Diagram of Apparatus for Isobaric Integral Heat of Vaporization

After all high pressure components had been thoroughly evacuated, a charge of gas was released from the storage cylinders and liquefied in a high pressure bomb, Marison ICC3AA4000, 4-1/2 in. O.D. x 15 in. long. After the liquefied charge had returned to ambient temperature, the calorimeter was cooled down and thermostatic fluid added to the three constant-temperature zones. (See Figure 13 for a detailed description of the thermostatic fluid system.) When the calorimeter was sufficiently cooled down, a weighed portion of the charge was condensed in the calorimeter reservoir. Hallikainen Thermotrols were adjusted to give the temperature necessary to produce the desired operating pressure. The heater was turned on, and after allowing an hour or so for establishing steady state, a sample was taken in the external condenser, an MGM No. 61E/AL, 500 ml., 3000 pound test aluminum bomb. Pressures were measured on the Budenburg Dead Weight Gauge Model No. 280L, certified for 0.05 per cent accuracy, as transmitted through the Ruska Differential Pressure Indicator (DPI) Cell. Thermocouple emf's and potential drops across the standard resistors were measured on the potentiometer, as described in detail in the following section.

Electrical Apparatus

The power for the heater, the heart of the calorimeter, was furnished by a Dressen-Barnes 17-22 volt, 1.5 amps DC power supply with 0.01 per cent regulation and one millivolt rms ripple. This precise unit was necessary to produce a very constant voltage throughout each run. Experience had shown that wet storage batteries were inadequate. A schematic circuit diagram is presented in Figure 14.

On-off control of the heater was achieved by a SPST switch, and approximate voltage and amperage were indicated on inexpensive meters.

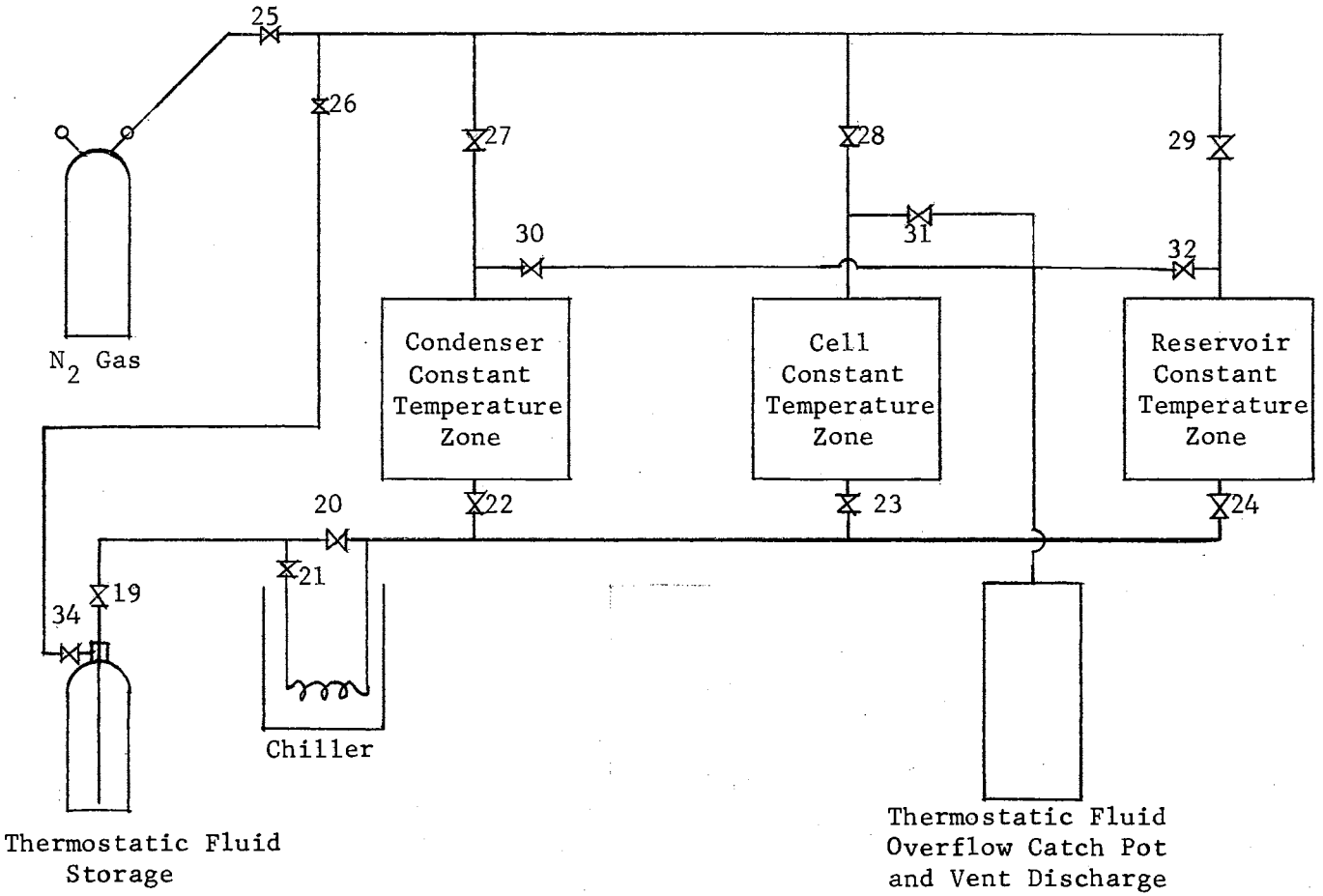

Figure 13

Schematic Diagram
Thermostatic Fluid, Nitrogen Blow-Down, and Vent Systems

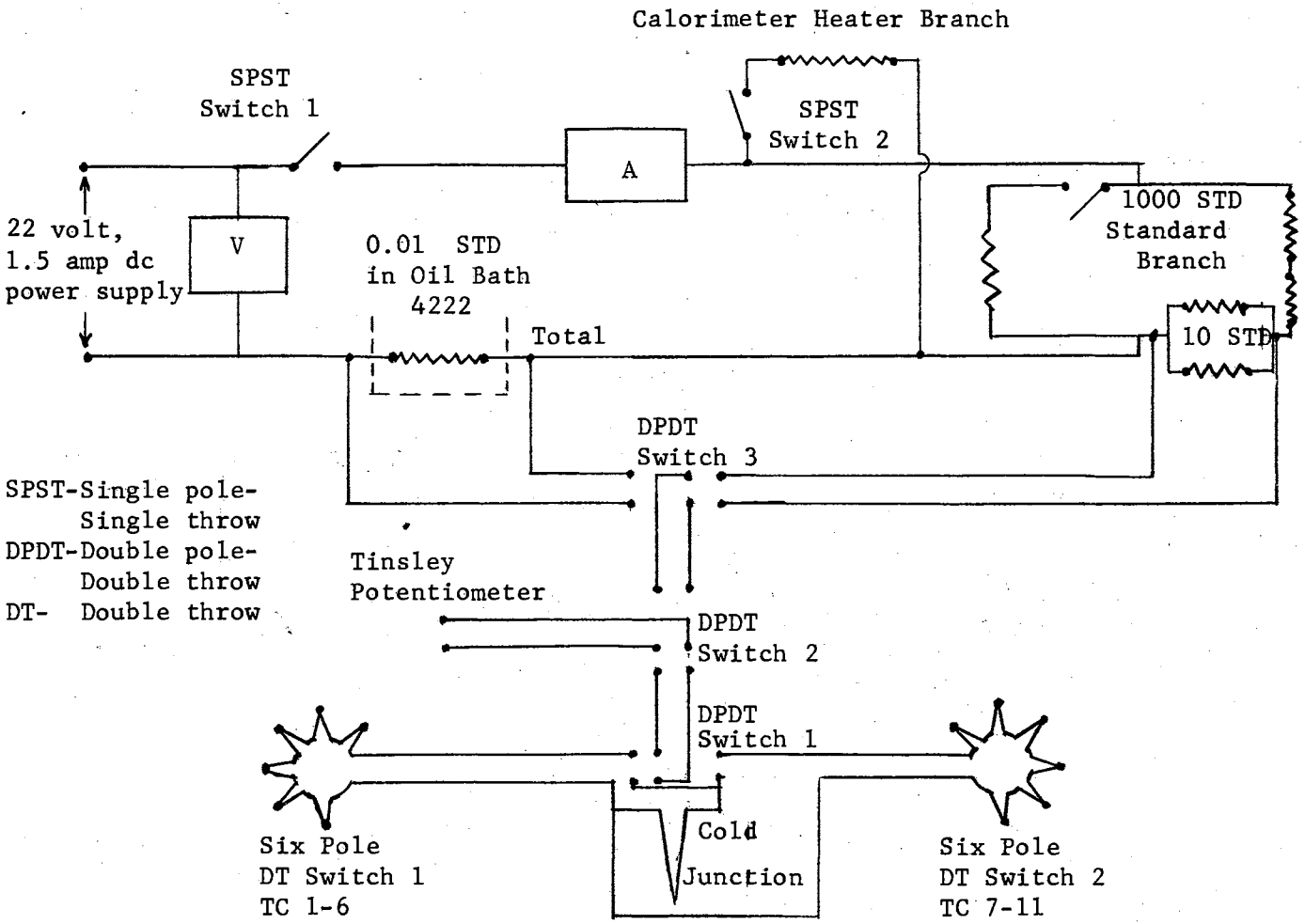

Figure 14

Schematic Diagram of Energy and Temperature Measuring Circuits

All of the current passed through an oil-cooled, 0.01 Ω standard resistor, Leeds and Northrup No. 4222. Measurement of the voltage drop across this resistor permitted calculation of the total current flowing. The circuit split into a series-parallel arrangement. Inasmuch as the resistance of the heater branch was about 15 ohms and the resistance of the standard branch was 2005 ohms, most of the current flowed through the heater. Measurement of potential drop across the two 10-ohm standard resistors, Leeds and Northrup No. 4025-B, wired in parallel (to produce an effective resistance of 5 ohms) permitted calculation of the small amount of current flowing in that branch. The difference between the total and standard branch currents was the current flowing in the heater branch. Sample calculations are presented in Appendix F.

All of the 20-gauge copper-constantan thermocouple junctions were purchased from Conax Corp. Two six-pole double throw switches were used in conjunction with a double pole-double throw (DPDT) switch as thermocouple selectors. A cold-junction crushed ice bath was placed in series with the potentiometer and each hot junction as the selector switches were rotated. Thermocouple locations are as follows: TC 1, charge in reservoir; TC 2, condensate; TC 3, reservoir constant-temperature zone; TC 4, reboiler; TC 5, below bubble tray; TC 6, on bubble tray; TC 7, above bubble tray; TC 8, equilibrium cell constant-temperature zone; TC 9, condenser constant-temperature zone; TC 10, atmospheric pressure liquefaction chiller, not used; TC 11, external condenser constant-temperature zone; TC 12, not installed.

A photograph of major electrical components appears in Plate VIII. The potentiometer was a five-dial Tinsley Diesselhorst pattern, thermo-

Plate VIII

Potentiometer Rack

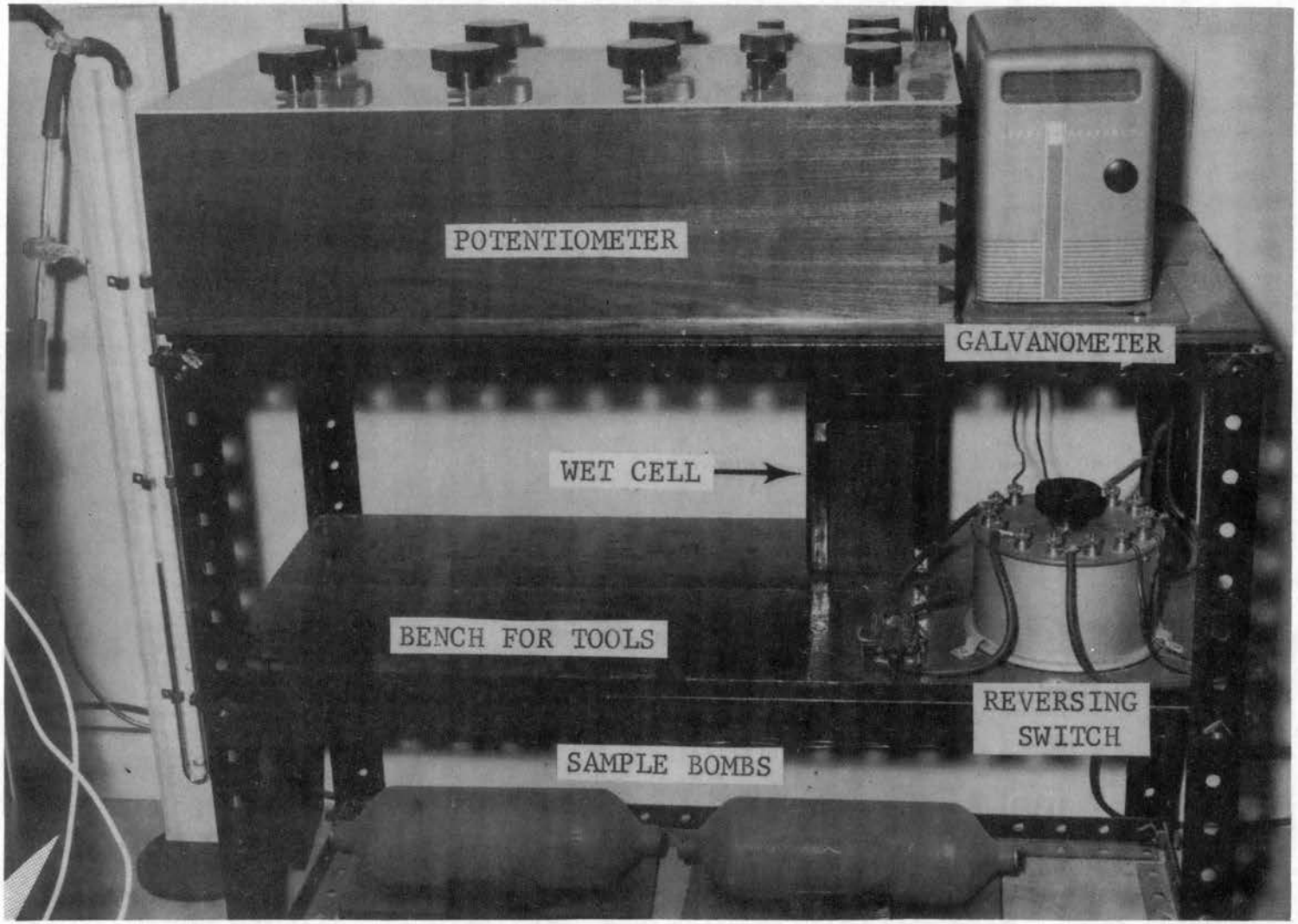

electric free, Model 3589R. Two voltage ranges were available, 0.111110 to -0.011001 volts and 0.0111110 to -0.0011001 volts. Any stray potential effects were eliminated by a Tinsley reversing switch Type 4092, which reversed the terminal connections of the battery, galvanometer, and leads simultaneously. A Leeds and Northrup galvanometer No. 2430 having a sensitivity of 0.0029 microamps/mm was used to balance the potentiometer. A saturated standard cell, Guildline Instruments Type 4305, was used as reference voltage and was placed in an insulated box. The temperature of the cell was determined by a mercury-in-glass thermometer inserted in the box, and the corresponding emf read from the calibration chart supplied with the cell.

Charge Gases and Mixture Analyses

The methane and ethylene used in the heat of vaporization determinations were provided by Phillips Petroleum Co. Both components were Pure Grade, 99 mole per cent minimum, and were supplied in standard 220 SCF cylinders. The principal contaminants of the methane were carbon dioxide, nitrogen, and ethane. A carbon dioxide scrubber filled with potassium hydroxide flakes was placed in the line to purify the gas prior to liquefaction. The ethylene contained a few tenths of a per cent methane, which was inconsequential, as well as traces of ethane.

All mixtures were analyzed on an F and M Hydrogen Flame Ionization Chromatograph, Model 609, using a 1/4 in. O. D. copper tubing column 18 feet long, packed with 20 weight per cent SE-30 on Chromosorb P. Inasmuch as the hydrogen flame detector will not pick up hydrogen, oxygen, nitrogen, air, carbon dioxide, helium and other rare gases, or water, it was not possible to detect the presence of the impurities

mentioned above. The amount of ethane present was not noticeable on the range and attenuations used during analysis.

The chromatograph was calibrated for methane and ethylene using the procedure described in detail in Appendix C.

A five cubic centimeter, gas-tight Hamilton syringe was used to transport samples from the calorimeter sample ports to the chromatograph injection port. No difficulty with two-phase mixtures was encountered because the critical temperature of all methane-ethylene binaries is below room temperature. Total elution time was about four minutes.

CHAPTER V

EXPERIMENTAL PROCEDURES AND DATA

In this chapter, the details of operating the calorimeter and auxiliary apparatus are presented. Following this are the special heat leak determination and the calculated results.

Procedures

Purging and Evacuating

Initially, the vacuum pump was started and the concentration of air within the calorimeter and piping was reduced to a negligible level by three successive evacuations and purgings with ethylene. Ethylene was used because of its odor, methane having little or no odor. Thus, the presence of ethylene in the laboratory could be readily detected.

Refer to the Schematic Flow diagram, Figure 12, for the location of valves and fittings. Valve No. 1 will be designated as V 1, etc. After the vacuum pump had reduced the pressure to about 10^{-1} torr, V 12 was closed and ethylene was admitted by opening the regulator and V 1, until a slight positive pressure was indicated on the manometer, after which V 1 was closed. The system was vented by opening V 9 momentarily. V 12 was reopened, and the entire cycle repeated twice. The system was left under a slight positive ethylene pressure, and all valves were closed.

Preparation of Charges

Since the volume of the reservoir was about 675 cubic centimeters and volume of the liquid hold-up on the bubble tray was about 75 cubic centimeters, it was necessary to liquefy about 400 grams of charge to prevent running out of mixture during a run. The liquefaction bomb, hereafter known as the thermal compressor, was evacuated by connecting it at the tubing cross between V 4 and 5, weighed, filled with pure ethylene to about 300 psig, and reweighed. This final tare weight represented the amount of gas that would be left in the thermal compressor if the entire charge was transferred to the calorimeter, assuming a 20 atmosphere bubble point.

A dry-ice-and-methanol bath was prepared for liquefying pure ethylene and the methane mixtures to be used, while a liquid nitrogen bath was required for liquefying pure methane, whose critical temperature is 5° K below the dry ice point, 195° K (-109° F). After the thermal compressor had been cooled down and loosely reconnected to the tubing cross, a small amount of gas was admitted by momentarily opening V 4. This served to purge the cross of air, which would accumulate in the calorimeter as a non-condensable. After the thermal compressor connection had been tightened, and the cold bath raised into position, liquefaction was started. A charge of ethylene, about 400 grams, required about 20 minutes to prepare with the regulator set at 200 psi. A charge of methane, about 275 grams, required about 15 minutes to liquefy with the regulator set at 300 psi.

New mixtures were always prepared by adding methane to pure ethylene or to existing mixtures. Weighing and analyzing the existing mixture permitted the calculation of the number of moles of each

component present. With this information the number of moles of additional methane needed to produce the new mixture was calculated. Methane was condensed in the mixture at a rate of about 30 grams per minute at a regulator pressure of 600 psi. Small increments were added until the desired total was attained, after which the compressor was brought to room temperature as rapidly as practical. The composition of the new mixture was verified on the chromatograph; adjustments were made if necessary. The mixture was reweighed on the day of use to guarantee that sufficient charge was on hand.

Cooling Down the Calorimeter

A dry-ice-and-methanol bath was used for runs requiring zone temperatures of 200° K (-100° F) minimum. This included the pure ethylene runs, all mixtures at 40 atmospheres, and the 13.7 per cent methane binary at 20 atmospheres. The 43.6 and 75.6 per cent mixtures at 20 atmospheres and pure methane at both pressures required a liquid nitrogen bath.

If a dry-ice bath was required, preparations were started the day before a run was to be made. The methanol to be used in the bath was dried over a bed of freshly dehydrated silica gel. This removed the water dissolved in the methanol during a previous run. It was found that as the water content of the methanol increased, foaming increased when the dry ice was added, and would eventually foam enough to overflow the calorimeter dewar. Therefore it was dried regularly.

About 12 hours before start-up, the reservoir zone was insulated with pieces of expanded polystyrene to reduce dry-ice-and-methanol requirements. The calorimeter dewar was raised into position. About 30 pounds of finely pulverized dry ice was added. Dried methanol was

poured over the dry ice a liter or so at a time until 8 or 10 liters had been added. More dry ice was added until the dewar was full of dry ice, and then more methanol, until the methanol level was about four inches from the top. It was important to maintain a surplus of dry ice at all times to prevent the methanol from warming up. Adding dry ice to methanol as cold as 225° K (-55° F) usually caused the dewar to overflow. A large catch pan was placed under the elevated dewar to receive the overflow. The calorimeter was allowed to cool down overnight.

If a liquid nitrogen bath was required, cooling down was started on the same day as the run to conserve liquid nitrogen. About 10 liters was required in the initial charge, and additional amounts were added as needed.

Usual Start-Up Procedures

On the day of a run, certain preliminary, routine checks and procedures were carried out. The supply of dry ice in the calorimeter dewar was checked first and more added as indicated. The crushed-ice bath for the thermocouple cold junction was prepared and placed in service. The barometer was read and the reading recorded. After turning on the galvanometer, the potentiometer was balanced and all thermocouples spot-checked for operability. All temperature controllers were turned on and checked to insure they were operating properly. The set-points were set very low after the check-out to prevent the heaters from coming on. The 0.01-ohm standard resistor oil bath stirrer was turned on, followed by the DC power supply. The power supply switch was wired in series with the oil bath stirrer switch so that the oil bath stirrer had to be turned before the power supply.

The calorimeter heater was turned on momentarily to verify that it was working properly. With all of the auxiliary equipment in running order, start-up procedures continued.

The DPI cell was balanced to zero by opening V 18 and V 9 to the atmosphere. The valve on the reference manometer was opened and the oil level adjusted to a previously determined mark by the screw press on the dead weight gauge. The sensitivity on the DPI control box was brought up to the operating level (pointer vertical) and the milliammeter balanced with the zero-adjust knob. The cell was balanced, and all three valves were closed. The air was evacuated via V 17.

The three constant-temperature zones were filled with thermostatic fluid using the system shown in Figure 13. If dry ice was used in the dewar, methanol was used in the zones; if liquid nitrogen was used, Phillips Petroleum Company commercial Grade iso-octane was used. Valves 25 and through 29 were closed and the nitrogen regulator set at about 5 psig. The regulator was kept at this low setting to minimize the mass flow of thermostatic fluid to the calorimeter. Extra precooling was provided by another dry-ice-and-methanol bath at the chiller.

The reservoir zone was filled first because cooling capacity was greater there. The first portion of the fluid coming from the chiller was warmer than the latter portions. To accomplish filling this zone, V 19, 21, 24, 30, 31, and 32 were opened and V 20, 22, and 23 were closed. Nitrogen pressure was then applied to the storage vessel by opening V 25, 26, and 34. Filling of the reservoir zone usually required about four minutes.

Each section of the zone overflow header contained a short piece

of transparent Tygon tubing. When the fluid appeared, V 24 was closed and flow switched to the equilibrium cell zone by opening V 23 immediately. When that zone was full--about 8 minutes later--the flow was switched to the condenser zone by closing V 23 and opening V 22. Three minutes was usually required to fill the last zone, at which time V 22 was closed, followed immediately by V 19 and 25. The nitrogen line was then disconnected at V 34 and the storage cylinder vented.

Valves 30, 31, and 32 were always left open for two reasons; (1) if a leak occurred in any of the high-pressure components, the escaping gas would be vented via these valves, and (2) the thermostatic fluid was expanding and contracting as the set points in the zones were changed. The end of the line to the overflow catch pot was also made of Tygon tubing and arranged in a U-shape to trap a segment of liquid in the line. Flow of gas or liquid was easily spot-checked throughout an experiment by observing the action of the trapped liquid. If action in the trap was overlooked, the presence of a leak was easily detected by the odor of ethylene in the laboratory.

Charging and Liquid Level Adjusting

The reservoir and its zone were cooled down to 10 or 15° K below the bubble-point temperature of the experiment, as indicated by TC 1, 2, and 3. The equilibrium cell zone temperature (TC 8) was adjusted to 10 or 15° K above the bubble point to prevent condensation there. The condenser zone temperature (TC 9) was usually near the bubble point. It was not necessary to wait for this last zone to reach any certain temperature because most of the condensation occurred in the reservoir.

The thermal compressor was check weighed again and loosely connected to the tubing cross between V 4 and 5, shown in Figure 12. V 4 was opened momentarily to purge the air from the connection. The connection was closed tightly and V 33 was opened slowly. The pressure in the compressor was usually between 1500 and 2000 psig. Valve settings were checked; V 7, 18, and 5 open, V 17 and 6 closed. Flow to the calorimeter was controlled by V 6.

If about nine-tenths of the charge in the compressor was to be transferred to the calorimeter, a good approximation was obtained by allowing the pressure in the compressor to fall nine-tenths of the way between the initial thermal compressor pressure and the bubble-point pressure corresponding to the reservoir temperature. This approach worked fairly well for pure-component charges because the necessary vapor pressure and density data were available (see Figures 15 through 18). The resulting level of liquefied charge in the reservoir was only known approximately by reading TC 1, 4 through 7. (See Recommendation No. 3).

Since the level of liquid in the system was very important to successful operation of the calorimeter, and more important for running mixtures than pures, a more definite way of checking the level was used on mixtures. This method could not be applied to pure components because it utilized the difference in compositions of the coexisting phases.

After the charge had been warmed up to approximately the desired bubble-point temperature and the liquid had expanded to nearly the density it would have during the experiment, samples were taken one at a time from the four sample ports in the calorimeter and analyzed.

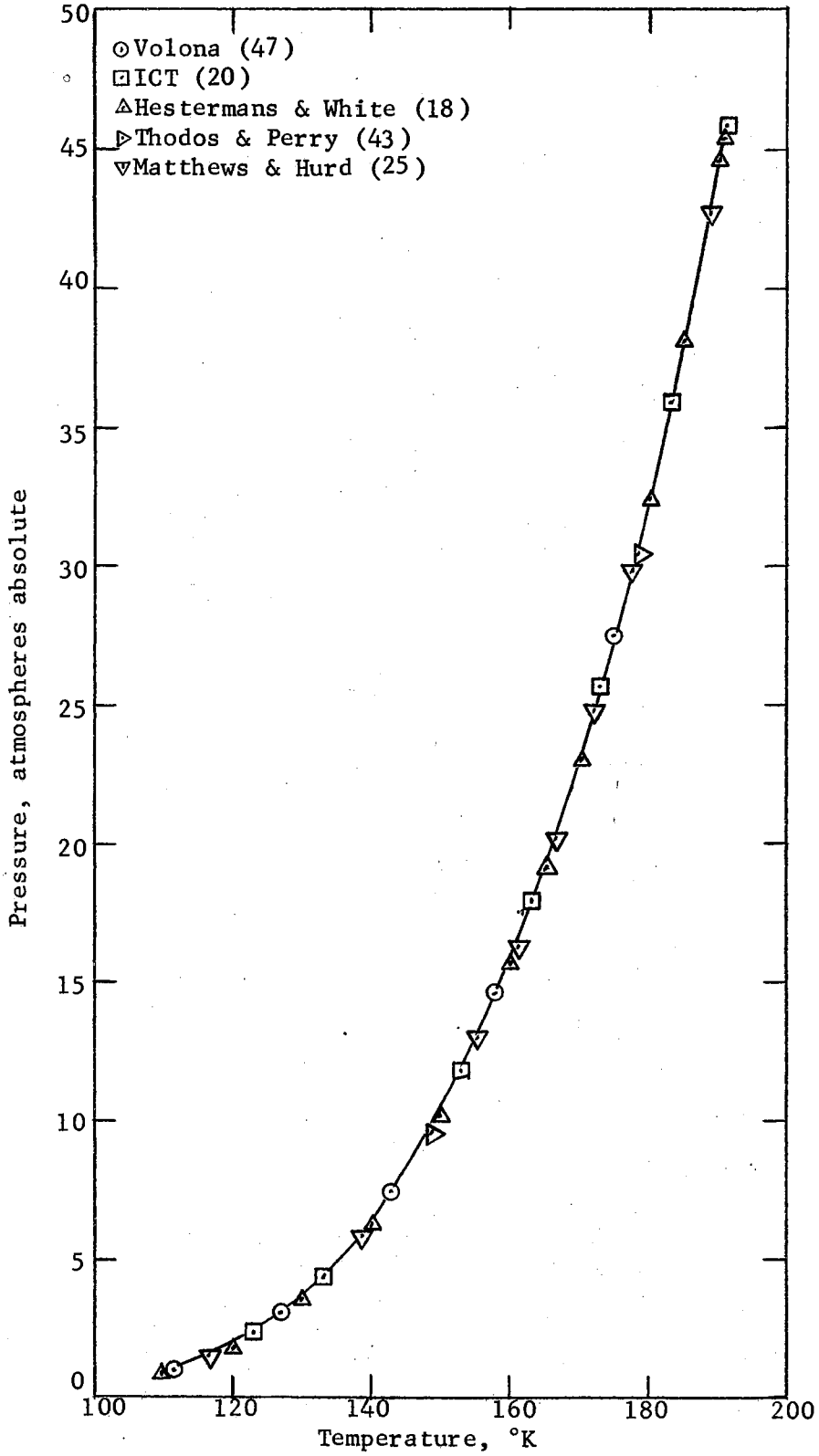

Figure 15

Methane Vapor Pressure

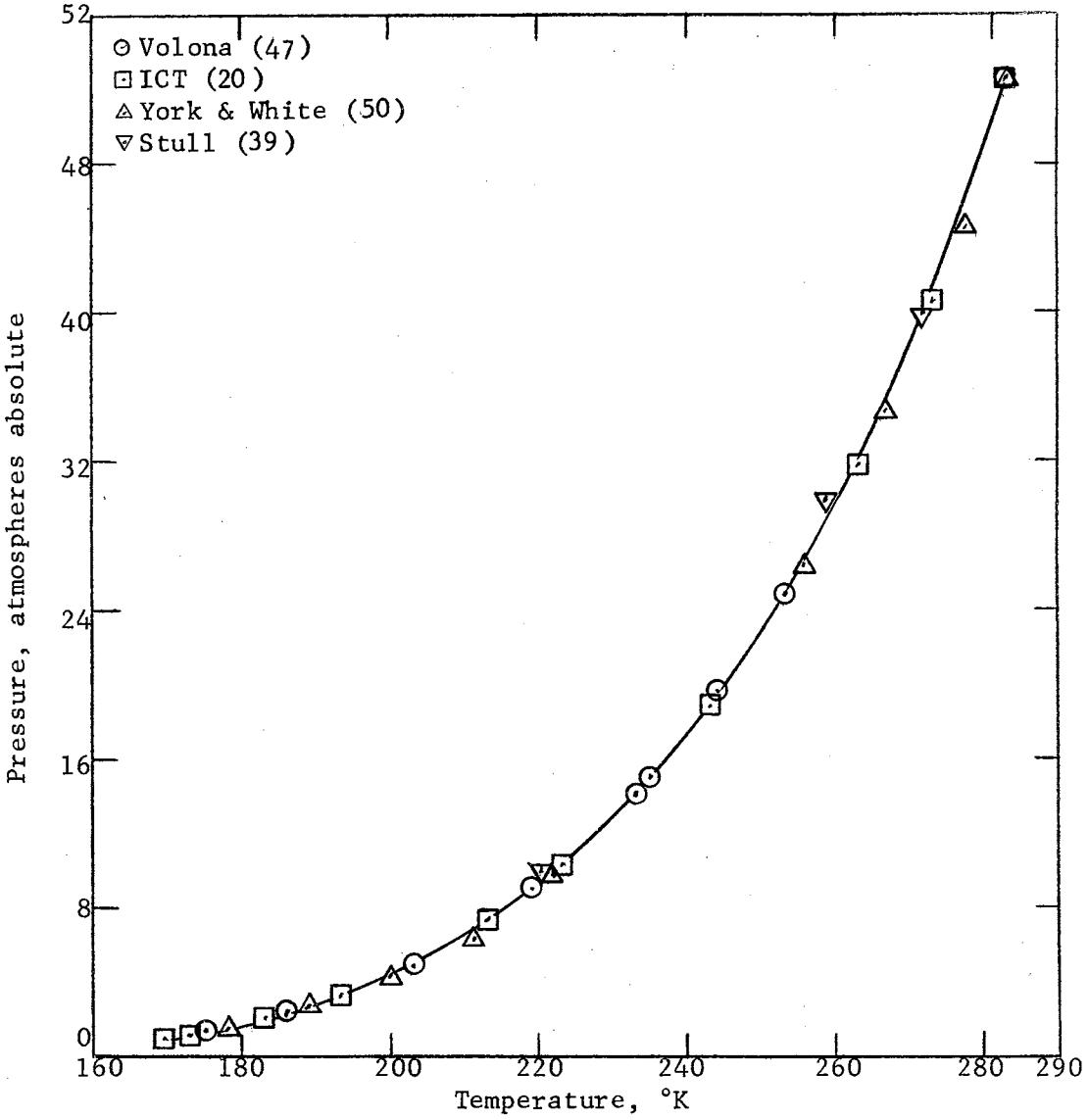

Figure 16

Ethylene Vapor Pressure

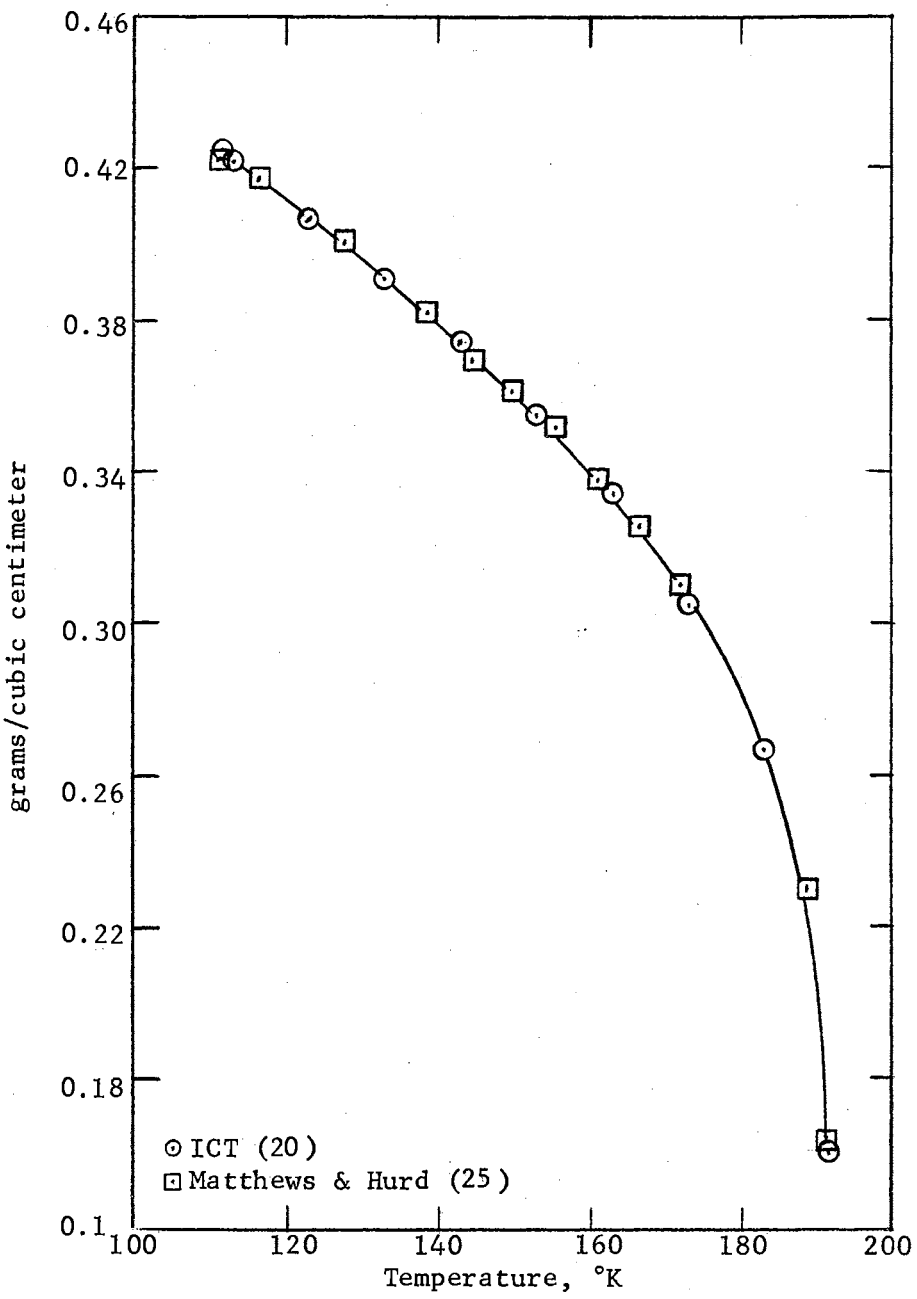

Figure 17

Liquid Methane Densities

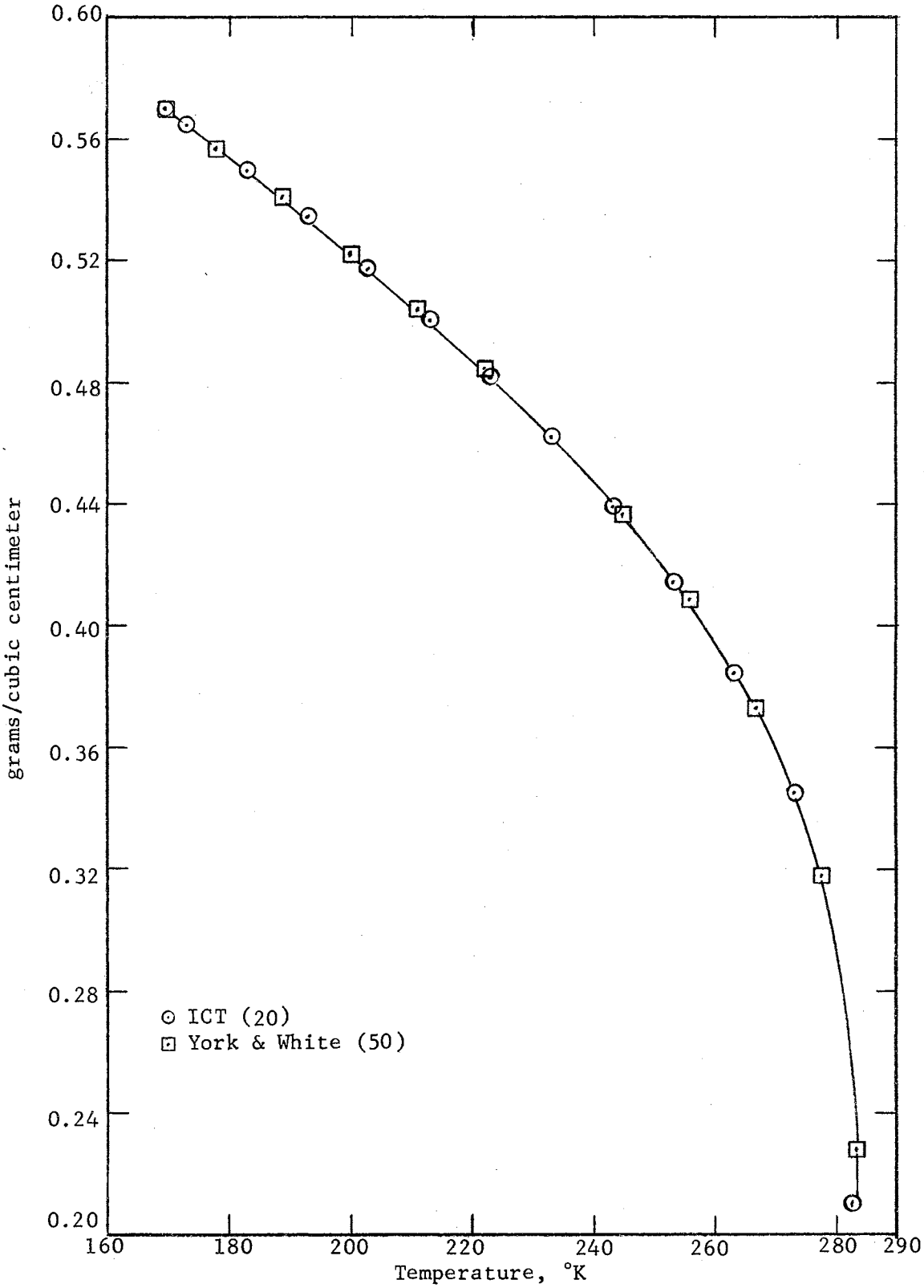

Figure 18

Liquid Ethylene Densities

These were located at the top of the reservoir, in the reboiler, below the tray and on the tray. The chromatograms told immediately whether liquid or vapor existed at any particular sample port. To reduce the charge level, liquid was withdrawn. This prevented the loss of methane from the methane-rich vapor phase.

Withdrawal was accomplished by attaching an evacuated bomb directly to the reboiler sample port. Filled bombs were carried outside the building and vented to the atmosphere prior to reevacuating. After a prudent number of the cycles, samples were taken from the four sample ports to ascertain the new liquid level. This was repeated until a vapor sample was obtained from the reservoir.

Final adjustments were made in the reservoir temperature zone to bring the pressure up to the desired level, 20 or 40 atmospheres absolute, as determined by the dead weight gauge. The smallest weight supplied with the Budenburg Dead Weight Gauge was for 10 psi. A number of various sized weights were weighed on the 6 kg Volard balance to determine the actual weight required to represent 1 psi, which was 28.36 grams. Weight Set No. 4775 was used to measure pressures to the nearest 5 gram weight, which was equivalent to the nearest 0.012 atmospheres. It was almost impossible to control the temperature well enough to produce exactly the desired pressure.

Turning on the Heater

At this point, the voltage of the power supply was set and the calorimeter heater turned on. For pure components, the voltage was set at the minimum value, about 16.5 volts, because the pures had a lower heat of vaporization than the mixtures, and there was no energy

required for heat leak. This low voltage setting kept the boil-up rate low enough so that all of the vapor produced could be properly condensed. For mixtures, the setting was made near the maximum, about 23.5 volts. The pressure increased slightly as the result of the heater being turned on.

Setting Up the External Condenser

An hour or so was usually required to reach steady state in the calorimeter. During this time, an external condenser constant-temperature zone was set up. A special, double-walled, six-liter glass beaker with expanded polystyrene in the annular space was made for this zone. This makeshift glass vessel proved to be very successful because the rate of heat loss to the heat sink could be adjusted to suit the wide range of temperature differences encountered throughout the experimental program. This was done by pouring various quantities of methanol or iso-octane (depending on whether dry ice or liquid nitrogen was being used) into the annular space. When the ΔT was high, no liquid was used at all; when it was low, the annular space was about half full.

The inner vessel was approximately half-filled with the same constant-temperature bath fluid, enough to cover the condenser bomb. Initially dry ice was added directly to this liquid to cool it. The special glass beaker was placed in a stainless steel dewar, which had previously been prepared with dry ice and methanol or liquid nitrogen, as the experiment required.

This "dewar within a dewar" was placed on a small elevator which was designed to hoist the two nested dewars up around the external condenser sample bomb. This action is indicated in

Figure 12. The 300-watt immersion heater with TC 11 attached was lowered into the bath, and the evacuated, external condenser sample bomb, which had been precooled in a dry-ice-and-methanol bath, was loosely connected to V 9, which was opened momentarily to purge the air from the connection. The connection was tightened.

The external-condenser temperature sensor and stirrer were positioned next to the sample bomb. The elevator was raised until the bomb was submerged; the system was allowed to come to the set-point temperature, which was always below the bubble point in the reservoir.

Valves 9 and 10 were opened slowly and the sample bomb was filled with vapor at the temperature and pressure of the system. After the elevator was lowered, the bomb was removed for weighing. This weight was the external-condenser tare weight for the experiment.

The sample bomb was precooled again in dry ice and methanol before it was connected to V 9 and purged. The same procedure was followed every time the external-condenser sample bomb was connected, filled, and weighed.

Attaining Steady-State

Before a timed run could be made, the four sample ports were analyzed again to see if steady-state was actually attained. An indication of this was given by the rise in temperature in the reboiler (TC 4). Obviously, steady-state could not be reached if the equilibrium-cell temperature zone was below the dew point. The set point of that zone was gradually raised until its temperature, measured by TC 8, exceeded the reboiler temperature (TC 4). Valve 8 was always open. If the reboiler temperature had stabilized and readings from TC 5, 6, 7, and 8 were all higher than TC 4, nearness of steady-

state was indicated. The pre-run samples were taken. The analysis generally confirmed that steady-state had been attained, and a timed run could be made.

Making the Run

Just prior to actually starting a run, the potentiometer range switch was set on 0.1, the potentiometer was standardized, the reversing switch set to "direct," and DPDT switches 1 and 2, shown in Figure 14, set to read TC 1.

A run was actually started by "all but closing" V 8 and opening V 10, immediately after which V 9 was opened slowly as the stop watch was started. It was necessary to leave V 8 open slightly to prevent the establishment of a pressure differential between the condenser and the equilibrium cell, which would retard the flow of liquid into the reboiler. The ten thermocouples were read first, followed by the two standard resistances, which were easily connected to the potentiometer by throwing DPDT 2 and DPDT 3 (see Figure 14). It was necessary to use the 1.0 range of the Tinsley for the standard resistance readings. The reversing switch was used to average any stray potentials in the standard resistors. The pressure was measured last on the dead weight gauge.

These readings usually required from six to ten minutes, depending on how easily the potentiometer was balanced. Check readings could not be made because of the danger of the reboiler going dry. Valve 9 was closed simultaneously with the stopping of the stop watch, which was usually permitted to reach the next 15 second interval.

Valve 10 was closed immediately thereafter, followed by the opening of V 8, and the shutting-off of the heater.

The external-condenser sample bomb was removed from V 9 and weighed, after which it was allowed to come to room temperature so that a sample of the dense phase fluid thus created could be analyzed.

Only one run per day could be made.

Shutting Down

The shut-down procedure depended on what was planned for the following day. If the same mixture was to be run again at a higher pressure, it was left in the calorimeter, provided that enough dry ice was on hand to hold the calorimeter bath at the dry-ice point during the night. If both of these conditions were not met, the remainder of the charge was stripped from the calorimeter into the thermal compressor, which had been placed in a dry ice or liquid nitrogen bath, as the situation required. The stripping prevented a pressure rise due to warming of the calorimeter.

After the stripping was completed, the four temperature controllers were turned off and disconnected, and the thermostatic fluid was blown-down to storage. During the early stages of the experimental program, the fluid was allowed to remain in the calorimeter overnight. Next day, it was discovered that a considerable amount had leaked out of the two upper zones into the vacuum space. This caused an undue amount of heat transfer and limited evacuation of the vacuum jacket to the bubble-point pressure of the fluid, besides loading-up the cold trap just ahead of the vacuum pump.

Therefore, it was much easier and less time-consuming to drain the fluid at the end of each experiment. Before the experimental program was completed, it was necessary to disassemble the calorimeter, at which time the two zones were painted with white epoxy paint inside and out to stop these leaks. The bottom of the vacuum space was also filled with foamed-in-place insulation. The calorimeter has not been disassembled since to evaluate this treatment.

Blow-down was accomplished by closing V 21 and 26 (Figure 13) and the vent valve of the zone to be emptied (V 30, 31 or 32). This is the only time that a vent valve should ever be closed. The walls of each zone were not designed to withstand any pressure, other than the 5 psig required for blow-down. Valves 19, 20 and 25 were opened plus the correct combination of V 22, 23, and 24 with V 27, 28 and 29 respectively, depending on the zone to be emptied. After each zone was emptied, as noted by sound of bubbling nitrogen in the storage cylinder, the particular pair of opened valves was closed and the vent valve (V 30, 31, or 32) for the zone opened.

The shut-down procedure was completed by turning-off and disconnecting all electronic gear.

Special Heat-Leak Determination

The most important correction to be made to the data was the heat-leak correction, which occurred on mixture runs only. The cause of the heat leak is discussed in Appendix F. A schematic diagram, Figure F-1, is also presented there.

It was not possible to determine the magnitude of this heat leak using other methane-ethylene mixture data because they are not available in the literature. A different method was needed.

Pure ethylene was charged into the calorimeter and the reservoir temperature brought up to about 222° K, (-60° F) corresponding to a bubble-point pressure of about 10 atmospheres. A cylinder of Grade-A helium, whose pressure was in excess of 400 psig, was connected directly to V 2. Valves 1, 3, 33, 9, and 17 were closed and V 4, 5, 6, 7, 8, and 18 were opened. Weights corresponding to 20 atmospheres were placed on the dead weight gauge (DWG), and the helium cylinder was just barely opened. The rise in pressure was followed on the gauge between V 4 and 5 until the weights on the DWG were displaced upward, at which time the helium was shut off. The heater was turned on using minimum voltage. Reboiler temperature (TC 4) was monitored on the potentiometer. The temperature rose to the 20 atmosphere bubble point, about 244° K (-20° F), and stayed there. Evidence of the heat leak was very apparent at TC 1 and 3. After a few minutes at steady-state, a regular pure ethylene run (Run 46) was made. The calculation of the heat leak is presented in Appendix F.

Experimental Results

The pure-component and mixture heats of vaporization are given in Table I; the vapor-liquid equilibria data are given in Table II. The pure ethylene determinations were made first, followed by the mixtures. Pure methane was run next, followed by the heat-leak determination and replication of a pure ethylene run. Raw data were processed according to procedures outlined in Appendix F.

TABLE I

ISOBARIC INTEGRAL HEATS OF VAPORIZATION

Run	Pressure Atm. abs.	Feed Comp. %	Sample, grams	Gross Calories	Heat Leak Correction Calories	Heats of Vaporization cal/gm.	Heats of Vaporization Btu/lb-mol
				Pure-Grade Methane			
44	20.21	99+	24.2	2022.4	--	83.6	2413
45	40.09	99+	48.8	2019.1	--	41.4	1195
				Pure-Grade Ethylene			
27	19.59	99+	39.9	3184.0	--	79.8	4029
47	20.15	99+	26.1	2009.0	--	77.0	3887
31	38.42	99+	59.9	2856.1	--	47.7	2408
				Heat-Leak Calibration, Pure-Grade Ethylene			
46	19.94	99+	41.3	3628.8	415.5	77.8	3928
				Mixtures at 20 Atmospheres			
36	19.95	13.7	45.4	4632.1	216.8	97.2	4622
43	20.81	43.6	36.7	4064.6	338.1	101.5	4170
42	19.94	75.6	36.9	4068.6	373.4	100.1	3419
				Mixtures at 40 Atmospheres			
40	39.97	11.2	52.7	4042.4	119.8	74.4	3578
41	38.07	32.7	48.3	4044.3	211.9	79.3	3445
37	42.44	75.2	41.7	3523.7	282.4	77.7	2661

TABLE II

EXPERIMENTAL VAPOR-LIQUID EQUILIBRIA DATA

				Composition, mol % Methane					
		Corrected Temp., ° K		Bubble Point		Dew Point			
Run	Pressure Atm. Abs.	Bubble Point	Dew Point	Charge Liquid	Reservoir Vapor	Reboiler Liquid	Reboiler Vapor	Tray Liquid	Tray Vapor
				Mixtures at 20 Atmospheres					
36	19.95	226.8	241.7	13.7	40.8	2.3	14.1	2.6	14.3
43	20.81	199.4	226.3	43.6	75.2	14.0	41.5	14.3	42.0
42	19.94	176.5	206.3	75.6	94.2	32.4	69.7	32.5	70.2
				Mixtures at 40 Atmospheres					
40	39.97	253.7	263.3	11.2	36.4	6.5	13.1	6.6	13.1
41	38.07	235.3	252.2	32.7	68.5	18.9	39.4	19.2	39.3
37	42.44	199.4	225.2	75.2	92.8	40.7	75.0	41.1	75.5

CHAPTER VI

ANALYSIS OF RESULTS

The results of this research are analyzed in this chapter under three major headings: pure component data, mixture data, and consistency tests. Mixture data are subdivided into vapor-liquid equilibria data and calculation methods; consistency tests are subdivided into differential and integral forms.

Pure Component Data

The heats of vaporization of pure methane and ethylene were determined (Runs 27, 31, 44, 45, and 47) to establish the end points of the $(\Delta H_v)_{P,x}$ vs. composition diagrams, Figures 23 through 26, which are discussed in the next section. In addition, these pure component determinations served to establish the serviceability and reliability of the calorimeter. Pure Grade ethylene was run first because it imposed less severe temperature conditions (245° vs. 166° K or -19° vs. -161° F) on the calorimeter. The odor of ethylene also aided in leak detection, which was essential to improving and maintaining the serviceability of the apparatus. No leaks were detected after the Conax sealants were changed from Teflon to "lava", a natural magnesium silicate, or soap stone.

Table III is a comparison of pure-component experimental data determined in this work with that found in the literature.

TABLE III

A COMPARISON OF PURE-COMPONENT EXPERIMENTAL DATA

(cal/gm)

Run	Pressure Atm. Abs.	Heats of Vaporization This Work	Literature	Difference	Per Cent Difference
		Methane			
44	20.21	83.6	83.3 (25)	0.3	0.4
45	40.09	41.4	41.1 (25)	0.3	0.7
		Ethylene			
27	19.59	79.8	78.3 (50)	1.5	1.9
47	20.15	77.0	77.5 (50)	-0.5	-0.6
31	38.42	47.7	47.2 (50)	0.5	1.1

Standard Deviation = 0.71 cal/gm
= 1.28 Btu/lb

The positive differences exceed the combined effect of the errors in individual measurements (0.15% vs. 0.8%), as discussed in Appendix H. The differences are indicative of a very small heat leak. A correction for this was made in the heat-leak calibration.

The negative difference (Run 47) is indicative of a normal statistical variation. It could have been caused by a slightly flooded equilibrium cell. It was noted early that a flooded equilibrium cell plus a small negative temperature gradient between the cell and the external condenser would cause the liquid to vaporize in the cell and condense in the external condenser, without the calorimeter heater being on. Once this effect was discovered, precautions were taken, as described in the previous chapter, to prevent flooding.

Mixture Data

The vapor-liquid equilibria data are compared with values found in the literature, followed by the enthalpy-concentration diagrams and a comparison of the isobaric integral heats of vaporization with values calculated by the three calculation methods discussed in Chapter II.

Vapor-Liquid Equilibria Data

There are two published sets of vapor-liquid equilibria data for the methane-ethylene system: Guter, Newitt, and Ruhemann(15) and Volona (47). The former contains four isotherms of interest, 169°, 184°, 195° and 231° K (-155°, -128°, -109°, and -44° F); the latter contains nine isotherms, but no data at 40 atmospheres. The pertinent data of these investigators and the data obtained in this investigation are plotted on temperature-composition diagrams in Figures 19 and 20 at 20 and 40 atmospheres, respectively.

At 20 atmospheres, the liquid-phase data of this work are about 10 per cent richer in methane than the other investigators'. The vapor-phase data are about three per cent richer. These differences are attributed to vaporization during sampling. The other investigators sampled their systems under equilibrium conditions. A portion of these differences is attributed to the analytical method. The accuracy of the analyses is discussed in Appendix C. Briefly, mixtures of methane-ethylene prepared and analyzed by Phillips Petroleum Co. were reanalyzed on the chromatograph used in this work. Their mass spectrometer analyses agreed with the chromatographic results within 1.5 mole per cent.

The values of the partial derivatives used in the differential form

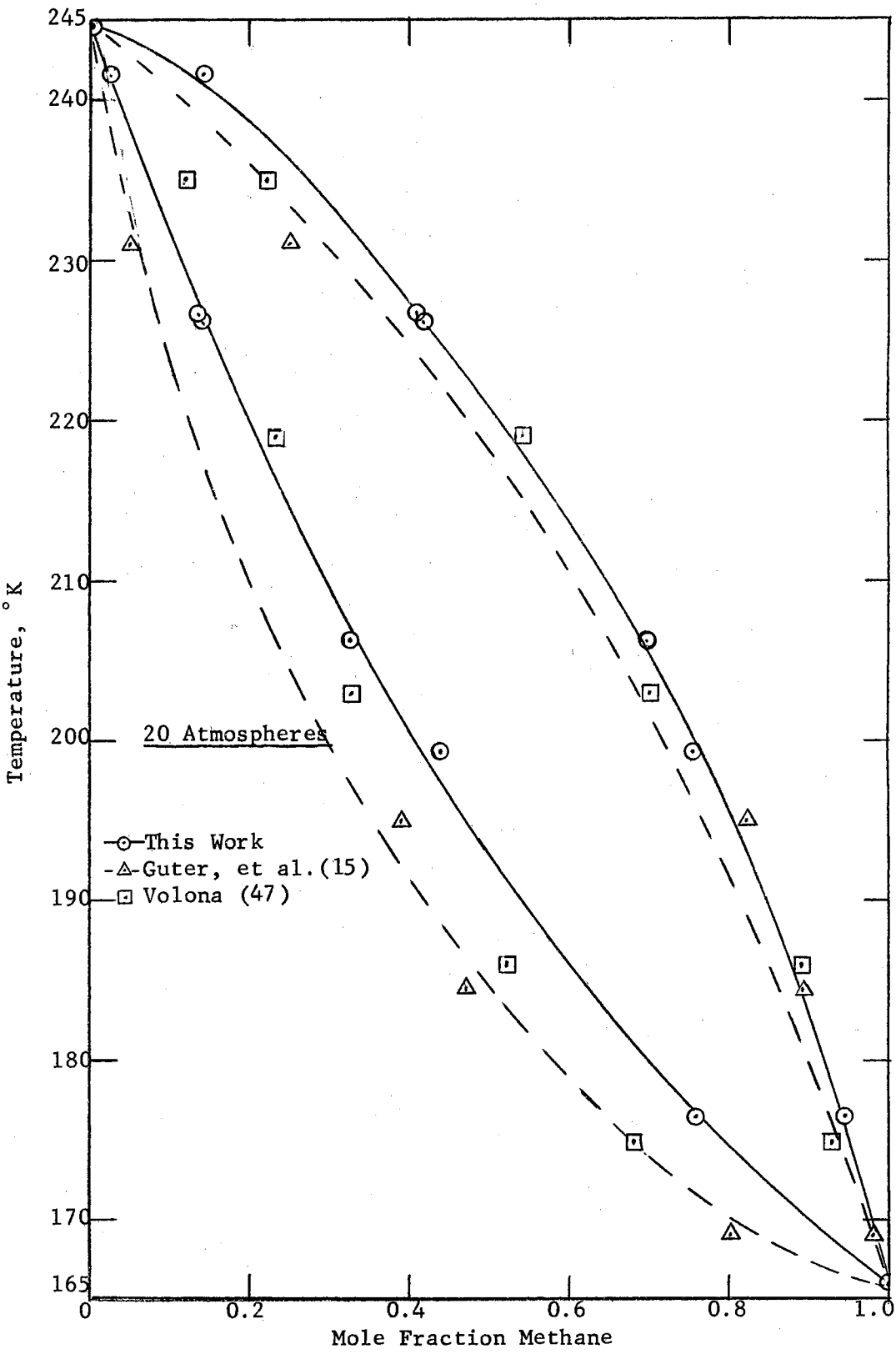

Figure 19

Temperature-Composition Diagram, Methane-Ethylene,
20 atmospheres

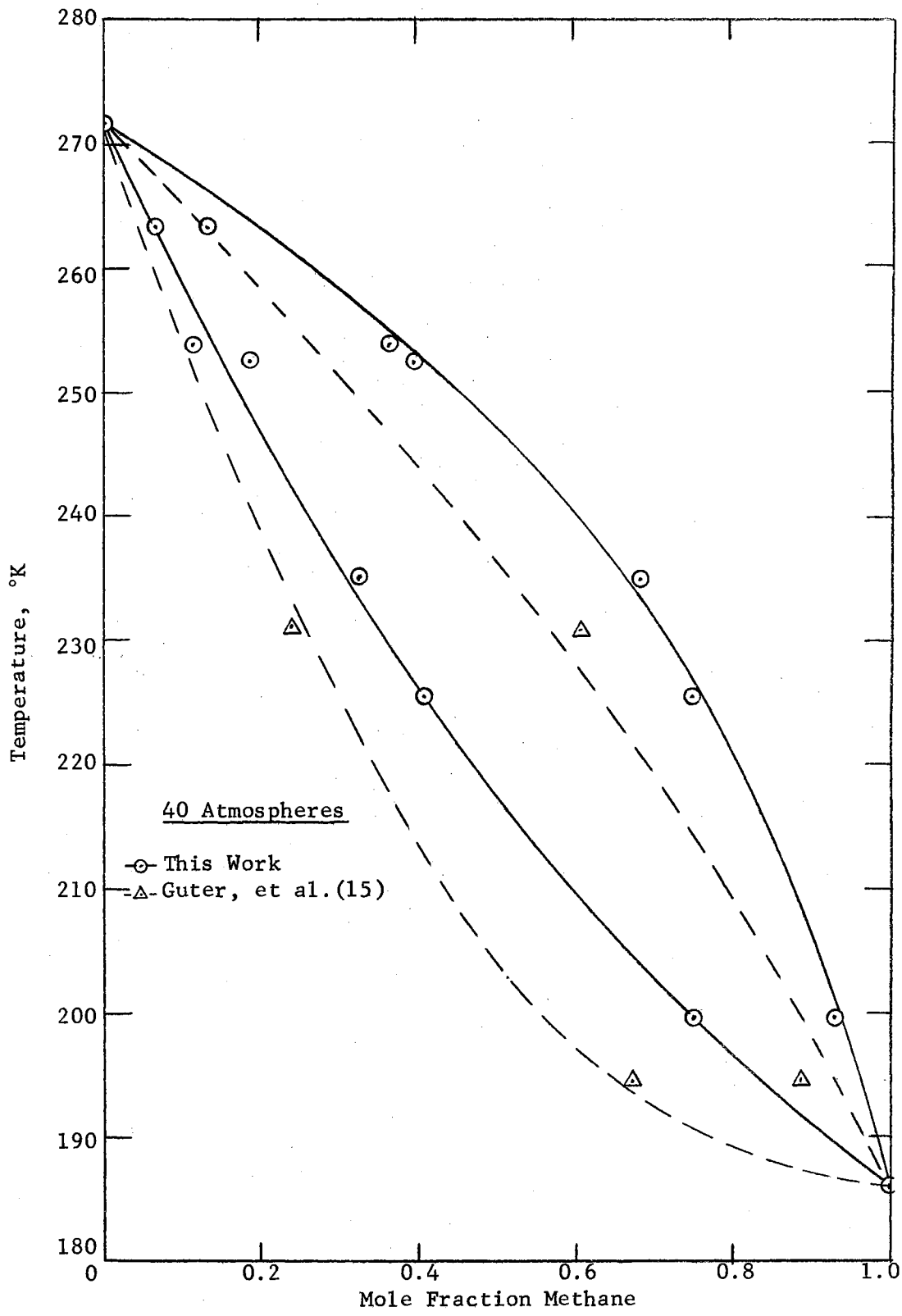

Figure 20

Temperature-Composition Diagram, Methane-Ethylene,
40 atmospheres

of the consistency test, given by Equation 138 and tabulated in Tables VIII and XIV, indicate that these composition differences have not affected the relative consistency of these two different sets of VLE data very much.

At 40 atmospheres, the liquid and vapor phase data of this work are about 10 per cent richer in methane than the two isotherms reported by Guter, et. al. A thorough analysis of these two data points can hardly be justified. A cursory examination of the consistency test results would indicate that Guter's liquid data might be slightly deficient in methane.

Enthalpy-Concentration Diagrams

The enthalpy-concentration diagrams for the methane-ethylene system at 20 and 40 atmospheres are shown in Figures 21 and 22, respectively. Values along the saturated vapor curves were determined using the EPE (11, 12) computer program, details of which are discussed in Chapter II and Appendix F. The saturated liquid curves were determined by subtracting the pure component and mixture enthalpy data from computed saturated vapor data. Values are tabulated in Table F-V.

Examination of the curves shows the liquid phase to be more non-ideal than the vapor phase, as would be expected. At 20 atmospheres the vapor phase has a slightly negative heat of mixing while at 40 atmospheres a definitely positive heat of mixing is shown. (This comes from the Redlich-Kwong (30) equation used to calculate the saturated vapor enthalpies.)

Calculational Methods

No prior experimental isobaric integral heats of vaporization at

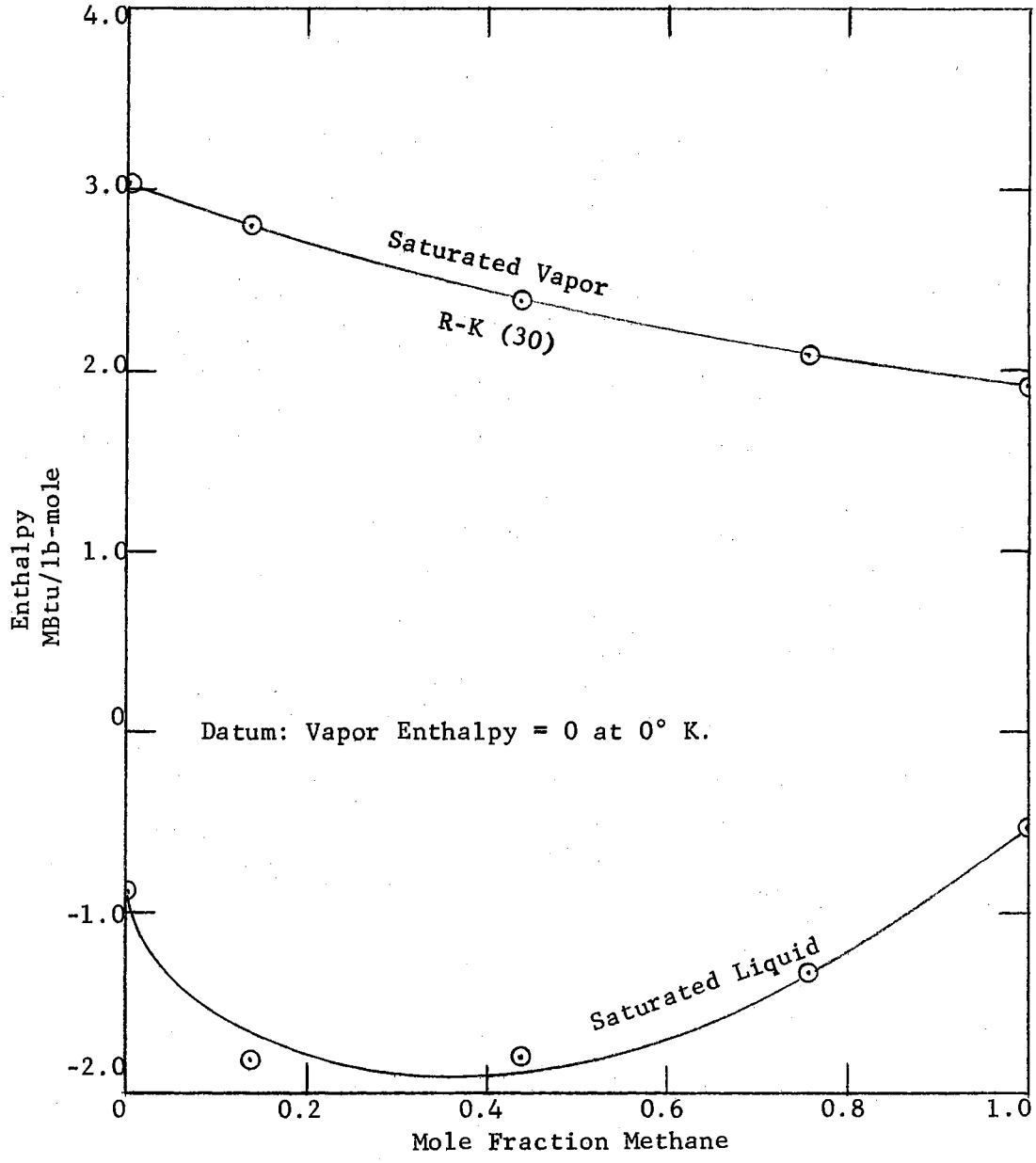

Figure 21

Enthalpy-Concentration Diagram, Methane-Ethylene,
20 atmospheres

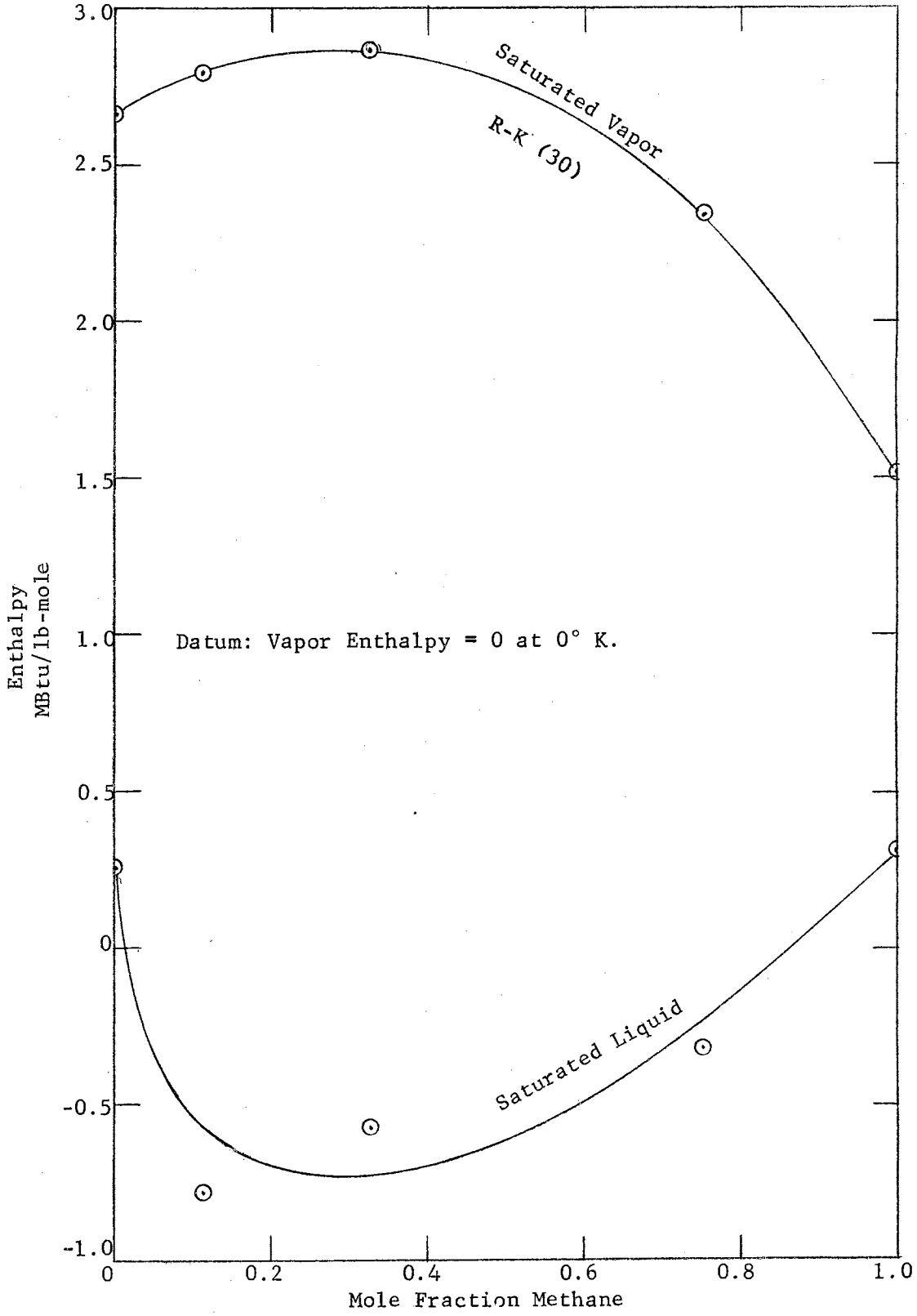

Figure 22

Enthalpy-Concentration Diagram, Methane-Ethylene,
40 atmospheres

high pressures are available for comparison. In lieu thereof, the results of this investigation are compared with values calculated by three different methods: the Edmister-Persyn-Erbar (EPE)(11, 12) method, the Yen-Alexander (49) method, and the Edmister (9) K-value approximation method. The details of each method are presented in Chapter II, and the results for 20 and 40 atmospheres are presented in Tables IV and V, respectively.

20 Atmospheres

At 20 atmospheres, the values of the isobaric integral heats of vaporization calculated by the Edmister-Persyn-Erbar (EPE)(11, 12) method were 8 per cent below the experimental values. These data are compared graphically in Figure 23. The difference is attributed to the inability of the Redlich-Kwong (30) equation to describe accurately the vapor-phase behavior of the methane-ethylene system. It is also attributed to the inability of the Pitzer, et. al. (23), correlation to predict accurately the departure from simple fluid.

The values calculated by the Yen-Alexander (49) method were also 8 per cent below the experimental values. This difference is attributed to the inability of their equations and the Lydersen, Greenkorn and Hougen (24) generalized enthalpy difference charts to predict mixture behavior.

The Edmister (9) K-value approximation values were 13 per cent below the experimental data. In this range, the temperature approximation ($T_{BP} \cong T_{BP}T_{DP} \cong T_{DP}^2$) will cause errors of about 10 per cent.

All three methods did not indicate a maximum value of the heat of vaporization for some mixture, as did the experimental data, but they

TABLE IV

COMPARISON OF EXPERIMENTAL AND CALCULATED VALUES OF THE ISOBARIC INTEGRAL HEATS OF VAPORIZATION OF METHANE-ETHYLENE MIXTURES AT 20 ATMOSPHERES

(M Btu/lb-mol)

Experimental			Calculated Values		
Mol % Methane	This Work	Literature	Edmister (9) K-value	Edmister-Persyn-Erbar (11)	Yen-Alexander (49)
0.0	4.029*	3.953 (50)	--	4.177	4.279
	3.887**	3.912 (50)	--	4.150	--
10.0	--	--	5.143	4.179	4.258
13.7	4.622	--	4.396	4.175	4.240
20.0	--	--	4.527	4.144	4.163
30.0	--	--	4.249	4.056	4.066
40.0	--	--	3.810	3.920	3.940
43.6	4.170	--	3.325	3.833	3.745
50.0	--	--	3.629	3.750	3.772
60.0	--	--	3.579	3.552	3.593
70.0	--	--	3.211	3.334	3.390
75.6	3.419	--	2.952	3.206	3.241
80.0	--	--	2.918	3.099	3.131
90.0	--	--	2.864	2.850	2.778
100.0	2.413	2.404 (25)	--	2.580	2.381

* 19.59 atms.
** 20.15 atms.

TABLE V

COMPARISON OF EXPERIMENTAL AND CALCULATED VALUES OF THE ISOBARIC INTEGRAL HEATS OF VAPORIZATION OF METHANE-ETHYLENE MIXTURES AT 40 ATMOSPHERES

(M Btu/lb-mol)

Experimental			Calculated Values		
Mol % Methane	This Work	Literature	Edmister (9) K-value	Edmister-Persyn-Erbar (11)	Yen Alexander (49)
0.0	2.408	2.383 (50)	--	3.152	2.498
10.0	--	--	4.166	3.203	2.520
11.2	3.578	--	4.640	3.228	2.462
20.0	--	--	5.151	3.262	2.505
30.0	--	--	4.670	3.242	2.420
32.7	3.445	--	4.237	3.308	2.349
40.0	--	--	3.743	3.152	2.301
50.0	--	--	3.226	2.998	2.123
60.0	--	--	3.011	2.766	1.926
70.0	--	--	2.975	--	1.664
75.2	2.611	--	2.853	--	1.315
80.0	--	--	2.860	--	1.364
90.0	--	--	2.526	--	1.061
100.0	1.195	1.187 (25)	--	--	0.855

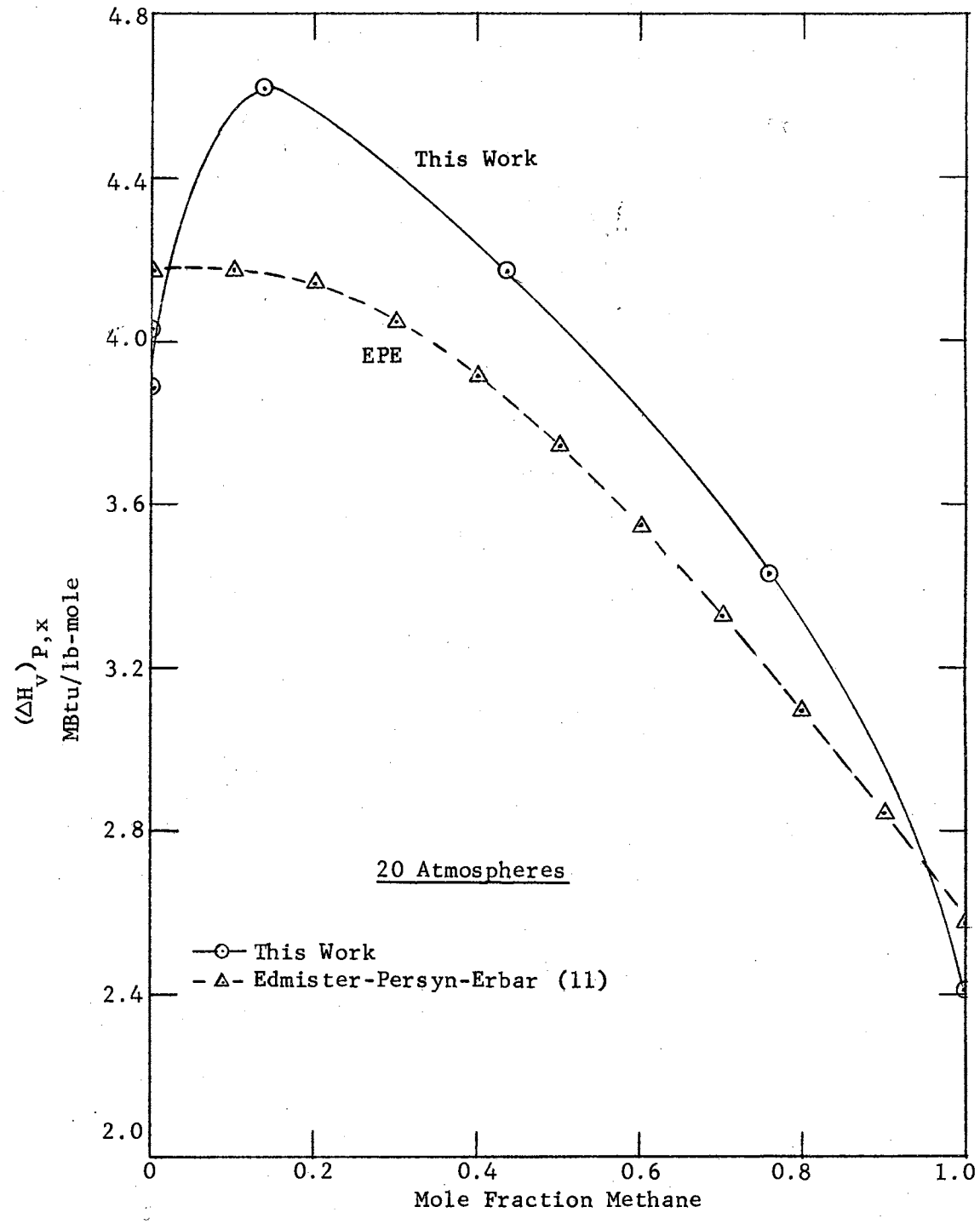

Figure 23

Isobaric Integral Heat of Vaporization, Methane-Ethylene, 20 atmospheres

did indicate a slightly positive heat of mixing. This is attributed to inadequate description of mixture behavior. In order to check into this non-ideal heat of mixing effect, the isobaric integral heats of vaporization of the methane-ethane system were examined using the values of Houser and Weber (19). These data are plotted in Figure 24. It is obvious that these calculated values indicate an even more non-ideal heat of mixing. It was not possible to apply this calculation method directly to the methane-ethylene system because there are no PVT data for this system, which are necessary for the Houser-Weber (19) method.

40 Atmospheres

The values calculated by the EPE (11, 12) method were 7 per cent below the experimental data. This comparison is shown in Figure 25. The Yen-Alexander (49) method values were 38 per cent below the experimental data. The Edmister (9) K-value method values were 20 per cent above the data. Reasons for these discrepancies are the same as stated for 20 atmospheres. In addition, non-ideal mixture behavior is more pronounced at higher pressures.

The values of Houser and Weber for methane-ethane at 40 atmospheres are plotted and compared in Figure 26. The magnitude of the heat of mixing is about the same. The methane-ethane maximum occurs at 40 per cent methane, while the methane-ethylene maximum is skewed to 11 per cent.

Consistency Tests

Three different isobaric thermodynamic consistency tests were applied to the experimental data. The tests used were (1) the Thompson-Edmister (45) test, derived in Appendix J, (2) the Edmister test (10),

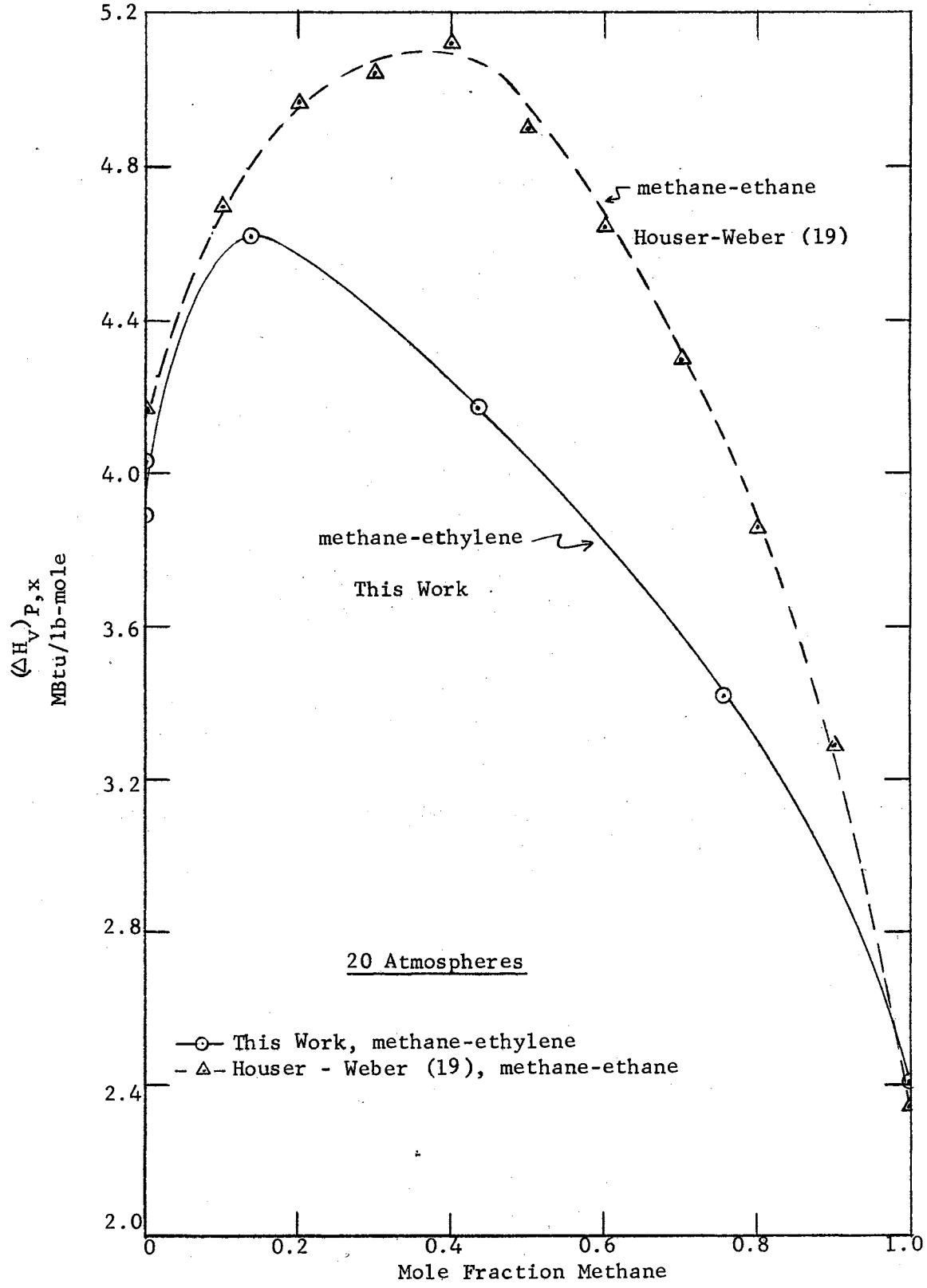

Figure 24

Comparison of Isobaric Integral Heats of Vaporization of Methane Binaries of Ethylene and Ethane at 20 atmospheres

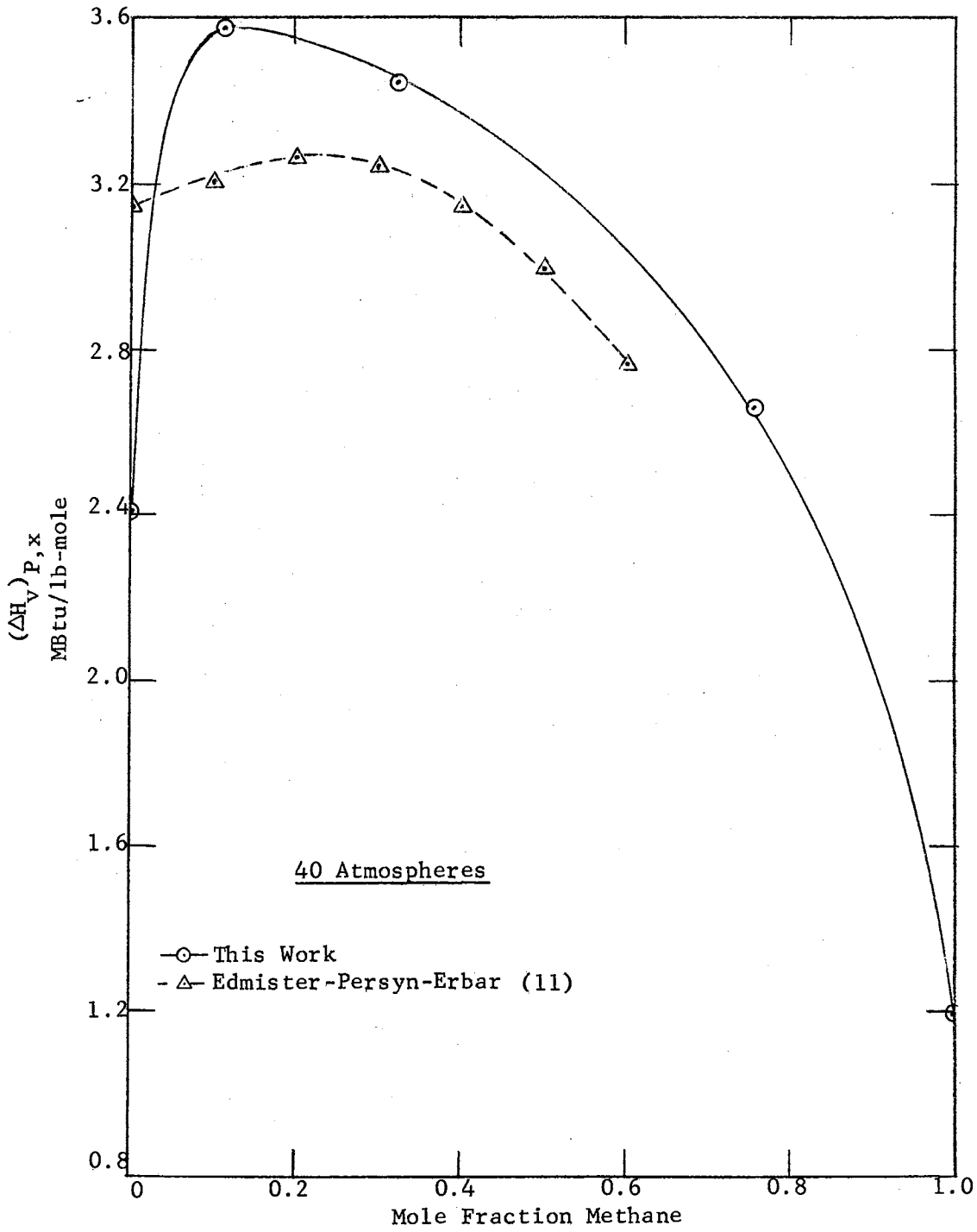

Figure 25

Isobaric Integral Heat of Vaporization, Methane-Ethylene, 40 atmospheres

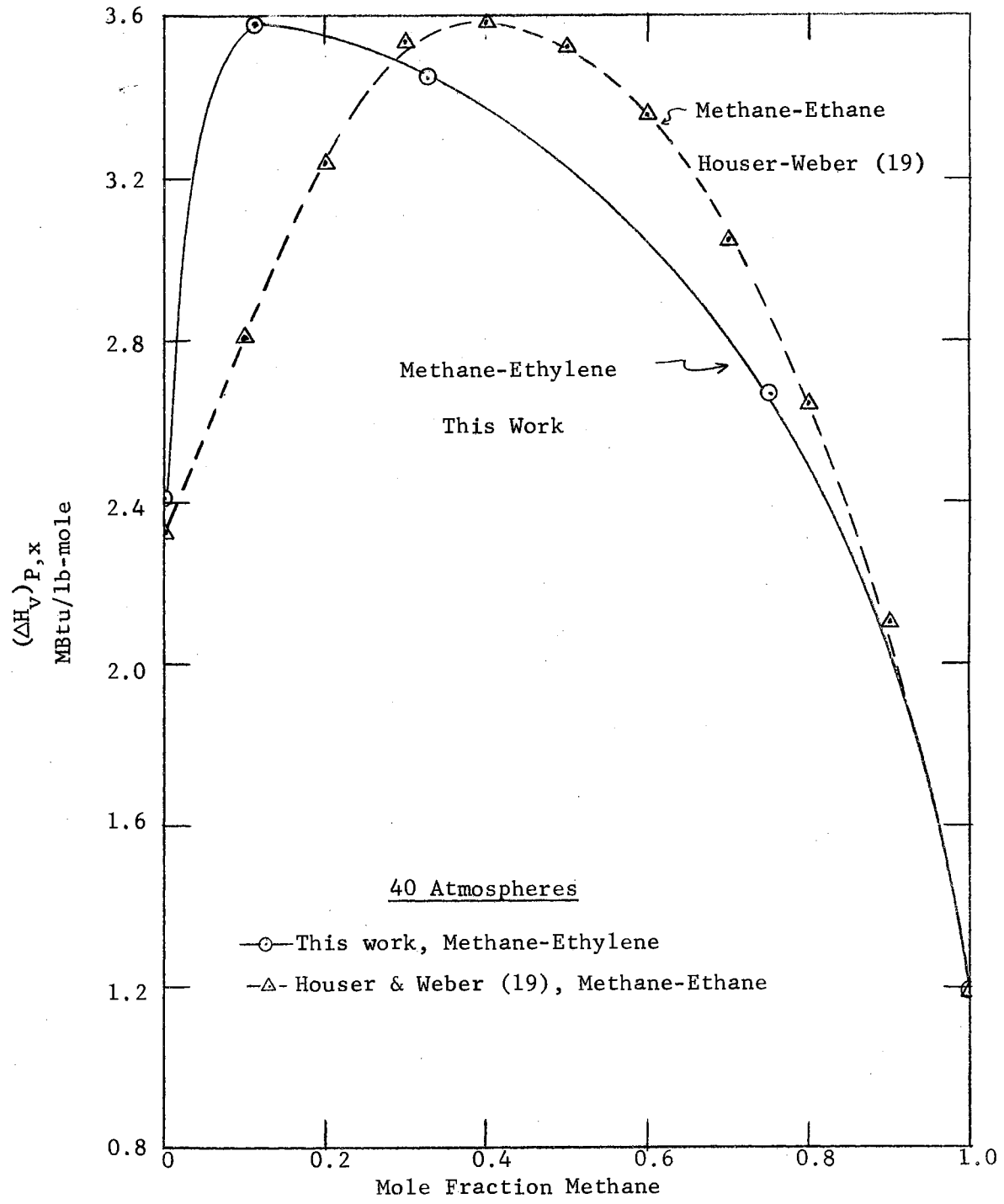

Figure 26

Comparison of Isobaric Integral Heats of Vaporization of Methane Binaries of Ethylene and Ethane at 40 Atmospheres

derived in Chapter II, and (3) a modified form of the Thompson-Edmister test, derived in Appendix J. Each test compares vapor-liquid equilibria (VLE) data with enthalpy data. The enthalpy data obtained in the calorimeter are the isobaric integral heats of vaporization, $(\Delta H_v)_{P,x}$ or $(H_y^V - H_x^L)_P$. The enthalpy values required for the tests are some form of the equilibrium enthalpy difference, $(H_y^V - H_x^L)_{P,T}$. The conversion of the experimental data to the necessary forms is treated in Appendix F. Each test was made in differential and integral form. A comparison is made of the different tests.

Thompson-Edmister Test

The Thompson-Edmister (45) consistency test, as given by Equations 138 and 139, requires the calculation of an enthalpy difference term ΔH^*, as defined by Equations 136 and 137. Since this term involves H^V and $\bar{H}_1^V$, the effect of the shape of the H-y (enthalpy-composition) diagram was studied first.

The saturated vapor enthalpy as a function of composition was calculated by four different methods, the Redlich-Kwong (30) equation of state, the Pitzer, et al. (23) tables, the Yen-Alexander equations (49), and the Benedict-Webb-Rubin (BWR)(4) equation of state. The results are given in Table VI-A and plotted in Figures 27 and 29. A least-squares quadratic curve was passed through the data, and the values of $\Delta H^*/RT^2$ calculated by the method described in Appendix F. The values of $\Delta H^*/RT^2$ vs. T are given in Table VI-B and plotted in Figures 28 and 30.

The Thompson-Edmister (45) test was then carried out in differential and integral form using IBM 1620 computer programs listed in Appendix M, Programs III, IV, and V. The results are tabulated in Table VII. Since

TABLE VI-A

VALUES OF H^V CALCULATED BY DIFFERENT METHODS
(MBtu/lb-mole)

Vapor Composition, Mole Fraction Methane	Method			
	Redlich-Kwong(30)	Pitzer, et al.(23)	Yen-Alexander(49)	Benedict-Webb-Rubin(4)
		20 Atmospheres		
.0	3.028	3.144	2.855	2.797
.137	2.803	2.933		2.846
.20			2.736	
.40			2.625	
.436	2.395	2.818		2.713
.60			2.475	
.756	2.094	2.570		2.515
.80			2.266	
1.0	1.903	2.369	1.870	1.837
		40 Atmospheres		
.0	2.669	3.050	2.422	2.442
.0932	2.794			
.112		2.600		2.339
.20			2.300	
.322	2.856			
.327		2.699		2.467
.40			2.171	
.60			2.009	
.752		2.517		2.402
.778	2.296			
.80			1.713	
1.0	1.511	1.951	1.488	1.601

TABLE VI-B

VALUES OF $\Delta H^*/RT^2$ [1/] USING DIFFERENT VALUES FOR H^V
($(°K^{-1})\times10^3$)

Composition, Mole Fraction Methane			Method for Calculating H^V			
x_1	y_1	T, °K	Redlich-Kwong(30)	Pitzer, et al.(23)	Yen-Alexander(49)	Benedict-Webb-Rubin(4)
			20 Atmospheres			
.0	.0	244.6	18.320	18.320	18.320	18.320
.137	.408	226.8	24.923	25.520	25.440	25.798
.436	.752	199.4	29.000	29.150	29.882	31.045
.756	.942	176.5	30.394	30.600	30.933	30.222
1.0	1.0	166.2	24.485	24.480	24.480	24.480
			40 Atmospheres			
.0	.0	272.0	9.100	9.100	9.100	9.100
.112	.364	253.7	16.231	16.720	15.687	16.600
.327	.685	235.3	19.008	17.950	17.737	19.214
.752	.928	199.4	19.255	17.720	18.827	17.927
1.0	1.0	186.8	9.658	9.658	9.658	9.658

1/ $\Delta H^* = \frac{H^V}{K_2} + y_1\bar{H}_1^V\left(\frac{1}{K_1} - \frac{1}{K_2}\right) - H^L$, Equations 136 and 137.

For pure components $= \Delta\bar{H}_i$, Equation 133.

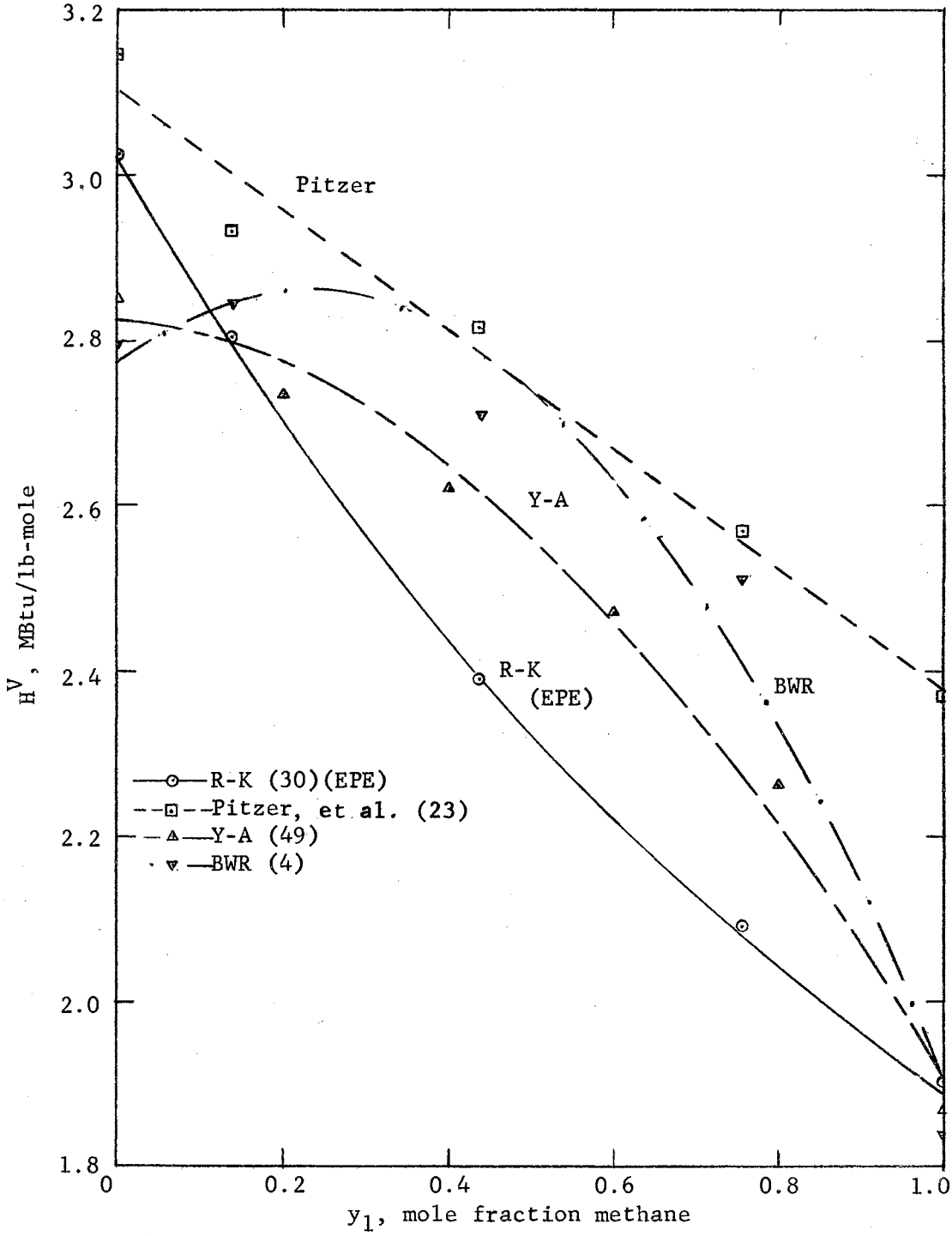

Figure 27

H^V vs. y_1, 20 Atmospheres

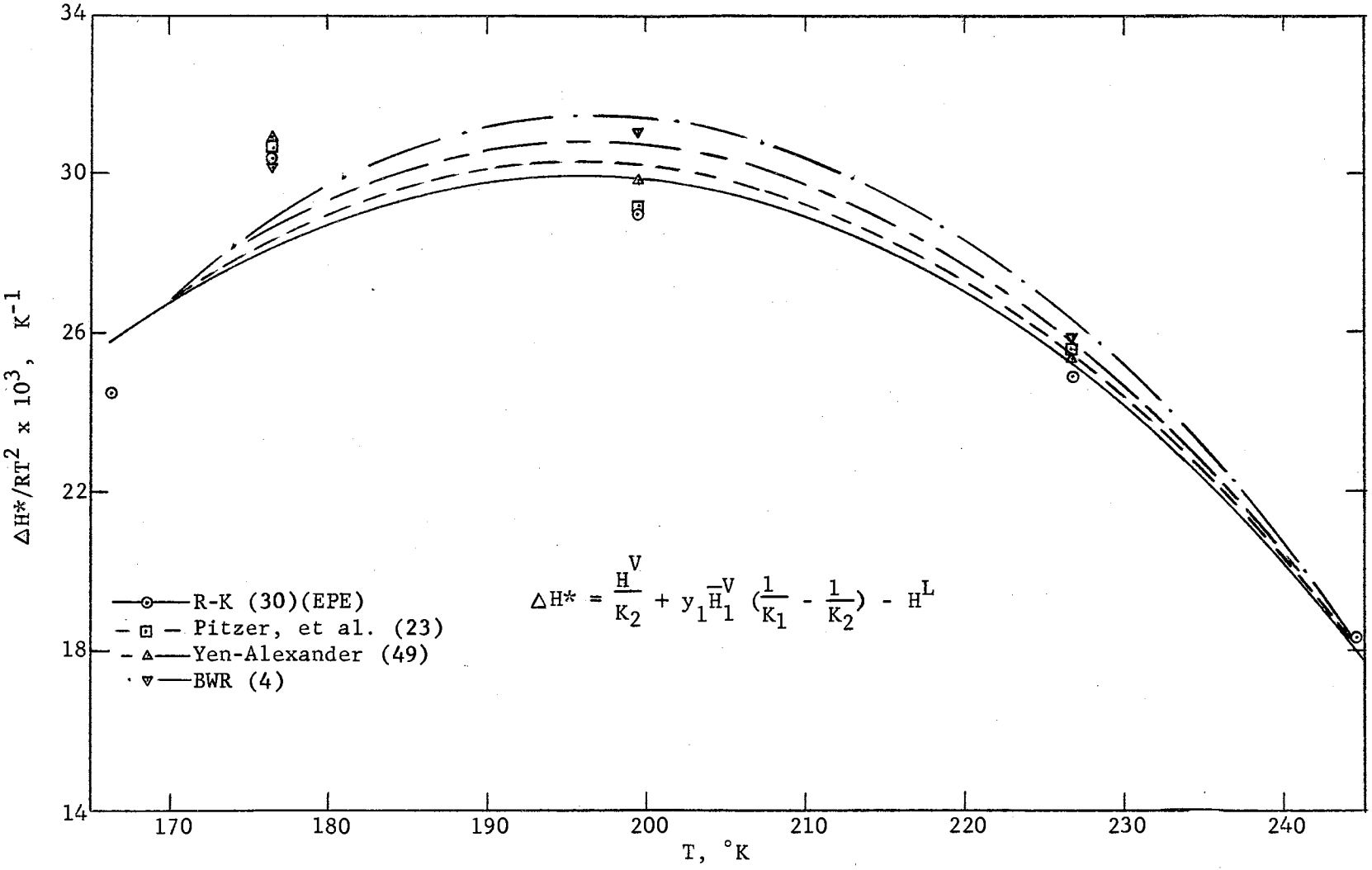

Figure 28

$\Delta H^*/RT^2$ vs. T, 20 Atmospheres

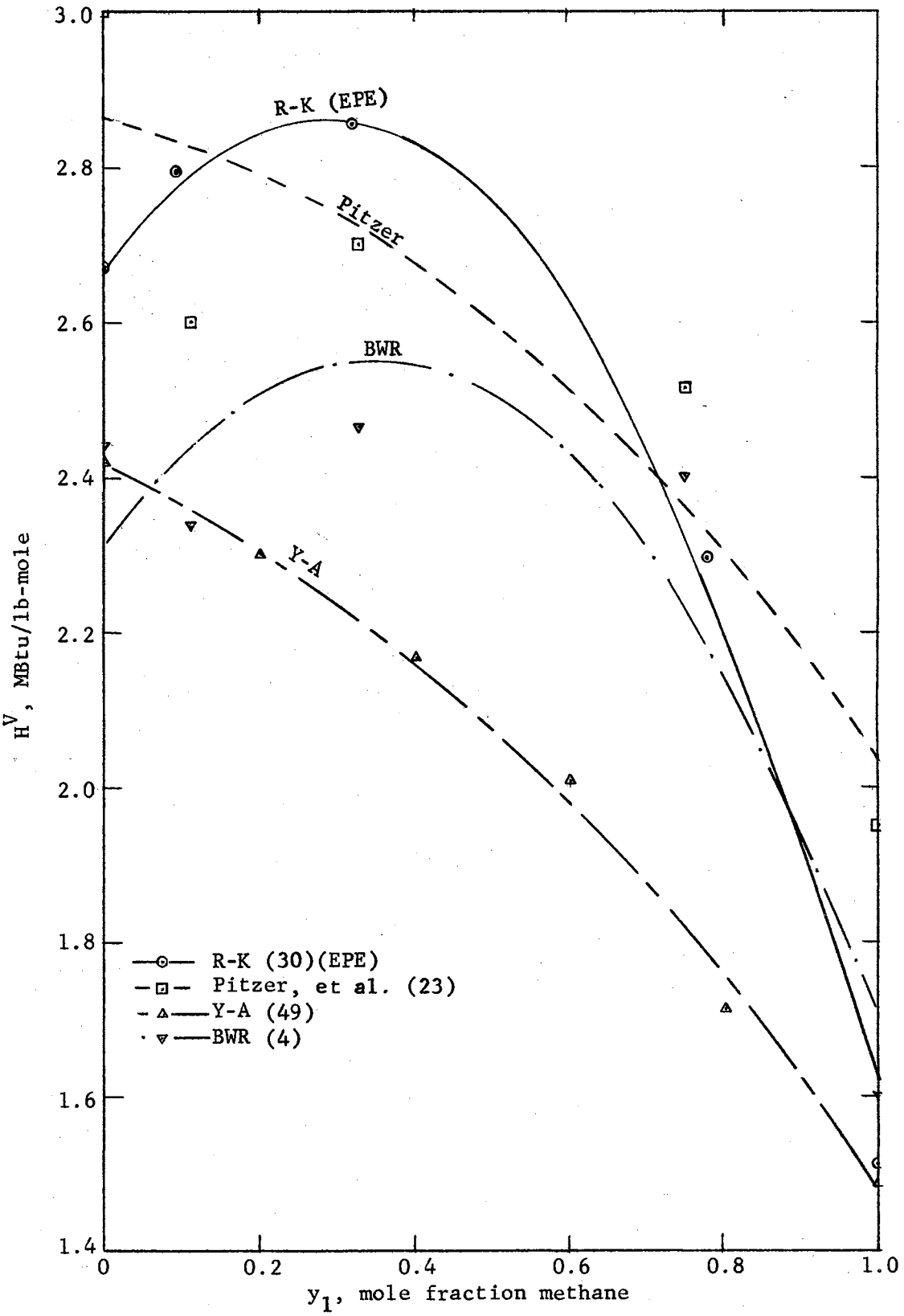

Figure 29

H^V vs. y_1, 40 Atmospheres

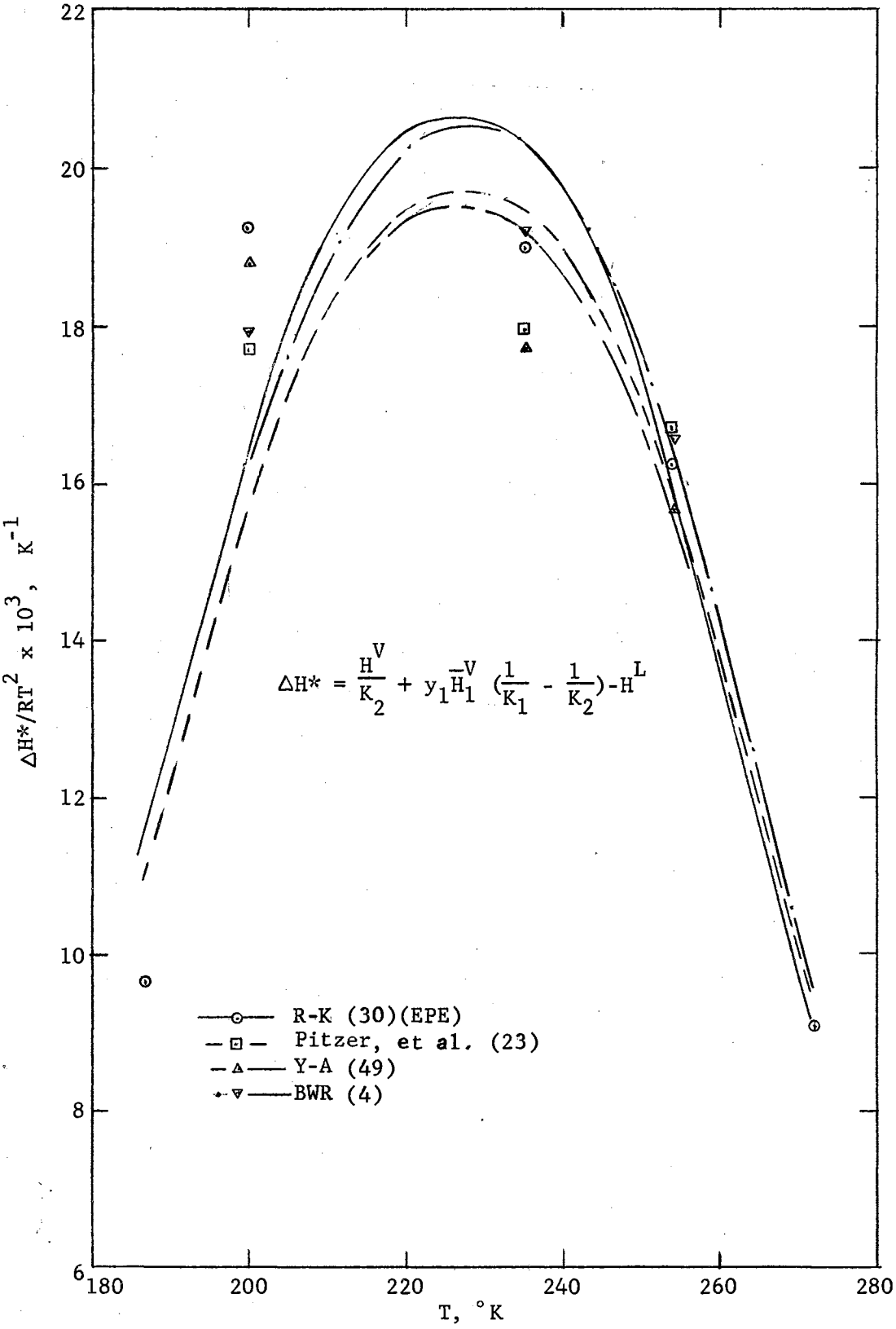

Figure 30

$\Delta H^*/RT^2$ vs. T, 40 Atmospheres

TABLE VII

THOMPSON-EDMISTER CONSISTENCY TEST USING DIFFERENT METHODS FOR CALCULATING H^V

	Method			
	Redlich-Kwong(30)	Pitzer, et al.(23)	Yen-Alexander(49)	Benedict-Webb-Rubin(4)
		Differential, 20 Atmospheres		
Run 36	15.9%	13.6%	13.9%	12.5%
43	10.9	10.4	7.8	4.0
42	10.7	10.0	8.9	11.3
Avr.	12.5%	11.3%	10.2%	9.3%
Std. Error	± 2.9%	± 2.6%	± 1.2%	± 2.5%
		Differential, 40 Atmospheres		
Run 40	-15.5%	-18.5%	-11.9%	-17.8%
41	- 7.1	- 1.1	+ 0.2	- 8.2
37	- 5.6	+ 3.2	- 3.3	+ 2.0
Avr.	- 9.4%	- 5.5%	- 5.0%	- 8.0%
Std. Error	± 5.3%	± 6.0%	± 2.5%	± 5.3%
		Integral, 20 Atmospheres		
	14.9%	15.8%	16.8%	17.9%
		Integral, 40 Atmospheres		
	0.8%	- 3.6%	- 3.8%	- 0.3%

the results did not differ as much as had been anticipated, the Redlich-Kwong (30) equation as utilized in the EPE (11, 12) method was selected as the most suitable. The Pitzer, et al. (23) tables required too many hand calculations, the Yen-Alexander (49) equations were based on a generalized approach, and the constants for the BWR equation were not determined for the temperature range of greatest interest.

The partial derivatives were determined by passing the best least-squares straight line through the experimental Ln K_i vs. (1/T) data. The line was constrained to pass through 0 at the bubble point temperature of component 1, since K_1 must be 1 (or ln K_1 must be 0) at this point. These data are plotted in Figures 31 through 34. The results of the differential test are given in Table VIII.

The positive average difference of 12.5% ± 2.9% at 20 atmospheres indicates that the experimental enthalpy values are high by 10 to 15%. In order to verify that the error was in the enthalpy and not in the VLE data, the slopes of the Ln K_i vs. (1/T) straight lines were determined for the data of Guter, et al. (15). The slopes were in close enough agreement to conclude that the discrepancy could be attributed primarily to the enthalpy determination.

The high experimental value of $(\Delta H_v)_{P,x}$ at 20 atmospheres is attributed to two factors, insufficient sample and insufficient heat leak correction. At 20 atmospheres, the 1/8" I.D. tubing between the internal and external condenser is not quite large enough to carry all of the vaporized sample. Consequently, some condensation occurs in the equilibrium cell. The heat leak determination was made on pure ethylene at temperatures above any of those encountered in the 20 atmosphere runs

TABLE VIII

RESULTS OF THOMPSON-EDMISTER DIFFERENTIAL CONSISTENCY TEST

Run	Experimental[1] T, K	Mole Fraction Methane x_1	y_1	ξ_1[2]	$\frac{\partial \ln K_1}{\partial(1/T)}$[3]	$\frac{\partial \ln K_2}{\partial(1/T)}$	Left Hand Side[4]	Right Hand Side[5]	% Diff.[6]
					20 Atmospheres				
36	226.8	.137	.408	.4224	-758.6	-944.7	-3854	-4585	15.9
43	199.4	.436	.752	.2519	-758.6	-944.7	-3673	-4124	10.9
42	176.5	.756	.942	.0549	-758.6	-944.7	-3024	-3386	10.7
								Avr.	12.5%
							Std. Estimate of Error		±2.9%
					40 Atmospheres				
40	253.7	.112	.364	.6119	-678.9	-1025.5	-4315	-3737	-15.5
41	235.3	.327	.685	.3439	-678.9	-1025.5	-4031	-3764	- 7.1
37	199.4	.752	.928	.0612	-678.9	-1025.5	-2891	-2738	- 5.6
								Avr.	- 9.4%
							Std. Estimate of Error		±5.3%

1/ See Table II.
2/ See Appendix L.
3/ This work. See Appendix F, Tables F-III and F-IV.
4/ See Equation 138.
5/ See Appendix F, Table F-V.
6/ % Diff. $= \left(\frac{\text{Right Side - Left Side}}{\text{Right Side}}\right)100 = \left(\frac{\text{Exp. - Calc.}}{\text{Experimental}}\right)100$

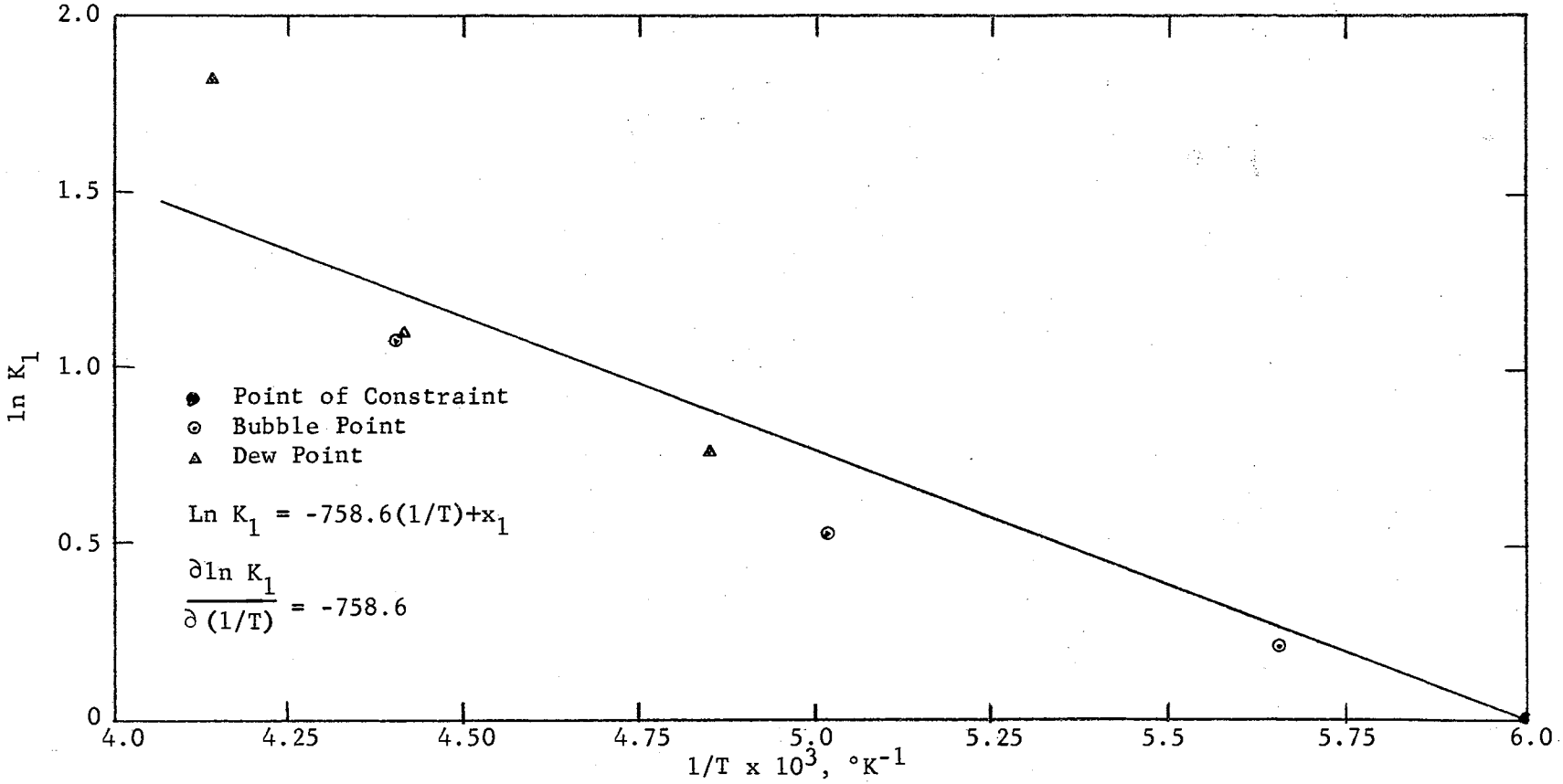

Figure 31

Ln K_1 vs. (1/T), 20 Atmospheres

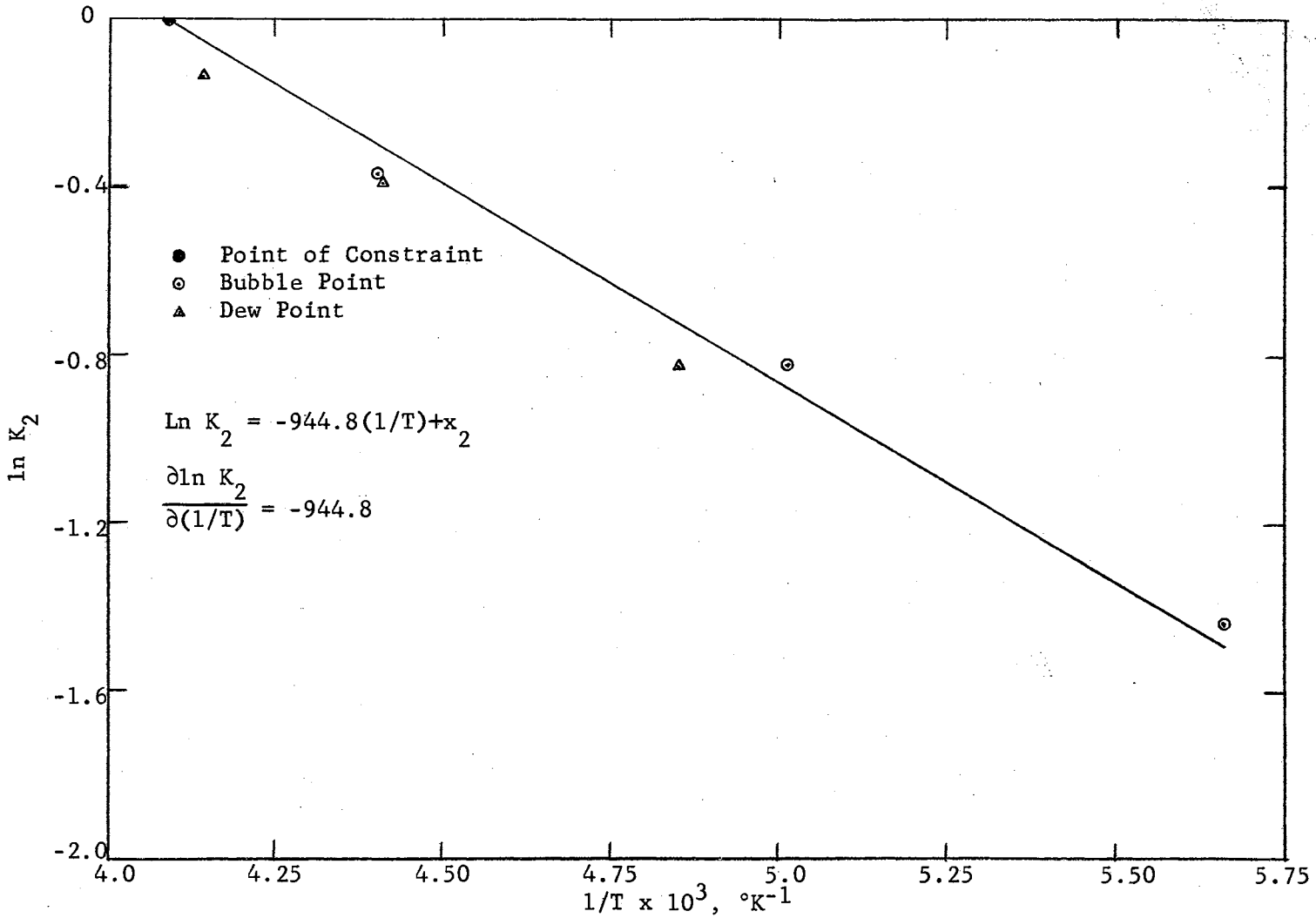

Figure 32

Ln K_2 vs. 1/T, 20 Atmospheres

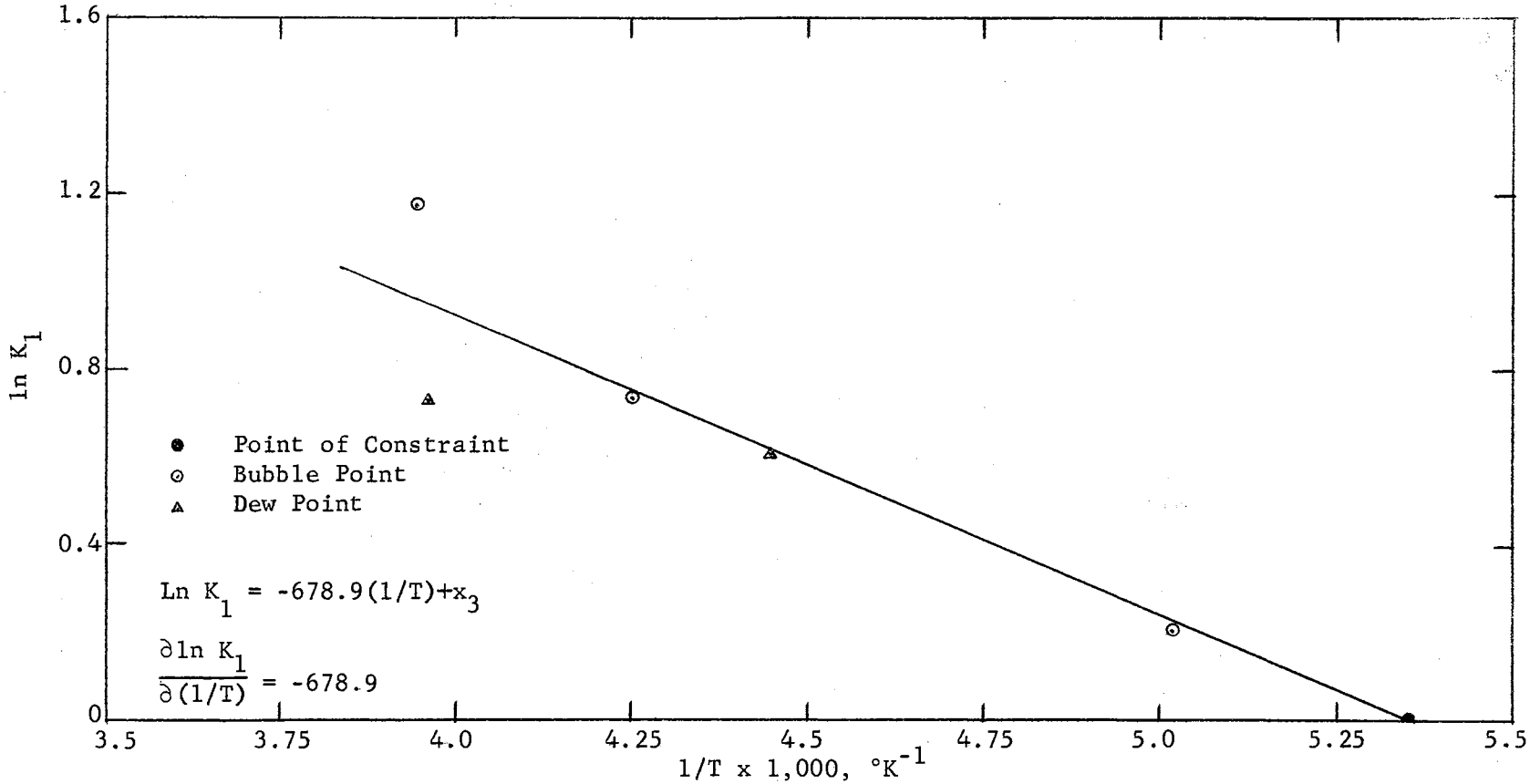

Figure 33

Ln K_1 vs. 1/T, 40 Atmospheres

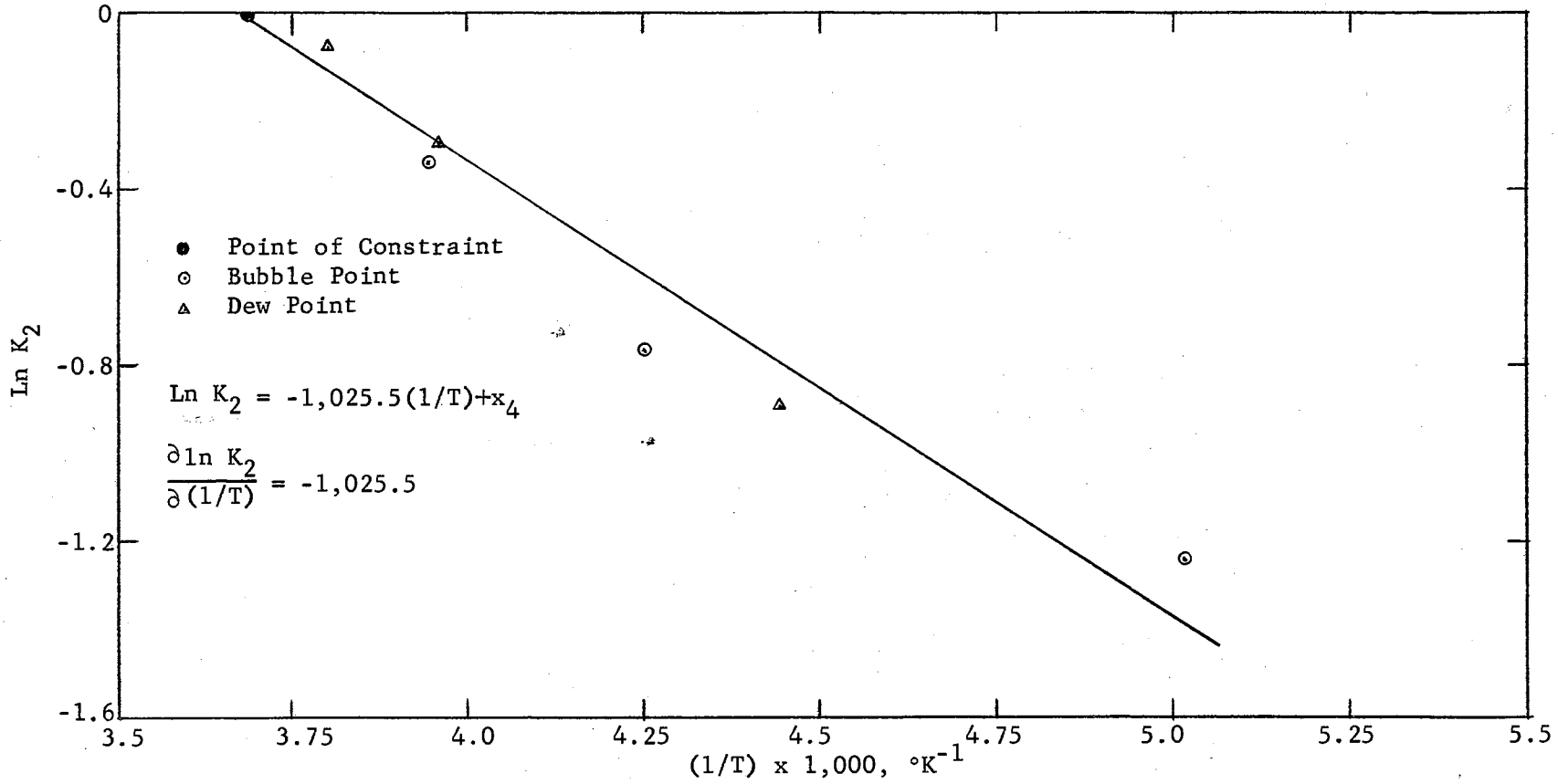

Figure 34

Ln K_2 vs. (1/T), 40 Atmospheres

(≈260° K vs. 226.8° K). It is possible that the heat leak is a function of temperature as well as temperature difference.

At 40 atmospheres, the negative average difference of 9.4% ± 5.3% indicates the experimental enthalpy values are low by that amount. This is attributed to a "thermal syphon" effect. (At this higher pressure, the 1/8" I.D. tubing is adequate to carry the vapors to the external condenser.) During the investigation, it was noted that it was possible to transfer liquid mixture (in vapor form) from the calorimeter to the external condenser by merely having the latter slightly sub-cooled below the bubble point temperature in the calorimeter. This temperature difference alone was enough to transfer the mixture, hence "thermal syphon". The temperatures encountered at 40 atmospheres coincide more closely with the heat leak correction temperatures (≈260° K vs. 253.7° K), so the correction factor is better at 40 atmospheres than it is at 20 atmospheres.

The sensitivity of the differential test to changes in the values of the isobaric integral heat of vaporization and vapor-liquid equilibria compositions was tested. The heats of vaporization were reduced by 10 per cent; liquid compositions were decreased by 1.5 mole per cent, the deviation in composition analysis; vapor compositions were increased by the same amount, producing the maximum possible error in K_1. The consistency tests were repeated using three combinations of these changes, namely enthalpy change, composition change, and enthalpy-and-composition change combined. The results are given in Table IX.

TABLE IX

SENSITIVITY OF DIFFERENTIAL CONSISTENCY TEST

Change	20 Atm.	40 Atm.
Original Data	12.5%	- 9.4%
Enthalpy, -10%	0.4%	-21.3%
Composition, 1.5%	3.5%	-38.0%
Combined	-10.1%	-47.9%

The test is more sensitive to composition changes (or errors) than to enthalpy changes. A 10 per cent change in enthalpy produced a 12 per cent change in the results. A 1.5 mole per cent change in composition produced a 9 per cent change in the results at 20 atmospheres and a 30 per cent change at 40 atmospheres. The slope of the ln K_2 vs. (1/T) curve is very sensitive to errors. Composition and negative enthalpy errors are additive.

The integral form of the Thompson-Edmister (45) consistency test was also applied to the experimental data of this investigation. The curves for integration are plotted in Figures 35 through 40. The results are given in Table X. A listing of the source program is given in Appendix M, Program V.

While the differential test is a point-by-point test, and as such is more sensitive to experimental errors, the integral test averages the results and smooths out the errors. Nevertheless, there should be some quantitative agreement between the average results of the differential test and the integral test of the same data. This agreement is good (12.5% vs. 14.9%) at 20 atmospheres and not so good (-9.4% vs. 0.8%) at 40 atmospheres. This is attributed to inconsistencies between the

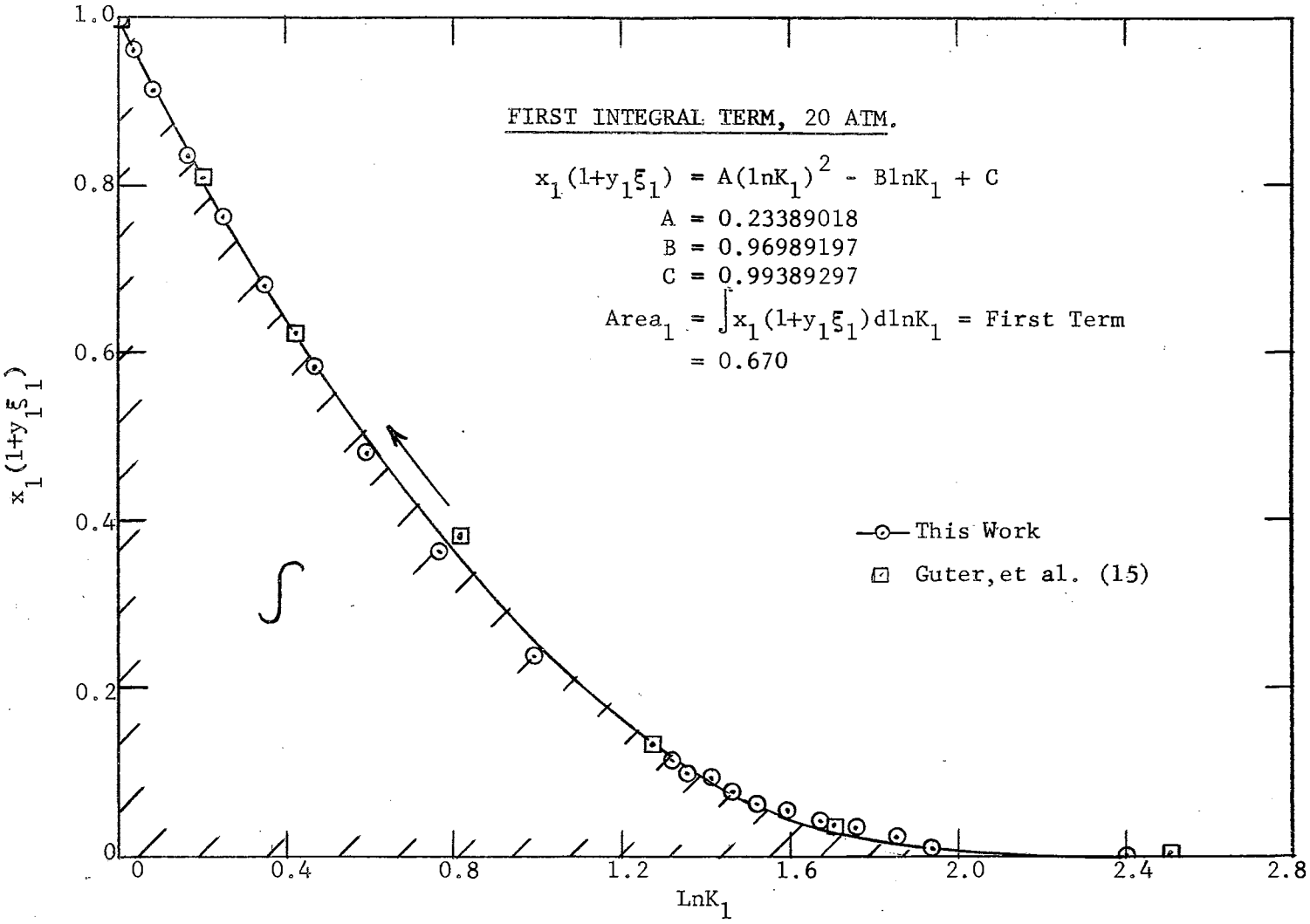

Figure 35

$x_1(1+y_1\xi_1)$ vs. $\ln K_1$, 20 Atmospheres

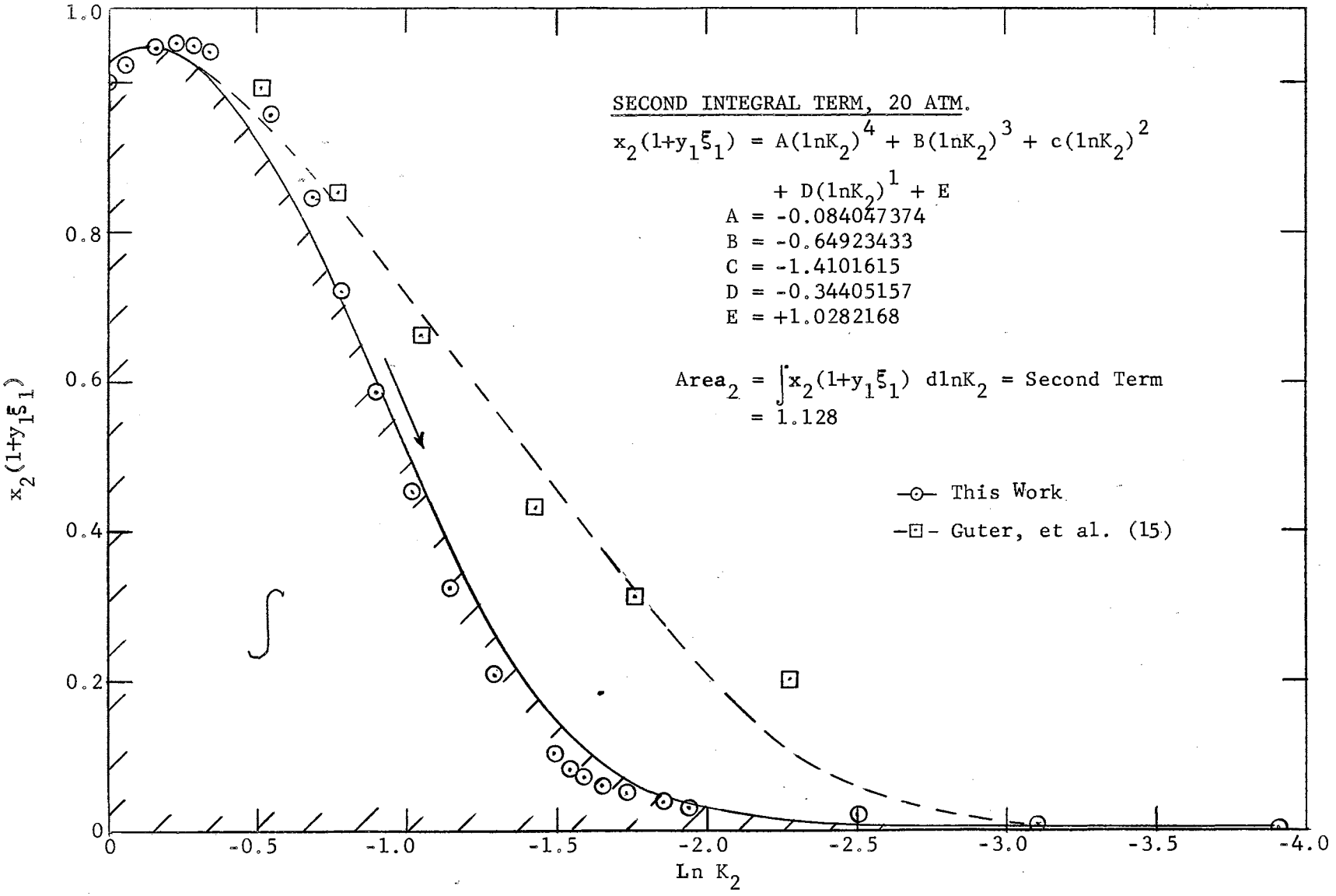

Figure 36

$x_2(1+y_1\xi_1)$ vs. $\ln K_2$, 20 Atmospheres

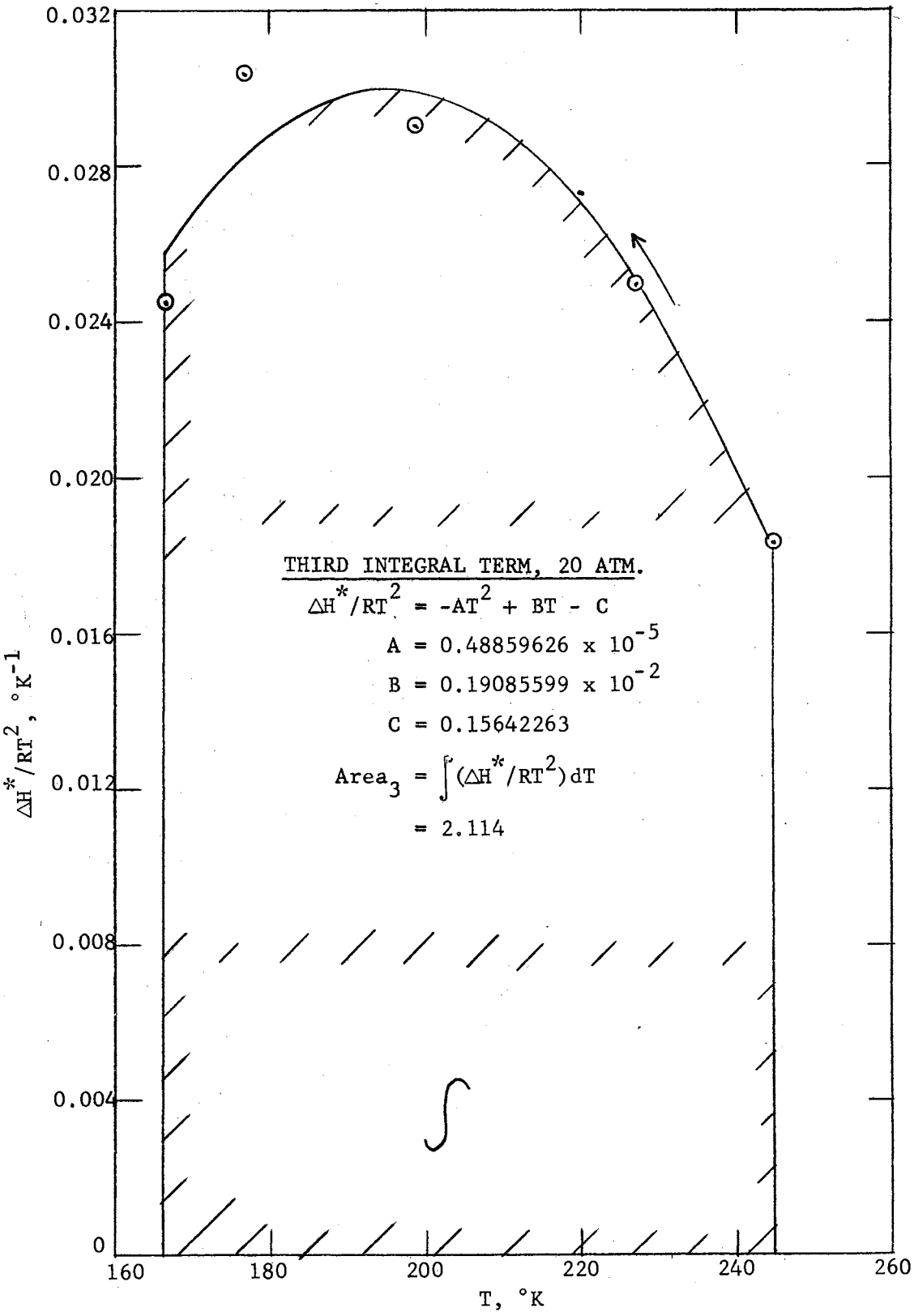

Figure 37

$\Delta H^*/RT^2$ vs. T, 20 Atmospheres

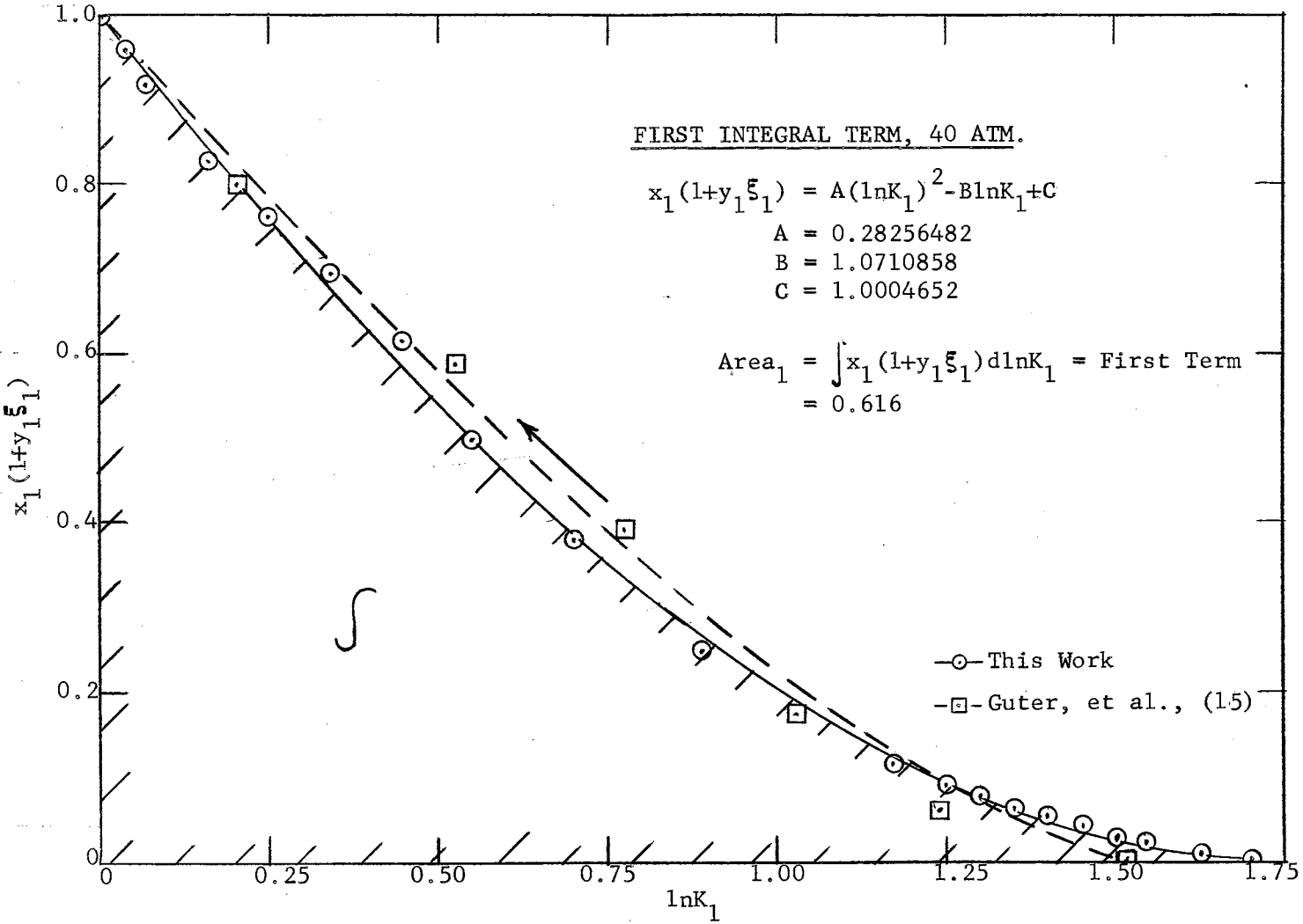

Figure 38

$x_1(1+y_1\xi_1)$ vs. Ln K_1, 40 Atmospheres

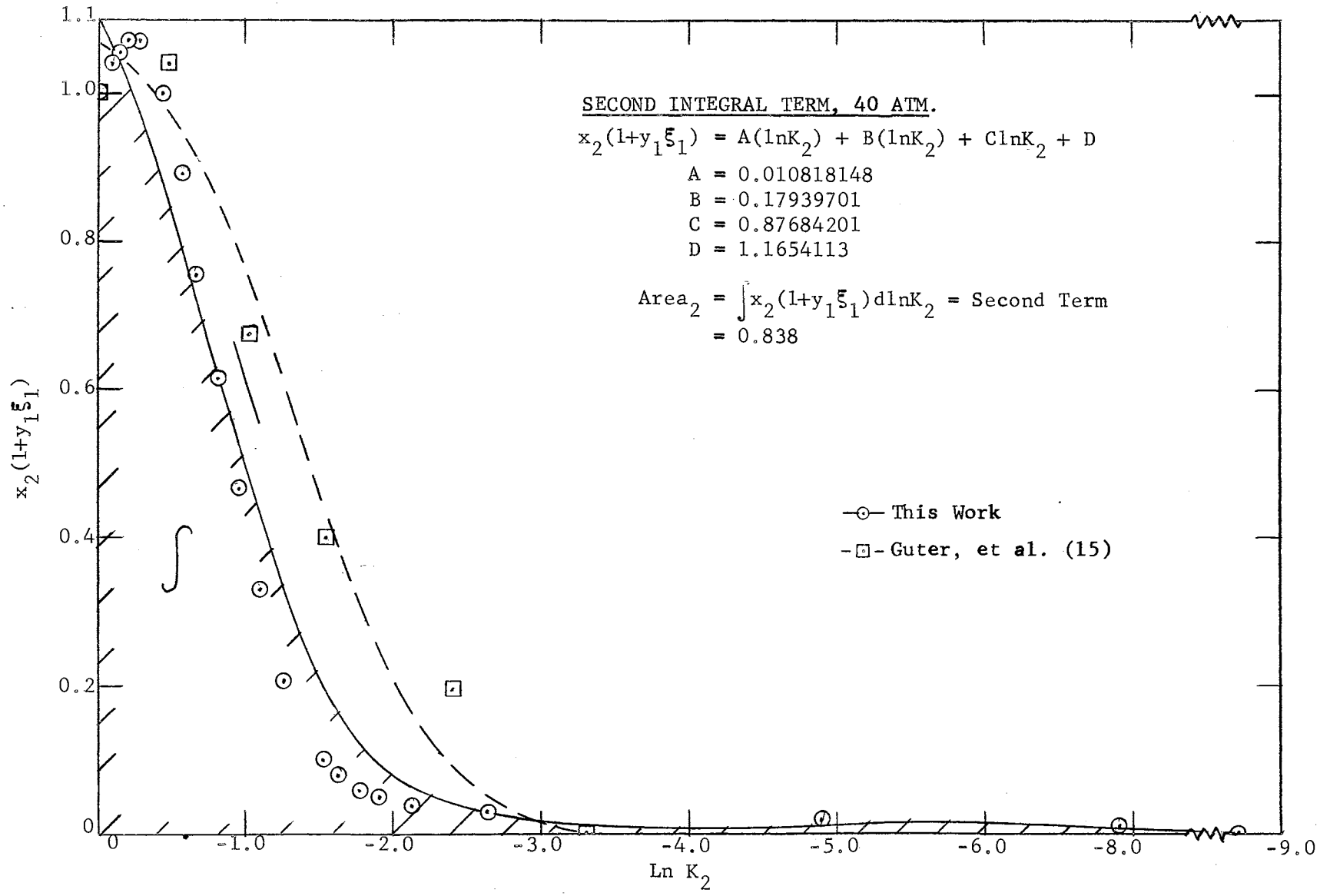

Figure 39

$x_2(1+y_1\xi_1)$ vs. $\text{Ln}K_2$, 40 Atmospheres

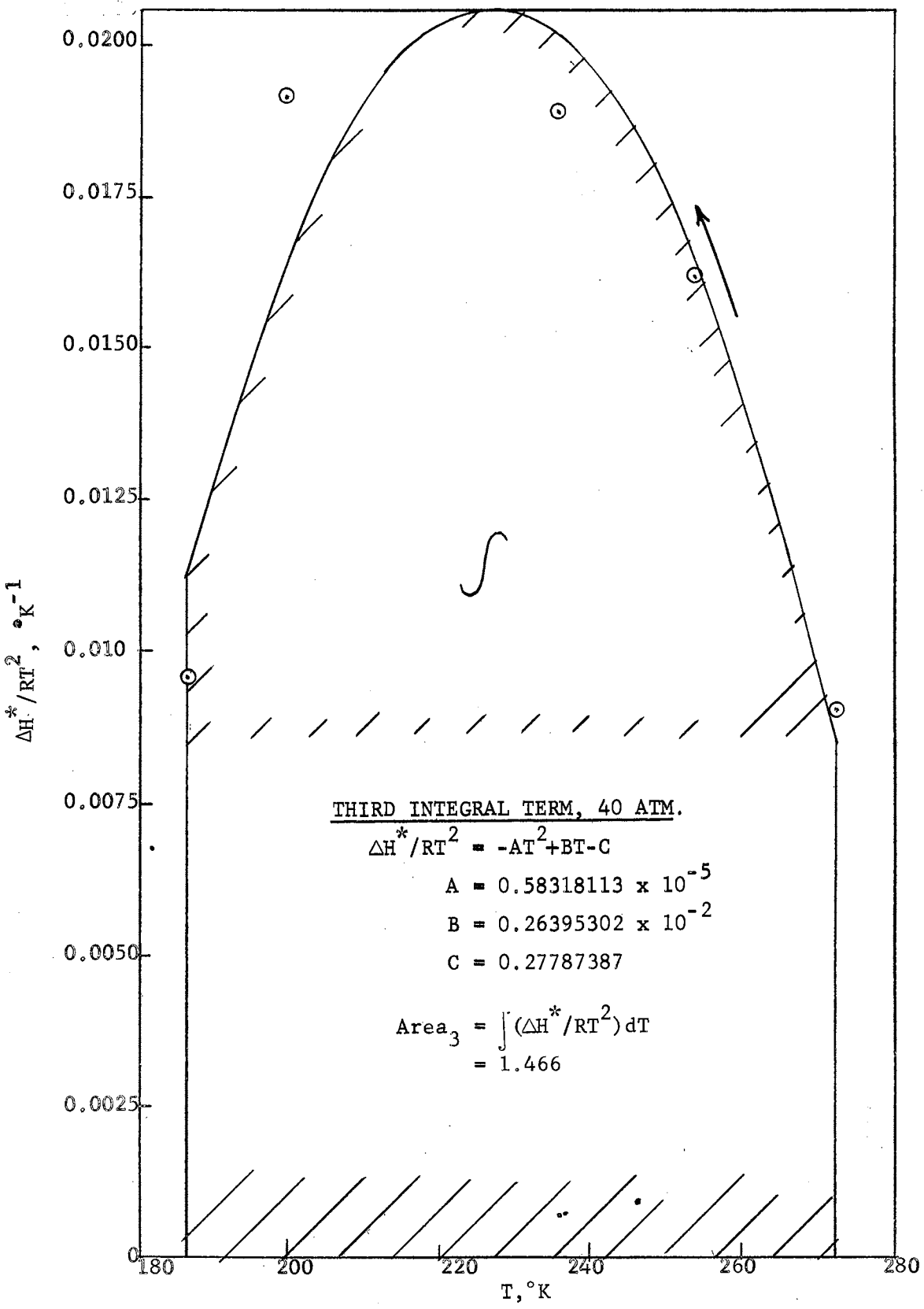

Figure 40

$\Delta H^*/RT^2$ vs. T, 40 Atmospheres

TABLE X

RESULTS OF THOMPSON-EDMISTER INTEGRAL CONSISTENCY TEST

First Term, Left Side[1/] Limits, LnK_1			Second Term, Left Side Limits, LnK_2			Area 1 Plus	Third Term, Right Side Limits, °K			Percent[2/]
Upper	Lower	Area 1	Upper	Lower	Area 2	Area 2	Upper	Lower	Area 3	Difference
					20 Atmospheres					
0	2.4	0.670	-3.9	0	1.128	1.798	166.2	244.6	2.114	14.9
					40 Atmospheres					
0	1.7	0.616	-8.7	0	0.838	1.454	186.8	272.0	1.466	0.8

1/ See Equation 139.
2/ Same as Table VIII.

form of data used in the differential test, Ln K_i vs. (1/T), and that used in the integral test, x_i $(1+y_1\xi_1)$ vs. Ln K_i. The Edmister (10) consistency test circumvents this difficulty, as will be discussed later.

The sensitivity of the integral form was also tested in the same manner as the differential form. Results are given in Table XI.

TABLE XI

SENSITIVITY OF INTEGRAL CONSISTENCY TEST

Change	20 Atm.	40 Atm.
Original Data	14.9%	0.8%
Enthalpy, -10%	29.0%	10.1%
Composition, 1.5%	17.7%	76.0%
Combined	32.1%	91.4%

The sensitivity of the integral form of the consistency test to deviations in enthalpy is approximately linear, as is the differential form. At 20 atmospheres, the effect of composition changes is small. At 40 atmospheres, the test is extremely sensitive to composition changes. This is caused by the extended range over which the $x_2(1+y_1\xi_1)$ vs. ln K_2 curve is integrated. This is not inherent in the test, but dependent on the equilibrium properties of the mixture. Negative enthalpy changes are additive to the composition changes, as in the differential form.

Edmister Test

More recently, Edmister (10) has developed a consistency test which eliminates the two principal difficulties encountered in the Thompson-

Edmister test. These difficulties are the determination of ξ_1 and the different forms of data required for integral test.

In the former test, ξ_1 is evaluated using a three-coefficient virial equation in Berlin form, as developed in Appendix K. This truncated expansion cannot adequately describe the complex behavior of gaseous mixtures. Any errors in ξ_1 are directly reflected in the test, due to the important part which this term plays in the test. Conversely in the Edmister test, the logarithm of the calculated fugacity coefficient ratio in Equations 27 and 28 is of little importance (-.00061, Table XII) compared to the logarithm of the observed vapor composition ratio (-.07218, ibid.).

For the former test, it is necessary to change the form of the data from Ln K_i vs. (1/T) to x_i $(1+y_1\xi_1)$ vs. Ln K_i. In the Edmister test, the Ln (ϕ_1/ϕ_2) and Ln (y_1/y_2) vs. T forms of the data are used in both the differential and integral tests. A third equation of the form (y_1-x_1) vs. T is also required for the latter. By using integration by parts, the integrations of the Edmister (10) test are carried out between limits of the same variable T, instead of the three variables, Ln K_1, Ln K_2 and T, required for the Thompson-Edmister test.

The Edmister (10) consistency test in differential and integral form was carried out on these experimental data. The data and equations are plotted in Figures 41 through 44 for the differential test and Figures 45 through 48 for the integral test. The results of the differential test are summarized in Table XII; the results of the integral test are summarized in Table XIII. The computer programs are listed in Appendix M, Programs I and II.

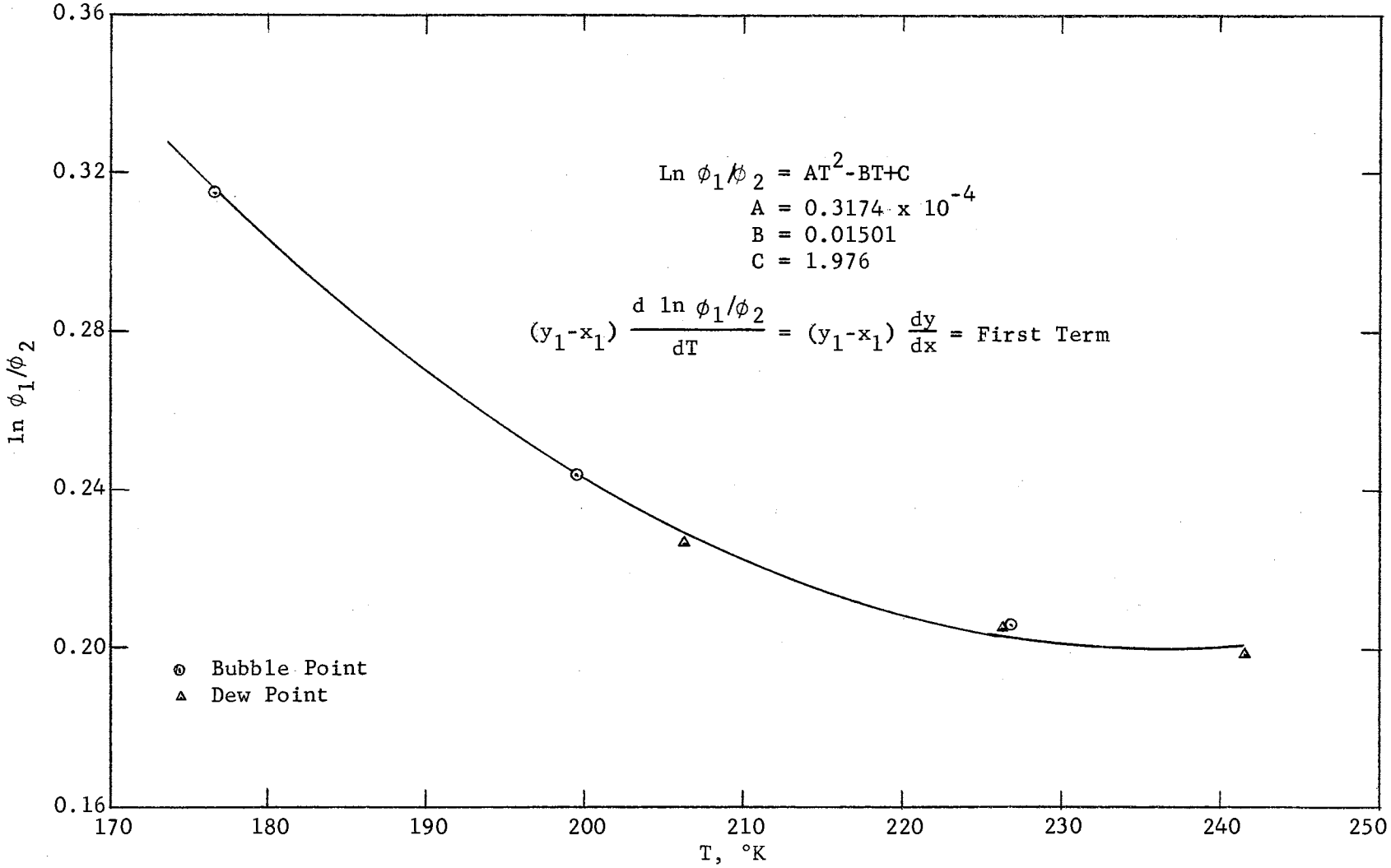

Figure 41

Ln ϕ_1/ϕ_2 vs. T, 20 Atmospheres

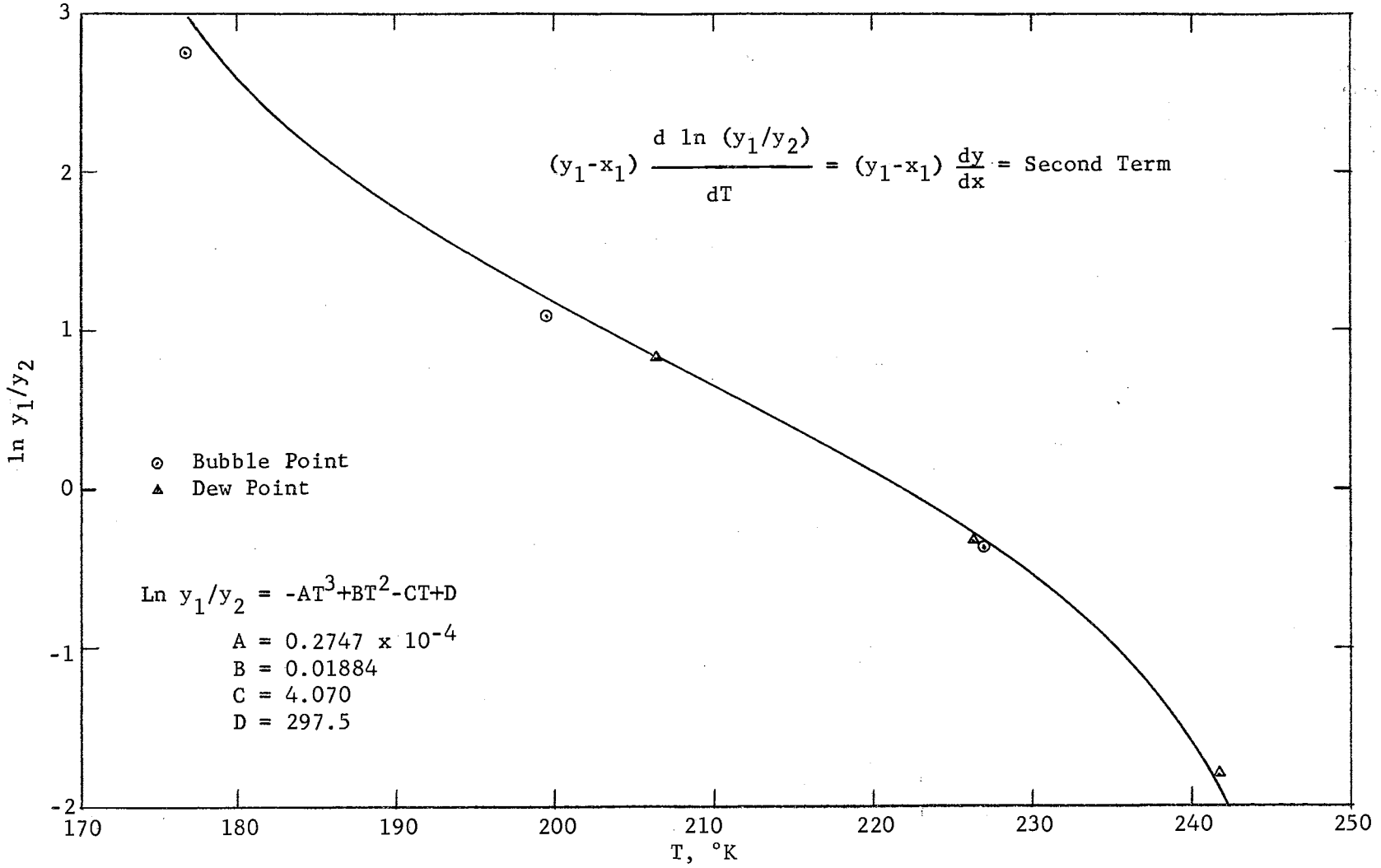

Figure 42

Ln y_1/y_2 vs. T, 20 Atmospheres

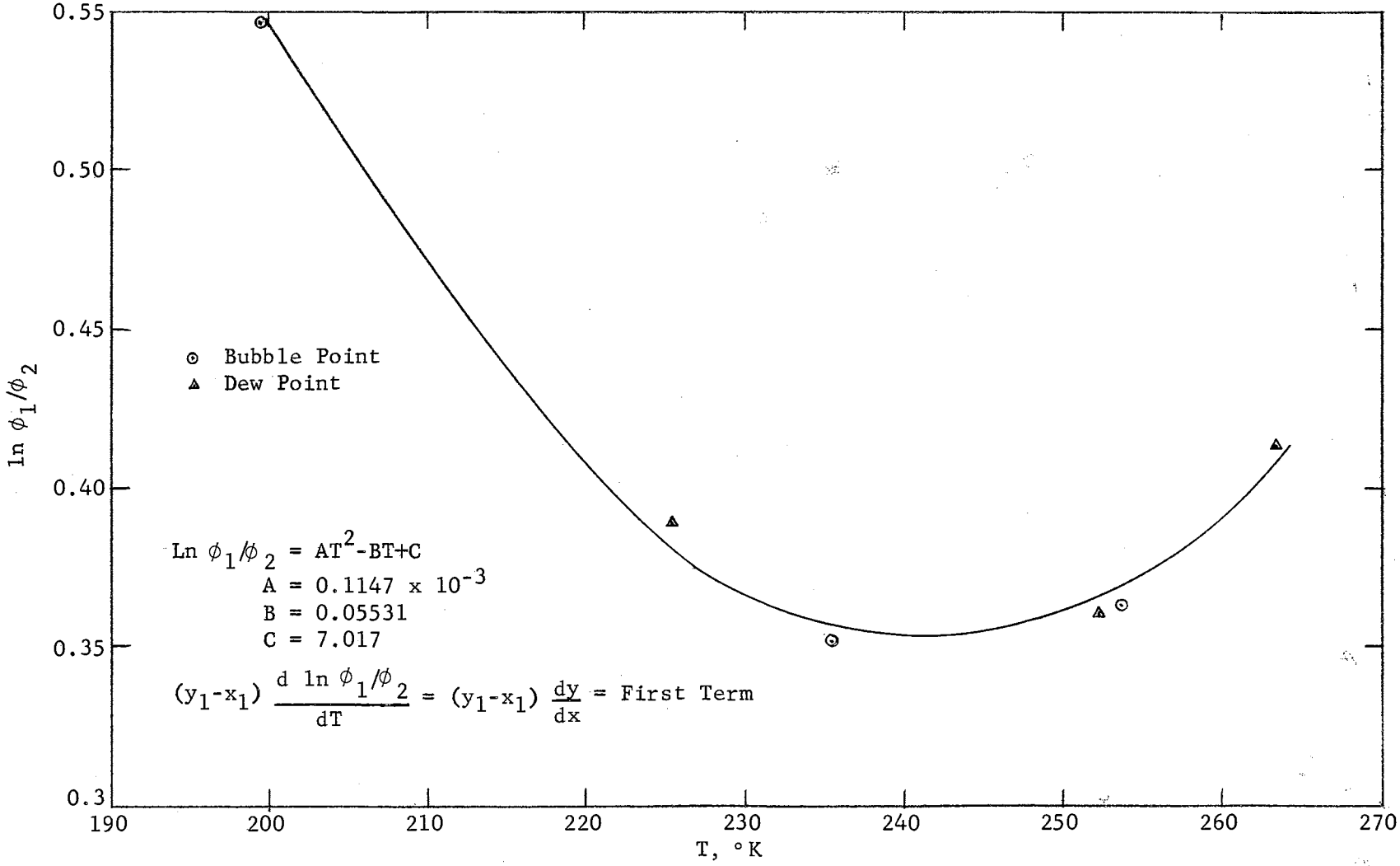

Figure 43

Ln ϕ_1/ϕ_2 vs. T, 40 Atmospheres

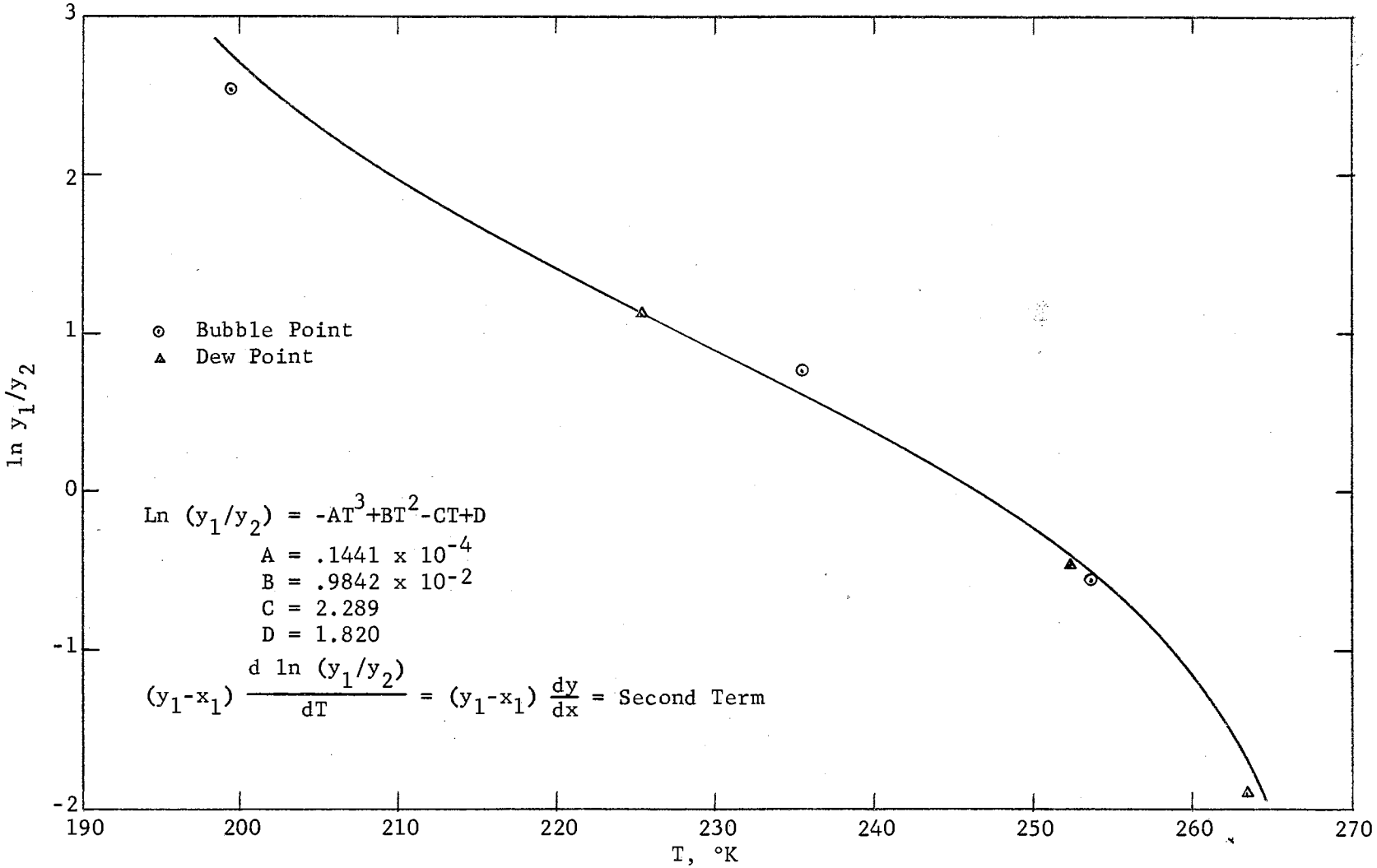

Figure 44

Ln y_1/y_2 vs. T, 40 Atmospheres

TABLE XII

RESULTS OF EDMISTER DIFFERENTIAL CONSISTENCY TEST

Run	Experimental[1] T, °K	mole fraction methane x_1	y_1	y_1-x_1	$\frac{d\ln(\phi_1/\phi_2)}{dT} \times 10^2$ [2]	$\frac{d\ln(y_1/y_2)}{dT} \times 10^2$	Left Hand Side [3] $\times 10^2$	Right Hand Side [4] $\times 10^2$	% Diff. [5]
					20 Atmospheres				
36	226.8	.137	.408	.271	-.061	-7.218	-1.972	-2.313	14.7
43	199.4	.436	.752	.316	-.235	-7.215	-2.354	-2.713	13.2
42	176.5	.756	.942	.186	-.380	-17.396	-3.306	-2.978	-11.0
									+ 5.6%
								Std. Estimate of Error	±14.4%
					40 Atmospheres				
40	253.7	.112	.364	.252	.290	-7.692	-1.865	-1.581	-18.0
41	235.3	.327	.685	.358	-.131	-5.021	-1.844	-1.544	-19.5
37	199.4	.752	.928	.176	-.955	-8.235	-1.617	-1.531	- 5.7
									-14.4
								Std. Estimate of Error	±10.7

1/ See Table II.
2/ See Appendix F, Table F-I.
3/ See Equation 27.
4/ See Appendix F, Table F-II
5/ % Diff. = $\left(\frac{\text{Right Side - Left Side}}{\text{Right Side}}\right) 100 = \left(\frac{\text{Exp. - Calc.}}{\text{Experimental}}\right) 100$

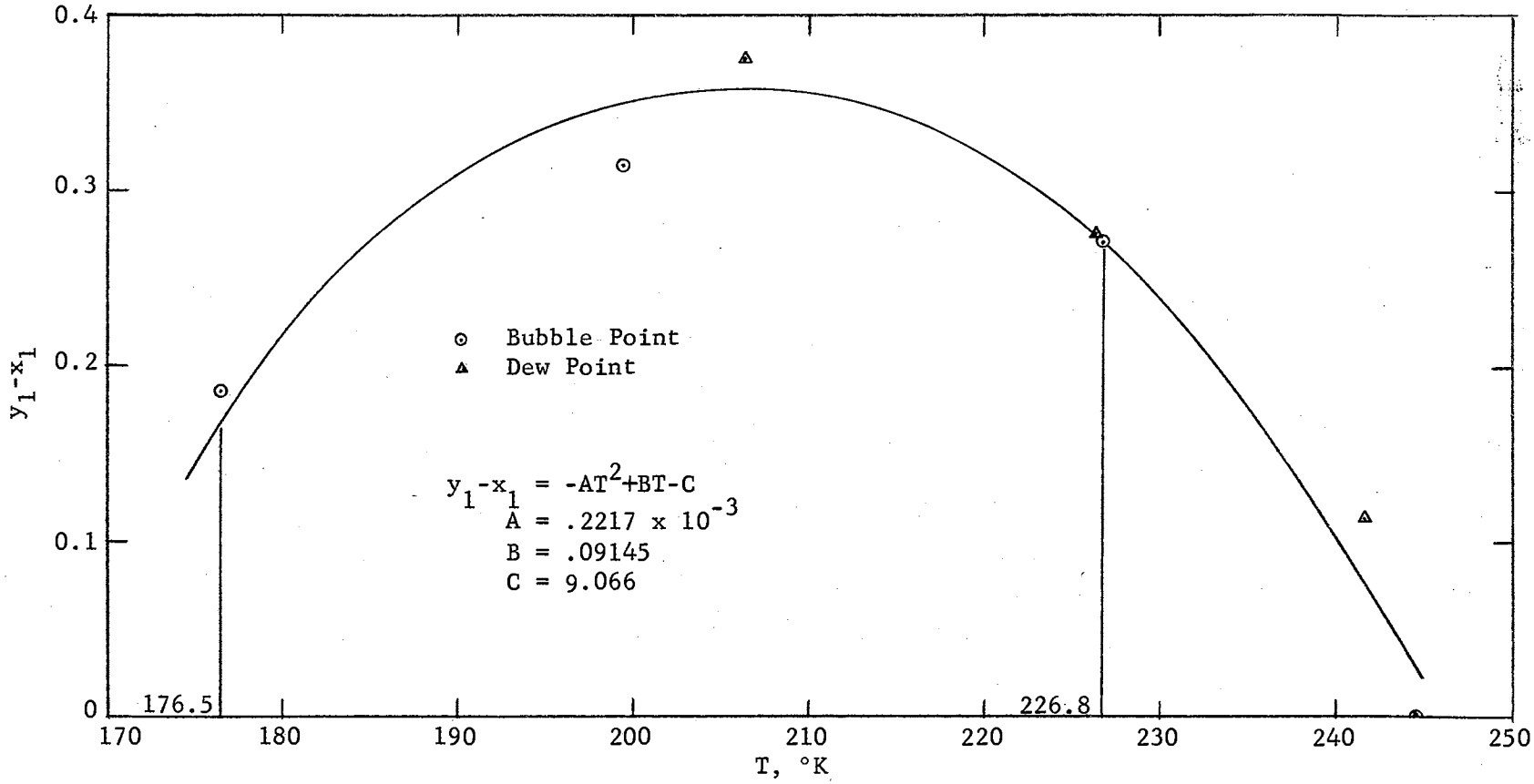

Figure 45

y_1-x_1 vs. T, 20 Atmospheres

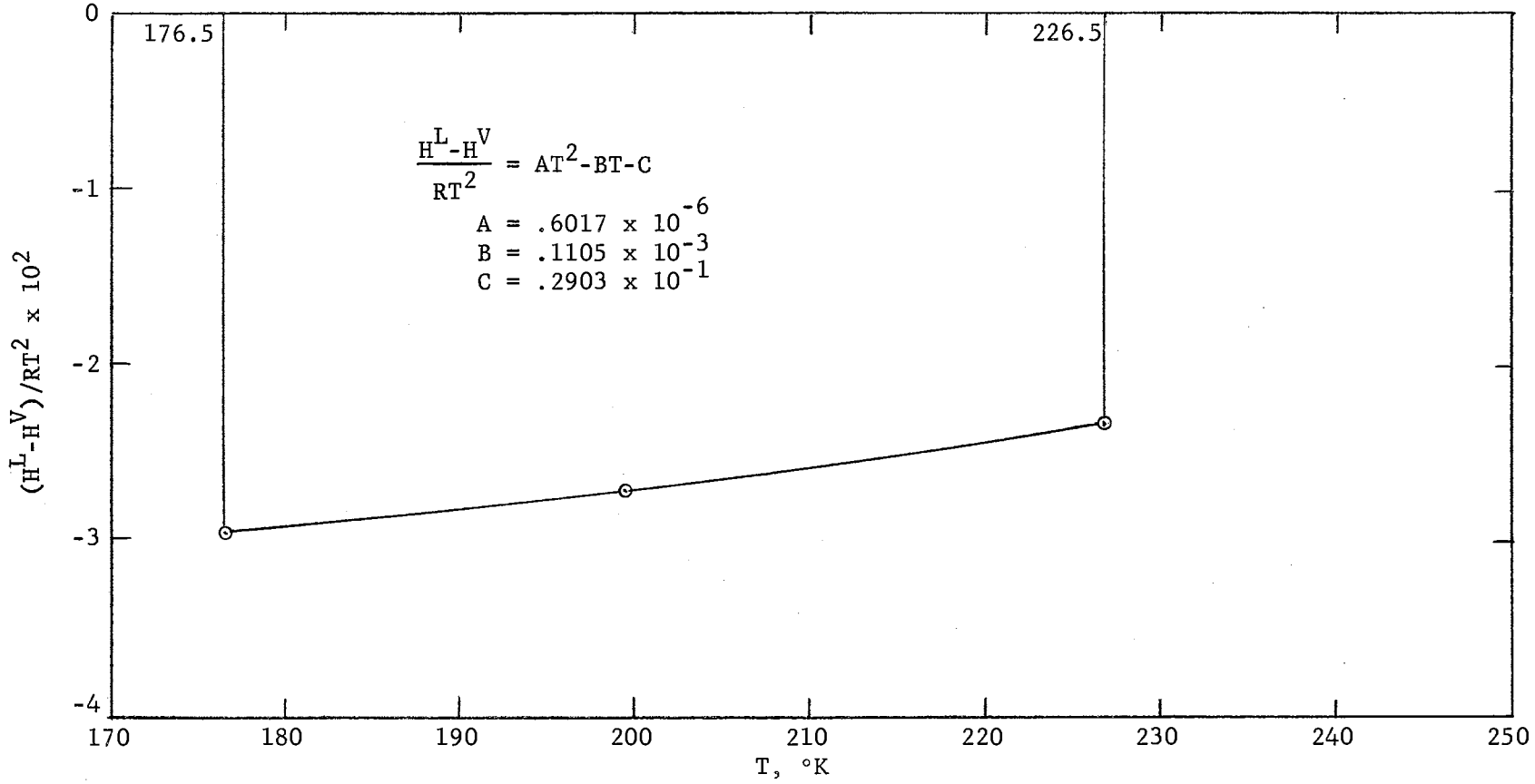

Figure 46

$(H^L-H^V)/RT^2$ vs. T, 20 Atmospheres

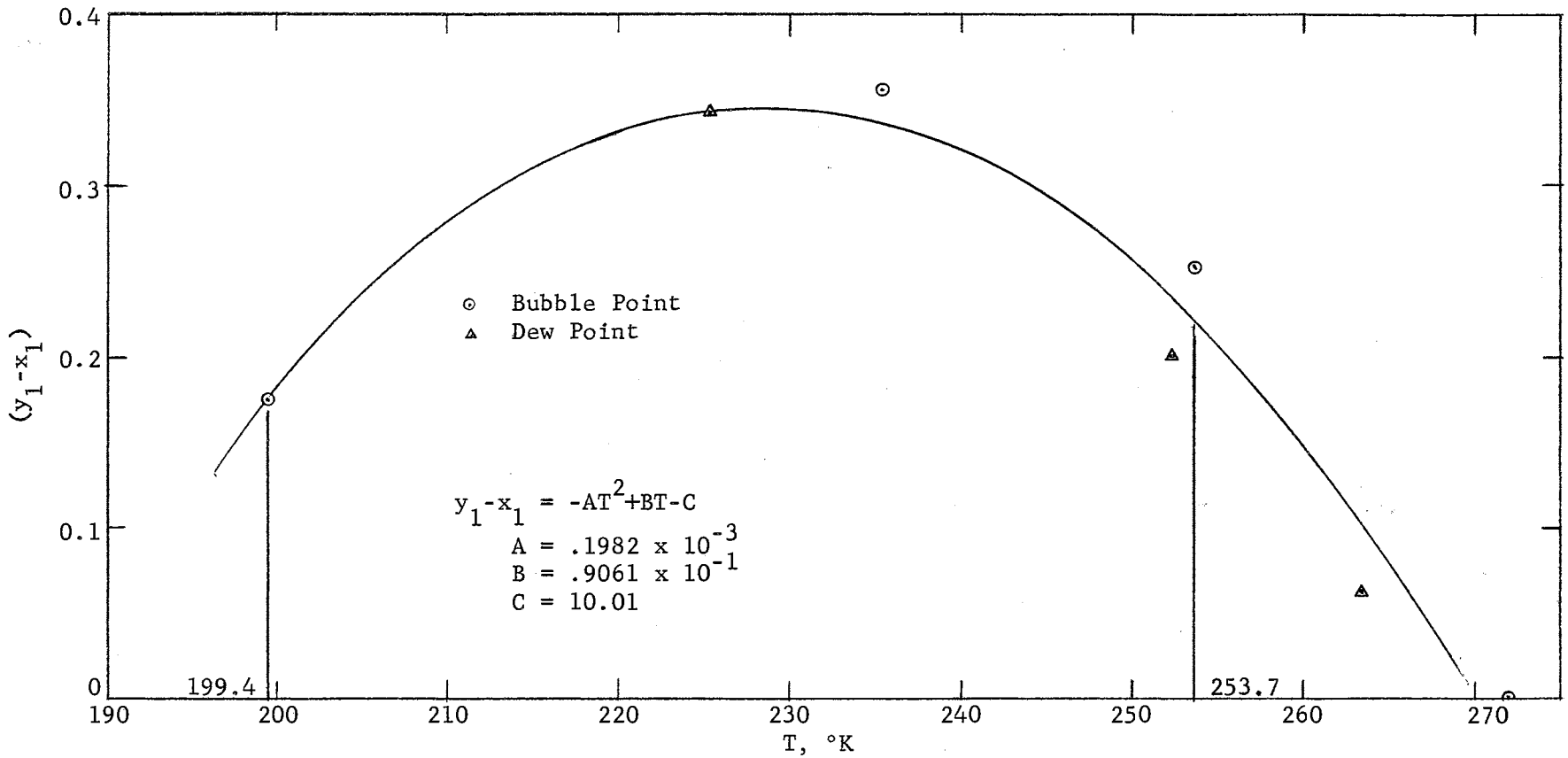

Figure 47

y_1-x_1 vs. T, 40 Atmospheres

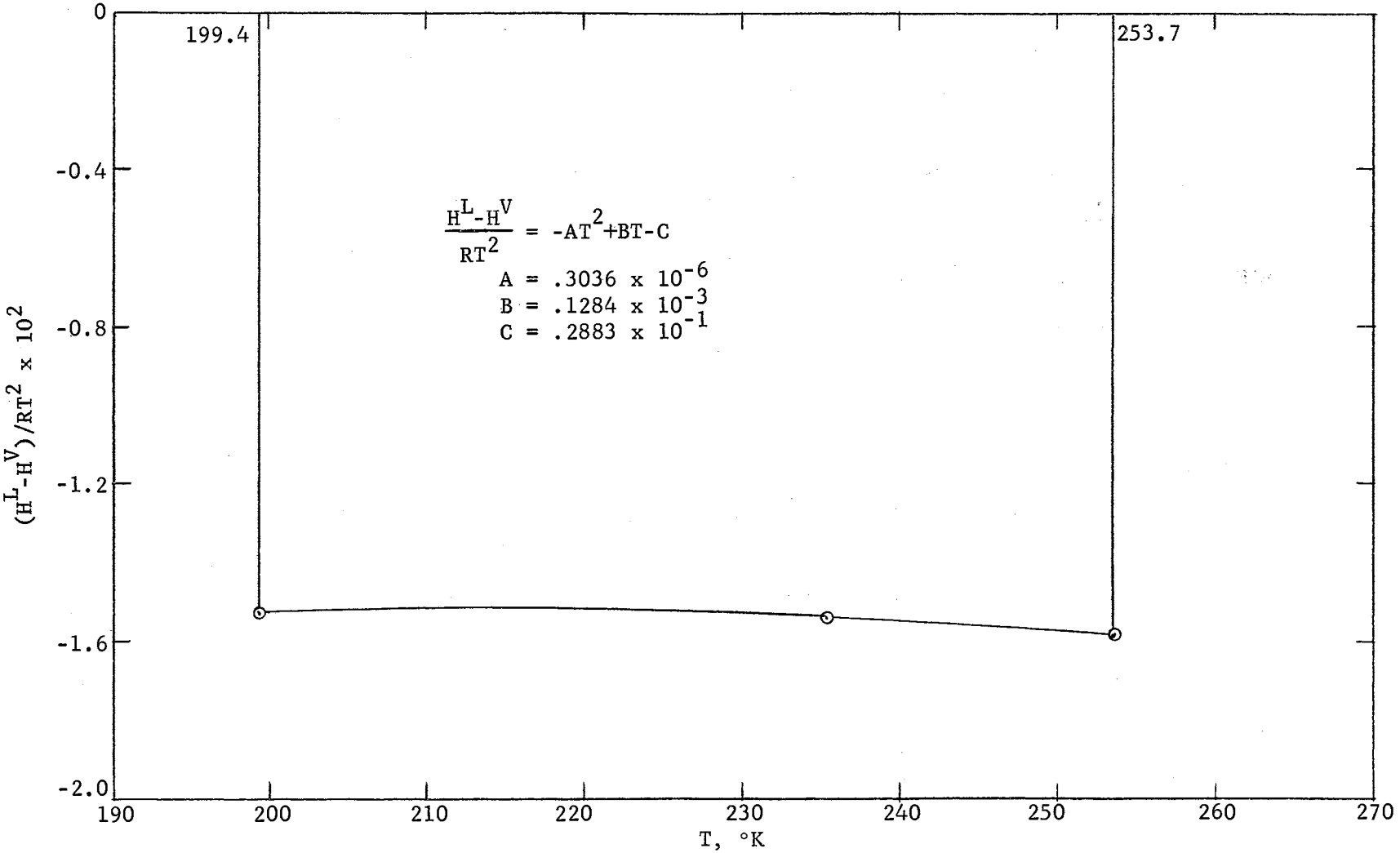

Figure 48

$(H^L-H^V)/RT^2$ vs. T, 40 Atmospheres

TABLE XIII

RESULTS OF EDMISTER INTEGRAL TEST

Limits of Integration, °K Upper	Lower	First Term,[1] Left Side, Area 1	Second Term, Left Side, Area 2	Area 1 Plus Area 2	Third Term, Right Side, Area 3	[2] % Diff.
			20 Atmospheres			
226.8	176.5	-.03319	-1.2616	-1.2948	-1.3434	3.6
			40 Atmospheres			
253.7	199.4	-.05119	- .9182	- .96947	- .8368	-15.8

1/ See Equation 28.

2/ % Diff. = $\left(\frac{\text{Right Side - Left Side}}{\text{Right Side}}\right)100 = \left(\frac{\text{Exp. - Calc.}}{\text{Experimental}}\right)100$

There is general agreement between the Thompson-Edmister test and the Edmister test. At 20 atmospheres the enthalpy data are only 5.6% high compared to 12.5% for the former test. At 40 atmospheres, the enthalpy data are 14.4% low instead of 9.4%. The standard estimates of error are larger for the Edmister test, which indicates a somewhat higher degree of sensitivity, which is good.

The agreement between the differential and integral tests is improved, as anticipated. At 20 atmospheres the difference is only -2.0% (5.6% - 3.6%) compared to 2.4% (14.9% - 12.5%) for the Thompson-Edmister test. The improvement is much more noticeable at 40 atmospheres, a 1.4% (-14.4% - 15.8%) difference vs. a -10.2% (-9.4% - 0.8%) difference.

Modified Thompson-Edmister Test

The Thompson-Edmister (45) test was rearranged to put it in a form analogous to the Edmister (10) test. This form is given by Equation 144. By doing this, the difference in form between the two tests is eliminated. The effect of the ξ_1 term remains.

The data and equations used in the modified differential test are the same as those used in the original test (Figures 31 through 34). The new equations for the modified integral test are plotted in Figures 49 through 52. The results are given in Tables XIV and XV, respectively. The integral test computer program is listed in Appendix M, Program VI.

The results of all three test methods are summarized in Table XVI. The agreement between differential and integral tests is better for the modified form than it is for the original form, as anticipated. The differences are now 0.6% vs. 2.4% at 20 atmospheres and 5.0% vs. 10.2% at 40 atmospheres. Comparing the differential tests of each method, it

TABLE XIV

RESULTS OF MODIFIED THOMPSON-EDMISTER DIFFERENTIAL CONSISTENCY TEST

Run	T, K	Experimental[1] Mole Fraction Methane x_1	y_1	$1+y\frac{\xi}{P}_1$[2]	$x_1 \frac{\partial \ln K_1}{\partial T}$[2] x 10	$x_2 \frac{\partial \ln K_2}{\partial T}$[2] x 10	Left Hand Side[3] x 10	Right Hand Side[4] x 10	% Diff.[5]
				20 Atmospheres					
36	226.8	.137	.408	1.1723	.02020	.15852	.20951	.24924	15.9
43	199.4	.436	.752	1.1894	.08318	.13402	.25834	.29000	10.9
42	176.5	.756	.942	1.0517	.18410	.07400	.27144	.30395	10.7
								Avr.	12.5
							Std. Estimate of Error		± 2.9
				40 Atmospheres					
40	253.7	.112	.364	1.2227	.01181	.14149	.18744	.16231	-15.5
41	235.3	.327	.685	1.2356	.04010	.12465	.20357	.19008	- 7.1
37	199.4	.752	.928	1.0568	.12840	.06396	.20329	.19255	- 5.6
								Avr.	- 9.4
							Std. Estimate of Error		± 5.3

1/ See Table II.
2/ See Table F-VI.
3/ See Equation 144.
4/ See Table F-V.
5/ Same as Table VIII.

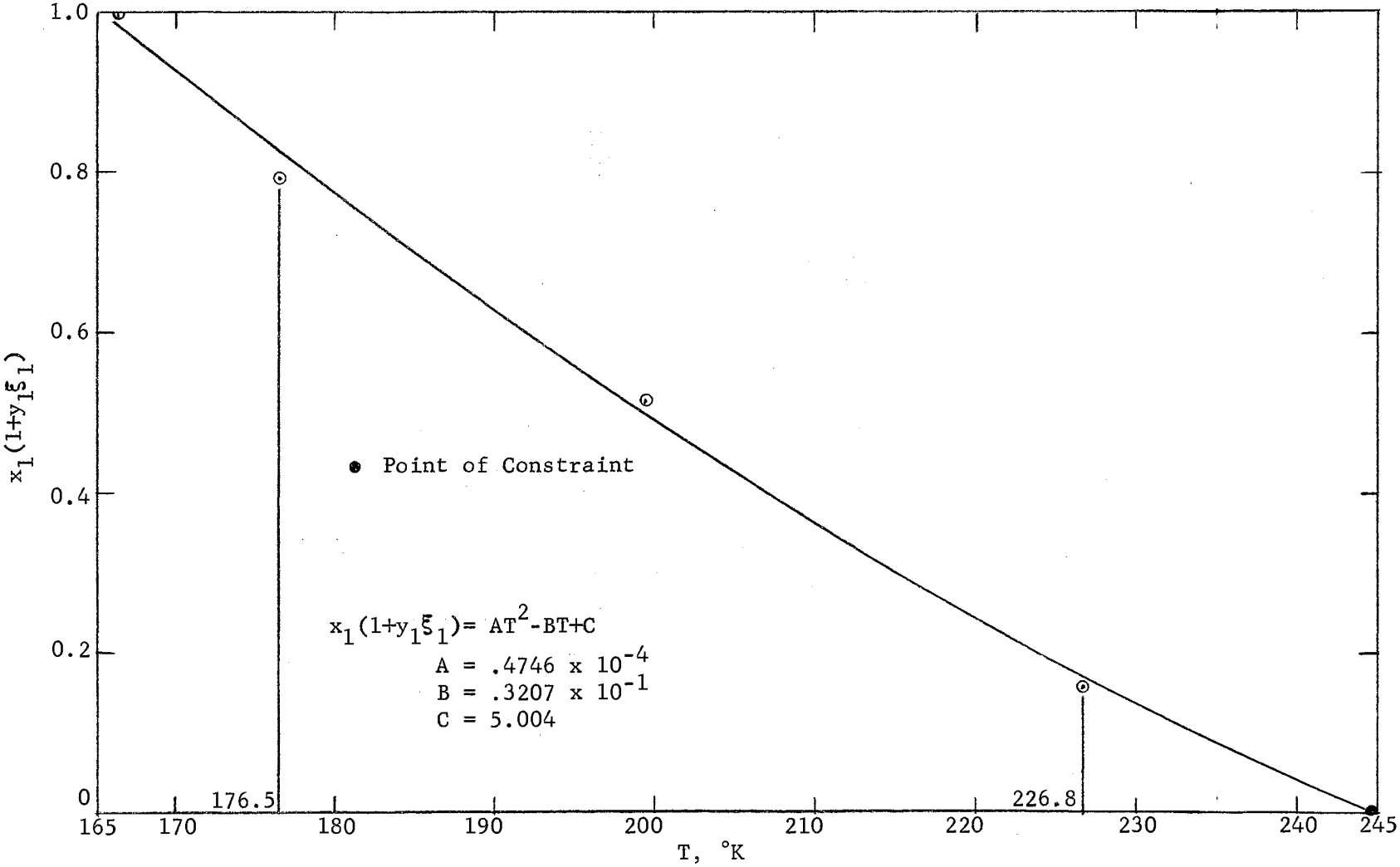

Figure 49

$x_1(1+y_1\xi_1)$ vs. T, 20 Atmospheres

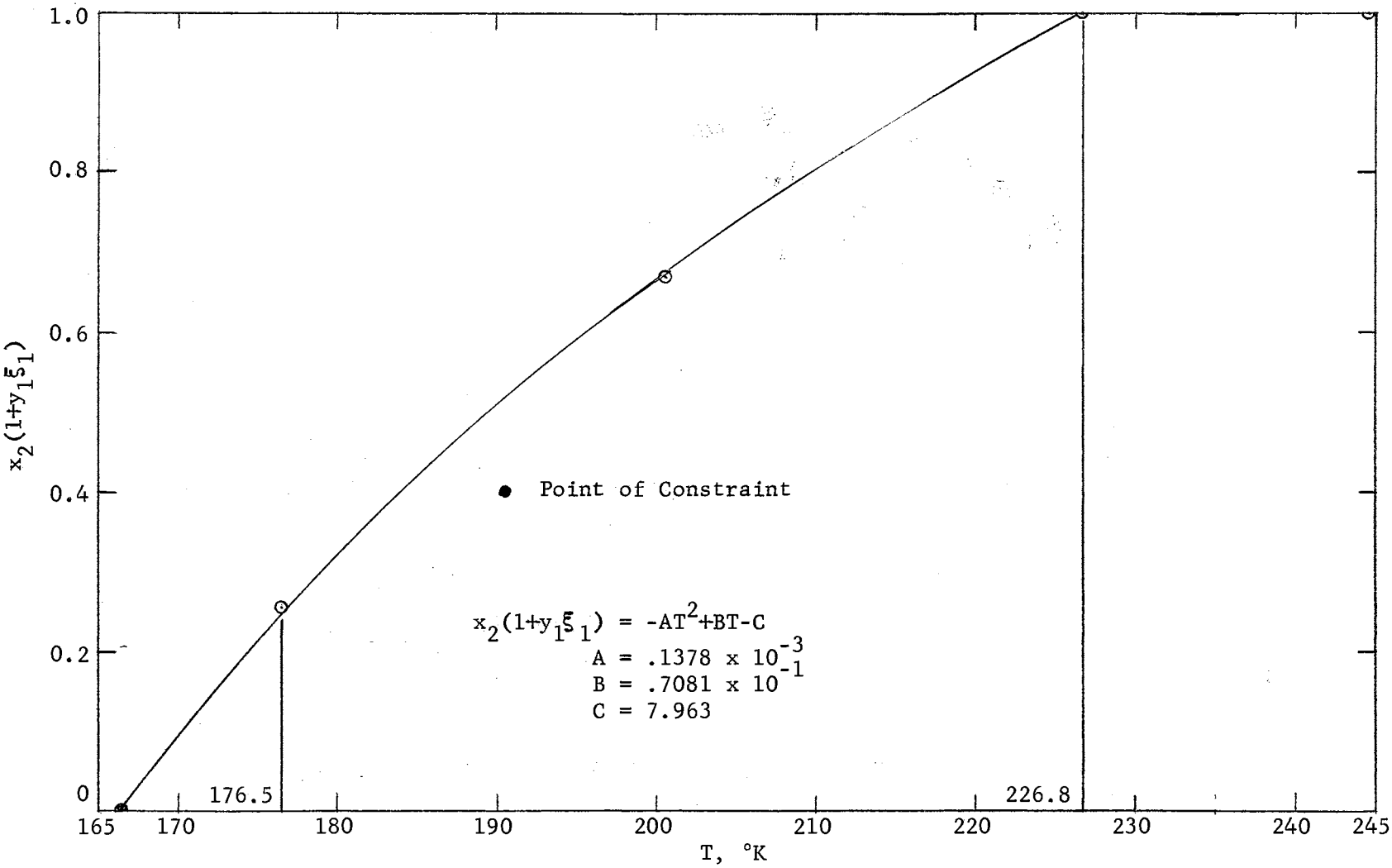

Figure 50

$x_2(1+y_1\xi_1)$ vs. T, 20 Atmospheres

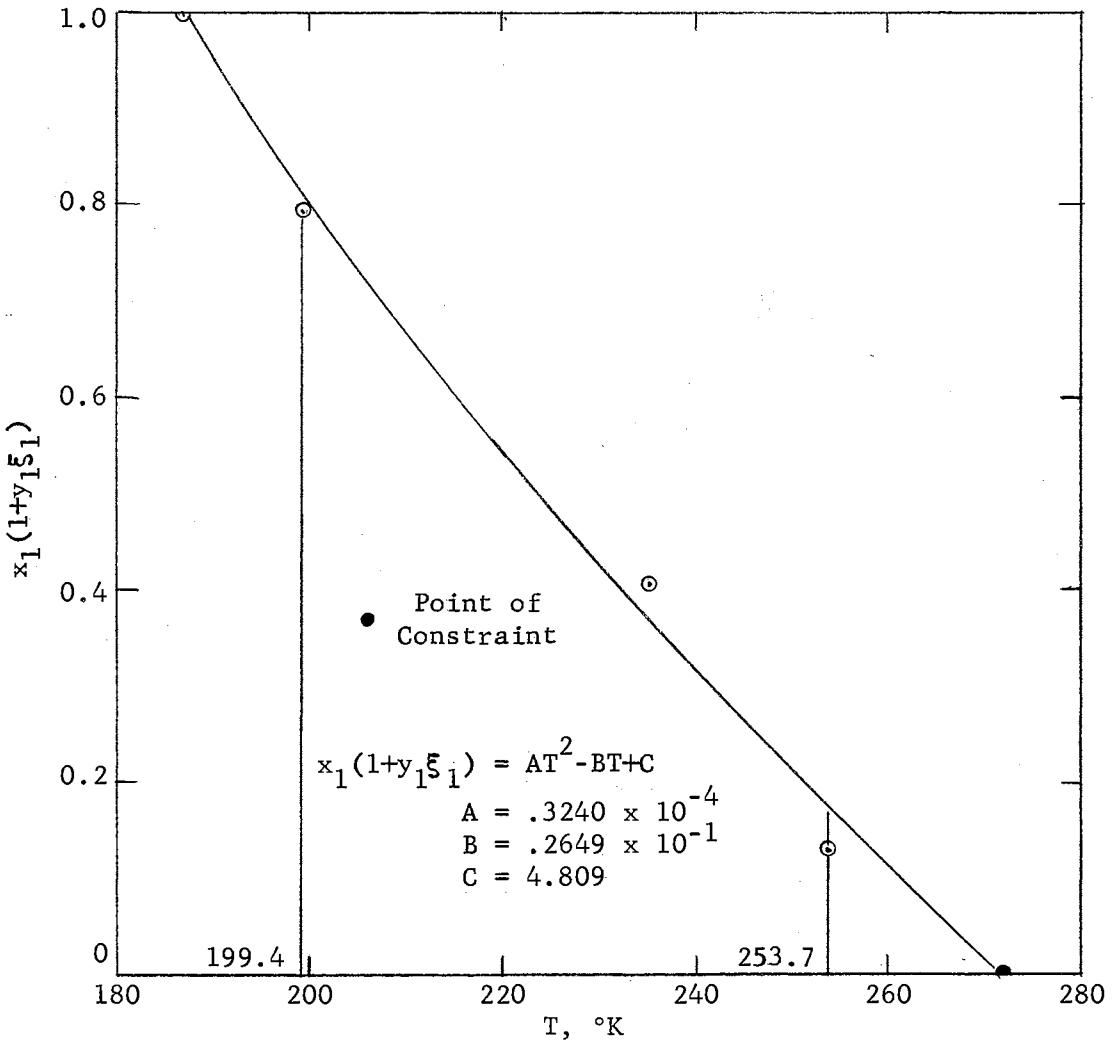

Figure 51

$x_1(1+y_1\xi_1)$ vs. T, 40 Atmospheres

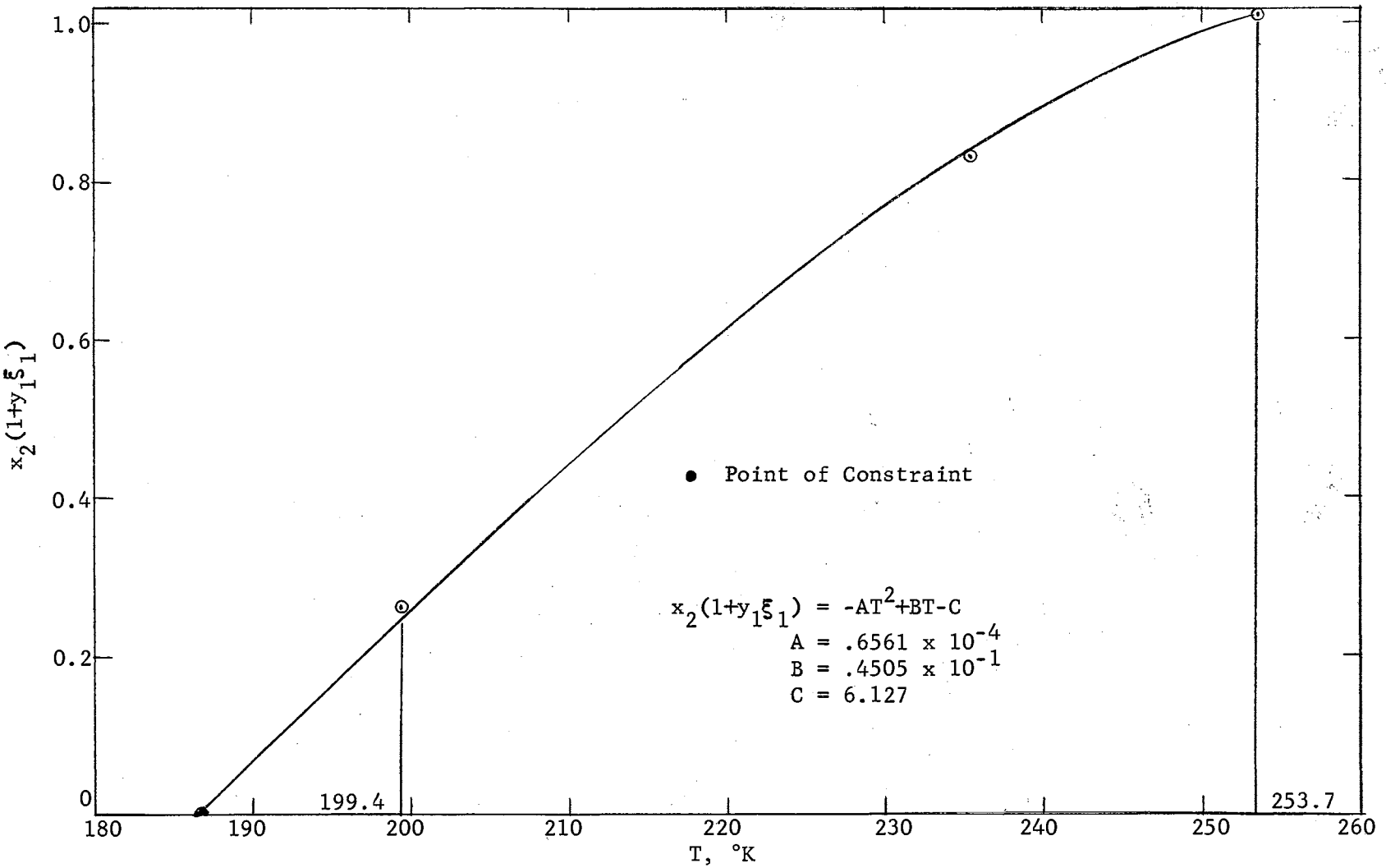

Figure 52

$x_2(1+y_1\xi_1)$ vs. T, 40 Atmospheres

TABLE XV

RESULTS OF MODIFIED THOMPSON-EDMISTER INTEGRAL CONSISTENCY TEST

Limits of Integration, °K Upper	Lower	First Term,[1] Left Side, Area 1	Second Term, Left Side, Area 2	Area 1 Plus Area 2	Third Term, Right Side, Area 3	[2] % Diff.
			20 Atmospheres			
226.8	176.5	.48133	.77418	1.2555	1.4452	13.1
			40 Atmospheres			
253.7	199.4	.36700	.73017	1.0971	1.0513	- 4.4

1/ See Equation 139.
2/ Same as Table VIII.

TABLE XVI

COMPARISON OF DIFFERENT CONSISTENCY TESTS

	Consistency Test		
	Edmister (10)	Thompson-Edmister (45)	Modified Thompson-Edmister
	Differential, 20 Atmospheres		
Run 36	14.7%	15.9%	15.9%
43	13.2	10.9	10.9
42	-11.0	10.7	10.7
Avr.	+ 5.6%	12.5%	12.5%
Std. Error	±14.4%	± 2.9%	± 2.9%
	Differential, 40 Atmospheres		
Run 40	-18.0%	-15.5%	-15.5%
41	-19.5	- 7.1	- 7.1
37	- 5.7	- 5.6	- 5.6
Avr.	-14.4%	- 9.4%	- 9.4%
Std. Error	±10.7%	± 5.3%	± 5.3%
	Integral, 20 Atmospheres		
	3.6%	14.9%	13.1%
	Integral, 40 Atmospheres		
	-15.8%	0.8%	- 4.4%

is noted that the modified test produced the same results as the original Thompson-Edmister (45) test, as anticipated. The results of the modified integral test are closer to the Edmister test than the original Thompson-Edmister (45) test. The difference in results is attributed to the different limits used for the original and modified integral tests. The original test was evaluated over the entire composition (0.0 to 1.0) range; the modified test was evaluated over the range of the mixture data, as was the Edmister test.

Analysis of Experimental Errors

The lack of agreement ($\approx \pm$ 10%) between the experimental data and the calculated consistency test values cannot be attributed to experimental errors other than those previously mentioned.

The combination of errors in individual measurements of standard resistor voltage drops, the value of the standard resistances, the elapsed time of a run, and the weight of a sample, which make up the total enthalpy error, amount to only 0.15%. The individual errors are itemized in Appendix H and combined by the method of Topping (46). In addition to the enthalpy error, there are errors in pressure measurement (.05%), temperature (0.2%), and sample composition (1.5 mole %).

The principal sources of error, heat leak correction, insufficient sample, and "thermal syphon", were discussed earlier.

CHAPTER VII

CONCLUSIONS AND RECOMMENDATIONS

The purpose of this research was to obtain experimental data to be used in the study of the non-ideal behavior of hydrocarbon mixtures. A calorimeter was built to obtain these data; the data obtained are reasonably thermodynamically consistent. They have been applied to the evaluation of methods for calculating the isobaric integral heat of vaporization. Specific conclusions and recommendations pertaining to the theoretical aspects are given, followed by the experimental conclusions and recommendations.

Theoretical

Conclusions

1. Of those consistency tests evaluated, the Edmister (10) test is the best. It is easy to evaluate the terms, the calculated ϕ term is of minor importance, the differential and integral forms use the same functions, and the integral test uses the same limits throughout.

2. The modified form of the Thompson-Edmister test is to be preferred over the original form because it does utilize the same functions in the differential and integral tests, and the same limits are used to evaluate each integral.

3. At 20 atmospheres, the enthalpy data are high by about 5%,

based on the consistency tests. At 40 atmospheres, they are low by about 14%.

4. The discrepancies in the enthalpy data indicated by the consistency tests are substantiated by the calculation methods.

5. Based on the enthalpy data as reported, the methods for calculating the isobaric integral heat of vaporization are ranked in order of preference as (1) Edmister-Persyn-Erbar (11, 12) method, observed value high by 8% and 7% for 20 and 40 atmospheres, respectively, (2) Edmister (9) K-value approximation method, 13% and -20% and (3) Yen-Alexander (49) equations, 8% and 38%. Based on the enthalpy data as adjusted by the results of the consistency tests, the order of the first two would be reversed.

Recommendations

1. More experimental data of this type should be taken to permit a more thorough investigation of the non-ideal behavior of hydrocarbon mixtures. These data could be used to verify the conclusions given above.

2. The consistency tests should be performed on high pressure isothermal vapor-liquid equilibria data to confirm the conclusions of this work.

3. The use of the Edmister (10) consistency test to calculate the isobaric integral heat of vaporization from VLE data should be investigated.

Experimental

Conclusions

1. It is possible and practical to obtain isobaric integral heats

of vaporization for hydrocarbon mixtures in a high-pressure, stainless steel calorimeter, simultaneously with vapor-liquid equilibria data.

2. Heats of vaporization of pure components are readily determined. The small deviation of these data with values found in the literature justify continuation of work on the calorimeter to perfect equipment and techniques for obtaining more and better data on various hydrocarbon mixtures.

3. The principal source of error was heat leak from the reboiler, at the dew-point temperature, to the contents of the reservoir and the reservoir thermostatic fluid, both of which were at the bubble-point temperature.

Recommendations

1. The reboiler tube should be insulated to minimize the heat-leak correction. (This obviously involves complete disassembling of the calorimeter.) The tube should be insulated inside the reservoir to prevent conduction to the charge in the reservoir. A suitable insulating material must be found which will not deteriorate in liquefied hydrocarbons. Urethane "foamed-in-place" should be tried. A materials development program could be conducted prior to disassembling the calorimeter.

The reboiler tube should also be insulated outside the reservoir to minimize heat conduction to the thermostatic fluid. This amounts to surrounding the reboiler tube Conax packing gland with a suitable material which will not deteriorate in the thermostatic fluid. Urethane foam could be tried in this application also.

The reboiler tube should have a check valve arrangement in the bottom which will prevent flow of dew-point mixture back into the

bubble-point charge. This should eliminate the possibility of convection heat transfer at this point. The check valve must not inhibit the flow into the reboiler in the slightest way.

2. It was necessary to use 20 atmospheres as a minimum operating pressure because overhead lines to the internal and external condensers were too small to permit complete transfer of all vaporized material. These lines should be made as large as possible---at least 1/4 in. I. D. This would permit good runs to be made at 10 atmospheres and lower.

3. An additional point liquid-level sensor (United Control Corp., Redmond, Washington, or Delta-Sonics, Hawthorne, Calif.) should be installed in the top of the reservoir to indicate when the reservoir is full. It is very important that the heater be flooded at all times. It is almost as important that the reboiler and condenser not be flooded. One sensor properly located would suffice.

The liquid-level sensor in the bubble cap should be replaced.

4. Considerable difficulty was encountered in transferring heat from the three constant-temperature zones to the heat sink. This was particularly true when the control temperatures were within 20° K of the sink temperature. Likewise, some difficulty was experienced in losing too much heat to the sink when the temperature difference exceeded 60° K.

To increase the heat transfer, it is recommended that the vacuum jackets be connected to a helium supply which could be introduced when needed. Additional Conax-type fittings could also be installed between the inner and outer walls of each zone. A copper plug could easily be inserted in the fitting for experiments requiring high heat transfer; a plastic plug would be used for runs requiring minimal heat transfer.

The two pieces of tubing running down from the condenser zone should be lengthened so they will reach the bottom of the calorimeter. Thus, they will always be in the heat sink fluid, regardless of its level.

To decrease the heat transfer, the vacuum jackets must be more highly evacuated--to the one micron or lower range. This requires locating and sealing the remaining minute vacuum leaks.

5. The constant-temperature bath stirring needs to be improved three ways: First, the impellers should be of an improved design; second, the speed should be increased; third, the noise of the gears should be minimized.

The existing packing glands were originally for static operation, but were modified to permit shaft rotation. At the time the original design was made, there was no satisfactory rotary seal for cryogenic, high-pressure and vacuum service. Hence, the adaptation of the static seal. Presently, such seals are available from Bal-Seal Engineering Co., La Habra, Calif.

6. The leads to the bubble-cap liquid-level sensor should be brought out through the top of the still instead of through the still wall to facilitate still assembly. This will require using a special "lava" sealant in one of the existing Conax packing glands.

7. Most of the Teflon Conax sealants have been replaced with magnesium silicate, or "lava" sealants. The remaining Teflon sealants should be replaced.

8. The dead weight gauge and differential pressure indicator cell could be replaced by a large dial, well-calibrated pressure gauge. The high degree of accuracy attainable with the dead weight piston gauge is

not necessary for enthalpy experiments and the manipulation of the weights is time-consuming. In addition, its lower pressure limit (about 100 psig) is a disadvantage.

9. Although pressure regulation did present a problem, it is believed that better heat transfer and better stirring should eliminate the need for a pressure regulator.

10. All wiring should be consolidated as much as possible and be converted from terminal strip connections to jack-and-plug arrangements.

11. Sample valves, thermostatic-fluid transfer valves, and nitrogen blow-down valves should be relocated for easier operation.

12. If the larger lines are installed (Recommendation No. 2), it would be worthwhile to consider the purchase of a larger DC power supply, say 100 watts or more. This would permit a wider variety of boil-up rates to be used at any particular composition and pressure.

13. The internal condenser should be enlarged to provide more heat transfer surface.

14. The internal condenser cut-off valve should be changed to some other type, rather than a needle valve, which has a high pressure drop. This new valve must be capable of venting the internal condenser during a run, i.e., being "all-but" closed.

15. The four hypodermic sampling tubes should have a 200-mesh metallic gauze "sock" over the inlet to prevent plugging of the line by small metal particles.

A SELECTED BIBLIOGRAPHY

1. Adler, S. B., L. Friend, R. L. Pigford and G. M. Rosselli, AIChE Journal 6, 104 (1960).

2. Am. Pet. Inst. Res. Proj. 44, Carnegie Inst. of Technology, Pittsburgh, Pa. (1953).

3. Bahlke, W. H. and W. B. Kay, Ind. Eng. Chem. 24, 291 (1932).

4. Benedict, M. G., B. Webb and L. C. Rubin, Chem. Eng. Prog. 47, 419 (1951).

5. Bird, R. B., E. L. Spotz and J. O. Hirschfelder, J. Chem. Phys. 18, 1395 (1950).

6. Chao, K. C. and J. D. Seader, AIChE Journal 7, 598 (1961).

7. Dana, L. I., Proc. Am. Acad. Arts and Sci. (Daedalus) 60, 241 (1925).

8. Dodge, B. F., "Chemical Engineering Thermodynamics", McGraw-Hill Book Co., Inc., New York (1944).

9. Edmister, W. C., AIChE Journal 1, 38 (1955).

10. Edmister, W. C., Private Communication, January 26, 1965.

11. Edmister, W. C., C. L. Persyn and J. H. Erbar, Proceedings of 42nd Annual Convention of Natural Gas Processors Association, Houston, Texas, March 1963.

12. Erbar, J. H., C. L. Persyn and W. C. Edmister, Proceedings of 43rd Annual Convention of Natural Gas Processors Association, New Orleans, La., March 1964.

13. Grayson, H. G. and C. W. Streed, Sixth World Petroleum Congress, Frankfurt/Main, June 1963.

14. Guggenheim, E. A. "Thermodynamics", North-Holland Publishing Co., Amsterdam (1957).

15. Guter, M., D. M. Newitt and M. Ruhemann, Proc. Roy. Soc. (London) A176, 140 (1940).

16. Gyorog, D. A. and E. F. Obert, AIChE Journal 10, 621 (1964).

17. Hala, E., J. Pick, V. Fried and O. Vilim, "Vapor-Liquid Equilibrium", Pergamon Press, New York (1958).

18. Hestermans, P. and D. White, J. Phys. Chem. 65, 362 (1961).

19. Houser, C. G. and J. H. Weber, J. Chem. Eng. Data 6, No. 4, 510, (1961).

20. International Critical Tables, III, 230 (1928).

21. Kumar, S., M. S. Thesis, Oklahoma State University (1965).

22. Lewis, G. N. and M. Randall, "Thermodynamics and the Free Energy of Chemical Substances", McGraw-Hill Book Co., Inc., New York (1923).

23. Lewis, G. N. and M. Randall, "Thermodynamics", Revised by K. S. Pitzer and L. Brewer, 2nd Ed., McGraw-Hill Book Co., Inc., New York (1961).

24. Lydersen, A. L., R. A. Greenkorn and O. A. Hougen, Wisconsin University Eng. Exp. Sta., Report No. 4 (October 1955).

25. Matthews, C. J. and C. O. Hurd, Trans. Am. Inst. Chem. Eng. 42, 55 (1946).

26. Plewes, A. C., D. A. Jardine and R. M. Butler, Can. J. Tech. 32, 133, (1954).

27. Plewes, A. C., D. C. Pei and R. K. Code, Can. J. Tech. 37, 121 (1959).

28. Plewes, A. C., R. M. Butler and K. Pugi, Can. J. Tech. 34, 152 (1956).

29. Powell, R. L., L. P. Caywood, Jr. and M. D. Bunch, "Temperature, Its Measurement and Control in Science and Industry", Vo. III, Pt. 2, Edited by C. M. Herzfeld, Reinhold Publishing Corp., New York (1962), p. 65.

30. Redlich, O. and J. N. S. Kwong, Chem. Rev. 44, 233 (1949).

31. Roper, E. E., J. Phys. Chem. 44, 835 (1940).

32. Sage, B. H. and W. H. Lacey, API Research Project No. 37, "Thermodynamic Properties of the Lighter Paraffin Hydrocarbons and Nitrogen", 12 (1950).

33. Schnelle, K. B., Jr., Ph. D. Thesis, Carnegie Inst. Tech. (1959).

34. Schnelle, K. B., Jr., and L. N. Canjar, Chem. Eng. Sci. 17, 189 (1962).

35. Schroeder, D. W., Ph. D. Thesis, Carnegie Inst. Tech. (1952).

36. Schroeder, D. W. and W. C. Edmister, Paper Presented at National AIChE Convention, San Francisco, Calif., September 1953.

37. Stein, F. P. and J. J. Martin, Chem. Eng. Prog. Symp. Series 59, No. 44, 112 (1963).

38. Stiehl, J. G., M. Hobson and J. H. Weber, AIChE Journal 2, 389 (1956).

39. Stull, D. R., Ind. Eng. Chem. 39, 517 (1947).

40. Tallmadge, J. A., Ph. D. Thesis, Carnegie Inst. Tech. (1953).

41. Tallmadge, J. A. and L. N. Canjar, Ind. Eng. Chem. 46, No. 6, 1297 (1954).

42. Tallmadge, J. A., D. W. Schroeder, W. C. Edmister and L. J. Canjar, Chem. Eng. Prog. Symp. Series 50, No. 10, 137 (1954).

43. Thodos, G. and R. E. Perry, Ind. Eng. Chem. 44, 1649 (1952).

44. Thompson, R. E., Private Communication to W. C. Edmister, June 1964.

45. Thompson, R. E. and W. C. Edmister, AIChE Journal 11, 457 (1965).

46. Topping, J., "Errors of Observation and Their Treatment", Reinhold Publishing Corp., New York (1960).

47. Volona, L. M., J. Phys. Chem. USSR 14, 268 (1940).

48. Yarborough, L., Ph. D. Thesis, Oklahoma State University (1964).

49. Yen, L. C. and R. E. Alexander, Paper Presented at 53rd National AIChE Convention, Pittsburgh, Pa., May 1964.

50. York, R., Jr. and E. F. White, Jr., Trans. AIChE 40, 227 (1944).

APPENDIX A

CALORIMETER ASSEMBLY AND PRESSURE TESTING

Stepwise pressure testing of the calorimeter for gas leaks was very important because of the time required to assemble it.

Reservoir

The first opportunity for a pressure test occurred when the reservoir was completely assembled. Assembly was started by sealing the reboiler tube and reservoir stirrer in their Conax packing glands in the lid of the reservoir (see Plate II). (The condenser was permanently attached to the lid during the first assembly.) Conax "lava" sealants were used wherever possible because of their superiority in low temperature service. The high torque requirements for lava sealants necessitated putting the lid in a vise and using a wrench with an extension handle to tighten the jam nuts. Opposing octagonal faces of the lid were always clamped in the vise jaws, rather than the top and bottom of the lid, to prevent any damage to the latter, which was the sealing surface. The packing gland for TC 2 was also assembled and tightened. This completed the assembly of the reservoir lid.

Assembly of the reservoir body was completed by installing TC 1 in its packing gland, which was used for measuring the temperature of the reservoir. The lead wire from the packing gland to the junction was about 10 inches long, which was held in place around the inside

wall of the reservoir by wire "spider" to prevent it from becoming entangled in the stirrer. This extra lead wire was provided to insure that the temperature measured at the junction was that of the fluid in the reservoir only, and that the junction temperature was not affected by any heat flowing in the lead wire as a result of a temperature gradient between the reservoir fluid and its surroundings. This procedure of providing extra lead wire is known as "tempering", and was used wherever possible. The leads for TC 1 and TC 2 were tempered again before passing them through their glands in the wall of the constant-temperature zone.

The reservoir lid and the O-ring groove were cleaned with a soft rubber eraser to remove any foreign particles. The teflon-coated, 4-inch O-ring was placed in the groove. A thin copper gasket was cut for the 1/4 in. NPT union seat, using a five cent coin as a template and a cork borer to cut the inside hole. The gasket was gently formed to the union seat before the opposite side was brought into position. The reservoir body was placed in a vise and the lid was lowered into place, taking care not to touch the O-ring with the stirrer. The union collar was made finger tight, followed by the eight Allen cap screws. Opposing cap screws were tightened about an eighth of a turn at a time with an Allen wrench until all eight had been pulled-up by the same amount. The procedure was repeated until the screws were as tight as possible, using only the unaided hand on the Allen wrench. In this way the O-ring was compressed gradually, uniformly and completely. After this the union collar was tightened, using a 12 in. adjustable wrench. This completed the assembly of the reservoir.

First Pressure Test

To prepare the reservoir for pressure testing, a 1/4 in. female NPT to 1/4 in. stainless steel tubing adapter was screwed onto the top of the condenser and a 3/8 in. NPT plug was screwed into the end of the reboiler tube, shown on Plate II. Bucking wrenches were used in both instances to positively prevent any turning of the condenser and reboiler tube. The reservoir was submerged in methanol in a suitable vessel. A connection of 1/4 in. high-pressure tubing was made between the condenser and V7, and a cylinder of nitrogen gas, whose pressure was considerably above 1000 psig, was connected directly to V1 or 2 without a regulator. (Valve numbers refer to Fig. 8). If a high-pressure regulator for a nitrogen bottle is available, it should be used. Valves 2, 3, 9, 17, and 18 were closed and V4, 5, 6, and 7 were opened. A plug was placed in the cross between V4 and 5 to replace the liquefaction cylinder (thermal compressor) which was disconnected during pressure testing. The gas flow was controlled by the valve on the cylinder.

In order to start the test at a low pressure (50 to 100 psig) in the reservoir V6 was closed and gas admitted into this small section of line until the pressure was about 500 psig, as noted on the gauge between V4 and 5. The gas was expanded into the calorimeter by opening V6 slowly, which resulted in less than 100 psig in the entire system. The methanol was examined thoroughly for tell-tale bubbles. If none appeared, the expansion process was repeated.

The pressure was increased to about 100 psig, and corrections made as indicated. Pressure was raised successively to 250, 500, 750, 1000 and 1100 psig. If no visible leaks were noticed at this level, the DPI cell was introduced as a leak detector by opening V18, because it was

much more sensitive than the eye. A test was considered satisfactory if the nitrogen leak rate was one gram per hour or less.

If all of these tests were successful, the procedure was repeated at the dry-ice point (195° K or -109° F) by adding dry ice to the methanol. For the cold test, only the DPI cell was used, because of the bubbling carbon dioxide. The lava sealants were rated to only 90° K. (-298° F), so tests were not conducted with liquid nitrogen (77° K. or -321° F.). The probability of successful ambient temperature test resulting in a successful dry-ice test, as determined by the DPI cell test mentioned above, was quite high if lava sealants were used; it was very low if teflon sealants were used.

Reservoir Constant-Temperature Zone

The reservoir constant-temperature zone heater and the booster heater were placed in their zone and connected to the lead wires, shown in Plate I. The reservoir was inserted in the zone, rotating it slightly. The leads from TC1 and 2 were sealed in their respective packing glands. A 1/8 in. NPT to 1/4 in. flare adapter was inserted in its 1/8 in. NPT collar in the reservoir zone wall and tightened, and the blowdown dip tube connected thereto. Next, the lead wires of TC3 and the temperature controller sensor were coiled around inside the zone for tempering, placed on top of the reservoir and tied down so they could not come in contact with the stirrers. Finally, the zone stirrer was set in position.

To facilitate the assembly of the zone cover and the vacuum jacket to the reservoir zone, two or three alignment studs were screwed into the zone flange, also shown in Plate I, and a teflon gasket was placed on the flange. The pressure-test adapter was removed from the condenser,

and the zone cover was lowered over the two stirrers, condenser, reboiler tube and alignment studs. All of the Conax glands in the cover were tightened and the 3/8 in. NPT plug removed from the reboiler. Another teflon gasket was placed on top of the cover, followed by the vacuum jacket. The #10-32 Allen cap screws were inserted in the lower vacuum jacket flange, shown in Plate V, and tightened with a special Allen wrench. Finally the alignment studs were replaced by cap screws, and all cap screws were tightened again using a regular Allen wrench.

Condenser Constant-Temperature Zone

With the outer vacuum jacket in place, the condenser constant-temperature zone was ready for assembling. The Conax gland in the bottom of the zone was tightened first using a special wrench. The zone heater consisted of approximately 50 feet of yellow asbestos-covered Chromel wire, which was coiled in a helix one inch in diameter, wrapped around the condenser and connected to its lead wires, soldered and insulated. The 1/8 in. NPT by 1/4 in. flare elbow and the 1/8 in. NPT by 1/4 in. flare union were screwed into their respective collars in the zone wall, and the refrigerant coil was connected to these two fittings. The adapter was replaced on the condenser and connected to V8 via the condenser tee. Lead wires for the thermocouple and temperature controller sensor were tempered in the zone and assembled through their respective packing glands.

Equilibrium Cell Constant-Temperature Zone, Phase I

The equilibrium cell constant-temperature zone was assembled next in preparation for the second pressure test. Two complete wraps of teflon joint tape were applied to the 3/4 in. male NPT thread at the

bottom of the cell body, shown in Plate III, prior to screwing the cell into the bottom of the constant-temperature zone. The cell was tightened until the hole in the body was in a position to permit insertion of a plugged MTG-20-A2, also shown in Plate III, with teflon tape on the thread. The aluminum tee brace was placed between the MTG-20-A2 and the inner wall of the zone to prevent rotation of the cell while the PG-5 in the bottom of the cell was being tightened with the special wrench. To develop the torque required for tightening this lava sealant, it was necessary to use a strap wrench with a three-foot handle on the exterior of the vacuum jacket to oppose the special wrench with a three-foot handle being used to tighten the jam nut. This Conax fitting was the most difficult to tighten. It was also one of the most important pressure seals.

Second Pressure Test

Before proceeding to install the internal components of the equilibrium cell, it was advisable to pressure test the seal mentioned above. All of the cell top (lens ring) Conax glands shown in Plate III, were plugged with wire of the appropriate size, and tightened. The mating surfaces of the lens ring were cleaned with a soft rubber eraser and the lens ring was bolted down with the aluminum tee brace still in place. It was found that tightening of the Allen cap screws a little bit at a time, proceeding clockwise around the bolt circle, produced more gas-tight seals than the method of tightening opposing cap screws did. A plugged elbow was connected to the cell overhead line to complete the closure. The condenser tee was connected to V7 as before, and the pressure testing procedures repeated, proceeding

all the way to 1100 psig in dry-ice-and-methanol baths made in each of the two upper zones.

Equilibrium Cell Constant-Temperature Zone, Phase II

Having passed the second pressure test, the cell top, etc., were removed and the thermocouples and heater leads connected to the bubble cap. The two heater lead wires were soldered to the leads coming down through the bubble cap. TC4 (refer to Electrical Apparatus, Chapter IV) and the reboiler-liquid sample line were passed through the bubble cap, and both were tied to the heater lead wires just above the heater to hold them firmly in place. TC5 and the reboiler vapor sample line were inserted through the top of the bubble cap and through the bubble-cap riser to a point just even with the bottom of the tray. All packing sets were removed from the plugged lens ring Conax glands. Then all thermocouples and leads plus TC 6 and 7 were passed through their respective Conax packing glands in the lens ring and the glands assembled. (See Recommendation 6.) A spring was placed between the bubble cap and the lens ring to insure good contact between the tray and its seating ring. The bubble-cap assembly was now ready to be placed in the cell body in the order shown in Plate IV. A thin coat of silicone stopcock grease was placed on the periphery of the bottom of the tray to help seal the tray to its seating ring in the cell. The heater, thermocouple and sample tube were guided into the reboiler tube, followed by inserting the tray into the cell. It was very important to keep the tray perpendicular to the axis of the cell. This was done by gently tapping the tray around its entire periphery with a 1/8 in. steel rod. The spring between the bubble cap and the lens ring was

compressed by pushing the lens ring to its seat. With this held in place, the lens-ring bolt circle was screwed into the cell and the cap screws tightened as before. The overhead tee was connected between the lens ring and V8 as shown in Plate III.

Third Pressure Test

This test was conducted on the completed assembly of high-pressure components to insure they were devoid of leaks before the equilibrium zone sensor, thermocouple and heaters were put in the zone.

The overhead tee was sealed by connecting a plugged elbow to the line. The pressure tests were conducted as before, proceeding from ambient temperature and low pressure to 195° K. (dry ice temperature, -109° F.) and 1100 psig, making corrections as indicated.

Equilibrium Cell Constant-Temperature Zone, Phase III

The condenser tee connection nut and ferrule, the stem of V8 and the plugged elbow on the overhead line were removed, along with the aluminum tee brace. The 300-watt immersion heater and the 450-watt booster heater were placed in the constant-temperature bath fluid space around the cell, connected to their respective leads and insulated. TC8 and the cell zone sensor were coiled inside (tempered in) their zone, as TC9 and the condenser zone sensor had been coiled in their zone. All heater leads were also coiled in the cell zone to temper them. The cell overhead extension was screwed into the overhead tee and each stirrer was placed in its respective zone. The bolt flange of each zone was coated with silicone stopcock grease, followed by placing the teflon gaskets on the flanges. Each zone lid was maneu-

vered into position and the copper gaskets placed on top of the lids. The #5-40 Allen cap screws were started and tightened with the special Allen wrenches. The stirring shaft length was adjusted to the proper height and all Conax glands were tightened. Plate VI shows the calorimeter at this point of assembly. The universal-joint valve stem was added to V8.

Fourth Pressure Test

With the addition of the cell overhead extension mentioned above, another joint was made, which was tested before proceeding with the final stages of assembly.

The usual testing connections were made: the plugged elbow was connected to the cell overhead extension line, and the condenser tee was connected to V7. This test was abbreviated by conducting it at room temperature only and using the DPI cell to detect any leaks at 1100 psig, dispensing with the dry-ice-and-methanol bath. If an excessive leak rate (>1 gm/hr) was observed, the cell overhead extension joint was tightened. If this did not eliminate the leak, the joint was completely dismantled and reassembled, repeating the test thereafter. Upon completion of a successful test, the testing connections were removed and assembly continued.

Calorimeter Lid and Superstructure

The upper calorimeter flange shown in Plates V and VI, was coated with silicone stopcock grease, and a teflon gasket placed on the grease. The calorimeter lid was bolted in place using copper washers under each bolt head for a vacuum seal. All Conax packing glands were assembled and tightened.

The plugged tee was connected to the condenser tee, providing an auxiliary pressure or vacuum connection to the calorimeter, which has not been used to date. The valve handle was put on the stem of V8, the stirring shaft collars were tightened on their respective shafts, and additional lead wires soldered to the heater leads, and insulated. The four 5/16 in. all-threads were screwed into the calorimeter lid, using copper washers as before, and the phenolic plate secured to the all-threads via lock nuts.

The aluminum bearing plate, with bearings and drive gears "floating" in their holes, was bolted to the phenolic plate using all-threads and spacers. The bull gear was placed between the drive gears, and the stirring collars tightened to the gear shafts. The drive gears were aligned and locked in place with locking nuts. The calorimeter was ready to be placed in the tower.

The calorimeter was placed on a box about 15 inches high, which was on the calorimeter elevator. Before the apparatus was raised to the gear motor, all of the heater and sensor leads were attached to the terminal strip in the back of the tower, starting at the left with the reservoir heater. The two booster heaters and the calorimeter heater were attached to their terminal strip on the right side. The calorimeter was then raised slightly to permit the connection of TC1, 2, 3, 8, and 9, starting at the front of the terminal strip on the left of the tower.

The calorimeter was raised to its full height and the bull gear tightened on the shaft of the gear motor. The aluminum bearing plate was bolted to the two cross members using all-threads and spacers. The elevator was lowered slowly and the box removed.

The high-pressure tie-in was made by joining the cell overhead line to V7. TC4, 5, 6, and 7 were connected to their terminal strip (left center). The three vent lines, the three thermostatic-fluid transfer lines and the two vacuum lines were connected to V30, 31, 32, 22, 23, 24, 15, and 16 respectively to complete the installation.

Final Pressure Test

The final pressure test was made using the DPI cell, tightening any leaky external connections as indicated by the "soap test."

Cooling Down

To cool down the calorimeter, the calorimeter dewar was placed on the elevator, which had been lowered to the floor. The dewar was raised by hand (not using the elevator) until the 15-inch box could be inserted between the elevator platform and the dewar. The elevator was then raised to its maximum height. Safety bolts were inserted through the elevator frame and tower to prevent the dewar from falling to the floor, in the event of a cable failure.

Disassembly

Disassembly, when required, was essentially the reverse of the above assembly procedure.

APPENDIX B

BALANCE AND WEIGHT CALIBRATIONS

Sample bombs were weighed to the nearest 0.1 gram on the 6 kg. Voland and Sons balance using weight sets No. 4775 and Sargent Set No. 5-Y-2748, as described by Yarborough (48). These weights deviated from their nominal values in the second and third places only. Consequently, no adjustments were necessary when weighing to the nearest 0.1 gram.

APPENDIX C

CALIBRATION OF CHROMATOGRAPH

The relative response of the F and M Hydrogen Flame ionization detector to methane-ethylene mixtures separated by the 18 ft. column of SE-30 on Chromosorb P was determined by injecting known quantities of the pure components. The settings on the F and M Model 609 unit were as follows:

Column Temperature	Ambient
Detector Variac	40
Injection Port Variac	Off
Hydrogen Flow Meter Setting	8.0
Helium Flow Meter Setting	6.5
Air Flow Meter Setting	6.5
Range	10,000
Attenuation	2,4,8

Six 0.3 cubic centimeter samples of methane were injected and the Disc Chart Integrator area units noted. Six additional samples at 0.4, 0.6, 0.9, 1.2, and 1.5 cubic centimeters each were also injected and the area units noted, adjusting attenuation as required. The same injection program was used on pure ethylene.

The number of gram-moles in each volume was calculated using the ideal gas law, corrected barometric pressure, and room temperature. The six values of area units were averaged and a least-squares regression made, using gram-moles as ordinate and area units as abscissa. The best curves passed through the data were linear, which resulted in the following equations:

$$\text{Gm-mols methane} = (1.6596 \times 10^{-12})(\text{Range})(\text{Attenuation})(\text{Area Units}) - 1.5427 \times 10^{-6} \quad (34)$$

$$\text{Gm-mols ethylene} = (7.5824 \times 10^{-13})(\text{Range})(\text{Attenuation})(\text{Area Units}) - 1.6299 \times 10^{-6} \quad (35)$$

A program was written for the IBM 1620 Digital Computer which would calculate mole per cent methane using range, attenuation, and area units for methane and ethylene as input data.

To verify the quality of the calibration, four methane-ethylene mixtures previously prepared and analyzed on a mass spectrograph by Phillips Petroleum Co. were reanalyzed. The results are compared below.

Phillips mol% methane	This Work mol% methane	Difference mol% methane
18.4	17.5	-0.9
38.4	37.0	-1.4
57.2	56.1	-1.1
78.8	78.9	0.1

The agreement was good enough to warrant continued use of the calibration equations.

All subsequent analyses were made using chromatograph settings which were as close as possible to those used during the calibration and verification.

APPENDIX D

CALIBRATION OF THERMOCOUPLES

Originally, all thermocouples were calibrated in place against an NBS calibrated platinum resistance thermometer, Leeds and Northrup No. 8163, over the entire expected use-range, 150° to 300° K (-190° to 80° F). There was considerable irregularity in the results. This was attributed to insufficient immersion of the resistance thermometer, the calorimeter not having been designed with thermocouple calibration in mind.

It was decided to calibrate the bubble-point temperature thermocouple, TC1, and the dew-point temperature thermocouple TC4, using the vapor pressure of ethylene. The system pressure was measured accurately (0.05%) using the Budenburg Dead Weight Gauge and Ruska DPI cell. The corresponding temperature was calculated on the IBM 1620 computer using the York and White (50) vapor-pressure equation in the implicit T form,

$$T,°K = (-646.275\ 1.880472\ T \log_{10}T - 0.00224072\ T^2)/\log_{10}P_{atm} \qquad (36)$$

Thermocouple emf's were converted to ° K via the Powell, et al., (29) Tables. The calibration data is given in Table D-I, and the results are plotted in Figure D-1.

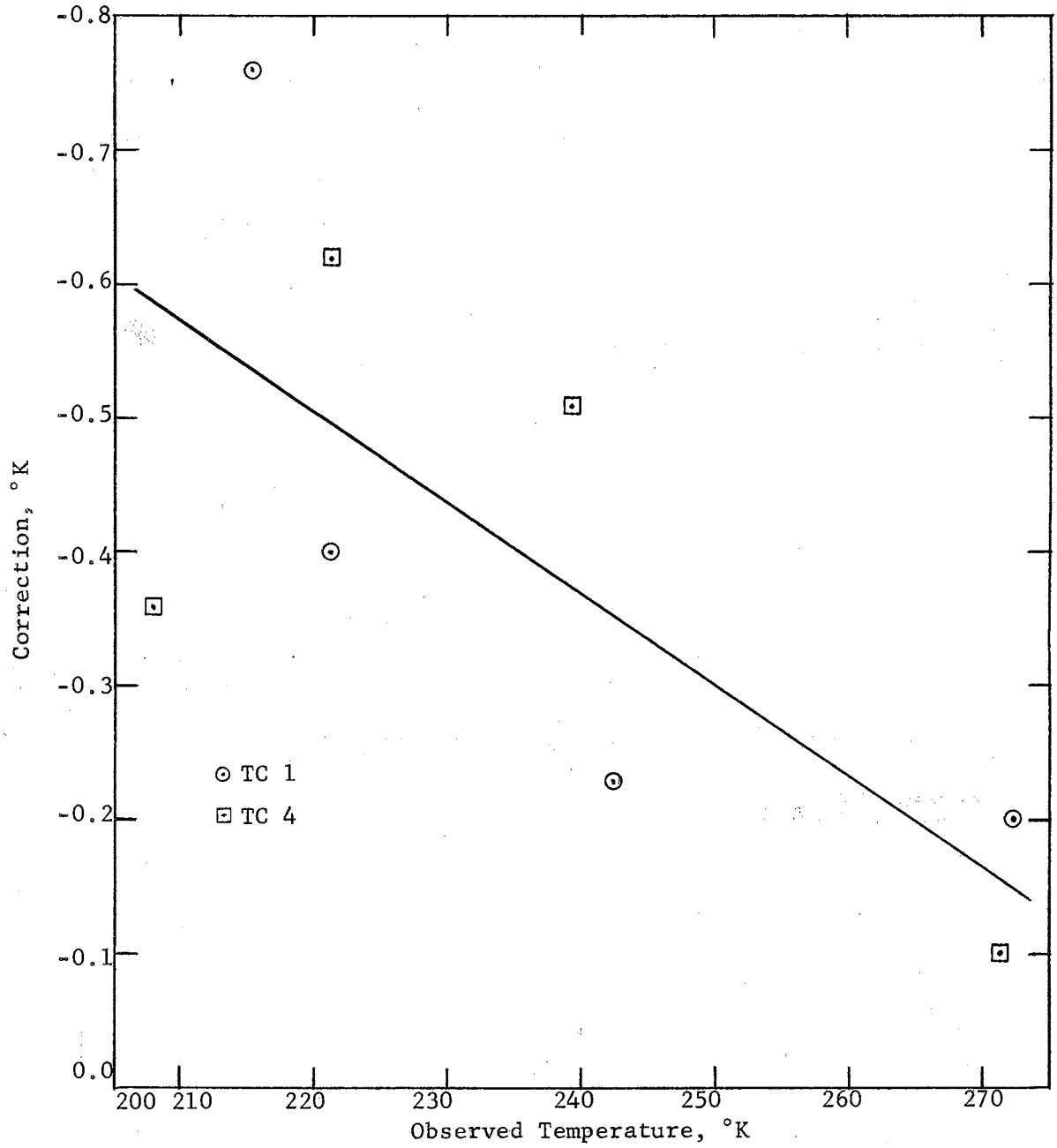

Figure D-I

Thermocouple Calibration Chart

TABLE D-I

THERMOCOUPLE CALIBRATION DATA

Run	Emf, mv	Actual T, °K	Dead Weight Gage lbs.	Dead Weight Gage gms.	Pressure, atms. abs.	Theoretical T, °K	Correction, °K
			Thermocouple #1, Bubble-Point Temperature				
1002	2.076	215.36	100	7	7.80	214.60	-0.76
2	1.833	222.63	130	190	10.27	222.59	-0.04
1026	1.145	242.43	260	5	18.69	242.20	-0.23
1031	0.020	272.64	560	170	39.48	272.44	-0.20
			Thermocouple #4, Dewpoint Temperature				
1001	2.321	207.85	70	101	5.97	207.49	-0.36
121	1.840	222.43	130	80	10.01	221.81	-0.62
1004	1.252	239.42	230	167	17.02	238.91	-0.51
31	0.071	271.32	550	10	38.42	271.22	-0.10

APPENDIX E

CALIBRATION OF STANDARD RESISTORS

TABLE E-I

CALIBRATION OF STANDARD RESISTORS

Nominal Size, Ohm	Leeds & Northrup Cat. Number	Serial Number	Date Calibrated	Resistance Ohms	Accuracy %
0.01	4222-B	1592716	Aug. 1962	0.010000	.01
10.0	4025-B	1609309	Aug. 1962	10.0000	.005
		1612893	Oct. 1962	10.0000	.005
1000.	4035-B	1611766	Nov. 1962	999.99	.005
		1611768	Nov. 1962	1000.02	.005

APPENDIX F

CALCULATIONS AND CORRECTIONS

The isobaric integral heat of vaporization of a mixture was calculated from the quotient of net power required for vaporization and weight of sample vaporized. The net power was calculated by subtracting the power lost by heat leak from the measured, or gross power.

The heat leak occurs in the reservoir constant-temperature zone from the reboiler tube to the charge in the reservoir and to the reservoir constant-temperature bath fluid, as shown schematically in Fig. F-1.

Originally the reboiler tube was jacketed and the annular space evacuated to minimize the heat leak. The thin walls of the outer vacuum jacket could not withstand the compressive forces within the Conax glands. Consequently gas leaks occurred at the reservoir and equilibrium cell glands.

The heat leak, the lesser of the two evils, was chosen in preference to a gas leak, and the reboiler tube was redesigned. The double-walled tube was replaced by a heavy, single-walled tube of the same O.D., which withstood the compressive forces and stopped the gas leak.

Gross Power Calculation

The gross power dissipated in the calorimeter was calculated by applying Ohm's Law (E = IR) to the heater circuit, shown in Figure 14,

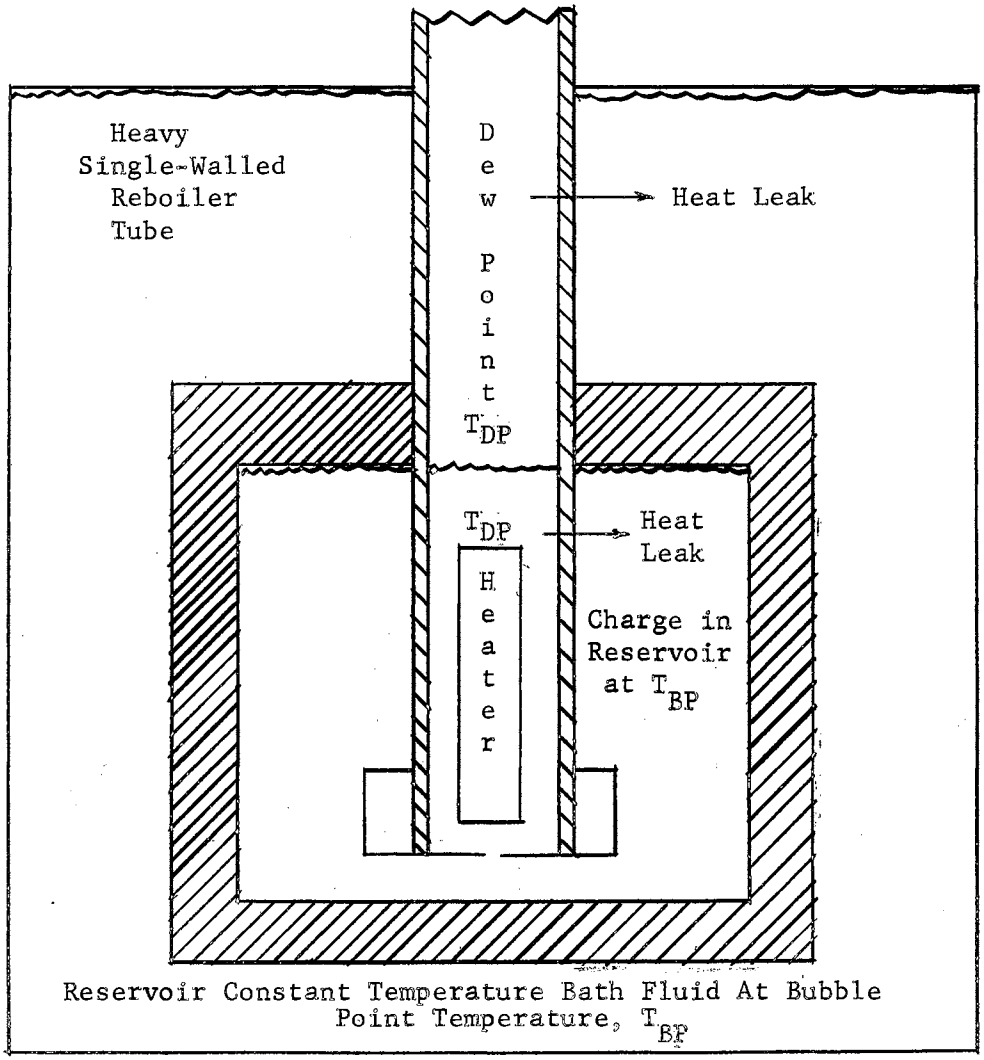

Figure F-1

Schematic Diagram of Heat Leak in Reservoir Constant Temperature Zone

as follows:

$$I_{total} = \frac{E_{total}}{R_{total}} = \frac{E_{0.01r}}{R_{0.01r}} = \frac{E_{0.01r}}{0.01} \tag{37}$$

$$I_{\substack{std \\ branch}} = I_{5.0r} = \frac{E_{5.0r}}{R_{5.0r}} = \frac{E_{5.0r}}{5.0} \tag{38}$$

$$I_{\substack{heater \\ branch}} = I_{total} - I_{std} = \frac{E_{0.01r}}{0.01} - \frac{E_{5.0r}}{5.0} \tag{39}$$

where the subscripts indicate that portion of the circuit in which the quantity was measured. The voltage drops across parallel branches of a circuit are equal. Therefore,

$$E - (IR)_{\substack{heater \\ branch}} = (IR)_{\substack{std \\ branch}} = \frac{E_{5.0r}}{5.0}\ (2000.01 + 5.0) \tag{40}$$

Since

$$\text{Energy} = EI = (IR)(I) \tag{41}$$

$$\text{Energy}_{heater} = (IR)_{heater}\ (I)_{heater} \tag{42}$$

$$= \frac{E_{5.0r}}{5.0}\ (2005.01)\left(\frac{E_{0.01r}}{0.01} - \frac{E_{5.0r}}{5.0}\right) \tag{43}$$

Run 46 is selected for purposes of illustration. Data appear in Table G-I.

$$\text{Energy}_{heater} = \frac{0.058485}{5.0}\ (2005.01)\left(\frac{0.015530}{0.01} - \frac{0.058485}{5.0}\right)$$

$$= (23.454)(1.541) = 36.20 \text{ watts}$$

Power = (Energy)(Time) = (36.20)(7.0) = 253.4 watt-min.

$$= (253.4)\left(14.34\ \frac{cal}{watt\text{-}min}\right) = 3{,}628.8 \text{ calories}$$

which appears in Table I.

Heat Leak Correction

To determine this correction, it was necessary to make a run on a substance whose heat of vaporization as a function of pressure was known. This eliminated the possibility of using a mixture; pure ethylene was selected.

An artificial dew point-bubble point temperature difference, or $T_{DP}-T_{BP}$ as shown in Figure F-1, was established by vaporizing the ethylene under a blanket of helium gas. Thus the charge in the reservoir and the reservoir constant-temperature bath fluid were sub-cooled at T_{BP}, as maintained by the temperature controller, and the ethylene vaporized by the heater was at its bubble point, T_{DP}, corresponding to the total pressure of ethylene and helium. Enough helium was introduced into the system to raise the bubble point of the ethylene about 20° K.

The increase in sensible heat of the liquid ethylene in rising from T_{BP} to T_{DP} was supplied by the heater. Therefore, the gross power measured was actually the sum of the increase in sensible heat, the heat leak, and the true heat of vaporization. The first term was calculated using the ideal gas state enthalpies given in API 44 (2) and the Yen-Alexander (49) equations, which are based on the improved Lydersen, Greenkorn and Hougen (24) "Corrections to Ideal Enthalpy Charts." The Yen-Alexander (49) equation for the saturated liquid region for $Z_c = 0.27$ (ethylene) is

$$(H^\circ-H)/T_c = \frac{5.8 + 5.19(-\ln P_r)^{0.4963}}{1.0 - 0.1(\ln P_r)} \qquad (44)$$

For Run 46, this increase in liquid enthalpy was 271 Btu/lb-mol or 5.37 cal/gm.

The true heat of vaporization was calculated by using the York and White (50) equation.

$$\lambda_{true} = 15.1906\ (T_c - T)^{0.5} - 0.426028\ (T_c - T) \qquad (45)$$

$$= 77.8 \text{ cal/gm}$$

The gross power, 3629 cal, was calculated using Equation 43 and expressed as the apparent heat of vaporization, $\lambda_{app.}$, by dividing by the weight of the sample, or 87.86 cal/gm.

$$\lambda_{app.} = \lambda_{true} + \text{sensible heat} + \text{heat leak},$$

$$\text{Heat leak} = \lambda_{app.} - \lambda_{true} - \text{sensible heat}$$

$$= 87.86 - 77.8 - 5.37$$

$$= 4.69 \text{ cal/gm, which is equivalent to}$$

$$\frac{(4.69 \text{ cal/gm})(41.3 \text{gm})}{(7.0 \text{ min})(243.93 - 226.93^{\circ}\text{K})} = 1.628 \text{ cal/min/}^{\circ}\text{K}.$$

In these units, this heat-leak correction factor was readily applied to all heat of vaporization calculations.

Barometric Correction

The most significant barometric correction is that for the expansion of the mercury, which is given by Hala, et al., (17),

$$P_o = P_t / (1 + 1.818 \times 10^{-6} T) \qquad (46)$$

where P_o = pressure, mm Hg, at 0° C

P_t = pressure, mm Hg, at temperature T, °C

Pressure Calculations

The Budenburg dead weight gauge has been certified to be accurate to 0.05% of reading, or 1 psi in 2,000, yet the smallest weight provided was equivalent to 10 psi. To measure pressures to the accuracy

capability of the dead weight gauge, an ordinary 1 to 300-gm weight set was used to span the 10 psi interval.

The various weights supplied with the dead weight gauge were weighed to determine the gms/psi ratio, which was 28.36. Thus, pressure readings appearing in the experimental data (Appendix G) are reported in lbs. and gms.

Consistency Tests

Edmister Test, Differential Form

The first term of Equation 27, d ln $(\phi_1/\phi_2)/dT$, was calculated by taking the dy/dx derivative of an analytical expression of the ln (ϕ_1/ϕ_2) vs. T data. The best quadratic equation passed through the bubble and dew point data was determined by a least-squares regression. The various ln (ϕ_1/ϕ_2) values were determined by the R-K (30) equation. The best cubic equation was obtained for the ln (y_1/y_2) vs. T data. The second term was calculated from the dy/dx derivative of this equation. These data are given in Table F-I and plotted in Figures 41 through 44.

The liquid enthalpy term on the right side of Equation 27 was calculated by subtracting the observed isobaric heat of vaporization from the enthalpy of a saturated vapor of the same composition. The saturated vapor enthalpies as a function of composition were determined by the R-K (30) equation and a least-squares quadratic equation passed through the data. The enthalpy of the vapor in equilibrium with the liquid was determined from this equation at the equilibrium vapor composition. These data are presented in Table F-II.

The Fortran source program for Equation 27 is listed in Appendix M, Program I.

TABLE F-I

TERMS FOR EDMISTER CONSISTENCY TEST

Run	T, °K	Mole Fraction Methane x_1	y_1	ϕ_1	ϕ_2	$\ln\phi_1/\phi_2$	$\ln y_1/y_2$
				20 Atmospheres			
36	226.8	.137	.408	0.9339	0.7600	0.2060	- .3722
	241.7	.023	.143	0.9676	0.7925	0.1995	-1.791
43	199.4	.436	.752	0.8771	0.6871	0.2442	1.1093
	226.3	.140	.420	0.9325	0.7591	0.2057	- .3228
42	176.5	.756	.942	0.8176	0.5963	0.3155	2.7876
	206.3	.324	.702	0.8908	0.7102	0.2265	0.8568
				40 Atmospheres			
40	253.7	.112	.364	0.9347	0.6496	0.3639	-0.5580
	263.3	.065	.131	1.0165	0.6714	0.4147	-1.892
41	235.3	.327	.685	0.8621	0.6070	0.3508	0.7768
	252.2	.189	.393	0.9274	0.6461	0.3615	-0.4347
37	199.4	.752	.928	0.7498	0.4336	0.5477	2.5564
	225.2	.407	.755	0.8365	0.5665	0.3897	1.125

TABLE F-II

TERMS FOR EDMISTER CONSISTENCY TEST

Run	T, °K	Mole Percent Methane[1/] x_1	y_1	$y_1 - x_1$	H_y^V #	Btu/lb-mole $(\Delta H_v)_{P,x}$	H_x^L	H_y^V	$\frac{H^L - H^V}{RT^2}$
				20 Atmospheres					
36	226.8	.137	.408	.271	2803	4622	-1819	2437	-0.02313
43	199.4	.436	.752	.316	2395	4170	-1775	2084	-0.02713
42	176.5	.756	.942	.186	2094	3419	-1325	1944	-0.02978
				40 Atmospheres					
40	253.7	.112	.364	.252	2797	3578	- 781	2860	-0.01581
41	235.3	.327	.685	.358	2871	3445	- 574	2483	-0.01544
37	199.4	.752	.928	.176	2339	2661	- 322	1855	-0.01531

1/ Experimental data from Table II.

Edmister Test, Integral Form

An analytical expression for (y_1-x_1) vs. T was required to perform the integral test of Equation 28. This quadratic equation was also determined by a least-squares regression of the experimental data. They are shown in Figures 45 and 47. The two left hand terms were integrated by parts. Details are given at the end of this appendix.

A least-squares quadratic equation was passed through the enthalpy data of the differential test to obtain an analytical function for $(\underline{H}^L-\underline{H}^V)/RT^2$ vs. T which could be integrated. These functions are shown in Figures 46 and 48.

A listing of the source program for Equation 28 is presented in Appendix M, Program II.

Thompson-Edmister Test, Differential Form

The partial derivative terms of Equation 138 were calculated by taking the dy/dx derivative of an analytical equation obtained by a least-squares regression of the ln K_i vs. (1/T) data, shown in Tables F-III and F-IV. This provided only six points for each pressure. To obtain more points, particularly near the pure component region, additional regressions were made using the T-x and T-y data. These equations were programmed to generate about 30 additional points of ln K_i vs. (1/T) data, which were incorporated into the first regression. Values of ln K_i at infinite dilution were obtained by extrapolation. These final equations (ln K_i vs. 1/T) are given in Figures 31 through 34. Plotted points were selected from Tables F-III and F-IV and the output from the temperature-composition program.

The IBM 1620 II source program for Equation 138 is given in

TABLE F-III

Ln K_i vs. (1/T), 20 Atmospheres

Run	T,°K	(1/T) x 10^3	x_1	y_1	K_1	$\ln K_1$	x_2	y_2	K_2	$\ln K_2$
					Bubble Point					
36	226.8	4.409	.137	.408	2.9781	1.0912	.863	.592	0.6860	-0.3769
43	199.4	5.015	.436	.752	1.7248	.5451	.564	.248	0.4397	-0.8217
42	176.5	5.666	.756	.942	1.2460	.2199	.244	.058	0.2377	-1.4367
					Dew Point					
36	241.7	4.137	.026	.143	5.5000	1.7047	.974	.857	0.8799	-0.1279
43	226.3	4.419	.143	.420	2.9371	1.0774	.857	.580	0.6768	-0.3904
42	206.3	4.847	.325	.702	2.1600	.7701	.675	.298	0.4415	-0.8176
					Pure Components					
Pure C_1	166.2	6.017	1.0	1.0	1.0	0	0	0	-	-3.9
Pure C_2	244.6	4.088	0	0	-	2.4	1.0	1.0	1.0	0

TABLE F-IV

Ln K_i vs. (1/T), 40 Atmospheres

Run	T,°K	$(1/T) \times 10^3$	x_1	y_1	K_1	$\ln K_1$	x_2	y_2	K_2	$\ln K_2$
					Bubble Point					
40	253.7	3.942	.112	.364	3.2500	1.1786	.888	.636	0.7162	-0.3337
41	235.3	4.250	.327	.685	2.0948	0.7395	.673	.315	0.4680	-0.7593
37	199.4	5.015	.752	.928	1.2340	0.2102	.248	.072	0.2903	-1.2368
					Dew Point					
40	263.3	3.798	.065	.131	2.0154	0.7008	.935	.869	0.9294	-0.0732
41	252.2	3.965	.189	.394	2.0846	0.7346	.811	.606	0.7472	-0.2914
37	225.2	4.440	.407	.750	1.8428	0.6113	.593	.250	0.4216	-0.8637
					Pure Components					
Pure C_1	186.8	5.353	1.0	1.0	1.0	0	0	0	-	-8.7
Pure C_2	272.0	3.676	0	0	-	1.7	1.0	1.0	1.0	0

Appendix M, Program III.

The values of ΔH^*_{exp}, as defined by Equation 137, were calculated by Program IV, Appendix M. The essential elements of this calculation are tabulated in Table F-V. Points on the saturated vapor enthalpy curve, $H_y^{V\#}$, were calculated using the EPE (11,12) program. An abbreviated EPE program was written to produce values for compositions higher than 60% methane at 40 atmospheres, which could not be obtained from the original EPE program. An analytical quadratic equation was obtained for the enthalpy-concentration data by least-squares regression, from which the values of $H_y^{V\#}$ were calculated at the experimental compositions. The saturated liquid enthalpies were calculated from the experimental data by

$$H_x^L = H_y^{V\#} - (\Delta H_v)_{exp} \tag{47}$$

The enthalpy-concentration diagrams are given in Figures 21 and 22. The values of H_y^V, the enthalpy of the saturated vapor in equilibrium with the saturated liquid x, were calculated from the equations of the enthalpy-concentration curves. The values of dH/dy were calculated from the derivatives of those equations evaluated at y. The partial molal enthalpies $\bar{H}_1^V$ at y_1 were calculated by

$$\bar{H}_1^V = \underline{H}^V + (1-y_1)(dH/dy) \tag{48}$$

The calculation of ξ_1 is detailed in Appendix K. The final results are given in Table VIII.

Thompson-Edmister Test, Integral Form

The value of the right hand integral of Equation 139 was determined by integrating the quadratic equation of $\Delta H^*/RT^2$ vs. T, which

was determined by a least-squares regression of those data from Table F-V. Equations of the curves are given in Figures 37 and 40.

The values of the two left hand integrals were determined by integrating the $x_i(1 + y_1\xi_1)$ vs. $\ln K_i$ curves between limits. The equations of the curves are given in Figures 35, 36, 38, and 39.

Modified Thompson-Edmister Test

Equation 138 was modified to Equation 144 and the differential test repeated using the same equations used in the original Thompson-Edmister (45) test. The derivatives were determined analytically. The integral test given by Equation 145 was integrated by parts. The first term will be used for illustration.

Let
$$\text{Ln } K_1 = K(T) \tag{48a}$$
$$x_1(1+y_1\xi_1) = x(T) \tag{48b}$$
$$\int x_1(1+y_1\xi_1)\frac{d\ln K_1}{dT} = \int udv \tag{48c}$$
Then
$$\int_{T_1}^{T_2} udv = uv\Big]_{T_1}^{T_2} - \int_{T_1}^{T_2} vdu \tag{48d}$$
$$= (x(T))(K(T))\Big]_{T_1}^{T_2} - \int_{T_1}^{T_2} (K(T))\frac{dx(T)}{dT}\,dT \tag{48e}$$

The derivative was determined analytically. The integral product was integrated easily. The source program of the resulting expression is given in Appendix M, Program VI.

TABLE F-V

CALCULATION OF ΔH^*_{exp}

Run	Experimental[1] T, °K	x_1	y_1	$(\Delta H_v)_{P,x}$	$H_y^{V\#}$ [2]	H_x^L	H_y^V [2]	dH^V/dy [3]	$\bar{H}_1^V$ [3]	K_1	K_2	ΔH^*_{exp}	$\Delta H^*/RT^2$
						20 atm.							
36	226.8	.137	.408	4.622	2.803	-1.819	2.437	-1.215	1.718	2.978	0.686	4.585	.02492
43	199.4	.436	.752	4.170	2.395	-1.775	2.084	-0.840	1.875	1.725	0.440	4.124	.02900
42	176.5	.756	.942	3.419	2.094	-1.325	1.944	-0.632	1.907	1.246	0.238	3.386	.03039
						40 atm.							
40	253.7	.112	.364	3.578	2.797	-0.781	2.860	-0.377	2.620	3.250	0.716	3.737	.01623
41	235.3	.327	.685	3.445	2.871	-0.574	2.483	-1.976	1.860	2.095	0.468	3.764	.01901
37	199.4	.752	.928	2.661	2.339	-0.322	1.855	-3.186	1.626	1.234	0.290	2.738	.01925

1/ See Tables I and II

2/ From EPE (11, 12) Program

3/ From Equation 48 programmed in Program IV, Appendix M.

TABLE F-VI

TERMS FOR MODIFIED THOMPSON-EDMISTER CONSISTENCY TEST

Run	T, °K	Experimental[1] Mole Fraction Methane x_1	y_1	ξ_1	$1+y_1\xi_1$	$T^2 \times 10^{-4}$	$\frac{\partial \ln K_1}{\partial T}$[2] x 10	$\frac{\partial \ln K_1}{\partial T}$[3] x 10	$\frac{\partial \ln K_2}{\partial (\frac{1}{T})}$[4]	$\frac{\partial \ln K_2}{\partial T}$[3] x 10
					20 Atmospheres					
36	226.8	.137	.408	.4224	1.1723	5.1438	-758.6	.14748	-944.8	.18368
43	199.4	.436	.752	.2519	1.1894	3.9760	-758.6	.19079	-944.8	.23763
42	176.5	.756	.942	.0549	1.0517	3.1152	-758.6	.24352	-944.8	.30329
					40 Atmospheres					
40	253.7	.112	.364	.6119	1.2227	6.4364	-678.9	.10548	-1025.5	.15933
41	235.3	.327	.685	.3439	1.2356	5.5366	-678.9	.12262	-1025.5	.18522
37	199.4	.752	.928	.0612	1.0568	3.9760	-678.9	.17075	-1025.5	.25792

1/ See Table II.
2/ See Figures 31 and 33.
3/ See Equation 48a.
4/ See Figures 32 and 34.

APPENDIX G

EXPERIMENTAL DATA

TABLE G-I

EXPERIMENTAL THERMOCOUPLE DATA

Negative Emf, mv

Run	Pressure, Atms. abs.	Feed Comp. %	TC 1	TC 2	TC 3	TC 4	TC 5	TC 6	TC 7	TC 8	TC 9	TC 11
						Pure-Grade Methane						
44	20.21	99+	3.506	3.529	3.556	3.498	3.339	3.159	3.054	3.066	3.302	3.551
45	40.09	99+	3.080	3.081	2.999	3.044	3.066	2.998	2.889	2.900	3.121	3.210
						Pure-Grade Ethylene						
27	19.59	99+	1.064	1.080	1.039	1.070	1.075	1.069	0.977	0.912	1.125	1.166
47	20.15	99+	1.052	1.063	1.173	0.789	1.064	1.016	0.984	0.994	1.537	1.145
31	38.42	99+	0.063	0.095	0.138	0.071	0.080	0.079	0.051	0.003	-0.026	0.096
						Heat-Leak Calibration, Pure Grade Ethylene						
46	19.94	99+	1.687	1.664	1.723	1.091	1.131	1.124	1.047	1.072	1.566	1.132
						Mixtures at 20 Atmospheres						
36	19.95	13.7	1.020	0.906	1.062	0.050	0.713	0.529	0.432	0.380	1.477	1.657
43	20.81	43.6	2.571	2.432	2.537	1.690	1.978	1.710	1.544	1.561	2.473	2.865
42	19.94	75.6	3.255	3.476	3.550	2.351	3.041	2.744	2.552	2.570	2.900	2.831
						Mixtures at 40 Atmospheres						
40	39.97	11.2	0.725	0.561	0.594	0.370	0.351	0.084	-0.050	-0.114	1.544	1.526
41	38.07	32.7	1.382	1.640	1.534	0.868	1.125	0.842	0.741	0.707	2.338	2.354
37	42.44	75.2	1.407	1.791	1.524	0.660	1.290	1.096	0.999	0.950	2.333	2.319

TABLE G-II

EXPERIMENTAL DATA

Run	Pressure Atms. abs.	Feed Comp. %	5 Ohm Resistor Emf 1, mv	5 Ohm Resistor Emf 2,mv	0.01 Ohm Resistor Emf 1, mv	0.01 Ohm Resistor Emf 2,mv	Dead Weight Gage lbs.	Dead Weight Gage gms.	Sample, gms.	Time, min.
					Pure-Grade Methane					
44	20.21	99+	41.328	41.349	11.055	11.066	280	80	24.2	7.75
45	40.09	99+	41.323	41.330	11.044	11.048	570	140	48.8	7.75
					Pure-Grade Ethylene					
27	19.59	99+	41.265	41.276	13.497	13.503	270	105	39.9	10.00
47	20.15	99+	41.288	41.379	10.988	10.991	280	55	26.1	7.75
31	38.42	99+	41.374	41.364	12.087	12.093	550	10	59.9	10.00
					Heat-Leak Calibration, Pure-Grade Ethylene					
46	19.94	99+	58.470	58.510	15.513	15.547	270	250	41.3	7.00
					Mixtures at 20 Atmospheres					
36	19.95	13.7	58.750	58.970	15.327	15.321	270	255	45.4	9.00
43	20.81	43.6	58.771	58.795	15.618	15.618	290	48	36.7	7.75
42	19.94	75.6	58.803	58.809	15.638	15.647	270	252	36.9	7.75
					Mixtures at 40 Atmospheres					
40	39.97	11.2	58.706	58.733	15.558	15.572	570	95	52.7	7.75
41	38.07	32.7	58.719	58.700	15.574	15.576	540	150	48.3	7.75
37	42.44	75.2	58.724	58.726	15.570	15.583	600	275	41.7	6.75

APPENDIX H

LIMITS OF EXPERIMENTAL ERROR

The error in each result and the individual fractional errors in each measurement used to calculate that result are given in Table H-1. The individual errors were combined by the method of Topping (46).

TABLE H-I

LIMITS OF EXPERIMENTAL ERROR
IN RESULTS AND MEASUREMENTS

Result	Measurement or Instrument	Limit of Error
Enthalpy		0.15%
	Potentiometer	0.01%
	Standard Resistors	0.01%
	Time	0.1 %
	Weight	0.01%
Pressure	Dead Weight Gauge	0.05%
Temperature	Thermocouples	0.2 %
Composition	Gas Chromatograph	1.5 mol%

APPENDIX I

DERIVATION OF CALCULATION METHODS

FOR THE

ISOBARIC INTEGRAL HEAT OF VAPORIZATION

Edmister K-Value Approximation Method

Edmister (9) developed a method for calculating the isobaric integral heat of vaporization of multicomponent hydrocarbon mixtures from K-values and bubble and dew point temperatures. For either phase the basic equation derived from the definition of fugacity is

$$\bar{L}_i = \bar{H}_i - H_i^\circ = -RT^2\left(\frac{\partial \ln \bar{f}_i}{\partial T}\right)_{P,x} \tag{49}$$

where $\bar{L}_i$ = partial molal quantity

$^\circ$ = ideal gas value

i = i th component

For the constant pressure-composition case

$$x = y^{\#} = z$$

where z = mole fraction of a component in any mixture.

Defining a new enthalpy difference term

$$D = \sum_{i=1}^{n} y_i \bar{L}_i^V - \sum_{i=1}^{n} x_i \bar{L}_i^L \tag{50}$$

Expanding and rearranging

$$D = \sum_{i=1}^{n} z_i \left[(\bar{H}_i^V - H_i^\circ)_{T_{DP}} - (\bar{H}_i^L - H_i^\circ)_{T_{BP}} \right] \tag{51}$$

$$= \sum z_i \left(\bar{H}_{i_{T_{DP} y_{DP}^{\#}}}^V - \bar{H}_{i_{T_{BP} x_{BP}}}^L \right) - \sum z_i \left(H_{i_{T_{DP}}}^\circ - H_{i_{T_{BP}}}^\circ \right) \tag{52}$$

$$= (\Delta H_v)_{P,x} - \sum z_i \, \Delta H_i^\circ \tag{53}$$

Substituting Equation 49 into Equation 50

$$D = \sum z_i RT_{BP}^2 \left(\frac{\partial \ln \bar{f}^L_{i_{T_{BP}x_{BP}}}}{\partial T}\right)_{P,x_{BP}} - \sum z_i RT_{DP}^2 \left(\frac{\partial \ln \bar{f}^V_{i_{T_{DP}y^{\#}_{DP}}}}{\partial T}\right)_{P,y^{\#}_{DP}} \quad (54)$$

where $x_{BP} = y^{\#}_{DP}$

Equation 54 is next expressed in difference form instead of differential form as

$$D\,(T_{DP}-T_{BP}) = \sum z_i RT_{BP}^2 \left(\ln \bar{f}^L_{i_{T_{DP}x_{BP}}} - \ln \bar{f}^L_{i_{T_{BP}x_{BP}}}\right)_{P,x_{DP}}$$

$$- \sum z_i RT_{DP}^2 \left(\ln \bar{f}^V_{i_{T_{DP}y^{\#}_{DP}}} - \ln \bar{f}^V_{i_{T_{BP}y^{\#}_{DP}}}\right)_{P,y^{\#}_{DP}} \quad (55)$$

from which

$$D = \frac{R}{(T_{DP}-T_{BP})}\left[\sum z_i \; T_{BP}^2 \ln \left(\frac{\bar{f}^L_{i_{T_{DP}}}}{\bar{f}^L_{i_{T_{BP}}}}\right)_{x_{BP}} - T_{DP}^2 \ln \left(\frac{\bar{f}^V_{i_{T_{DP}}}}{\bar{f}^V_{i_{T_{BP}}}}\right)_{y^{\#}_{DP}}\right]_P \quad (56)$$

The first of two approximations will now be made, namely that

$$\left(\frac{\bar{f}^L_{i_{T_{DP}}}}{\bar{f}^L_{i_{T_{BP}}}}\right)_{x_{BP}} \approx \left(\frac{\bar{f}^L_{i_{T_{DP}x_{DP}}}}{\bar{f}^L_{i_{T_{BP}x_{BP}}}}\right) \quad (13a)$$

and

$$\left(\frac{\bar{f}^V_{i_{T_{DP}}}}{\bar{f}^V_{i_{T_{BP}}}}\right)_{y^{\#}_{DP}} \approx \left(\frac{\bar{f}^V_{i_{T_{DP}y_{DP}}}}{\bar{f}^V_{i_{T_{BP}y_{BP}}}}\right) \quad (13b)$$

Substituting Equations 13a and 13b into Equation 56 and dividing by x and y as indicated,

$$D = \frac{R}{(T_{DP}-T_{BP})} \sum z_i \left[T_{BP}^2 \ln \frac{(\bar{f}_i^L/x_i)_{T_{DP}x_{DP}}}{(\bar{f}_i^L/x_i)_{T_{BP}x_{BP}}} - T_{DP}^2 \ln \frac{(\bar{f}_i^V/y_i)_{T_{DP}y_{DP}}}{(\bar{f}_i^V/y_i)_{T_{BP}y_{BP}}} \right] \quad (57)$$

The second approximation will now be made, namely that

$$T_{BP}^2 \approx T_{BP}T_{DP} \approx T_{DP}^2 \quad (14)$$

Substituting Equation 14 into Equation 57

$$D = \frac{RT_{BP}T_{DP}}{(T_{DP}-T_{BP})} \sum z_i \ln \left[\frac{(\bar{f}_i^L/x_i)_{DP}(\bar{f}_i^V/y_i)_{BP}}{(\bar{f}_i^L/x_i)_{BP}(\bar{f}_i^V/y_i)_{DP}} \right] \quad (58)$$

In terms of K-values

$$K_{i_{BP}} = \frac{y_{i_{BP}}}{x_{i_{BP}}} \quad (59a)$$

and

$$K_{i_{DP}} = \frac{y_{i_{DP}}}{x_{i_{DP}}} \quad (59b)$$

Equation 58 becomes

$$D = \frac{RT_{BP}T_{DP}}{T_{DP}-T_{BP}} \sum z_i \ln \frac{K_{i_{DP}}}{K_{i_{BP}}} \quad (60)$$

Equating Equations 60 and 53 and rearranging

$$(\Delta H_v)_{P,x} = \frac{RT_{BP}T_{DP}}{(T_{DP}-T_{BP})} \sum z_i \ln \frac{K_{i_{DP}}}{K_{i_{BP}}} + \sum z_i \Delta H_i^\circ \qquad (15)$$

While Equation 15 utilizes the two assumptions of Equations 13 and 14, values of $(\Delta H_v)_{P,x}$ calculated by it are fairly good, considering the minimum amount of information required, K-values and bubble and dew point temperatures. Edmister (9) also gives ways of estimating these quantities, if necessary. Equation 15 was programmed on the IBM 1620 computer to carry out the calculations included herein.

Edmister has also derived Equation 15 by an alternate method, as follows:

For an isobaric process

$$\left(\frac{\partial \ln \bar{f}_i^L}{\partial T}\right)_{P,x} = \left(\frac{\partial \ln \bar{f}_i^L/x_i}{\partial T}\right)_{P,x} = \frac{H_i^\circ - \bar{H}_i^L}{RT^2} \qquad (61)$$

Since

$$\ln \bar{f}_i^L/x_i = \ln K_i \gamma_i^V + \ln f_i^V \qquad (62)$$

$$\left(\frac{\partial \ln \bar{f}^L/x_i}{\partial T}\right)_{P,x} = \left(\frac{\partial \ln K_i \gamma_i^V}{\partial T}\right) + \left(\frac{\partial \ln f_i^V}{\partial T}\right)_{P,x} \qquad (63)$$

Two additional relationships are needed.

$$\left(\frac{\partial \ln f^V}{\partial T}\right)_{P,x} = \frac{H_i^\circ - H_i^V}{RT^2} \qquad (64)$$

and

$$\left(\frac{\partial \ln \gamma^V}{\partial T}\right)_{P,x} = \frac{H_i^V - \bar{H}_i^V}{RT^2} \qquad (65)$$

Combining Equations 61, 63, 64, and 65

$$\left(\frac{\partial \ln K_i \gamma_i^V}{\partial T}\right)_{P,x} - \left(\frac{\partial \ln \gamma_i^V}{\partial T}\right)_{P,x} = \frac{(\overline{\Delta H}_v)_{P,x} - \Delta H_i^\circ}{RT^2} \qquad (66)$$

where $(\overline{\Delta H}_v)_{P,x} = (\bar{H}^V_{DP} - \bar{H}^L_{BP})_i$

$$\Delta H^\circ_i = (H^\circ_{DP} - H^\circ_{BP})_i$$

Since $dT = -T^2 d(1/T)$, Equation 66 may also be written

$$R\left[\left(\frac{\partial \ln K_i \gamma^V_i}{\partial(1/T)}\right)_{P,x} - \left(\frac{\partial \ln \gamma^V_i}{\partial(1/T)}\right)_{P,x}\right] = \Delta H^\circ_i - (\overline{\Delta H}_v)_{P,x} \qquad (67)$$

When $\gamma^V_i = 1.0$; i.e., when the Lewis and Randall fugacity rule applies, Equation 67 becomes

$$R\left(\frac{\partial \ln K_i}{\partial(1/T)}\right)_{P,x} = \Delta H^\circ_i - (\overline{\Delta H}_v)_{P,x} \qquad (68)$$

The differential term on the left side is now replaced with a difference term

$$\frac{d \ln K}{d(1/T)} = \frac{T_{BP} T_{DP}}{T_{BP} - T_{DP}} \ln \frac{K_{DP}}{K_{BP}} \qquad (69)$$

Substituting Equation 69 into Equation 68, rearranging, and summing over components

$$(\Delta H_v)_{P,x} = \frac{R T_{BP} T_{DP}}{T_{DP} - T_{BP}} \sum z_i \ln \frac{K_{i_{DP}}}{K_{i_{BP}}} + \sum z_i \Delta H^\circ_i \qquad (15)$$

Edmister-Persyn-Erbar Method

Edmister, Persyn and Erbar (11, 12) have developed a computer program for calculating consistent K-values, saturated liquid and vapor enthalpies, and partial enthalpies of multicomponent hydrocarbon mixtures. Only the saturated vapor and liquid portions of their work will be discussed here.

The saturated vapor enthalpy of mixtures was computed using the API 44 (2) ideal gas state values H_i° and the Redlich-Kwong (R-K) (30) equation to calculate the pressure effect on the enthalpy. A cubic polynominal equation was developed for each component to represent the ideal gas state values; the R-K equation was used in the enthalpy form. These were combined to give

$$H^V_{Mix} = \sum y_i H_i^\circ - RT\left[\frac{3}{2}\frac{A^2}{B}\ln\left(1+\frac{BP}{Z}\right) + 1 - Z\right] \qquad (70)$$

where $A^2 = \dfrac{a}{R^2T^{2.5}} = 0.4278\,\dfrac{T_c^{2.5}}{P_cT^{2.5}}$

$$B = \frac{b}{RT} = 0.0867\,\frac{T_c}{P_cT}$$

$$Z = \frac{PV}{RT} = \frac{1}{(1-h)} - \frac{A^2}{B}\,\frac{h}{(1+h)}$$

$$h = \frac{BP}{Z}$$

and using $A = \sum y_i A_i$

$$B = \sum y_i B_i$$

for mixtures.

The method for calculating the saturated liquid enthalpy given in the original paper (11) was improved in a later paper (12). This latter approach will now be discussed.

The saturated liquid mixture enthalpy was calculated in three parts: the ideal state H_i°, the simple fluid enthalpy difference from the ideal state $\left(\dfrac{H_i^\circ - H_i}{RT_c}\right)^\circ$, and the departure from a simple fluid $\left(\dfrac{H_i^\circ - H_i}{RT_c}\right)'$. In equation form,

$$H^{L}_{Mix} = \sum x_i \left[H^{\circ}_i + \left(\frac{H^{\circ}_i - H_i}{RT_c}\right)^{\circ} + \omega \left(\frac{H^{\circ}_i - H_i}{RT_c}\right)' \right] \tag{71}$$

where ω = acentric factor

API 44 (2) values were used for the ideal state. For the ideal difference and simple fluid departure contributions, the authors developed correction term equations Δ and Δ', which were added to the Grayson-Streed (13) equations.

Grayson and Streed modified and extended the work done by Chao-Seader (6) who used the simple fluid model developed by Pitzer, et al. (23). The values of the difference terms calculated using the Erbar-Persyn-Edmister correction equations agreed very well with the original Pitzer values. The final equations are (12)

$$\left(\frac{H^{\circ}_i - H_i}{RT_c}\right)^{\circ} = 2.30259\, T_r \left[-A_1 T_r^{-1} + A_2 + 2A_3 T_r + 3A_4 T_r^2 \right.$$

$$\left. + (A_6 + 2A_7 T_r)\, P_r + A_9 P_r^2 \right] + \Delta \text{ (or } \Delta_1) \tag{72}$$

where A_1, etc., are the Grayson-Streed (13) constants given in Table I-I of Appendix I and

$$\Delta = C_o + C_1 T_r \qquad (T_r < 1.0) \tag{73a}$$

$$= 0 \qquad (T_r > 1.0) \tag{73b}$$

For methane, a special correction term was required which was

$$\Delta_1 = E_o + E_1 T_r + E_2 T_r^2 \qquad (T_r < 1.0) \tag{74a}$$

$$= 0 \qquad (T_r > 1.0) \tag{74b}$$

For the generalized departure from the enthalpy of a simple fluid another equation is required, namely

$$\left(\frac{H_i^\circ - H_i}{RT_c}\right)' = 2.30259\ T_t \left[8.65808 + 1.22020\ T_r^{-2} - 9.45672\ T_r^2\right] + \Delta' \qquad (75)$$

where $\Delta' = D_o + D_1 T_r + D_2 T_r^2 \qquad (T_r < 1.0) \qquad (76a)$

$= 0 \qquad (T_r > 1.0) \qquad (76b)$

Calculations used in this investigation were carried out on an IBM 1401 computer using a program supplied by the authors (12).

Yen-Alexander Method

Yen and Alexander (49) have developed mathematical expressions for the generalized enthalpy correction charts of Lydersen, Greenkorn and Hougen (24). These equations are primarily for computer application. For the saturated vapor line

$$\frac{H^\circ - H}{T_c} = \frac{5.4\ P_r^{0.6747}}{1+1.227(-\ln P_r)^{0.503}} \qquad (Z_c = 0.29, \text{ methane}) \qquad (77a)$$

$$= \frac{5.8\ P_r^{0.63163}}{1+1.229(-\ln P_r)^{-.55456}} \qquad (Z_c = 0.27, \text{ ethylene}) \qquad (77b)$$

For the saturated liquid line

$$\frac{H^\circ - H}{T_c} = \frac{5.4+3.6485(-\ln P_r)}{1-0.0056942(\ln P_r)} \qquad (Z_c = 0.29) \qquad (78a)$$

$$= \frac{5.8+5.19(-\ln P_r)^{0.4963}}{1-0.1(\ln P_r)} \qquad (Z_c = 0.27) \qquad (78b)$$

The suggested mixing rules are

$$Z_{Pc} = \sum x_i Z_{c_i}$$

$$T_{Pc} = \sum x_i T_{c_i}$$

$$P_{Pc} = \sum x_i P_{c_i}$$

These equations and others representing the API 44 (2) ideal state enthalpies of methane and ethylene were programmed for the IBM 1620 computer to calculate values to compare with the experimental data obtained in this investigation.

TABLE I-I

CONSTANTS FOR PURE LIQUID ENTHALPY, EQUATION 72

Source: Grayson-Streed (13)

	General	Methane	Hydrogen
A_1	-2.10899	-1.54831	2.74283
A_2	0.0	0.0	-0.02110
A_3	-0.19396	0.02889	0.00011
A_4	0.02282	-0.01076	0.0
A_6	0.0	-0.02529	0.0
A_7	-0.00872	0.0	0.0
A_9	0.00203	0.0	0.0

TABLE I-II

CONSTANTS FOR PURE LIQUID ENTHALPY CORRECTION EQUATIONS

Source: Erbar-Persyn-Edmister (12)

Simple Fluid Equation 73a	
C_0	2.0048
C_1	-2.3958

Departure from Simple Fluid Equation 76a	
D_0	36.778
D_1	-103.02
D_2	68.616

Methane Equation 74a	
E_0	-0.4479
E_1	8.0837
E_2	-8.0012

APPENDIX J

DERIVATION OF THOMPSON-EDMISTER CONSISTENCY TEST

Thermodynamic consistency tests are derived from basic equations to compare two types of experimental data. Isobaric consistency tests usually compare enthalpy data with fugacities or vapor-liquid equilibria (VLE) data. As mentioned in the previous chapter, the experimental apparatus used in this investigation was especially designed to collect enthalpy and VLE data simultaneously for use in the isobaric test.

Until recently, the consistency equations of Adler, et al. (1), provided the best approach to experimental thermodynamic consistency because they used observables (equilibrium compositions, volumetric data and enthalpy differences), rather than derived quantities. The derivation of the equations assumed that the vapor obeyed the Lewis and Randall rule (22). Since deviations from this rule are more significant at high pressures the results of applying the equations to these high pressure data would be questionable.

Recently, Thompson and Edmister (45) made a rigorous derivation of similar equations which do not assume that the Lewis and Randall rule applies, as given below.

Consider a reversible process acting on a closed system wherein pressure is the only acting force, then by the First and Second Laws of Thermodynamics

$$H = U + PV \tag{79a}$$

$$dH = dU + PdV + VdP \tag{79b}$$

$$dU = TdS - PdV \tag{79c}$$

Combining Equations 79b and 79c

$$dH = TdS + VdP \tag{80}$$

The Gibbs-Duhem equation will now be derived in general form. The Gibbs free energy function G is defined by

$$G = H - TS \tag{81}$$

from which

$$dG = dH - TdS - SdT \tag{82}$$

Substituting Equation 80 into Equation 82

$$dG = VdP - SdT \tag{83}$$

Now consider an open (variable mass) system, where

$$G = G(T,P,n_1,\cdots n_n) \tag{84}$$

By the chain rule

$$dG = \left(\frac{\partial G}{\partial T}\right)_{P,n_i} dT + \left(\frac{\partial G}{\partial P}\right)_{T,n_i} dP + \sum_{i=1}^{n} \left(\frac{\partial G}{\partial n_i}\right)_{T,P} dn_i \tag{85}$$

By comparison of Equations 83 and 85

$$\left(\frac{\partial G}{\partial P}\right)_{T,n_i} = V \tag{86}$$

$$\left(\frac{\partial G}{\partial T}\right)_{P,n_i} = -S \tag{87}$$

and Equation 85 becomes

$$dG = -SdT + VdP + \sum \left(\frac{\partial G}{\partial n_i}\right) dn_i \tag{88}$$

Guggenheim (14) has shown that Equation 88 can be integrated under conditions of constant P and T, where

$$dP = dT = 0 \tag{89}$$

to

$$G = \sum \mu_i n_i \tag{90}$$

where $\mu_i = \left(\frac{\partial G}{\partial n_i}\right)_{T,P}$ (91)

Differentiating Equation 90

$$dG = \sum \mu_i dn_i + \sum n_i d\mu_i \quad (92)$$

Comparing Equations 88 and 92

$$\sum n_i d\mu_i = -SdT + VdP \quad (93)$$

which is the Gibbs-Duhem equation in general form.

Equation 93 will now be written for a closed system in equilibrium. Dividing Equation 93 by the total number of moles, Σn_i

where $x_i = n_i/\Sigma n_i$

$$\Sigma x_i d\mu_i = -\underline{S}dT + \underline{V}dP \quad (94)$$

Since $\mu_i = \mu_i (P,T,x_i)$

$$d\mu_i = \left(\frac{\partial \mu_i}{\partial P}\right)_{T,x_i} dP + \left(\frac{\partial \mu_i}{\partial T}\right)_{P,x_i} dT + \left(\frac{\partial \mu_i}{\partial x_i}\right)_{T,P} dx_i \quad (95)$$

$$= \bar{V}_i dP - \bar{S}_i dT + \left(\frac{\partial \mu_i}{\partial x_i}\right)_{T,P} dx_i \quad (96)$$

Combining Equations 94 and 96 at constant P and T,

$$\sum x_i \left(\frac{\partial \mu_i}{\partial x_i}\right)_{P,T} dx_i = 0 \quad (97)$$

Equations 96 and 97 can be written separately for liquid and gas phases, or

$$d\mu_i^L = \bar{V}_i^L dP - \bar{S}_i^L dT + \left(\frac{\partial \mu_i^L}{\partial x_i}\right)_{P,T} dx_i \quad (98a)$$

$$d\mu_i^V = \bar{V}_i^V dP - \bar{S}_i^V dT + \left(\frac{\partial \mu_i^V}{\partial y_i}\right)_{P,T} dy \quad (98b)$$

$$\sum x_i \left(\frac{\partial \mu_i^L}{\partial x_i}\right)_{P,T} dx_i = 0 \tag{99a}$$

$$\sum y_i \left(\frac{\partial \mu_i^V}{\partial y_i}\right)_{P,T} dy_i = 0 \tag{99b}$$

If the phases coexist in equilibrium an additional condition is imposed, which is

$$d\mu_i^L = d\mu_i^V \tag{100}$$

Substituting Equations 98a and 98b into Equation 100 and rearranging

$$\left(\frac{\partial \mu_i^L}{\partial x_i}\right)_{P,T} dx_i - \left(\frac{\partial \mu_i^V}{\partial y_i}\right)_{P,T} dy_i = \left(\bar{V}_i^V - \bar{V}_i^L\right) dP - \left(\bar{S}_i^V - \bar{S}_i^L\right) dT \tag{101}$$

$$= \Delta\bar{V}_i dP - \Delta\bar{S}_i dT \tag{102}$$

where $\Delta\bar{S}_i$ = partial molal entropy difference between equilibrium vapor and liquid.

Equation 102 is now written for the liquid phase of a binary system

$$x_1 \left(\frac{\partial \mu_1^L}{\partial x_i}\right)_{P,T} dx_1 + x_2 \left(\frac{\partial \mu_2^L}{\partial x_2}\right)_{P,T} dx_2 - x_1 \left(\frac{\partial \mu_1^V}{\partial y_1}\right)_{P,T} dy_1 - x_2 \left(\frac{\partial \mu_2^V}{\partial y_2}\right)_{P,T} dy_2$$

$$= (x_1\Delta\bar{V}_1 + x_2\Delta\bar{V}_2)\, dP - (x_1\Delta\bar{S}_1 + x_2\Delta\bar{S}_2)\, dT \tag{103}$$

Expanding Equation 99a for a liquid phase,

$$x_1 \left(\frac{\partial \mu_1^L}{\partial x_1}\right)_{P,T^1} dx_1 + x_2 \left(\frac{\partial \mu_2^L}{\partial x_2}\right)_{P,T^2} dx_2 = 0 \tag{104}$$

and 99b for the vapor phase

$$y_1 \left(\frac{\partial \mu_1^V}{\partial y_1}\right)_{P,T^1} dy_1 + y_2 \left(\frac{\partial \mu_2^V}{\partial y_2}\right)_{P,T^2} dy_2 = 0 \tag{105}$$

Rearranging and recalling that $dy_1 = -dy_2$

$$\left(\frac{\partial \mu_2^V}{\partial y_2}\right)_{P,T} = \frac{y_1}{y_2}\left(\frac{\partial \mu_1^V}{\partial y_1}\right)_{P,T} \tag{106}$$

Substituting Equations 104 and 106 into Equation 103 and collecting terms

$$\left(\frac{y_1 - x_1}{1 - y_1}\right)\left(\frac{\partial \mu_1^V}{\partial y_1}\right)_{P,T} dy_1 = (x_1\Delta\bar{V}_1 + x_2\Delta\bar{V}_2)\, dP - (x_1\Delta\bar{S}_1 + x_2\Delta\bar{S}_2)\, dT \tag{107}$$

An expression will now be derived for $\left(\frac{\partial \mu_1^V}{\partial y_1}\right)_{P,T}$. By definition (22) of the fugacity f at constant T

$$d\underline{G} = RT\, d \ln f \qquad (dT = 0) \tag{108}$$

Dodge (8) also defines

$$d\mu_i^V = RT\, d \ln \bar{f}_i^V \qquad (dT = 0) \tag{109}$$

and

$$\mu_i^V = RT \ln \bar{f}_i^V + \mu_i^{\circ V} \tag{110}$$

from which

$$\left(\frac{\partial \mu_i^V}{\partial P}\right)_T = RT\left(\frac{\partial \ln \bar{f}_i^V}{\partial P}\right)_T \tag{111}$$

From Equation 86

$$\left(\frac{\partial \mu_i^V}{\partial P}\right)_{T,n_j} = \left[\frac{\partial}{\partial n_i}\left(\frac{\partial G}{\partial P}\right)_{T,n_j}\right]_{T,P} = \left(\frac{\partial V}{\partial n_i}\right)_{T,P} = \bar{V}_i \tag{112}$$

Substituting Equation 112 into Equation 111

$$\left(\frac{\partial \ln \bar{f}_i^V}{\partial P}\right)_T = \frac{\bar{V}_i}{RT} \tag{113}$$

Integrating

$$\ln \frac{\bar{f}_{i_2}^V}{\bar{f}_{i_1}^V} = \frac{1}{RT}\int_{P_1}^{P_2} \bar{V}_i dP \qquad \text{(T constant)} \tag{114}$$

If state 1 is chosen such that $\bar{f}_i = Py_i$, then

$$\ln \frac{\bar{f}^V_{i_2}}{P_1 y_i} = \frac{1}{RT} \int_{P_1}^{P_2} \bar{V}_i dP = \frac{1}{RT} \int_{P_1}^{P_2} \left(\frac{RT}{P} - \bar{\alpha}_i \right) dP \tag{115}$$

where $\bar{\alpha}_i = \frac{RT}{P} - \bar{V}_i$ (116)

Expanding and rearranging Equation 115

$$RT \ln \bar{f}^V_{i_2} - RT \ln P_1 - RT \ln y_i = RT \ln P_2 - RT \ln P_1 - \int_{P_1}^{P_2} \bar{\alpha}_i dP \tag{117}$$

or

$$RT \ln \frac{\bar{f}^V_{i_2}}{P_2 y_i} = - \int_{P_1}^{P_2} \bar{\alpha}_i dP \tag{118}$$

Letting $P_1 \rightarrow 0$ and $P_2 \rightarrow P$

$$RT \ln \frac{\bar{f}^V_i}{Py_i} = - \int_0^P \bar{\alpha}_i dP = - \int_0^P \left(\frac{RT}{P} - \bar{V}_i \right) dP \tag{119}$$

In terms of the chemical potential

$$\mu^V_i - \mu^o_i = RT \ln \bar{f}^V_i \tag{120}$$

$$= RT \ln y_i P + \int_0^P \left(\bar{V}_i - \frac{RT}{P} \right) dP \tag{121}$$

Differentiating

$$\left(\frac{\partial \mu^V_i}{\partial y_i} \right)_{P,T} = \frac{RT}{y_i} + \int_0^P \left(\frac{\partial \bar{V}_i}{\partial y_i} \right)_{P,T} dP \tag{122}$$

Dodge p. 123

If we let

$$\xi_i = \frac{1}{RT}\int_0^P \left(\frac{\partial \bar{V}_i}{\partial y_i}\right)_{P,T} dP \tag{123}$$

then

$$y_i \left(\frac{\partial \mu_i^V}{\mu y_i}\right)_{P,T} = RT\,(1 + y_i \xi_i) \tag{124}$$

The equilibrium distribution ratios (K-values) will now be incorporated. From the definition of K-value

$$K_i = \frac{y_i}{x_i} \tag{125}$$

it follows that

$$\ln K_1 = \ln y_1 - \ln x_1 \tag{126}$$

Differentiating and multiplying both sides by x_1

$$x_1\, d \ln K_1 = \frac{x_1\, d\, y_1}{y_1} - dx_1 \tag{127}$$

Similarly for the other component

$$x_2\, d \ln K_2 = \frac{x_2\, d\, y_2}{y_2} - dx_2 \tag{128}$$

Adding Equations 127 and 128

$$x_1\, d \ln K_1 + x_2\, d \ln K_2 = \frac{x_1\, d\, y_1}{y_1} + \frac{x_2\, d\, y_2}{y_2} \tag{129}$$

$$= \left(-\frac{y_1 - x_1}{1 - y_1}\right)\left(\frac{dy_1}{y_1}\right) \tag{130}$$

The chemical potential and K-value expressions will now be incorporated into the equilibrium equation. Substituting Equations 130 and 124 into Equation 107

$$x_1 \, d \ln K_1 + x_2 \, d \ln K_2 = \frac{(x_1\Delta\bar{S}_1 + x_2\Delta\bar{S}_2)dT - (x_1\Delta\bar{V}_1 + x_2\Delta\bar{V}_2)dP}{RT\,(1 + y_1\xi_1)} \quad (131)$$

Restricting Equation 131 to an isobaric path, and recalling that $dT = -T^2 d(1/T)$ and $\Delta\bar{S}_i = \Delta\bar{H}_i/T$

$$x_1\left(\frac{\partial \ln K_1}{\partial(1/T)}\right)_P + x_2\left(\frac{\partial \ln K_2}{\partial(1/T)}\right)_P = -\frac{x_1\Delta\bar{H}_1 + x_2\Delta\bar{H}_2}{R(1+y_1\xi_1)} \quad (132)$$

Expanding the numerator of the right hand side

$$-\left(x_1\Delta\bar{H}_1 + x_2\Delta\bar{H}_2\right) = -\left[x_1\left(\bar{H}_1^V - \bar{H}_1^L\right) + x_2\left(\bar{H}_2^V - \bar{H}_2^L\right)\right] \quad (133)$$

$$= H^L - x_1\bar{H}_1^V - x_2\bar{H}_2^V \quad (134)$$

$$= H^L - \frac{y_1}{K_1}\bar{H}_1^V - \frac{y_2}{K_2}\left(\frac{H^V - y_1\bar{H}_1^V}{y_2}\right) \quad (135)$$

$$= H^L - y_1\bar{H}_1^V\left(\frac{1}{K_1} - \frac{1}{K_2}\right) - \frac{H^V}{K_2} \quad (136)$$

$$\equiv -\Delta H^* \quad (137)$$

where the vapor whose enthalpy is H^V is in equilibrium with the liquid whose enthalpy is H^L. Substituting Equation 137 into Equation 132 and rearranging

$$R\,(1 + y_1\xi_1)\left[x_1\left(\frac{\partial \ln K_1}{\partial(1/T)}\right)_P + x_2\left(\frac{\partial \ln K_2}{\partial(1/T)}\right)_P\right] = -\Delta H^* \quad (138)$$

Equation 138 can be expressed in integral form

$$\int_{\ln K_1, x_1=0}^{\ln K_1, x_1=1} x_1(1+y_1\xi_1)\,d\ln K_1 + \int_{\ln K_2, x_1=0}^{\ln K_2, x_1=1} x_2(1+y_1\xi_1)\,d\ln K_2 = \int_{T_1, x_1=0}^{T_2, x_1=1} (\Delta H^*/RT^2)\,dT \quad (139)$$

For completeness, the isothermal path of Equation 131 is given, which is

$$x_1 \left(\frac{\partial \ln K_1}{\partial P}\right)_T + x_2 \left(\frac{\partial \ln K_2}{\partial P}\right)_T = - \frac{x_1\Delta\bar{V}_1 + x_2\Delta\bar{V}_2}{RT(1+y_1\xi_1)} \tag{140}$$

$$= \frac{V^L - x_1\bar{V}_1^V - x_2\bar{V}_2^V}{RT(1+y_1\xi_1)} \tag{141}$$

This can be expressed in terms of the compressibility factors

$$Z^L = \frac{PV^L}{RT}, \quad \bar{Z}_1^V = \frac{P\bar{V}_1}{RT}, \text{ and } \bar{Z}_2^V = \frac{P\bar{V}_2}{RT}.$$

$$x_1 \left(\frac{\partial \ln K_1}{\partial \ln P}\right)_T + x_2 \left(\frac{\partial \ln K_2}{\partial \ln P}\right)_T = \frac{Z^L_{Mix} - y_1\bar{Z}_1^V(1/K_1 - 1/K_2) - Z^V_{Mix}/K_2}{(1+y_1\xi_1)} \tag{142}$$

Equation 142 can also be expressed in integral form, as used by Thompson and Edmister (45)

$$\int_{\ln K_1, x=0}^{\ln K_1, x=1} x_1(1+y_1\xi_1)d\ln K_1 + \int_{\ln K_2, x=0}^{\ln K_2, x=1} x_2(1+y_1\xi_1)d\ln K_2$$

$$= \int_{P_1, x=0}^{P_2, x=1} \left[Z^L_{Mix} + y_1\bar{Z}_1^V(1/K_2 - 1/K_1) - Z^V_{Mix}/K_2\right]d\ln P \tag{143}$$

If the Lewis and Randall rule holds for the vapor, $\xi_1 = 0$ and Equations 139 and 143 reduce to those derived by Adler, et al (1).

Thompson (44) has derived an expression for ξ_1 in terms of the second and third virial coefficients which is given in Appendix K. Values of ξ_1, as a function of x_1, are given in Appendix L.

The isobaric thermodynamic consistency tests were calculated in differential and integral form, as given by Equations 138 and 139, respectively. Results are discussed in Chapter VI.

Modified Thompson-Edmister Test

The Thompson-Edmister (45) consistency test has been modified so that the same analytical expressions used in the differential test could be incorporated into the integral test. This technique was employed in the Edmister (10) consistency test. Equation 138 becomes

$$(1 + y_1\xi_1)\left[x_1\left(\frac{\partial \ln K_1}{\partial T}\right) + x_2\left(\frac{\partial \ln K_2}{\partial T}\right)\right] = \frac{\Delta H^*}{RT^2} \qquad (144)$$

The form of the integral test (Equation 139) remains the same but the limits are changed, or

$$\int_{T_1}^{T_2} x_1(1+y_1\xi_1)\, d\ln K_1 + \int_{T_1}^{T_2} x_2(1+y_1\xi_1)\, d\ln K_2 = \int_{T_1}^{T_2} (\Delta H^*/RT^2)dT \qquad (145)$$

In addition to the equations obtained for the differential test ($\ln K_i$ vs. $1/T$) equations are obtained for $x_i(1 + y_1\xi_1)$ vs. T, which makes it possible to integrate by parts.

APPENDIX K

VIRIAL EXPRESSION FOR ξ_1

Thompson (44) has derived an expression for ξ_1 using the Berlin form virial equation. Following is Thompson's derivation

$$\underline{V} = \frac{RT}{P} + B' + C'P \qquad (146)$$

and

$$V = (n_1+n_2)\underline{V} = \frac{(n_1+n_2)RT}{P} + (n_1+n_2)B' + (n_1+n_2)C'P \qquad (147)$$

The Berlin form second and third virial coefficients are expressed in Leyden form equivalents because of their preponderance in the literature

$$B' = B = y_1^2 B_{11} + 2y_1y_2B_{12} + y_2^2B_{22} \qquad (148)$$

$$= \frac{n_1^2}{(n_1+n_2)^2} B_{11} + \frac{2n_1n_2}{(n_1+n_2)^2} B_{12} + \frac{n_2^2}{(n_1+n_2)^2} B_{22} \qquad (149)$$

$$C' = \frac{C-B^2}{RT} = \frac{1}{RT}\left[\frac{n_1^3}{(n_1+n_2)^3} C_{111} + \frac{3n_1^2n_2}{(n_1+n_2)^3} C_{112} + \frac{3n_1n_2^2}{(n_1+n_2)^3} C_{122}\right.$$

$$\left. + \frac{n_2^3}{(n_1+n_2)^3} C_{222}\right] - \frac{1}{RT}\left[\frac{n_1^4}{(n_1+n_2)^4} B_{11}^2 + \frac{4n_1^2n_2^2}{(n_1+n_2)^4} B_{12}^2\right.$$

$$+ \frac{n_2^4}{(n_1+n_2)^4} B_{22}^2 + \frac{4n_1^3n_2}{(n_1+n_2)^4} B_{11}B_{12} + \frac{2n_1^2n_2^2}{(n_1+n_2)^4} B_{11}B_{22} + \left(\frac{4n_1n_2^3}{(n_1+n_2)^4}\right)$$

$$\left.(B_{12}B_{22})\right] \qquad (150)$$

Substituting Equations 149 and 150 into Equation 147

$$V = \frac{(n_1+n_2)RT}{P} + \left[\frac{n_1^2}{n_1+n_2} B_{11} + \frac{2n_1n_2}{n_1+n_2} B_{12} + \frac{n_2^2}{n_1+n_2} B_{22}\right]$$

$$+ \frac{P}{RT}\left[\frac{n_1^3}{(n_1+n_2)^2} C_{111} + \frac{3n_1^2n_2}{(n_1+n_2)^2} C_{112} + \frac{3n_1n_2^2}{(n_1+n_2)^2} C_{122}\right.$$

$$\left. + \frac{n_2^3}{(n_1+n_2)^2} C_{222}\right] - \frac{P}{RT}\left[\frac{n_1^4}{(n_1+n_2)^3} B_{11}^2 + \frac{4n_1^2n_2^2}{(n_1+n_2)^3} B_{12}^2 + \frac{n_2^4}{(n_1+n_2)^3} B_{22}^2\right.$$

$$\left. + \frac{4n_1^3n_2}{(n_1+n_2)^3} B_{11}B_{12} + \frac{2n_1^2n_2^2}{(n_1+n_2)^3} B_{11}B_{22} + \frac{4n_1n_2^3}{(n_1+n_2)^3} B_{12}B_{22}\right] \qquad (151)$$

The definition of ξ_1, Equation 123, contains the partial molal volume

$$\bar{V}_1 = \left(\frac{\partial V}{\partial n_1}\right)_{P,T,n_2} = \frac{RT}{P} + \left[\frac{n_1^2+2n_1n_2}{(n_1+n_2)^2} B_{11} + \frac{2n_2^2}{(n_1+n_2)^2} B_{12} - \frac{n_2^2}{(n_1+n_2)^2} B_{22}\right]$$

$$+ \frac{P}{RT}\left[\frac{(n_1^3+3n_1^2n_2)}{(n_1+n_2)^3} C_{111} + \frac{6n_1n_2^2}{(n_1+n_2)^3} C_{112} + \frac{(3n_1^3-3n_1n_2^2)}{(n_1+n_2)^3} C_{122}\right.$$

$$\left. - \frac{2n_2^3}{(n_1+n_2)^3} C_{122}\right] - \frac{P}{RT}\left[\frac{(n_1^4+4n_1^3n_2)}{(n_1+n_2)^4} B_{11}^2 + \frac{(8n_1n_2^3 - 4n_1^2n_2^2)}{(n_1+n_2)^4} B_{12}^2\right.$$

$$- \frac{3n_2^4}{(n_1+n_2)^4} B_{22}^2 + \frac{12n_1^2n_2^2}{(n_1+n_2)^4} B_{11}B_{12} + \frac{4n_1n_2^3-2n_1^2n_2^2}{(n_1+n_2)^4} B_{11}B_{22}$$

$$\left. + \frac{4n_2^4-8n_1n_2^3}{(n_1+n_2)^4} B_{12}B_{22}\right] \qquad (152)$$

Dividing by RT, subtracting 1/P, and expressing the coefficients in mol fractions

$$\frac{\bar{V}_1}{RT} - \frac{1}{P} = \frac{1}{RT}\left[(y_1^2+2y_1y_2)B_{11} + 2y_2^2B_{22} - y_2^2B_{22}\right] + \frac{P}{R^2T^2}\left[(y_1^3+3y_1^2y_2)C_{111}\right.$$

$$\left. + 6y_1y_2^2C_{112} + (3y_2^3-3y_1y_2^2)C_{122} - 2y_2^3C_{222}\right] - \frac{P}{R^2T^2}\left[(y_1^4+4y_1^3y_2)B_{11}^2\right.$$

$$\left. + (8y_1y_2^3-4y_1^2y_2^2)B_{12}^2 - 3y_2^4B_{22}^2 + 12y_1^2y_2^2B_{11}B_{12} + (4y_1y_2^3-2y_1^2y_2^2)\right.$$

$$\left.(B_{11}B_{12}) + (4y_2^4-8y_1y_2^3)B_{12}B_{22}\right] \qquad (153)$$

Integrating and expressing concentration in y_1 exclusively

$$\int_0^P\left(\frac{\bar{V}_1}{RT} - \frac{1}{P'}\right)dP' = \frac{P}{RT}\left[(2y_1-y_1^2)B_{11} + (2-4y_1+2y_1^2)B_{12} - (1-2y_1+y_1^2)B_{22}\right.$$

$$\left. + \frac{P^2}{2R^2T^2}\left[(3y_1^2-2y_1^3)C_{111} + (6y_1-12y_1^2+6y_1^3)C_{112} + (3-12y_1+15y_1^2\right.\right.$$

$$\left.\left. - 6y_1^3)C_{122} - (2-6y_1+6y_1^2-2y_1^3)C_{222}\right] - \frac{P^2}{2R^2T^2}\left[(4y_1^3-3y_1^4)B_{11}^2\right.\right.$$

$$\left.\left. + (8y_1-28y_1^2+33y_1^3-12y_1^4)B_{12}^2 - (3-12y_1+18y_1^2-12y_1^3+3y_1^4)B_{22}^2\right.\right.$$

$$\left.\left. + (12y_1^2-24y_1^3+12y_1^4)B_{11}B_{12} + (4y_1-14y_1^2+16y_1^3-6y_1^4)B_{11}B_{12}\right.\right.$$

$$\left.\left. + (4-24y_1+48y_1^2-40y_1^3+12y_1^4)B_{12}B_{22}\right.\right. \qquad (154)$$

Equation 123, the definition of ξ_1, can be written

$$\xi_1 = \frac{\partial}{\partial y_1}\left[\int_0^P\left(\frac{\bar{V}_1}{RT} - \frac{1}{P'}\right)dP'\right] \qquad (155)$$

Performing the indicated differentiation and expressing concentration in y_2 where convenient

$$\xi_1 = \frac{P}{RT}\left[2y_2B_{11}-4y_2B_{12}+2y_2B_{22}\right] + \frac{P^2}{2R^2T^2}\left[6y_1y_2C_{111}+6y_2(y_2-2y_1)C_{112}\right.$$
$$\left. - 6y_2(2y_2-y_1)C_{122} + 6y_2^2C_{222}\right] - \frac{P^2}{2R^2T^2}\left[12y_1^2y_2B_{11}^2+8y^2(1-6y_1y_2)B_{12}^2\right.$$
$$+ 12y_2^3B_{22}^2 + 24y_1y_2(y_2-y_1)B_{11}B_{12} + 4y_2(1-6y_1y_2)B_{11}B_{22}$$
$$\left. - 24y_2^2(y_2-y_1)B_{12}B_{22}\right] \qquad (156)$$

$$\xi_1 = \frac{2Py_2}{RT}\left[B_{11}+B_{22}-2B_{12}\right] + \frac{3P^2y_2}{R^2T^2}\left[y_1C_{111}+(y_2-2y_1)C_{112} + (y_1-2y_2)C_{122}\right.$$
$$\left. + y_2C_{222}\right] - \frac{2P^2y_2}{R^2T^2}\left[3y_1^2B_{11}^2+3y_2^2B_{22}^2+(1-6y_1y_2)(B_{11}B_{22}+2B_{12}^2)\right.$$
$$\left. + 6(y_2-y_1)(y_1B_{11}B_{12}-y_2B_{12}B_{22})\right] \qquad (157)$$

$$\xi_1 = \frac{2Py_2}{RT}\left(\left[B_{11}+B_{22}-2B_{12}\right] + \frac{3P}{2RT}\left[y_1C_{111}+(y_2-2y_1)C_{112}\right.\right.$$
$$\left. + (y_1-2y_2)C_{122} + y_2C_{222}\right] - \frac{P}{RT}\left[3(y_1^2B_{11}^2+y_2^2B_{22}^2)\right.$$
$$\left.\left. + (1-6y_1y_2)(B_{11}B_{22}+2B_{12}^2) + 6B_{12}(y_2-y_1)(y_1B_{11}-y_2B_{22})\right]\right) \qquad (158)$$

Attempts to derive an expression for ξ_1, from the Leiden form virial equation of state were unsuccessful, as were attempts to derive an expression from the Redlich-Kwong equation.

APPENDIX L

CALCULATION OF ξ_1

The second and third virial coefficients of methane used to determine ξ_1, by the method given in Appendix K were those given by Gyorog and Obert (16). The second virials of ethylene were those of Roper (31). The third virials of ethylene were calculated by the method of Bird, Spotz and Hirschfelder (5). The values of ξ_1, thus calculated using the VLE data of this work are given in Table L-I.

TABLE L-I

VALUES OF ξ_1

Liquid Compositions, Mol fraction, methane	20 Atm.	40 Atm.
0.01	.486	.701
.02	.471	.674
.03	.459	.656
.04	.450	.642
.05	.443	.630
.06	.436	.619
.07	.430	.610
.08	.424	.601
.09	.419	.593
.10	.414	.585
.20	.370	.520
.30	.327	.451
.40	.280	.381
.50	.221	.289
.60	.159	.194
.70	.100	.106
.80	.050	.040
.90	.015	.005
.91	.013	.003
.92	.010	.002
.93	.008	.0007
.94	.006	.0006
.95	.004	.0005
.96	.003	.0004
.97	.002	.0003
.98	.0006	.0002
.99	.0004	.0001

APPENDIX M

SELECTED COMPUTER PROGRAMS

PROGRAM I

```
C      EDMISTER (10) CONSISTENCY TEST IN DIFFERENTIAL FORM
C      SS1, NEW EQUATIONS,SAME EQUATIONS
  900 READ 500
  500 FORMAT(55H                                                    )
      PRINT 500
  901 READ 501,COLLP,IOLLP,C1LLP,I1LLP,C2LLP,I2LLP
  501 FORMAT(3(E22.16,14))
      READ 501,COLLY,IOLLY,C1LLY,I1LLY,C2LLY,I2LLY
      READ 501, C3LLY,I3LLY
      READ 501,COHLP,IOHLP,C1HLP,I1HLP,C2HLP,I2HLP
      READ 501,COHLY,IOHLY,C1HLY,I1HLY,I2HLY
      READ 501, C3HLY,I3HLY
      PRINT501,COLLP,IOLLP,C1LLP,I1LLP,C2LLP,I2LLP
      PRINT501,COLLY,IOLLY,C1LLY,I1LLY,C2LLY,I2LLY
      PRINT 501, C2LLY,I3LLY
      PRINT501,COHLP,IOHLP,C1HLP,I1HLP,C2HLP,I2HLP
      PRINT501,COHLY,IOHLY,C1HLY,I1HLY,C2HLY,I2HLY
      PRINT 501,C3HLY,I3HLY
      EOLLP=IOLLP
      E1LLP=I1LLP
      E2LLP=I2LLP
      EOLLY=IOLLY
      E1LLY=I1LLY
      E2LLY=I2LLY
      E3LLY=I3LLY
      EOHLP=IOHLP
      E1HLP=I1HLP
      E2HLP=I2HLP
      EOHLY=IOHLY
      E1HLY=I1HLY
      E2HLY=I2HLY
      E3HLY=I3HLY
  902 READ 502,RUN,P,T,X,Y,RHSEXP
  502 FORMAT(6F10.5)
      IF(P-25.0)103,103,104
  103 DLPDT=(E2LLP*C2LLP*T)+(E1LLP*C1LLP)
      DLYDT=(E2LLY*C2LLY*T)+(E1LLY*C1LLY)+(E3LLY*C3LLY*T*T)
      GO TO 105
  104 DLPDT=(E2HLP*C2HLP*T)+(E1HLP*C1HLP)
      DLYDT=(E2HLY*C2HLY*T)+(E1HLY*C1HLY)+(E3HLY*C3HLY*T*T)
  105 RHSCAL=(DLPDT+DLYDT)*(Y-X)
      DIFF=RHSEXP-RHSCAL
      PCTDF= (DIFF/RHSEXP)*100.0
      PRINT 601,RUN,P,T,X,Y,DLPDT,DLYDT,RHSCAL,RHSEXP,DIFF,PCTDF
  601 FORMAT(F4.0,F6.0,F8.1,2F7.3,5F8.5,F8.2)
      PRINT 801
  801 FORMAT (/)
      IF(SENSE SWITCH 1)901,902
      END
```

PROGRAM II

```
*FANDK1605
C     EDMISTER (10) CONSISTENCY TEST IN INTEGRAL FORM CONSISTENT WITH
C     THE DIFFERENTIAL TEST, USING INTEGRATION BY PARTS.
      DIMENSION T1(2),T2(2),T3(2),T4(2),T5(2),FTLS1(2),FTLS2(2),
     1STLS1(2),STLS2(2),RHS(2)
  900 READ 500
  500 FORMAT(55H                                                    )
      PUNCH 500
      PUNCH 801
  801 FORMAT(/)
  901 READ 501,T1(1),T1(2)
  501 FORMAT(8F10.5)
      PUNCH 501,T1(1),T1(2)
      PUNCH 801
  902 READ 502,C,N1,B,N2,A,N3
  502 FORMAT(3(E22.16,14))
      READ 502,G,N4,F,NS,E,N6
      READ 502,D,N7
      READ 502,R,N8,Q,N9,P,N10
      READ 502,W,N11,V,N12,U,N13
      PUNCH502,C,N1,B,N2,A,N3
      PUNCH502,G,N4,F,N5,E,N6
      PUNCH502,D,N7
      PUNCH502,R,N8,Q,N9,P,N10
      PUNCH502,W,N11,V,N12,U,N13
      PUNCH 801
  701 DO 200 1=1,2
      T2(I)=(T1(I))**2
      T3(I)=(T1(I))**3
      T4(1)=(T1(I))**4
      T5(I)=(T1(I))**5
      TERM1=(P*T2(I))+(Q*T1(I))+R
      TERM2=(A*T2(I))+(B*T1(I))+C
      FTLS1(I)=TERM1*TERM2
      TERM3=0.5*A*P*T4(I)
      TERM4=(((2.0*B*P)+(A*Q))*T3(I))/3.0
      TERM5=0.5*((2.0*P*C)+(B*Q))*T2(I)
      TERM6=C*Q*T1(I)
      FTLS2(I)=TERM3+TERM4+TERM5+TERM6
      TERM7=(D*T3(I))+(E*T2(I))+(F*T1(I))+G
      STLS1(I)=TERM1*TERM7
      TERM8=0.4*P*D*T5(I)
      TERM9=0.25*((2.0*P*E)+(D*Q))*T4(I)
      TERM10=(((2.0*P*F)+(E*Q))*T3(I))/3.0
      TERM11=0.5*((2.0*P*G)+(F*Q))*T2(I)
      TERM12=Q*G*T1(I)
      STLS2(I)=TERM8+TERM9+TERM10+TERM11+TERM12
      TERM13=U*T3(I)/3.0
      TERM14=V*T2(I)*0.5
      TERM15=W*T1(I)
```

```
      RHS(I)=TERM13+TERM14+TERM15
      PUNCH 503,T1(I),T2(I),T3(I),T4(I),T5(I)
  503 FORMAT(6(2X,E11.5))
      PUNCH 503,TERM1,TERM2,FTLS1(I)
      PUNCH 503,TERM3,TERM4,TERM5,TERM6,FTLS2(I)
      PUNCH 503,TERM1,TERM7,STLS1(I)
      PUNCH 503,TERM8,TERM9,TERM10,TERM11,TERM12,STLS2(I)
      PUNCH 503,TERM13,TERM14,TERM15,RHS(I)
      PUNCH 801
  200 CONTINUE
      PUNCH 802
  802 FORMAT(//)
      FIRST=(FTLS1(1)-FTLS2(1))-(FTLS1(2)-FTLS2(2))
      SECOND=(STLS1(1)-STLS2(1))-(STLS1(2)-STLS2(2))
      RHSEXP=RHS(1)-RHS(2)
      RHSCAL=FIRST+SECOND
      DIFF=RHSEXP-RHSCAL
      PCTDF=(DIFF/RHSEXP)*100.0
      PUNCH 503,FIRST,SECOND,RHSCAL,RHSEXP,DIFF,PCTDF
      PUNCH 805
  805 FORMAT(/////)
      GO TO 900
      END
```

PROGRAM III

```
C     ISOBARIC THERMODYNAMIC CONSISTENCY TEST IN DIFFERENTIAL FORM AS
C     DERIVED BY THOMPSON AND EDMISTER(45). USE XI COMPUTED BY PREVIOUS
C     PROGRAM AND EQUATIONS OF LN KI VS L/T TO COMPUTE FIRST AND SECOND
C     TERMS AT 20 AND 40 ATMOSPHERES.
C     SS1, 101, 102. NEW LN KI VS (1/T) CURVES
C     SS2,PRINT-PUNCH
  101 READ 500
  500 FORMAT(55H                                                      )
      READ 501,COK1L1,N1,COK1L2,N2
  501 FORMAT(3(E22.16,14))
      READ 501,COK2L1,N3,COK2L2,N4
      READ 501,COK1H1,N5,COK1H2,N6
      READ 501,COK2H1,N7,COK2H2,N8
      PUNCH501,COK1L1,N1,COK1L2,N2
      PUNCH 501,COK2L1,N3,COK2L2,N4
      PUNCH 501,COK1H1,N5,COK1H2,N6
      PUNCH 501,COK2H1,N7,COK2H2,N8
  102 READ 502,RUN,P,T,XA,YA,DELHSR
      READ 502, XI
      IF (P-25.0) 103,103,104
  103 TK1L=(1.0/T)-(1.0/166.2)
      TK2L=(1.0/T)-(1.0/244.6)
      TKADT=COK1L1+(2.0*COK1L2*TK1L)
      DKBDT=COK2L1+(2.0*COK2L2*TK2L)
      GO TO 105
  104 TK1H=(1.0/T)-(1.0/186.8)
      TK2H=(1.0/T)-(1.0/272.0)
      DKADT=COK1H1+(2.0*COK1H2*TK1H)
      DKBDT=COK2H1+(2.0*COK2H2*TK2H)
  105 ALS = XA*DKADT
      BLS = (1.0-XA)*DKBDT
      RHSCAL=ALS+BLS
      XIY = XI*YA
      COEFF = 1.987*1.8*(1.0+XIY)
      RHSEXP=-DELHSR/COEFF
      DIFF=RHSEXP-RHSCAL
      PCTDF=(DIFF/RHSEXP)*100.0
      IRUN = RUN
      IF(SENSE SWITCH 2)110,115
  110 PRINT 500
      PRINT 601,IRUN,P,T,DKADT,DKBDT,XI,XIY,RHSCAL,RHSEXP,DIFF
      PRINT 602,PCTDF
      PRINT 801
      GO TO 120
  115 PUNCH 500
      PUNCH 601,IRUN,P,T,DKADT,DKBDT,XI,XIY,RHSCAL,RHSEXP,DIFF
      PUNCH 602,PCTDF
      PUNCH 801
  120 IF (SENSE SWITCH 1) 101,102
```

```
502 FORMAT (6F10.5)
601 FORMAT(I3, F5.1, F7.2, (2E11.5), (2F7.4), (3(1XF7.1)))
602 FORMAT(68XF7.2)
801 FORMAT(/)
    END
```

PROGRAM IV

```
C     THIRD TERM, RIGHT SIDE, ISOBARIC INTEGRAL CONSISTENCY TEST OF
C     THOMPSON AND EDMISTER(45)
C     SS1,NEW EQUATION FOR HVAPOR VS COMPOSITION,USE SAME EQUATION
  900 READ 500
  500 FORMAT(55H                                                    )
  901 READ 501,COEFA,COEFB,COEFC
  501 FORMAT(3E14.8)
  902 READ 502,RUN,T,X,Y,EXHOV,EPEHVX
  502 FORMAT(6F10.5)
      AHLX=EPEHVX-EXHOV
      AHVY=(COEFA*Y*Y)+(COEFB*Y)+COEFC
      AK1=Y/X
      AK2=(1.0-Y)/(1.0-X)
      DHDYY=(2.0*COEFA*Y)+COEFB
      BARHV1=AHVY+(DHDYY*(1.0-Y))
      AK1IN=1.0/AK1
      AK2IN=1.0/AK2
      DIFKIN=AK1IN-AK2IN
      T1= AHVY/AK2
      T2=Y*BARHV1*DIFKIN
      T3=AHLX
      ANUM=T1+T2-T3
      RITSID=ANUM/(1.8*1.987*T*T)
      PRINT 500
      PRINT 601,COEFA,COEFB,COEFC
  601 FORMAT(3(6XE14.8))
      PRINT 602,RUN,T,X,Y,EXHOV,EPEHVX
  602 FORMAT(F10.0,F10.1,2F10.3,2F10.1)
      PRINT 603,AHLX,AHVY,AK1,AK2,DHDYY,BARHV1,DIFKIN,T1,T2,T3
  603 FORMAT(2F8.1,2F8.4,2F8.1,F8.4,3F8.1)
      PRINT 604,T,RITSID,ANUM
  604 FORMAT(F10.1,6X,E14.8,F15.5)
      PUNCH 605,T,RITSID
  605 FORMAT(2E13.7)
      PRINT 804
  804 FORMAT(////)
      IF(SENSE SWITCH 1)900,902
      END
```

PROGRAM V

```
C     ISOBARIC THERMODYNAMIC CONSISTENCY TEST IN INTEGRAL FORM AS DERIVED
C     BY THOMPSON AND EDMISTER(45). USE EQUATIONS OF X(1+Y*XI) VS LN KI
C     FOR FIRST AND SECOND TERMS. USE EQUATIONS OF (DELH/RT**2) VS T FOR
C     THIRD TERM AT 20 AND 40 ATMOSPHERES.
      DIMENSION DLNKA(2),DLNKB(2),T(2),FTLS(2),STLS(2),RS(2)
  101 READ 500
  500 FORMAT(50H                                                  )
      PUNCH 500
  102 READ 501,FA,FB,FC,FD,FE,FF
  501 FORMAT(6E13.7)
      READ 501,SA,SB,SC,SD,SE,SF
      READ 501,RA,RB,RC,RD,RE,RF
      READ 501,DLNKA(1),DLNKA(2),DLNKB(1),DLNKB(2),T(1),T(2)
      DO 200 I=1,2
      DLKAS=DLNKA(1)**2
      DLKAC=DLNKA(1)**3
      DLKAQ=DLNKA(1)**4
      DLKAV=DLNKA(1)**5
      DLKAX=DLNKA(1)**6
      FTLS(1)=((FA*DLKAX)/6.0)+((FB*DLKAV)/5.0)+((FC*DLKAQ)/4.0)+((FD*DL
     1KAC)/3.0)+((FE*DLKAS)/2.0)+(FF*DLNKA(1))
      DLKBS=DLNKB(1)**2
      DLKBC=DLNKB(1)**3
      DLKBQ=DLNKB(1)**4
      DLKBV=DLNKB(1)**5
      DLKBX=DLNKB(1)**6
      STLS(1)=((SA*DLKBX)/6.0)+((SB*DLKBV)/5.0)+((SC*DLKBQ)/4.0)+((SD*DL
     1KBC)/3.0)+((SE*DLKBS)/2.0)+((SF*DLNKB(1)))
      TS=T(1)**2
      TC=T(1)**3
      TQ=T(1)**4
      TV=T(1)**5
      TX=T(1)**6
      RS(1)=((RA*TX)/6.0)+((RB*TV)/5.0)+((RC*TQ)/4.0)+((RD*TC)/3.0)+((RE
     1*TS)/2.0)+(RT*T(1))
  200 CONTINUE
      FT=FTLS(2)-FTLS(1)
      ST=STLS(2)-STLS(1)
      TT=RS(2)-RS(1)
      SUMT=FT+ST
      DIFT=SUMT=TT
      PCTT=(DIFT/TT)*100.0
      PUNCH 601,FT,ST,SUMT,TT,DIFT,PCTT
  601 FORMAT(6(2XE11.5))
      PUNCH 801
  801 FORMAT(/)
      GO TO 101
      END
```

PROGRAM VI

```
*FANDK1605
C     THOMPSON-EDMISTER CONSISTENCY TEST IN INTEGRAL FORM CONSISTENT
C     WITH THE DIFFERENTIAL TEST, USING INTEGRATION BY PARTS
      DIMENSION T1(2),T2(2),T3(2),T4(2),T5(2),FTLS1(2),FTLS2(2),STLS1
     1,STLS2(2),RHS(2)
      DIMENSION ALNT(2)
  900 READ 500
  500 FORMAT(55H                                                      )
      PUNCH 500
      PUNCH 801
  801 FORMAT(/)
  901 READ 501,T1(1),T1(2),BP1,BP2
  501 FORMAT(8F10.5)
      PUNCH501,T1(1),T1(2),BP1,BP2
      PUNCH 801
  902 READ 502,B,N1
  502 FORMAT(3(E22.16,14))
      READ 502,E,N3
      READ 502,R,N8,Q,N9,P,N10
      READ 502,Z,N14,Y,N15,X,N16
      READ 502,W,N11,V,N12,U,N13
      N2=0
      C=-(B/BP1)
      F=-(E/BP2)
      PUNCH 502,C,N2,B,N1
      PUNCH 502,F,N2,E,N3
      PUNCH502,R,N8,Q,N9,P,N10
      PUNCH502,Z,N14,Y,N15,X,N16
      PUNCH502,W,N11,V,N12,U,N13
      PUNCH 801
  701 DO 200 I=1,2
      T2(I)=(T1(I))**2
      T3(I)=(T1(I))**3
      ALNT(I)=LOG(T1(I))
      TERM1=(P*T2(I))+(Q*T1(I))+R
      TERM2=(B/T1(I))+C
      FTLS1(I)=TERM1*TERM2
      TERM3=((2.0*B*P)+(C*Q))*T1(I)
      TERM4=C*P*T2(I)
      TERM5=B*Q*ALNT(I)
      FTLS2(I)=TERM3+TERM4+TERM5
      TERM7=(X*T2(I))+(Y*T1(I))+Z
      TERM8=(E/T1(I))+F
      STLS1(I)=TERM7*TERM8
      TERM9=((2.0*E*X)+(F*Y))*T1(I)
      TERM10=F*X*T2(I)
      TERM11=E*Y*ALNT(I)
      STLS2(I)=TERM9+TERM10+TERM11
      TERM13=U*T3(I)/3.0
      TERM14=V*T2(I)*0.5
```

```
      TERM15=W*T1(I)
      RHS(I)=TERM13+TERM14+TERM15
  503 FORMAT(6(2X,E11.5))
      PUNCH 503,T1(I),T3(I),ALNT(I)
      PUNCH 503,TERM1,TERM2,FTLS1(I)
      PUNCH 503,TERM3,TERM4,TERM5,FTLS2(I)
      PUNCH 503,TERM7,TERM8,STLS1(I)
      PUNCH 503,TERM9,TERM10,TERM11,STLS2(I)
      PUNCH 503,TERM13,TERM14,TERM15,RHS(I)
      PUNCH801
  200 CONTINUE
      PUNCH802
  802 FORMAT(//)
      FIRST=(FTLS1(1)-FTLS2(1))-(FTLS1(2)-FTLS2(2))
      SECOND=(STLS1(1)-STLS2(1))-(STLS1(2)-STLS2(2))
      RHSEXP=RHS(1)-RHS(2)
      RHSCAL=FIRST+SECOND
      DIFF=RHSEXP-RHSCAL
      PCTDF=(DIFF/RHSEXP)*100.0
      PUNCH 503,FIRST,SECOND,RHSCAL,RHSEXP,DIFF,PCTDF
      PUNCH 805
  805 FORMAT(/////)
      GO TO 900
      END
```

NOMENCLATURE

A = parameter of Redlich-Kwong equation

= EPE method coefficient

a = parameter of Redlich-Kwong equation

B = second virial coefficient

b = paramter of Redlich-Kwong equation

= parameter of Redlich-Kwong equation

C = third virial coefficient

= EPE method correction term

= heat capacity

D = $\Sigma y_i \bar{L}_i^V - \Sigma x_i \bar{L}_i^L$, Equation 50

= EPE method correction term

d = differential quantity or operator

E = voltage

= EPE method correction term

f = fugacity

G = Gibbs free energy

H = enthalpy

h = parameter of Redlich-Kwong equation = $\frac{BP}{Z}$

I = current

K = vapor-liquid equilibria phase distribution ratio, y/x

= Kelvin temperature

L = $H-H^\circ$, Equation 49

n = number of moles

= number of components

P = pressure

R = universal gas constant

= resistance

S = entropy

T = temperature

U = internal energy

V = volume

x = liquid-phase composition

y = vapor-phase composition in equilibrium with x

$y^{\#}$ = vapor-phase composition = liquid-phase composition

Z = compressibility factor, PV/RT

z = composition of any mixture

Greek Letters

α = $RT/P - V$

γ = $\bar{f}_i/y_i f_i$

Δ = change in a quantity

= EPE correction term

δ = partial differentiation operator

λ = heat of vaporization

μ = chemical potential

ξ_1 = $1/RT \int_0^P \left(\frac{\partial \bar{V}_i}{\partial y_i}\right)_{P,T} dP$

Σ = summation

ϕ = $\bar{f}_i^V/Py_i$

Ω = ohm

ω = acentric factor

Subscripts

app. = apparent

BP = bubble point

c = critical property

= condensation

calc = calculated

com = compression

DP = dew point

exp = experimental

i = i^{th} component

Mix = mixture

N = number of moles

n = number of moles constant

nr = quantity measured across n-ohm resistor

P = pressure constant

Pc = pseudocritical property

r = reduced property

T = temperature constant

v = vaporization

x = liquid composition

= liquid composition constant

y = vapor composition in equilibrium with liquid x

= vapor composition constant

1 = lighter component

2 = heavier component

subbar = molal quantity

Superscripts

L = liquid state

V = vapor state

° = ideal state

′ = Berlin form

= correction term

super-
bar = partial molal quantity

* = a quantity defined in an unusual way

Abbreviations

AC = alternating current

BWR = Benedict-Webb-Rubin

DC = direct current

DPDT = double pole-double throw (switch)

DPI = differential pressure indicator

DWG = dead weight gauge

EPE = Edmister-Persyn-Erbar

ICT = International Critical Tables

ln = logarithm to the base e

NPT = National Pipe Thread

PVT = pressure-volume-temperature

R-K = Redlich-Kwong

SCF = standard cubic foot

SPST = single pole-single throw (switch)

TC = thermocouple

V = valve

VITA

Philip Cochran Tully

Candidate for the Degree of

Doctor of Philosophy

Thesis: THE SIMULTANEOUS INVESTIGATION OF THE ISOBARIC INTEGRAL HEAT OF VAPORIZATION AND VAPOR-LIQUID EQUILIBRIA DATA OF METHANE-ETHYLENE MIXTURES

Major Field: Chemical Engineering

Biographical:

Personal Data: Born in Grand Island, Nebraska, January 11, 1923, the son of C. Franklin and Marian Alice Tully.

Education: Attended grade and junior high school in Grand Island, Nebraska; graduated from Grand Island High School in 1940; received the Bachelor of Science degree from the Iowa State University, with a major in Chemical Engineering, in August, 1947; received the Master of Science degree from the University of Pittsburgh, with a major in Chemical Engineering, in February 1955; completed requirements for the Doctor of Philosophy degree in August 1965 at Oklahoma State University.

Professional experience: From April 1943 to August 1946, was First Lieutenant in the Field Artillery of the United States Army; following graduation from the Iowa State University, was employed by Koppers Co., Inc., Plastics Division, for thirteen years as process engineer, production superintendent, and chief engineer.